CAPTURE OF BCR-ABL FOR INDUCTION OF APOPTOSIS IN CHRONIC MYELOGENOUS LEUKEMIA: FROM INHIBITION TO NUCLEAR ESCORT

by

Andrew S. Dixon

A dissertation submitted to the faculty of
The University of Utah
in partial fulfillment of the requirements for the degree of

Doctor of Philosophy

Department of Pharmaceutics and Pharmaceutical Chemistry

The University of Utah

December 2011

The University of Utah Graduate School

STATEMENT OF DISSERTATION APPROVAL

The dissertation of **Andrew S. Dixon**

has been approved by the following supervisory committee members:

Coral S. Lim	, Chair	**Aug. 1, 2011** Date Approved
Jindrich Kopecek	, Member	**Aug. 1, 2011** Date Approved
James N. Herron	, Member	**Aug. 2, 2011** Date Approved
Darin Y. Furgeson	, Member	**Aug. 1, 2011** Date Approved
Michael S. Kay	, Member	**Aug. 1, 2011** Date Approved

and by **David W. Grainger** , Chair of

the Department of **Pharmaceutics and Pharmaceutical Chemistry**

and by Charles A. Wight, Dean of The Graduate School.

ABSTRACT

The primary cause of chronic myelogenous leukemia (CML) is the presence of the Philadelphia chromosome, resulting in the oncoprotein Bcr-Abl. The constitutive tyrosine kinase activity of Bcr-Abl, localized intracellularly in the cytoplasm, activates numerous oncogenic signaling pathways. Conversely, Bcr-Abl trapped in the cell nucleus induces apoptosis. This work is aimed at turning the oncogenic Bcr-Abl signaling into apoptotic signaling through redirecting Bcr-Abl, found only in the cancerous cells, to the nucleus.

First, this work validated that Bcr-Abl could be directed to the nucleus with nuclear localization signals, and that nuclear Bcr-Abl does induce apoptosis. Ectopic expression of a nuclear localized Bcr-Abl construct in CML cells activated apoptotic signaling.

Next, this worked focused on the design and isolation of Bcr-Abl binding domains. The first approach was the rational design of the Bcr-Abl coiled-coil domain which led to identification of mutations that could be made to enhance the oligomerization properties with Bcr-Abl. A nuclear translocation assay was then developed for studying protein interactions inside a live cell, and confirmed the modifications to the coiled-coil domain improved the binding to the wild-type coiled-coil domain representative of Bcr-Abl. In addition to the application to translocating Bcr-Abl

to the nucleus, the improved oligomerization domain (CCmut2) was found to function as an inhibitor of Bcr-Abl. A second generation modification to the Bcr-Abl coiled-coil domain, CCmut3, was found to exhibit even greater binding than CCmut2 and also inhibited Bcr-Abl.

As an alternative binding approach we used the intracellular antibody capture (IAC) methodology to isolate single domain antibodies (iDabs). Two Bcr-Abl regions with potential implications in the cytoplasmic retention of Bcr-Abl were targeted in the iDabs screens, the actin binding domain and Dbl homology/Pleckstrin homology domains. These screens produced ABI7, and when co-expressed with Bcr-Abl, caused a redistribution of the normal Bcr-Abl localization pattern.

Both CCmut3 and ABI7 were tested for their ability to translocate Bcr-Abl into the nucleus and together were found to efficiently redirect Bcr-Abl to the nucleus. The culmination of this work is an established method to efficiently redirect Bcr-Abl from the cytoplasm into the nucleus where it is known to induce apoptosis.

TABLE OF CONTENTS

ABSTRACT……...iii

LIST OF FIGURES……..viii

LIST OF ABBREVIATIONS ……...x

ACKNOWLEDGMENTS…….xii

Chapter

1. BACKGROUND AND SIGNIFICANCE……..……1

Summary……...……..…...1
Background and Significance……...…….5
References…….....27

2. CONTROLLING SUBCELLULAR LOCALIZATION TO ALTER FUNCTION: SENDING ONCOGENIC BCR-ABL TO THE NUCLEUS CAUSES APOPTOSIS……..……..41

Abstract……41
Introduction……..42
Materials and Methods……43
Results…….....48
Discussion/Conclusions……...56
Acknowledgments……59
References……60

3. THE NUCLEAR TRANSLOCATION ASSAY FOR INTRACELLULAR PROTEIN-PROTEIN INTERACTIONS AND ITS APPLICATION TO THE BCR COILED-COIL DOMAIN……..63

Abstract……63

Introduction……..64
Materials and Methods……69
Results and Discussion……....73
Acknowledgments……78
References……79

4. DISRUPTION OF BCR-ABL COILED-COIL OLIGOMERIZATION BY DESIGN……...82

Abstract……82
Introduction……..83
Materials and Methods……87
Results…….....96
Discussion……..108
Acknowledgments……..111
Supplemental Data…….111
References……..……118

5. SECOND-GENERATION MODIFICATIONS TO THE BCR COILED-COIL DOMAIN: FURTHER MUTANT HOMO-DIMER DESTABILIZATION FOR ENHANCED OLIGOMERIZATION WITH BCR-ABL…….124

Abstract……..124
Introduction……125
Materials and Methods……...131
Results…….....137
Conclusions……147
Acknowledgments…….….149
References……..150

6. RATIONALLY DESIGNED BCR-ABL CAPTURE MOTIFS FOR ESCORT TO THE NUCLEUS…….154
Abstract……..154
Introduction……155
Materials and Methods……...162
Results…….....169
Conclusions……184
Acknowledgments……..187
References……..188

7. CONCLUSIONS AND FUTURE WORK……..…….195

Conclusions..……..195
Future Work...……211
References……..226

LIST OF FIGURES

Figure		Page
1.1	Protein switch mechanism ……..3	
1.2	Bcr-Abl domains and signaling ……..…….....10	
1.3	Drug targeting to cellular organelles …….....14	
1.4	EGFP fused to the protein switch and transfected into 1471.1 murine adenocarcinoma cells..……..……..16	
1.5	Goals for the design of a mutant coiled-coil domain ……....19	
2.1	EGFP-Bcr-Abl localization in K562 cells ……49	
2.2	K562 cells transfected with 0NLS-, 1NLS-, or 4NLS-Bcr-Abl…….....50	
2.3	Healthy K562 cells……..…….....51	
2.4	Percent nuclear intensity of Bcr-Abl with and without 4NLS-Bcr-Abl…….....55	
2.5	Effect of Bcr-Abl localization on caspase activity...……..…….....57	
3.1	The nuclear translocation assay (NTA) concept …….....67	
3.2	Percent nuclear increase of protein-switch constructs and example cell images ……..….74	
3.3	NTA results for the Bcr coiled coil and mutant coiled coil……...76	
4.1	Ribbon diagrams, with the corresponding helical wheel diagram below, of the wild-type homodimer (A), wild-type:CCmut2 heterodimer (B), and CCmut2:CCmut2 homodimer (C) ……..85	
4.2	Circular dichroism wavelength scans and thermal denaturation …….....101	

4.3 Binding of the homo- and hetero-dimers tested through the nuclear translocation assay (NTA) and mammalian two-hybrid assay ……...103

4.4 Representative images of western blots to detect the phosphorylated form of Bcr-Abl ……..…105

4.5 Inhibition of the Bcr-Abl through expression of CCmut2 results in decreased proliferation of K562 cells and activation of apoptosis 107

4.6 Fluorescence microscopy for morphological evaluation of nuclei.…….....109

4.S1 One dimensional root mean square deviation (RMSd) of coiled-coil dimers derived from the Bcr protein-protein binding domain…….116

4.S2 Thermodynamic integration approaches to calculate the relative free energy of binding for coiled-coil dimers were based on a thermodynamic cycle……...117

5.1 Ribbon diagrams of the modified coiled-coil domains ……...129

5.2 Mammalian two-hybrid assay….…….138

5.3 Co-localization with Bcr-Abl ……..141

5.4 Effects of CCs on Bcr-Abl and proliferation of K562 cells..……...142

5.5 Annexin-APC/7AAD staining and caspase-3/7 assays……..…….144

5.6 Nuclear segmentation of K562 cells……146

6.1 Bcr-Abl domains and the targeting regions of the binding domains ……..161

6.2 Overview of IAC^3 screens against ABD and DHPH baits……..170

6.3 Mammalian two-hybrid assays ……...174

6.4 Co-localization between Bcr-Abl and the binding domains ..…….176

6.5 Redistribution of Bcr-Abl subcellular localization …….178

6.6 Nuclear translocation using the protein switch ……..180

6.7 Nuclear translocation using 4NLS-binding motif constructs ……....182

6.8 Representative images of nuclear Bcr-Abl resulting from 4NLS-CCmut3, and quantification of nuclear Bcr-Abl from all 4NLS constructs ….....183

LIST OF ABBREVIATIONS

AD	activation domain
ABD	Actin Binding Domain
Abl	abelson protein
ANOVA	analysis of variance
Bcr	breakpoint cluster region
Bcr-Abl	breakpoint cluster region-abelson protein
BD	binding domain
CC	coiled coil
CCmut	mutant coiled coil
CDR	compliment determining region
CML	chronic myelogenous leukemia
CPP	cell-penetrating peptide
CRM1	chromosome maintenance region 1
DBD	DNA binding domain
Dex	Dexamethasone
DH	Dbl-homology domain
DMSO	Dimethylsulfoxide
DNA	Deoxyribonucleic acid
EGFP	enhanced green fluorescent protein
GR	glucocorticoid receptor
IAC	intracellular antibody capture
iDab	intracellular/single domain antibody
JC-1	JC-1 cationic dye
LMB	Leptomycin B
LBD	ligand binding domain
Myc	Myelocytomatosis oncogene
NES	nuclear export signal
NLS	nuclear localization signal
NTA	nuclear translocation assay
PCR	polymerase chain reaction
PH	pleckstrin homology domain
Ph(+)	Philadelphia chromosome positive
Ph(-)	Philadelphia chromosome negative
PI	propidium iodide
PNI	percent nuclear increase
PS	protein switch
RLuc	Renilla luciferase

scFv	single chain variable fragment
SV40	Simian virus 40
SD	standard deviation
SDS-PAGE	sodium dodecylsulfate polyacrylamide gel electrophoresis
SEM	standard error of the mean
SFK	src family kinase
SH2	Src-homology 2 domain
SH3	Src-homolgy 3 domain
S/T kinase	serine/threonine kinase
TKI	tyrosine kinase inhibitor
V_H	variable domain from the heavy chain
V_L	variable domain from the light chain
Y kinase	tyrosine kinase

ACKNOWLEDGMENTS

I would like to thank my parents, Chris and Bonnie Dixon, for their seemingly endless support, encouragement, guidance, and unconditional love. They instilled in me at an early age not only the importance of education, but a love for learning. Their own efforts to further their education, at times in their lives that did not make returning to school simple, were outstanding examples and inspired me to pursue an advanced degree. Regardless of my specific aspiration, they have always supported me financially, emotionally, and, most importantly with their time. In addition, they taught me the value of hard work and integrity. Any successes I may have achieved can truly be accredited to their parenting, teaching, example, and sustaining vote of confidence. I will forever be grateful to them for molding me into the person I am today, and giving me the basis for future achievements.

I would also like to thank my loving wife Kati. I would never have made it through graduate school without her. I am grateful for her understanding that "done in 30 minutes" really means 2 more hours, and that "6 o'clock" really means 8 or 9 o'clock. Her support, encouragement, and pretending to act excited when I told her results gave me reason to keep going. She never hesitated, or complained about, staying up with babies so I could get sleep before tests. I am amazed at her tireless efforts to be the greatest wife and mother. She is a tremendous success that goes all too often unrecognized. During difficult times she has always been there to support me, and

knowing she always will be gives me strength to carry on. Her ability to envision me better than I actually am has inspired me to work to become it. She has made my life better and happier.

I want to thank my wonderful boys: Drew, Kade, and Miles. Thank you for helping me realize what truly is important in life, and inspiring me to work hard and be a better person. Thank you for cheering me up at the end of a long day.

The owners of the houses where my family has really lived the last five years, Karen and Laurice Lundberg and Ruth and Steve Hansen, are also due my sincere gratitude. I don't know what we would have done without your yards for the boys to play in, and for you playing with the boys and constantly feeding all of us. Your love and support go way beyond these acts, and I am genuinely appreciative for all that you do for me and my family.

I will always be grateful to Dr. Carol S. Lim for her exceptional mentoring. I cannot thank her enough for her sincere care and concern for me both as a scientist and a person. She has exerted enormous effort into ensuring all of her students are continually improving not just in laboratory skills where she might receive some benefit, but also as independent scientists, leaders, mentors, and well-rounded people. These great efforts reflect her sincere desire to see us succeed, and I have benefitted greatly from her incomparable outlook. She has helped me improve and fine-tune my laboratory, scientific writing, and presentation skills, and made me a better person in general. Throughout my graduate studies she has always been willing to provide valuable scientific insight and give meaningful feedback. Additionally, she has not only provided me the opportunity to expand my knowledge while working on a very interesting project,

but granting me the freedom to pursue some of my own ideas. I am grateful for the confidence and trust she has bestowed upon me.

I also need to thank all of the Lim Lab members. Not only was Mudit a great mentor/trainor, but also did much of the work leading up to this dissertation. I could not have done this work without the help and insight from the Bcr-Abl sub-group: Jonathan, David, Ben, and Geoff. Thanks to all other lab members who provided scientific insight and made a great work environment: Amy, Rian, Mohanad, Karina, Abdul, and Shams.

I would also like to express my gratitude to all of my supervisory committee: Dr. Herron, Dr. Furgeson, Dr. Kopecek, and Dr. Kay. Your scientific input has greatly enhanced the quality of this work, and made it possible by allowing me to come to your laboratories and use your equipment. Although he is not a member of my committee, I need to thank Dr. Cheatham for collaborations and guidance on the design of mutations in the coiled-coil domain. I am also grateful for the help and collaboration of Dr. Rabbitts at the University of Leeds.

CHAPTER 1

BACKGROUND AND SIGNIFICANCE

Summary

Proteins are essential to any organism due to their numerous biological roles including enzymatic reactions, structural integrity, and inter- and intracellular communication. These life dependent functions are both temporally and spatially regulated, and just as a mutated protein may not function, a protein in the wrong location may not function, or may have an alternate function in the new environment. Mislocalized proteins have been documented to be the cause of numerous diseases such as cancer, diabetes, schizophrenia, and cystic fibrosis (*1-3*). The ability to control the localization of a protein is a remarkable tool that not only provides a method for studying the effects of protein localization, but also exhibits the potential to be used therapeutically to overcome the results of a mislocalized protein. The control over the translocation between the cytoplasm and the nucleus has been previously optimized in the Lim Laboratory for the greatest nuclear translocation upon addition of ligand. The resulting chimeric protein was called a "protein switch" (*4*), and allows for the reversible translocation between two subcellular compartments through the addition or removal of a ligand. Although various other "protein switches" that translocate to other subcellular compartments have been constructed in the Lim Laboratory, the protein switch used in

the studies herein are based on the optimized nucleo-cytoplasmic shuttling protein switch and consist of the HIV Rev nuclear export signal (NES), the MycA8 nuclear localization signal (NLS), and the glucocorticoid ligand binding domain (LBD). In the absence of the synthetic glucocorticoid dexamethasone (dex), the NES is dominant and causes the protein switch to localize primarily to the cytoplasm. When dex is added, it induces a conformational change in the LBD, resulting in the NLS becoming dominant, and the protein switch translocates into the nucleus. A simple method of conveying control over the subcellular localization of a protein of interest is to genetically engineer a fusion protein consisting of the protein switch and the protein of interest. This fusion protein, and the ability to control its translocation between two compartments by adding or removing dex, allows for studying the function of the protein of interest in each of the compartments. Although fusing a protein of interest to the protein switch is a useful method to study the correlation between function and location of a protein, the therapeutic application is limited to diseases which may be treated by restoring a lost protein function. Potential problems with a treatment involving a protein known to have a role in causing the disease state are a further limitation. More broadly applicable is the ability to move an endogenous protein from one subcellular location to another. Critical to achieving this goal is a way to bind the protein switch to the protein of interest, enabling the targeting of a disease causing protein. By incorporating into the protein switch a domain/protein that interacts with a protein of interest, a mislocalized protein can be redirected to the appropriate location as a means of therapeutic intervention (see Figure 1.1). This type of protein switch, involving a binding motif, can target any protein

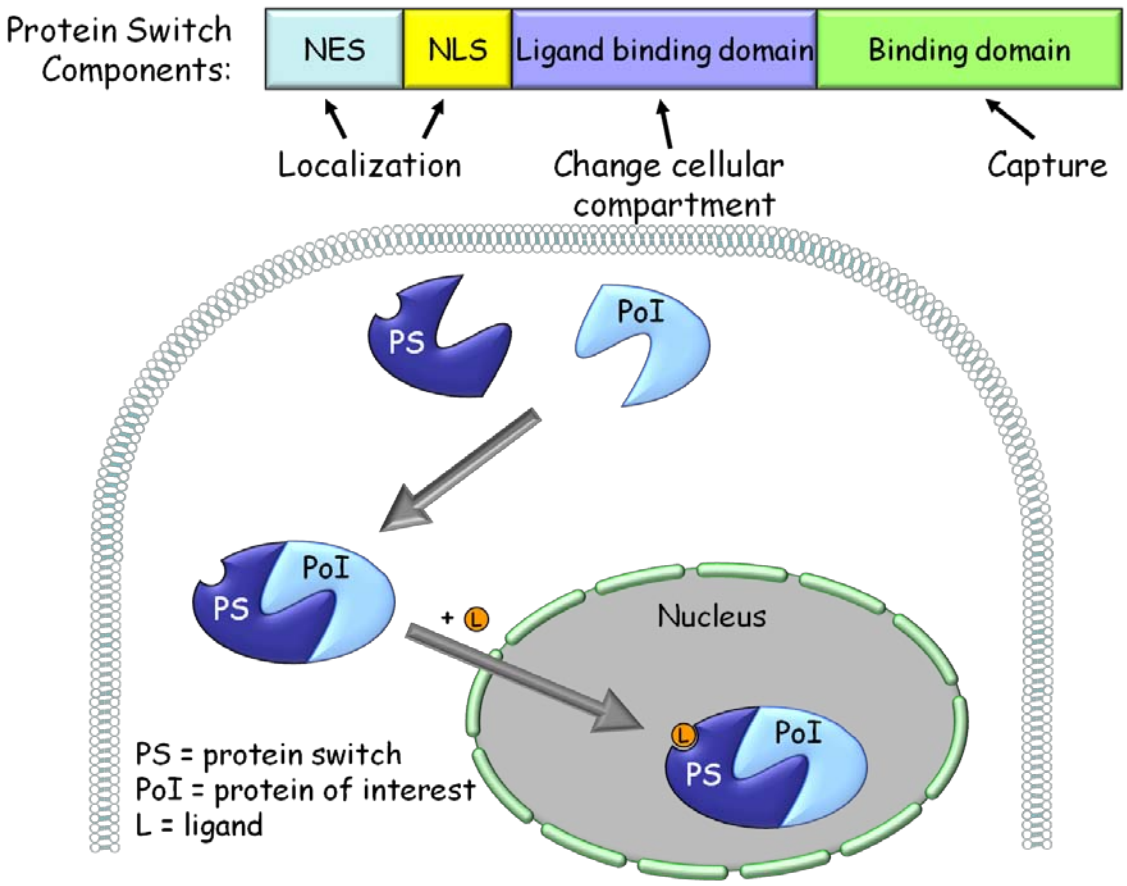

Figure 1.1 Protein switch mechanism. The PS, shown schematically (top diagram), consists of a NES, NLS, ligand-binding domain and binding domain. When PS plasmid is transfected into cells, the expressed PS captures a PoI in the cytoplasm. Upon addition of ligand, the PS-PoI complex translocates to the nucleus. L: Ligand; NES: Nuclear export signal; NLS: Nuclear localization signal; PoI: Protein of interest; PS: Protein switch. (Reprinted by permission from *Ther Deliv*. 2010 Jul 1;1(1):169-193.)

of interest so long as a binding motif to that protein has been identified or can be generated. As an alternative to the traditional attempt to stop the undesired function of the mislocalized protein, the protein switch allows for the redirection of the protein to the appropriate location to not only stop the aberrant function in the wrong compartment, but also restore the proper function in the right compartment.

The oncoprotein Bcr-Abl is the primary cause of chronic myeloid leukemia due to unregulated signaling of the tyrosine kinase domain in the cytoplasm of the leukemic cells (*5-7*). The constitutive activity of Bcr-Abl in the cytoplasm, which results in the uncontrolled cell proliferation, has the opposing role of inducing apoptosis in the nucleus (3, 5). Prior to the protein switch, there was no way of exploiting the apoptotic abilities of Bcr-Abl as a mode of fighting the Bcr-Abl containing cells. Moreover, the potential of using an active Bcr-Abl protein to induce apoptosis would be applicable to tyrosine kinase inhibitor (TKI) resistant cells (*8-11*) and even the cancer stem cells that are refractory towards TKI therapy (*12-15*). This first chapter will describe the etiology of chronic myelogenous leukemia (CML) and the pathogenic role of Bcr-Abl in CML. The protein switch concept will then be described in both the context of the application to escort Bcr-Abl to the nucleus for controlled induction of apoptosis in CML cells, as well as the context of the nuclear translocation assay. As a binding motif is pivotal in using the protein switch to move Bcr-Abl to the nucleus, the binding motifs will also be described.

Background and Significance

Chronic Myeloid Leukemia

The Philadelphia Chromosome

The Philadelphia chromosome (Ph), named after the city where it was identified, is responsible for 90-95% (*16-19*) of chronic myeloid leukemia and 20% of adult acute lymphoblastic leukemia (19, 20), and was the first abnormal chromosome to be directly correlated to a specific disease. The shortened chromosome 22 was first identified in leukocytes from people with CML by Peter Nowell and David Hungerford in 1960 (16, 21, 22), but at this time it was not known whether the chromosomal abnormality was the result of a deletion or a translocation. It was not until 13 years later that Janet Rowley was able to demonstrate the Ph was a result of a reciprocal translocation between chromosomes 9 and 22 (23). Further work by others more fully characterized the translocation as t(9:22)(q34:q11), involving the fusion of the Abelson kinase gene (abl) from chromosome 9 onto the Breakpoint Cluster Region gene (bcr) of chromosome 22 and the resulting expression of the oncoprotein Bcr-Abl (17, 24, 25). In most patients with CML the breakpoints are located between exons 12 and 16 of bcr, termed the major breakpoint cluster region, and between exon Ib and Ia of the abl gene, which generate a 210 kDa protein ($p210^{Bcr\text{-}Abl}$) (26, 27). Alternative breakpoints generate a 190 kDa protein ($p190^{Bcr\text{-}Abl}$) commonly found in Philadelphia chromosome positive (Ph^{+}) B cell acute lymphoblastic leukemia (B-ALL) and a 230 kDa protein ($p230^{Bcr\text{-}Abl}$) found in chronic neutrophilic leukemia (28-30). It has been demonstrated in a mouse model that expression of $p210^{Bcr\text{-}Abl}$ is sufficient to induce a myeloproliferative disorder typical of CML (31), directly indicating the Philadelphia chromosome provokes CML.

Disease Characterization and Progression

When a hematopoietic stem cell acquires the Ph, the resulting expression leads to an uncontrolled production of blast cells, and classification of CML into three distinct phases can be based on counts of these cells. As defined by the World Health Organization, the chronic phase is characterized by the leukocytes in the blood and marrow being comprised of less than 10% blast cells (32). Most CML patients are diagnosed in this chronic phase by the presence of the Ph after hypercellularity is detected in a medical examination as a periodic check-up or for an unrelated condition, a fact reflecting that this phase is not generally associated with noticeable symptoms. If undiagnosed and untreated, the chronic phase typically progresses to accelerated phase within 3-6 years (33), defined by 10-19% blasts in the blood and marrow (32). Even with treatment the chronic phase may advance to the accelerated phase due to additional chromosomal abnormalities, increased expression of Bcr-Abl, genomic instability, inactivation of tumor suppressor genes, and arrest of differentiation (34). Patients in the accelerated phase typically exhibit thrombocytopenia, neutropenia, anemia, and splenomegaly, which result in infections, contusions, hemorrhages, fatigue, weight loss, and a general loss of well-being. Within a couple months (untreated) the accelerated phase moves to blast phase (blast crisis) characterized by more than 20% blast cells in the blood and bone marrow (32). In blast crisis there is an increase in severity of the previously mentioned symptoms, and results in similar effects as acute myeloid leukemia or, less frequently, acute lymphoid leukemia. The fatal effects of blast crisis are primarily a result of the blast cells over whelming and limiting the number of mature and functional blood cells.

Prognosis and Treatment

It is estimated that approximately 5,000 people in the US will be diagnosed with CML in 2011, with the median age at diagnosis being 65 (35). In 2010 it was estimated that 440 people in the US died due to CML (35). Currently, the only cure for CML is allogenic stem cell transplantation, but this treatment is generally salvage therapy used for patients in accelerated phase, blast crisis, or otherwise resistant forms of CML. The rationale for considering stem cell transplantation as salvage therapy is the effective management of CML with tyrosine kinase inhibitors (TKIs) coupled with the risk of the stem cell transplant. Donor availability and recipient qualifications are also limiting factors. Stem cell transplantations are not generally used for patients older than 60, and, with the high median age at diagnosis of CML, this curative approach is not an option for a large percentage of CML patients. In addition, other factors such as phase of disease, matching of donor, and Bcr-Abl mutations affect the outcome and overall survival rate (36, 37).

The current first-line treatment of CML is one of three TKIs: imatinib (Gleevec®), nilotinib (Tasigna®), or dasatinib (Sprycel®). The first FDA approved TKI, imatinib, not only altered the treatment and prognosis of patients with CML, but validated the approach to rationally design drugs (38-40). Imatinib has exhibited astonishing results of 97% hematological response (normalization of the white blood cell counts), and 82% cytogenetic response (absence of Philadelphia chromosome in 20 metaphases on classical karyotyping on bone marrow) (41, 42) when treating CML patients in the chronic phase. Both nilotinib and dasatinib have lower IC_{50} values than imatinib and have further

enhanced the treatment of CML (43). However, in spite of the success observed with TKIs, they do not cure CML (44), and patients will require continual treatment to manage the disease. If treatment is discontinued, the disease rapidly returns (45, 46). The return of the disease is attributed the "residual disease," or the inability of TKIs to eliminate all the Ph cells (47-49). Specifically, TKIs do not induce apoptosis in the quiescent hematopoietic stem cells containing the Ph in spite of the over-expression of Bcr-Abl and the ability of the TKI to inhibit Bcr-Abl (50, 51). Given that any remaining stem cells containing the Ph will generate more Ph blast cells, it is easy to see why relapse occurs if treatment is discontinued or resistance develops. The inability to eliminate these leukemic stem cells underscores the necessity for alternative therapies with the ability to target these critical cells.

Resistance and Adverse Events

It is estimated that as many as 28% of patients on imatinib will have to stop treatment due to intolerance or resistance (41, 52). Resistance can be classified as primary resistance or secondary resistance. Failure to achieve complete hematologic response within 3-6 months, a partial cytogenic response by 12 months, or a complete cytogenic response within 18 months is defined as primary resistance. Secondary resistance, or acquired resistance, is the loss of response following an initial achievement of either complete hematologic or complete cytogenic response. The development of point mutations in the kinase domain of Bcr-Abl is the leading cause of secondary resistance, but ranges from 40-90% of cases due to variations in the definition of resistance, the method used to detect the mutation, and the phase in which the resistance

develops (8, 53, 54). Although more than 100 mutations have been identified in Bcr-Abl (54-56), all of these mutations can be treated with one of the approved TKIs except for T315I (57-59). This mutation, termed the gate keeper mutation, prevents the TKI from forming a critical hydrogen bond with Bcr-Abl and adds steric block to the ATP-binding region. The prevalence of this mutation is estimated to be up to 19% of patients with imatinib resistance (54, 60-62). However, two third-generation TKIs have demonstrated the ability to inhibit Bcr-Abl with the T315I mutation, ponatinib and DCC-2036, and are currently in clinical trials (63-66).

Although imatinib was found to induce cell death in cardiomyocytes through activation of the endoplasmic reticulum stress response (67), leading to the fear that imatinib and other inhibitors of c-Abl would cause cardiotoxicity, the incidence of cardiotoxicity in CML patients so far has been minimal, <0.1% (41, 42, 68, 69). There are, however, adverse events such as cytopenias, nausea, vomiting, fever, abdominal pain, and periorbital edema (42, 70).

Dr. Abl and Mr. Bcr: Cytoplasmic Oncogenicity and Nuclear Apoptosis

Bcr-Abl primarily localizes to the cytoplasm where it activates numerous pathways which result in cell proliferation, increased cell motility, and oncogenesis (Figure 1.2). Bcr-Abl is a complex protein consisting of numerous functional domains, and the signaling through Bcr-Abl is the cumulative result of these domains. As illustrated in Figure 1.2, the Bcr portion of $p210^{Bcr\text{-}Abl}$ contributes four domains; a coiled-coil domain (CC), serine/threonine kinase domain (S/T kinase), Dbl homology domain (DH), and Pleckstrin homology domain (PH). The Abl portion contributes five domains; Src

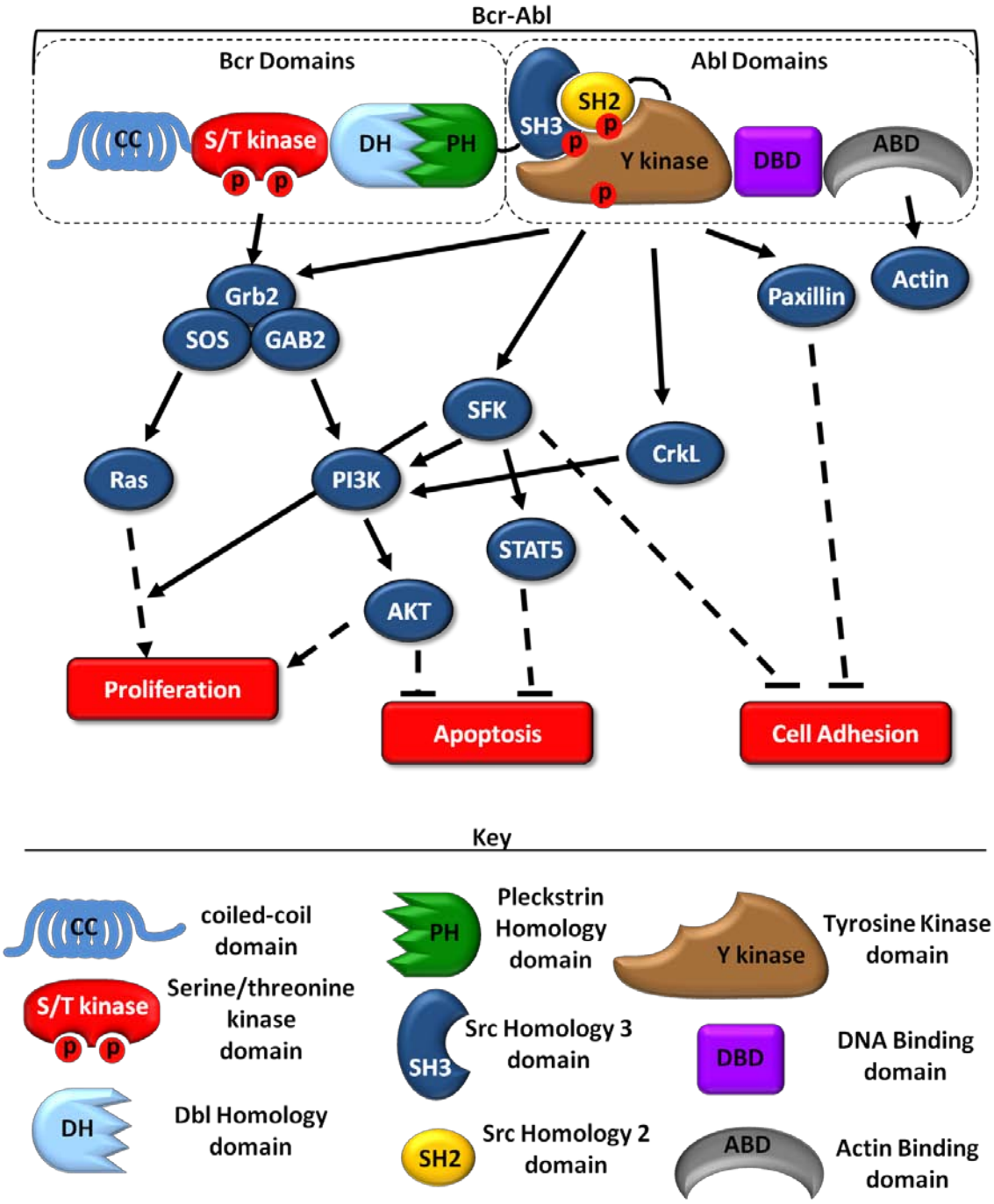

Figure 1.2. Bcr-Abl domains and signaling. Only some pathways affected by Bcr-Abl signaling are illustrated. The dashed lines indicate intermediate steps that are not depicted in the diagram.

homology 3 domain (SH3), Src homology 2 domain (SH2), tyrosine kinase domain (Y kinase), DNA binding domain (DBD), and an actin binding domain (ABD). The fusion of Abl onto Bcr relieves the autoinhibition of the Abl tyrosine kinase domain and generates a constitutively active protein (71) that signals cell proliferation, inhibition of apoptosis, and altered cell adhesion and motility (72-75). The Bcr coiled-coil domain is responsible for the oligomerization of the oncoprotein into first a dimer, and subsequently a tetramer (76, 77), and has been shown to be both essential and sufficient to activate the tyrosine kinase domain of Abl (78). Through the S/T kinase domain (specifically tyrosine 177) (79, 80), Bcr-Abl activates the Ras pathway which signals cell proliferation and transformation (78, 81-85). The combination of the S/T kinase and Y kinase domains also activate the phosphatidylinositol-3 kinase (PI3K)/AKT pathway (81, 86) associated with inhibition of apoptosis and inhibition of inhibitors of cell proliferation (78-80). As evident from the successes of imatinib, dasatinib, and nilotinib (tyrosine kinase inhibitors), the tyrosine kinase domain is of paramount importance in the oncogenesis of Bcr-Abl. This domain is responsible for phosphorylating and activating a list of proteins (81, 87-95). The SH3/SH2 domains play critical roles in regulating the tyrosine kinase activity and interacting with substrate proteins that are phosphorylated by the tyrosine kinase domain (96-98). In short, the pathogenesis of CML induced by Bcr-Abl is complex and is a cumulative effect of these various domains in concert.

The fusion of Abl onto Bcr results not only in the constitutive activity of Abl, but also an altered subcellular localization. While c-Abl is known to shuttle between the cytoplasm and the nucleus (99), Bcr-Abl is primarily cytoplasmic (100, 101). This subcellular localization is important in the regulation of the various functions of c-Abl

(99, 102). In the nucleus, c-Abl can bind distorted DNA structures and A/T duplexes (103, 104), interacts with retinoblastoma (RB) protein (105, 106), and regulates p73 (107-109) and RNA polymerase II (110-114). c-Abl is involved in cell cycle regulation and induction of apoptosis (99, 102), and the tyrosine kinase activity of c-Abl has been shown to be activated by several apoptotic agents such as cisplatin (107), ionizing radiation (115), mitomycin C (116, 117), etoposide (117), TNF (117)**,** and camptothecin (117). Cells with homozygous deletion of the c-Abl gene have also been shown to have a reduced apoptotic response to ionizing radiation (118).

The opposing roles of Bcr-Abl in cell proliferation and c-Abl in apoptosis are correlated to the subcellular localization of these two proteins. The theory that Bcr-Abl would also regulate apoptosis if located in the nucleus was initially validated by Vigneri and Wang who showed the nuclear accumulation of Bcr-Abl resulted in the induction of apoptosis (*5*) and subsequently by Aloisi et al. using samples from CML patients (3). The potency of the nuclear Bcr-Abl is evident by the induction of apoptosis by a small percentage of Bcr-Abl protein (20-25%) that became trapped inside the nucleus. We have further demonstrated in this work that an exogenously added Bcr-Abl, with additional nuclear localization signals to direct it to the nucleus, induced apoptosis in leukemia cells (119). The remainder of this work was aimed at identifying Bcr-Abl binding domains, and subsequently using those identified binding domains to translocate Bcr-Abl to the nucleus, as a means of exploiting this potent apoptotic potential as a novel therapeutic treatment.

Controlling Nucleo-Cytoplasmic Translocation of Bcr-Abl Using the Protein Switch

Since the pioneering work by Nobel Laureate Günter Blobel on signal sequences in proteins (120), numerous studies have been done to characterize these localization signals and use them to direct proteins, nucleic acid, and other macromolecules to a desired compartment within a cell (Figure 1.3). Nevertheless, while much work has been done with localization signals, the protein switch exhibits the unique property of the localization being controlled through the presence or absence of a ligand (121). Various ligand inducible transcription factors have been generated (122-127), and paved the way for the development of the bidirectional protein switch developed in our laboratory. Comprised of three components, the protein switch contains a nuclear localization signal (NLS), a nuclear export signal (NES), and a ligand binding domain (LBD). In the absence of the ligand, the NES is dominant and the protein switch localizes to the cytoplasm. When the ligand is added, it binds to the LBD and causes a conformational change that sends the protein switch to the nucleus. Nuclear import and export signals have been extensively studied (121, 128, 129) and optimized as protein switches (4, 128) that exhibit the most nuclear increase upon ligand induction. The optimized protein switch contains the NES sequence from the HIV-rev protein (LQLPPLERLTL), and the NLS sequence from the MycA8 protein (PAAKRVKADE) fused to the rat glucocorticoid receptor LBD containing the C656G mutation that renders it 10 times more sensitive to the agonistic ligand dexamethasone (130). The HIV-rev NES fits the typical leucine-rich sequences that are recognized by the classical export receptor, chromosomal region maintenance (CRM1 or exportin 1), which generally have the consensus sequence LX_{1-3}

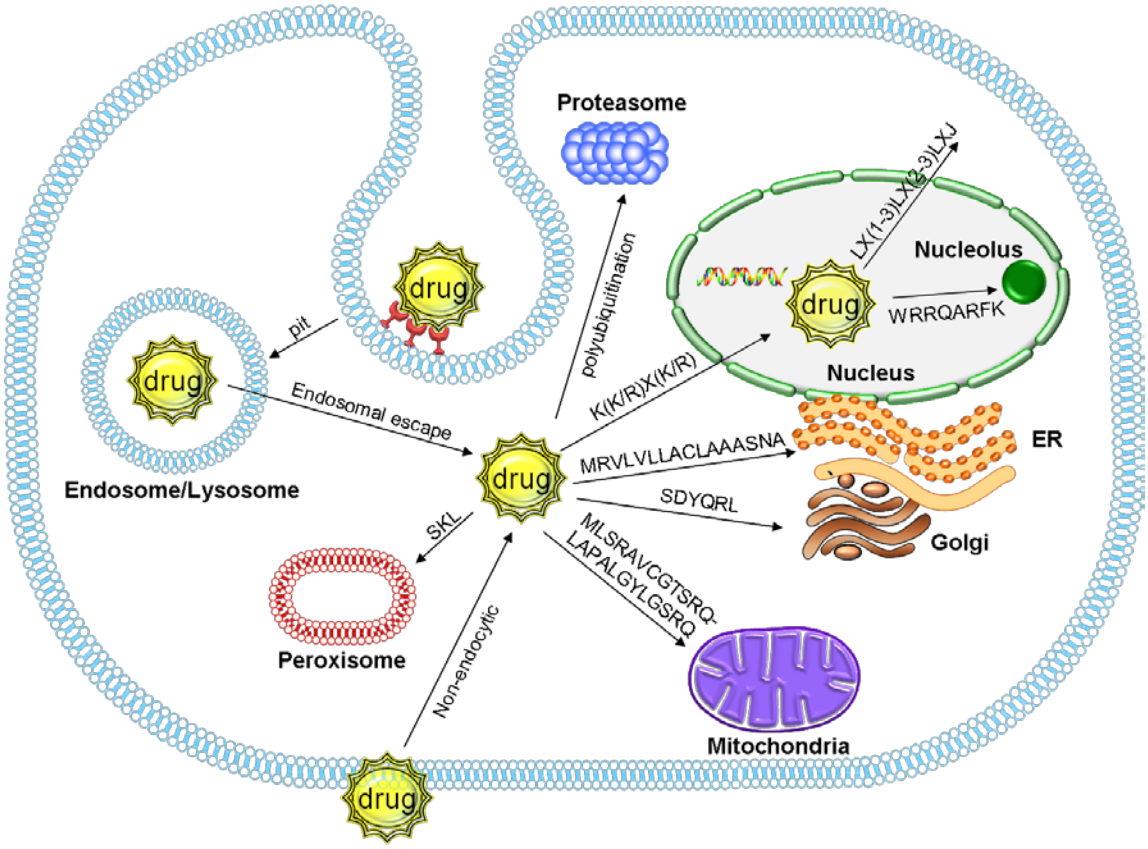

Figure 1.3. Drug targeting to cellular organelles. Text on arrows indicate consensus targeting sequence (if available), example of targeting signal, or mode of targeting. ER = endoplasmic reticulum. (Reprinted by permission from *Ther Deliv*. 2010 Jul 1;1(1):169-193.)

$LX_{2-3}LXJ$, where X is any amino acid and J is leucine, valine or isoleucine (128, 129, 131). The MycA8 NLS sequence contains 3 basic residues which are common to sequences recognized by importin-α and then transported to the nucleus by the importin-α/β heterodimer (132-134). This optimized protein switch provides a controlled method of shuttling between the cytoplasm and the nucleus. Representative images of the nucleo-cytoplasmic translocation of the protein switch are illustrated in Figure 1.4.

There are numerous examples in the literature of mislocalized proteins that result in diseases to which the protein switch would be useful (1, 134). As described in the previous section, the oncogenic Bcr-Abl is one of these proteins, and through relocalization with the protein switch, can be converted from an oncoprotein to an apoptosis inducing factor.

The Protein Switch Can Be Used to Study Protein Interactions in Live Cells

The main goal intended for the protein switch is the translocation of a disease causing protein for therapeutic intervention. However, the ability to translocate a second protein to the nucleus can be used as a measurement of the interaction between the protein switch and the second protein. This capability of the protein switch to monitor protein interactions has been termed the nuclear translocation assay, or NTA. While there are numerous methods to study protein interactions, there are relatively few assays for quantifying the interaction inside a live cell under the biological conditions wherein the interaction occurs. The NTA is a method of studying protein interactions in the native intracellular conditions. While interest in moving proteins as a therapeutic

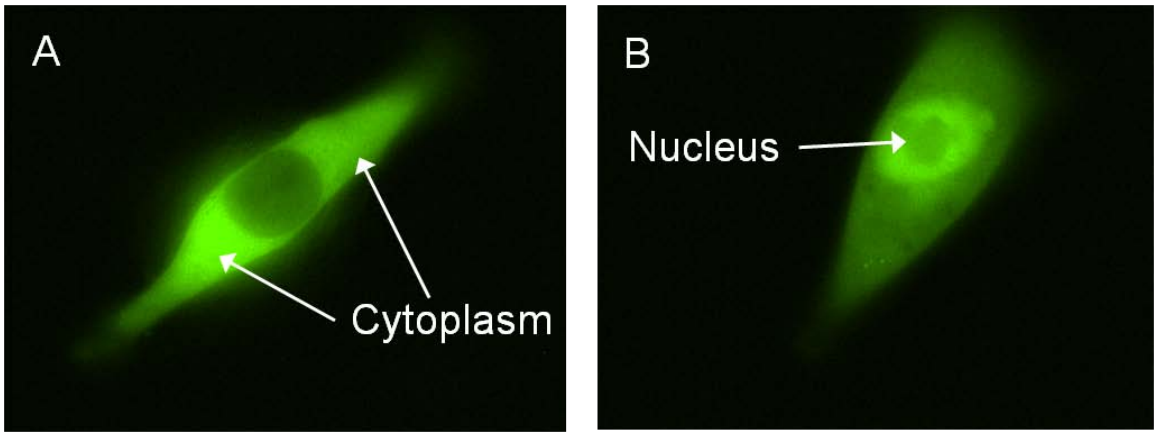

Figure 1.4. EGFP fused to the protein switch and transfected into 1471.1 murine adenocarcinoma cells. A) In the absence of ligand, the nuclear export signal (HIV NES) causes the protein switch to localize in the cytoplasm. B) The nuclear localization signal (MycA8 NLS) causes the protein switch to localize to the nucleus after the induction with ligand (dexamethasone). (Reprinted by permission from *Ther Deliv*. 2010 Jul 1;1(1):169-193.)

strategy is relatively limited, the application of the protein switch to studying protein interactions inside cells is more applicable to a broad range of scientists.

As already described, the protein switch localizes in the cytoplasm in the absence of ligand, and translocates to the nucleus upon addition of ligand (Figure 1.4) (4). A protein, or protein domain, can be fused to the protein switch through genetic engineering to grant control over the nucleo-cytoplasmic shuttling of that protein. If nuclear accumulation of a second protein that is not fused to the protein switch and is not responsive to the ligand occurs upon addition of ligand, it is due to the interaction with the protein switch construct. The translocation of both proteins is easily monitored through tagging one protein with EGFP, tagging the other with DsRed, and fluorescence microscopy. Thus, not only does the NTA allow protein interactions to be assayed inside a cell, but is relatively simple and essentially only requires a fluorescence microscope.

A Binding Domain Is Essential to the Protein Switch

As will be demonstrated in Chapter 2, it is possible to induce apoptosis by sending exogenous Bcr-Abl to the nucleus through the attachment of additional nuclear localization signals (119). This demonstrates the ability to induce apoptosis when inside the nucleus, without cytoplasmic depletion of endogenous Bcr-Abl. Further, this suggests the apoptotic signal from Bcr-Abl is greater than the proliferative signals in the cytoplasm, yet it is easy to speculate on the increased, and maybe even synergistic, effect when the removal of the cytoplasmic proliferative signal is combined with the nuclear apoptotic signal. Thus, the translocation of endogenous Bcr-Abl from the cytoplasm into the nucleus may produce an even greater apoptotic response due to removal of oncogenic

signaling through cytoplasmic depletion combined with apoptotic signaling due to the nuclear accumulation. Moreover, the delivery of exogenous Bcr-Abl to the nucleus may induce apoptosis in a wide range of cell types, not only CML cells. Altering the localization of Bcr-Abl, which is only present in the CML cells, is a way of specifically inducing apoptosis in only CML cells that express Bcr-Abl, and requires a binding domain that will efficiently bind Bcr-Abl to allow for nuclear translocation.

Binding Bcr-Abl with CCmut2 and CCmut3.

With the goal of translocating endogenous Bcr-Abl into the nucleus along with the protein switch, it is essential that the protein switch exhibits some method of binding Bcr-Abl. One method of binding Bcr-Abl is through the coiled-coil domain (76, 77), which may be incorporated into the protein switch. Nevertheless, incorporation of the wild-type coiled-coil domain into the protein switch would allow for protein switch dimerization, but would not preferentially oligomerize with Bcr-Abl over another protein switch molecule, potentially limiting the nuclear translocation of Bcr-Abl. Improving the specificity of the coiled-coil domain so as to not cause the oligomerization of the protein switch was the goal in designing CCmut2 and CCmut3. These design goals are illustrated in Figure 1.5.

Binding Bcr-Abl through the ABD and DHPH Domains with iDabs

Another method of binding Bcr-Abl is through an antibody. Antibodies specialize in high affinity and specific binding of molecules, yet typical antibodies consist of

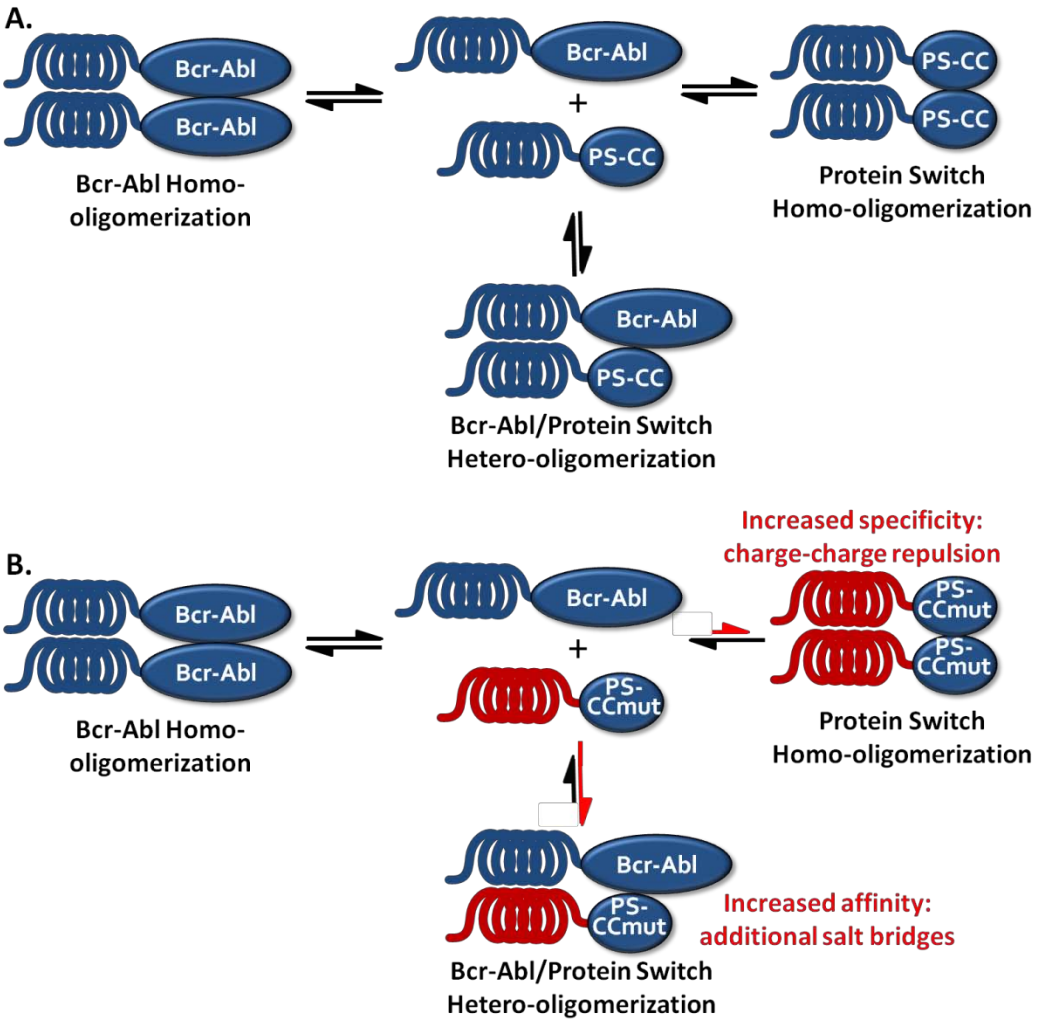

Figure 1.5. Goals for the design of a mutant coiled-coil domain. A) Depiction of the incorporation of the wild-type coiled-coil domain into the protein switch, and the resulting equal formation of protein switch homo-oligomers, Bcr-Abl homo-oligomers, and protein switch/Bcr-Abl hetero-oligomers. B) Improved equilibrium from a mutant coiled-coil domain incorporated into the protein switch. Through introduction of charge-charge repulsion the protein switch homo-oligomerization is reduced. Through formation of additional salt bridges the hetero-oligomerization is improved. Blue coil = wild-type coiled-coil domain, Red coil = mutant coiled-coil domain.

individual polypeptide chains held together through disulfide bonds (135). These disulfide bonds are stable in oxidizing conditions, but are reduced inside cells and can result in the intracellular instability of antibodies (136). This has been a major limitation in the usefulness of antibodies as therapeutics since most target antigens, including Bcr-Abl, are present inside cells. However, smaller antibody fragments have been identified that do not require disulfide bonds for their stability (135, 136). The first generation of intracellular antibodies, single chain variable fragments (scFv), contains the variable fragments from the heavy and light chains held together by a small peptide linker (137-139), and is roughly 250 amino acids (27 kDa), or one fifth the size of an IgG, and is stable inside cells. Recently it has been shown that one variable fragment can bind to an antigen with similar affinity and specificity (140, 141), further reducing the size to *one tenth* of an IgG antibody. The intracellular stability and minimal size make these single domain antibodies (iDabs) an ideal candidate for protein therapeutics. Technology termed intracellular antibody capture (IAC) (142-145) has been established to isolate intracellular antibodies that bind a desired target. The IAC protocol for isolation of single domain intracellular antibodies (iDabs) has been termed the third-generation intracellular antibody capture, or IAC^3 (146). The first report of the binding from iDabs isolated using IAC demonstrated binding to the Ras protein with affinities ranging from 20 nM to 200 nM (147). Unpublished data have also demonstrated iDabs to bind even in the picomolar range (personal communication with Dr. Terrence Rabbitts). Recently IAC^3 screening has produced iDabs binding LMO2, TP53, CRAF1, and Hoxa9 (148). Screening for single domain antibodies that bind Bcr-Abl at the actin binding domain (ABD) and Dbl homology/Pleckstrin homology (DHPH) domains are described in

Chapter 6.

Inhibition of Bcr-Abl through Oligomeric Disruption

While the original goal of studying the coiled-coil domain was to obtain an efficient binding partner for Bcr-Abl that could be used for nuclear translocation, an interesting alternative use is for the inhibition of Bcr-Abl through oligomeric disruption. Bcr-Abl is found predominantly as a tetramer, and achieves this homo-oligomerization through the coiled-coil domain at the N-terminus of the protein (77). The oligomerization through the coiled-coil domain is a critical part of the constitutive activity of the tyrosine kinase domain (149, 150). This oligomerization allows Bcr-Abl to undergo a trans-autophosphorylation wherein Bcr-Abl is activated. Bcr-Abl constructs that lack the coiled-coil domain have reduced levels of phosphorylation and reduced transformation potential (149). Interfering with the oligomeric state of Bcr-Abl prevents the activating trans-autophosphorylation and mimics the effects of a TKI. However, disruption of the oligomeric state through binding the coiled-coil domain may have the advantage of not binding the SH3, SH2, or Y-kinase domains where the point mutations have been described.

The Bcr-Abl coiled-coil domain consists of two parallel-oriented α-helices and a short linker connecting them to form an “N” (77). These helices interact with the helices from another coiled-coil domain in an anti-parallel orientation to form a dimer, which subsequently dimerizes with another dimer to form the tetramer (76). The dimer interface is composed primarily of the second helices of the coiled-coil domain, residues 28-67, while the first helices fold onto the backsides of the second helices in a swap-

domain fashion. Thus, helix two fits the typical α-helical coiled-coil model wherein residues at the "a" and "d" positions are hydrophobic and compose the hydrophobic core, and charged residues are found at the "e" and "g" positions where they can form salt bridges. The α-helix has been highly studied and characterized, greatly facilitating the rational design of modifications to an existing α-helical coiled-coil domain such as the one found in Bcr-Abl (151-155).

We aimed to improve the oligomerization between a modified coiled-coil domain and the Bcr-Abl coiled-coil domain, in attempt to reduce the homo-oligomerization of the mutant and increase the hetero-oligomerization with Bcr-Abl (the same concept illustrated in Figure 1.5 for the incorporation of the coiled-coil domain into the protein switch). The design of the coiled-coil domain focused on the helix at the dimer interface, helix two. In a simple fashion, uncharged residues in a position to form a salt bridge with a charged residue on the opposing helix were mutated to the appropriately charged residue to increase the number of salt bridges in the hetero-dimer. To decrease the homo-oligomer stability, residues were mutated to charged residues in positions in close proximity to the same-charged residue on the opposing helix in the homo-dimer. Through this simple approach the oligomerization properties were improved.

Therapeutic Potential of Nuclear Bcr-Abl

The introduction of tyrosine kinase inhibitors has revolutionized the treatment of CML and improved the prognosis and quality of life of CML patients. Nevertheless, the only cure for CML, allogenic stem cell transplantation, is not an option for the majority of patients due to age and donor availability. Moreover, resistance to TKI therapy (8-11),

the inability of TKIs to achieve a sustainable response for patients in advanced stages of the disease (156-162), and ineffectiveness of TKIs towards CML stem cells (13, 163-166) all remain major problems in CML therapy. More CML research is currently being done to generate additional TKIs that are efficacious against resistant cells and the CML stem cell niche. Yet, all indications from TKI therapy thus far indicate an inability to use this type of approach against leukemic stem cells. In addition, development of alternative TKIs that bind the kinase domain in distinct regions will create new selective pressures and may lead to resistance and identification of previously uncharacterized mutations. This work aims to induce apoptosis through translocating Bcr-Abl into the nucleus using a mutant form of the Bcr-Abl coiled-coil domain (alone or in combination with another Bcr-Abl-binding domain such as the iDab ABI7). Due to the essential role of oligomerization through the coiled-coil domain in activating Bcr-Abl, mutations affecting the oligomerization would alleviate the kinase activity driving the oncogenicity. Thus, by targeting Bcr-Abl through the coiled-coil domain, mutations leading to resistance to this type of therapy would be limited to mutations that only affect the hetero-oligomerization between Bcr-Abl and the therapeutic coiled-coil while not affecting the homo-oligomerization of Bcr-Abl. Whether or not such mutations are possible remains to be determined, but seem far less likely than mutations in the kinase domain that lead to increased transformation potential in addition to avoidance of the therapeutic interaction. Furthermore, the translocation of Bcr-Abl into the nucleus using a coiled-coil domain or iDab is not likely to be affected by any of the mutations generating TKI resistance, and is likely to be equally effective in all of the currently described mutant forms of Bcr-Abl including the T315I mutation.

In addition to the mutational advantages, sending the endogenous Bcr-Abl to the nucleus would also reduce oncogenic signaling from the cytoplasmic Bcr-Abl (167, 168). Cytoplasmic depletion of Bcr-Abl combined with the apoptotic signaling through nuclear Bcr-Abl will be a more potent therapeutic strategy. This approach is more likely to induce apoptosis in CML stem cells where inhibition of Bcr-Abl alone is not sufficient to induce apoptosis (13, 164, 166). Thus, the nuclear accumulation of at least 20-25% of Bcr-Abl (5) through the controlled translocation with the protein switch has the potential to address the two biggest problems with treatment of CML, and would be progress towards a possible cure for patients who do not have transplantation as an option.

Summary

In addition to demonstrating progress in the generation of a novel therapeutic, this work also demonstrates the ability to control the localization of an endogenous protein through an exogenously added protein. Both the oncoprotein Bcr-Abl and the disease CML are highly characterized and provide an ideal model system for validating this type of approach. The establishment that cytoplasmic Bcr-Abl is oncogenic and nuclear Bcr-Abl induces apoptosis was also critical in choosing Bcr-Abl as the target for this work. However, there are numerous other examples of proteins wherein the localization is a factor in the development of a disease (169-173), and where an alternate localization of that protein would relieve the disease causing conditions. Thus, the proof of concept demonstrated herein is not only applicable to CML, but a host of other diseases as well.

The translocation of other proteins by the protein switch can also be useful as an assay for intracellular protein-protein interactions relevant to the biochemistry field in

general. Currently, intracellular protein-protein interaction assays are limited, and alternative approaches to validate the interactions are needed. Hence, the significance of this work is the establishment of widely applicable methodology to alter the subcellular localization of an endogenous protein to alter the function, including a new biochemical assay for intracellular protein-protein interactions (nuclear translocation assay described in Chapter 3).

In summary, this dissertation is organized into the following chapters:

1. (This chapter) Background and significance. Some figures used in this chapter were taken from:

   Mossalam M, **Dixon AS**, Lim CS. *Ther Deliv.* 2010 Jul 1;1(1):169-193. "Controlling subcellular delivery to optimize therapeutic effect."

2. Demonstration that Bcr-Abl can be directed to the nucleus and that it does induce apoptosis when inside the nucleus

   Dixon AS, Kakar M, Schneider KM, Constance JE, Paullin BC, Lim CS. *J Control Release*. 2009 Dec 16;140(3):245-9. "Controlling subcellular localization to alter function: Sending oncogenic Bcr-Abl to the nucleus causes apoptosis."

3. Use of the protein switch for studying protein interactions (the nuclear translocation assay)

   Dixon AS, Lim CS. *Biotechniques*. 2010 Jul;49(1):519-24. "The nuclear translocation assay for intracellular protein-protein

interactions and its application to the Bcr coiled-coil domain."

4. Design of CCmut2 and demonstration of the inhibitory effects on Bcr-Abl and CML cells

   Dixon AS, Pendley SS, Bruno BJ, Woessner DW, Shimpi AA, Cheatham TE 3rd, Lim CS. *J Biol Chem.* 2011 Jun 9. [Epub ahead of print] "Disruption of BCR-ABL coiled-coil oligomerization by design."

5. Design of a second generation coiled-coil mutant, CCmut3, and demonstration of the inhibitory effects on Bcr-Abl and CML cells

   Dixon AS, Miller G., Bruno, BJ, Woessner DW, Constance JE, Cheatham TE, Lim CS. "Second generation modifications to the Bcr coiled-coil domain: further mutant homo-dimer destabilization for enhanced oligomerization with Bcr-Abl." In preparation for submission to *Mol. Pharmaceutics*.

6. Isolation of iDabs for binding Bcr-Abl, and use of binding domains for translocation of Bcr-Abl to the nucleus

   Dixon AS, Constance JE, Tanaka T, Rabbitts TH, Lim CS. "Rationally designed Bcr-Abl capture motifs for escort to the nucleus." In preparation for submission to *J. Control. Release*.

7. Conclusions and future work

References

1. Davis JR, Kakar M, Lim CS. Controlling protein compartmentalization to overcome disease. Pharm Res 2007; 24: 17-27.

2. Fabbro M, Henderson BR. Regulation of tumor suppressors by nuclear-cytoplasmic shuttling. Exp Cell Res 2003; 282: 59-69.

3. Aloisi A, Di Gregorio S, Stagno F, et al. BCR-ABL nuclear entrapment kills human CML cells: ex vivo study on 35 patients with the combination of imatinib mesylate and leptomycin B. Blood 2006; 107: 1591-8.

4. Kakar M, Davis JR, Kern SE, Lim CS. Optimizing the protein switch: altering nuclear import and export signals, and ligand binding domain. J Control Release 2007; 120: 220-32.

5. Vigneri P, Wang JY. Induction of apoptosis in chronic myelogenous leukemia cells through nuclear entrapment of BCR-ABL tyrosine kinase. Nat Med 2001; 7: 228-34.

6. Ren R. The molecular mechanism of chronic myelogenous leukemia and its therapeutic implications: studies in a murine model. Oncogene 2002; 21: 8629-42.

7. Ren R. Mechanisms of BCR-ABL in the pathogenesis of chronic myelogenous leukaemia. Nat Rev Cancer 2005; 5: 172-83.

8. Quintas-Cardama A, Kantarjian HM, Cortes JE. Mechanisms of primary and secondary resistance to imatinib in chronic myeloid leukemia. Cancer Control 2009; 16: 122-31.

9. Strout MP, Schatz DG. Imatinib resistance and progression of CML to blast crisis: somatic hypermutation AIDing the way. Cancer Cell 2009; 16: 174-6.

10. Deininger M. Resistance and relapse with imatinib in CML: causes and consequences. J Natl Compr Canc Netw 2008; 6 Suppl 2: S11-S21.

11. Volpe G, Panuzzo C, Ulisciani S, Cilloni D. Imatinib resistance in CML. Cancer Lett 2009; 274: 1-9.

12. Savona M, Talpaz M. Getting to the stem of chronic myeloid leukaemia. Nat Rev Cancer 2008; 8: 341-50.

13. Li S, Li D. Stem cell and kinase activity-independent pathway in resistance of leukaemia to BCR-ABL kinase inhibitors. J Cell Mol Med 2007; 11: 1251-62.

14. Graham SM, Jorgensen HG, Allan E, et al. Primitive, quiescent, Philadelphia-positive stem cells from patients with chronic myeloid leukemia are insensitive to STI571 in vitro. Blood 2002; 99: 319-25.

15. Copland M, Hamilton A, Elrick LJ, et al. Dasatinib (BMS-354825) targets an earlier progenitor population than imatinib in primary CML but does not eliminate the quiescent fraction. Blood 2006; 107: 4532-9.

16. Nowell PC, Hungerford DA. Chromosome studies on normal and leukemic human leukocytes. J Natl Cancer Inst 1960; 25: 85-109.

17. Groffen J, Stephenson JR, Heisterkamp N, de Klein A, Bartram CR, Grosveld G. Philadelphia chromosomal breakpoints are clustered within a limited region, bcr, on chromosome 22. Cell 1984; 36: 93-9.

18. Sandberg AA, Gemmill RM, Hecht BK, Hecht F. The Philadelphia chromosome: a model of cancer and molecular cytogenetics. Cancer Genet Cytogenet 1986; 21: 129-46.

19. Kurzrock R, Kantarjian HM, Druker BJ, Talpaz M. Philadelphia chromosome-positive leukemias: from basic mechanisms to molecular therapeutics. Ann Intern Med 2003; 138: 819-30.

20. Faderl S, Kantarjian HM, Thomas DA, et al. Outcome of Philadelphia chromosome-positive adult acute lymphoblastic leukemia. Leuk Lymphoma 2000; 36: 263-73.

21. Nowell PC, Hungerford DA. Chromosome studies in human leukemia. II. Chronic granulocytic leukemia. J Natl Cancer Inst 1961; 27: 1013-35.

22. Nowell PC. The minute chromosome (Phl) in chronic granulocytic leukemia. Blut 1962; 8: 65-6.

23. Rowley JD. Letter: A new consistent chromosomal abnormality in chronic myelogenous leukaemia identified by quinacrine fluorescence and Giemsa staining. Nature 1973; 243: 290-3.

24. Witte ON, Rosenberg NE, Baltimore D. A normal cell protein cross-reactive to the major Abelson murine leukaemia virus gene product. Nature 1979; 281: 396-8.

25. Konopka JB, Watanabe SM, Witte ON. An alteration of the human c-abl protein in K562 leukemia cells unmasks associated tyrosine kinase activity. Cell 1984; 37: 1035-42.

26. Ben-Neriah Y, Daley GQ, Mes-Masson AM, Witte ON, Baltimore D. The chronic myelogenous leukemia-specific P210 protein is the product of the bcr/abl hybrid gene. Science 1986; 233: 212-4.

27. Shtivelman E, Lifshitz B, Gale RP, Canaani E. Fused transcript of abl and bcr genes in chronic myelogenous leukaemia. Nature 1985; 315: 550-4.

28. Fainstein E, Marcelle C, Rosner A, et al. A new fused transcript in Philadelphia chromosome positive acute lymphocytic leukaemia. Nature 1987; 330: 386-8.

29. Clark SS, McLaughlin J, Crist WM, Champlin R, Witte ON. Unique forms of the abl tyrosine kinase distinguish Ph1-positive CML from Ph1-positive ALL. Science 1987; 235: 85-8.

30. Walker LC, Ganesan TS, Dhut S, et al. Novel chimaeric protein expressed in Philadelphia positive acute lymphoblastic leukaemia. Nature 1987; 329: 851-3.

31. Daley GQ, Van Etten RA, Baltimore D. Induction of chronic myelogenous leukemia in mice by the P210bcr/abl gene of the Philadelphia chromosome. Science 1990; 247: 824-30.

32. Vardiman JW, Harris NL, Brunning RD. The World Health Organization (WHO) classification of the myeloid neoplasms. Blood 2002; 100: 2292-302.

33. Kantarjian H, Sawyers C, Hochhaus A, et al. Hematologic and cytogenetic responses to imatinib mesylate in chronic myelogenous leukemia. N Engl J Med 2002; 346: 645-52.

34. Quintas-Cardama A, Cortes J. Molecular biology of bcr-abl1-positive chronic myeloid leukemia. Blood 2009; 113: 1619-30.

35. Cancer Facts and Figures 2011. 2011 [cited 2011 July 27, 2011]; Available from: http://www.cancer.org/acs/groups/content/@epidemiologysurveilance/documents/document/acspc-029771.pdf

36. Jabbour E, Cortes J, Santos FP, et al. Results of allogeneic hematopoietic stem cell transplantation for chronic myelogenous leukemia patients who failed tyrosine kinase inhibitors after developing BCR-ABL1 kinase domain mutations. Blood; 117: 3641-7.

37. Radich J. Stem cell transplant for chronic myeloid leukemia in the imatinib era. Semin Hematol; 47: 354-61.

38. Eck MJ, Manley PW. The interplay of structural information and functional studies in kinase drug design: insights from BCR-Abl. Curr Opin Cell Biol 2009; 21: 288-95.

39. Muller BA. Imatinib and its successors--how modern chemistry has changed drug development. Curr Pharm Des 2009; 15: 120-33.

40. Druker BJ, Lydon NB. Lessons learned from the development of an abl tyrosine kinase inhibitor for chronic myelogenous leukemia. J Clin Invest 2000; 105: 3-7.

41. Druker BJ, Guilhot F, O'Brien SG, et al. Five-year follow-up of patients receiving imatinib for chronic myeloid leukemia. N Engl J Med 2006; 355: 2408-17.

42. Hochhaus A, O'Brien SG, Guilhot F, et al. Six-year follow-up of patients receiving imatinib for the first-line treatment of chronic myeloid leukemia. Leukemia 2009; 23: 1054-61.

43. Tanaka R, Kimura S. Abl tyrosine kinase inhibitors for overriding Bcr-Abl/T315I: from the second to third generation. Expert Rev Anticancer Ther 2008; 8: 1387-98.

44. Soverini S, Martinelli G, Iacobucci I, Baccarani M. Imatinib mesylate for the treatment of chronic myeloid leukemia. Expert Rev Anticancer Ther 2008; 8: 853-64.

45. Cortes J, O'Brien S, Kantarjian H. Discontinuation of imatinib therapy after achieving a molecular response. Blood 2004; 104: 2204-5.

46. Guastafierro S, Falcone U, Celentano M, Coppola M, Ferrara MG, Sica A. Is it possible to discontinue imatinib mesylate therapy in Chronic Myeloid Leukemia patients with undetectable BCR/ABL? A case report and a review of the literature. Leuk Res 2009; 33: 1079-81.

47. Stentoft J, Pallisgaard N, Kjeldsen E, Holm MS, Nielsen JL, Hokland P. Kinetics of BCR-ABL fusion transcript levels in chronic myeloid leukemia patients treated with STI571 measured by quantitative real-time polymerase chain reaction. Eur J Haematol 2001; 67: 302-8.

48. Bhatia R, Holtz M, Niu N, et al. Persistence of malignant hematopoietic progenitors in chronic myelogenous leukemia patients in complete cytogenetic remission following imatinib mesylate treatment. Blood 2003; 101: 4701-7.

49. Lowenberg B. Minimal residual disease in chronic myeloid leukemia. N Engl J Med 2003; 349: 1399-401.

50. Corbin AS, Agarwal A, Loriaux M, Cortes J, Deininger MW, Druker BJ. Human chronic myeloid leukemia stem cells are insensitive to imatinib despite inhibition of BCR-ABL activity. J Clin Invest; 121: 396-409.

51. Hutchinson L. Human CML stem cells insensitive to imatinib even when BCR-ABL is inhibited. Nat Rev Clin Oncol; 8: 126.

52. Joske DJ. Chronic myeloid leukaemia: the evolution of gene-targeted therapy. Med J Aust 2008; 189: 277-82.

53. Gorre ME, Mohammed M, Ellwood K, et al. Clinical resistance to STI-571 cancer therapy caused by BCR-ABL gene mutation or amplification. Science 2001; 293: 876-80.

54. Shah NP, Nicoll JM, Nagar B, et al. Multiple BCR-ABL kinase domain mutations confer polyclonal resistance to the tyrosine kinase inhibitor imatinib (STI571) in chronic phase and blast crisis chronic myeloid leukemia. Cancer Cell 2002; 2: 117-25.

55. Hughes TP, Deininger MW, Hochhaus A, et al. Monitoring CML patients responding to treatment with tyrosine kinase inhibitors - Review and recommendations for 'harmonizing' current methodology for detecting BCR-ABL transcripts and kinase domain mutations and for expressing results. Blood 2006.

56. Mauro MJ. Mutational analysis and overcoming imatinib resistance in chronic myeloid leukemia with novel tyrosine kinase inhibitors. Curr Treat Options Oncol 2007; 8: 287-95.

57. Weisberg E, Manley PW, Breitenstein W, et al. Characterization of AMN107, a selective inhibitor of native and mutant Bcr-Abl. Cancer Cell 2005; 7: 129-41.

58. Kantarjian H, Giles F, Wunderle L, et al. Nilotinib in imatinib-resistant CML and Philadelphia chromosome-positive ALL. N Engl J Med 2006; 354: 2542-51.

59. Talpaz M, Shah NP, Kantarjian H, et al. Dasatinib in imatinib-resistant Philadelphia chromosome-positive leukemias. N Engl J Med 2006; 354: 2531-41.

60. Cortes J, Jabbour E, Kantarjian H, et al. Dynamics of BCR-ABL kinase domain mutations in chronic myeloid leukemia after sequential treatment with multiple tyrosine kinase inhibitors. Blood 2007; 110: 4005-11.

61. Hochhaus A, Kreil S, Corbin AS, et al. Molecular and chromosomal mechanisms of resistance to imatinib (STI571) therapy. Leukemia 2002; 16: 2190-6.

62. Jabbour E, Kantarjian H, Jones D, et al. Frequency and clinical significance of BCR-ABL mutations in patients with chronic myeloid leukemia treated with imatinib mesylate. Leukemia 2006; 20: 1767-73.

63. Eide CA, Adrian LT, Tyner JW, et al. The ABL switch control inhibitor DCC-2036 is active against the chronic myeloid leukemia mutant BCR-ABLT315I and exhibits a narrow resistance profile. Cancer Res; 71: 3189-95.

64. Thomas X. Is AP24534 (Ponatinib) the next treatment of Philadelphia chromosome-positive acute lymphoblastic leukemia? Bull Cancer.

65. Zhou T, Commodore L, Huang WS, et al. Structural mechanism of the Pan-BCR-ABL inhibitor ponatinib (AP24534): lessons for overcoming kinase inhibitor resistance. Chem Biol Drug Des; 77: 1-11.

66. Chan WW, Wise SC, Kaufman MD, et al. Conformational control inhibition of the BCR-ABL1 tyrosine kinase, including the gatekeeper T315I mutant, by the switch-control inhibitor DCC-2036. Cancer Cell; 19: 556-68.

67. Kerkela R, Grazette L, Yacobi R, et al. Cardiotoxicity of the cancer therapeutic agent imatinib mesylate. Nat Med 2006; 12: 908-16.

68. Orphanos GS, Ioannidis GN, Ardavanis AG. Cardiotoxicity induced by tyrosine kinase inhibitors. Acta Oncol 2009: 1-7.

69. Estabragh ZR, Knight K, Watmough SJ, et al. A prospective evaluation of cardiac function in patients with chronic myeloid leukaemia treated with imatinib. Leuk Res; 35: 49-51.

70. Hartmann JT, Haap M, Kopp HG, Lipp HP. Tyrosine Kinase Inhibitors - A Review on Pharmacology, Metabolism and Side Effects. Curr Drug Metab 2009.

71. Lugo TG, Pendergast AM, Muller AJ, Witte ON. Tyrosine kinase activity and transformation potency of bcr-abl oncogene products. Science 1990; 247: 1079-82.

72. Hazlehurst LA, Bewry NN, Nair RR, Pinilla-Ibarz J. Signaling networks associated with BCR-ABL-dependent transformation. Cancer Control 2009; 16: 100-7.

73. Van Etten RA. Mechanisms of transformation by the BCR-ABL oncogene: new perspectives in the post-imatinib era. Leuk Res 2004; 28 Suppl 1: S21-8.

74. Sattler M, Griffin JD. Molecular mechanisms of transformation by the BCR-ABL oncogene. Semin Hematol 2003; 40: 4-10.

75. Sattler M, Griffin JD. Mechanisms of transformation by the BCR/ABL oncogene. Int J Hematol 2001; 73: 278-91.

76. Taylor CM, Keating AE. Orientation and oligomerization specificity of the Bcr coiled-coil oligomerization domain. Biochemistry 2005; 44: 16246-56.

77. Zhao X, Ghaffari S, Lodish H, Malashkevich VN, Kim PS. Structure of the Bcr-Abl oncoprotein oligomerization domain. Nat Struct Biol 2002; 9: 117-20.

78. Zhang X, Subrahmanyam R, Wong R, Gross AW, Ren R. The NH(2)-terminal coiled-coil domain and tyrosine 177 play important roles in induction of a myeloproliferative disease in mice by Bcr-Abl. Mol Cell Biol 2001; 21: 840-53.

79. Pendergast AM, Quilliam LA, Cripe LD, et al. BCR-ABL-induced oncogenesis is mediated by direct interaction with the SH2 domain of the GRB-2 adaptor protein. Cell 1993; 75: 175-85.

80. Puil L, Liu J, Gish G, et al. Bcr-Abl oncoproteins bind directly to activators of the Ras signalling pathway. Embo J 1994; 13: 764-73.

81. Sattler M, Mohi MG, Pride YB, et al. Critical role for Gab2 in transformation by BCR/ABL. Cancer Cell 2002; 1: 479-92.

82. Million RP, Van Etten RA. The Grb2 binding site is required for the induction of chronic myeloid leukemia-like disease in mice by the Bcr/Abl tyrosine kinase. Blood 2000; 96: 664-70.

83. Kin Y, Li G, Shibuya M, Maru Y. The Dbl homology domain of BCR is not a simple spacer in P210BCR-ABL of the Philadelphia chromosome. J Biol Chem 2001; 276: 39462-8.

84. He Y, Wertheim JA, Xu L, et al. The coiled-coil domain and Tyr177 of bcr are required to induce a murine chronic myelogenous leukemia-like disease by bcr/abl. Blood 2002; 99: 2957-68.

85. Thomas EK, Cancelas JA, Zheng Y, Williams DA. Rac GTPases as key regulators of p210-BCR-ABL-dependent leukemogenesis. Leukemia 2008; 22: 898-904.

86. Skorski T, Kanakaraj P, Nieborowska-Skorska M, et al. Phosphatidylinositol-3 kinase activity is regulated by BCR/ABL and is required for the growth of Philadelphia chromosome-positive cells. Blood 1995; 86: 726-36.

87. Li S. Src-family kinases in the development and therapy of Philadelphia chromosome-positive chronic myeloid leukemia and acute lymphoblastic leukemia. Leuk Lymphoma 2008; 49: 19-26.

88. Warmuth M, Bergmann M, Priess A, Hauslmann K, Emmerich B, Hallek M. The Src family kinase Hck interacts with Bcr-Abl by a kinase-independent mechanism and phosphorylates the Grb2-binding site of Bcr. J Biol Chem 1997; 272: 33260-70.

89. Danhauser-Riedl S, Warmuth M, Druker BJ, Emmerich B, Hallek M. Activation of Src kinases p53/56lyn and p59hck by p210bcr/abl in myeloid cells. Cancer Res 1996; 56: 3589-96.

90. Ilaria RL, Jr., Van Etten RA. P210 and P190(BCR/ABL) induce the tyrosine phosphorylation and DNA binding activity of multiple specific STAT family members. J Biol Chem 1996; 271: 31704-10.

91. Chai SK, Nichols GL, Rothman P. Constitutive activation of JAKs and STATs in BCR-Abl-expressing cell lines and peripheral blood cells derived from leukemic patients. J Immunol 1997; 159: 4720-8.

92. Hamilton A, Elrick L, Myssina S, et al. BCR-ABL activity and its response to drugs can be determined in CD34+ CML stem cells by CrkL phosphorylation status using flow cytometry. Leukemia 2006; 20: 1035-9.

93. Hochhaus A, Kreil S, Corbin A, et al. Roots of clinical resistance to STI-571 cancer therapy. Science 2001; 293: 2163.

94. Bonati A, Carlo-Stella C, Lunghi P, et al. Selective expression and constitutive phosphorylation of SHC proteins [corrected] in the CD34+ fraction of chronic myelogenous leukemias. Cancer Res 2000; 60: 728-32.

95. Schaller MD, Schaefer EM. Multiple stimuli induce tyrosine phosphorylation of the Crk-binding sites of paxillin. Biochem J 2001; 360: 57-66.

96. Zhang X, Wong R, Hao SX, Pear WS, Ren R. The SH2 domain of bcr-Abl is not required to induce a murine myeloproliferative disease; however, SH2 signaling influences disease latency and phenotype. Blood 2001; 97: 277-87.

97. Smith KM, Yacobi R, Van Etten RA. Autoinhibition of Bcr-Abl through its SH3 domain. Mol Cell 2003; 12: 27-37.

98. Pendergast AM, Muller AJ, Havlik MH, Maru Y, Witte ON. BCR sequences essential for transformation by the BCR-ABL oncogene bind to the ABL SH2 regulatory domain in a non-phosphotyrosine-dependent manner. Cell 1991; 66: 161-71.

99. Taagepera S, McDonald D, Loeb JE, et al. Nuclear-cytoplasmic shuttling of C-ABL tyrosine kinase. Proc Natl Acad Sci U S A 1998; 95: 7457-62.

100. Wetzler M, Talpaz M, Van Etten RA, Hirsh-Ginsberg C, Beran M, Kurzrock R. Subcellular localization of Bcr, Abl, and Bcr-Abl proteins in normal and leukemic cells and correlation of expression with myeloid differentiation. J Clin Invest 1993; 92: 1925-39.

101. Dhut S, Chaplin T, Young BD. BCR-ABL and BCR proteins: biochemical characterization and localization. Leukemia 1990; 4: 745-50.

102. Wang JY. Regulation of cell death by the Abl tyrosine kinase. Oncogene 2000; 19: 5643-50.

103. David-Cordonnier MH, Hamdane M, Bailly C, D'Halluin JC. The DNA binding domain of the human c-Abl tyrosine kinase preferentially binds to DNA sequences

containing an AAC motif and to distorted DNA structures. Biochemistry 1998; 37: 6065-76.

104. Miao YJ, Wang JY. Binding of A/T-rich DNA by three high mobility group-like domains in c-Abl tyrosine kinase. J Biol Chem 1996; 271: 22823-30.

105. Welch PJ, Wang JY. Abrogation of retinoblastoma protein function by c-Abl through tyrosine kinase-dependent and -independent mechanisms. Mol Cell Biol 1995; 15: 5542-51.

106. Welch PJ, Wang JY. A C-terminal protein-binding domain in the retinoblastoma protein regulates nuclear c-Abl tyrosine kinase in the cell cycle. Cell 1993; 75: 779-90.

107. Gong JG, Costanzo A, Yang HQ, et al. The tyrosine kinase c-Abl regulates p73 in apoptotic response to cisplatin-induced DNA damage. Nature 1999; 399: 806-9.

108. Agami R, Blandino G, Oren M, Shaul Y. Interaction of c-Abl and p73alpha and their collaboration to induce apoptosis. Nature 1999; 399: 809-13.

109. Yuan ZM, Shioya H, Ishiko T, et al. p73 is regulated by tyrosine kinase c-Abl in the apoptotic response to DNA damage. Nature 1999; 399: 814-7.

110. Baskaran R, Dahmus ME, Wang JY. Tyrosine phosphorylation of mammalian RNA polymerase II carboxyl-terminal domain. Proc Natl Acad Sci U S A 1993; 90: 11167-71.

111. Baskaran R, Chiang GG, Mysliwiec T, Kruh GD, Wang JY. Tyrosine phosphorylation of RNA polymerase II carboxyl-terminal domain by the Abl-related gene product. J Biol Chem 1997; 272: 18905-9.

112. Duyster J, Baskaran R, Wang JY. Src homology 2 domain as a specificity determinant in the c-Abl-mediated tyrosine phosphorylation of the RNA polymerase II carboxyl-terminal repeated domain. Proc Natl Acad Sci U S A 1995; 92: 1555-9.

113. Baskaran R, Escobar SR, Wang JY. Nuclear c-Abl is a COOH-terminal repeated domain (CTD)-tyrosine (CTD)-tyrosine kinase-specific for the mammalian RNA polymerase II: possible role in transcription elongation. Cell Growth Differ 1999; 10: 387-96.

114. Baskaran R, Chiang GG, Wang JY. Identification of a binding site in c-Ab1 tyrosine kinase for the C-terminal repeated domain of RNA polymerase II. Mol Cell Biol 1996; 16: 3361-9.

115. Yuan ZM, Utsugisawa T, Huang Y, et al. Inhibition of phosphatidylinositol 3-kinase by c-Abl in the genotoxic stress response. J Biol Chem 1997; 272: 23485-8.

116. Liu ZG, Baskaran R, Lea-Chou ET, et al. Three distinct signalling responses by murine fibroblasts to genotoxic stress. Nature 1996; 384: 273-6.

117. Dan S, Naito M, Seimiya H, Kizaki A, Mashima T, Tsuruo T. Activation of c-Abl tyrosine kinase requires caspase activation and is not involved in JNK/SAPK activation during apoptosis of human monocytic leukemia U937 cells. Oncogene 1999; 18: 1277-83.

118. Takao N, Mori R, Kato H, Shinohara A, Yamamoto K. c-Abl tyrosine kinase is not essential for ataxia telangiectasia mutated functions in chromosomal maintenance. J Biol Chem 2000; 275: 725-8.

119. Dixon AS, Kakar M, Schneider KM, Constance JE, Paullin BC, Lim CS. Controlling subcellular localization to alter function: Sending oncogenic Bcr-Abl to the nucleus causes apoptosis. J Control Release 2009.

120. Heemels MT. Medicine Nobel goes to pioneer of protein guidance mechanisms. Nature 1999; 401: 625.

121. Kakar M, Cadwallader AB, Davis JR, Lim CS. Signal sequences for targeting of gene therapy products to subcellular compartments: the role of CRM1 in nucleocytoplasmic shuttling of the protein switch. Pharm Res 2007; 24: 2146-55.

122. Tang Y, Schmitt-Ott K, Qian K, Kagiyama S, Phillips MI. Vigilant vectors: adeno-associated virus with a biosensor to switch on amplified therapeutic genes in specific tissues in life-threatening diseases. Methods 2002; 28: 259-66.

123. Xu L, Zerby D, Huang Y, et al. A versatile framework for the design of ligand-dependent, transgene-specific transcription factors. Mol Ther 2001; 3: 262-73.

124. Burcin MM, Schiedner G, Kochanek S, Tsai SY, O'Malley BW. Adenovirus-mediated regulable target gene expression in vivo. Proc Natl Acad Sci U S A 1999; 96: 355-60.

125. Abruzzese RV, Godin D, Mehta V, et al. Ligand-dependent regulation of vascular endothelial growth factor and erythropoietin expression by a plasmid-based autoinducible GeneSwitch system. Mol Ther 2000; 2: 276-87.

126. Wang XJ, Liefer KM, Tsai S, O'Malley BW, Roop DR. Development of gene-switch transgenic mice that inducibly express transforming growth factor beta1 in the epidermis. Proc Natl Acad Sci U S A 1999; 96: 8483-8.

127. Beerli RR, Schopfer U, Dreier B, Barbas CF, 3rd. Chemically regulated zinc finger transcription factors. J Biol Chem 2000; 275: 32617-27.

128. Kanwal C, Mu S, Kern SE, Lim CS. Bidirectional on/off switch for controlled targeting of proteins to subcellular compartments. J Control Release 2004; 98: 379-93.

129. Kanwal C, Li H, Lim CS. Model system to study classical nuclear export signals. AAPS PharmSci 2002; 4.

130. Htun H, Barsony J, Renyi I, Gould DL, Hager GL. Visualization of glucocorticoid receptor translocation and intranuclear organization in living cells with a green fluorescent protein chimera. Proc Natl Acad Sci U S A 1996; 93: 4845-50.

131. Bogerd HP, Fridell RA, Benson RE, Hua J, Cullen BR. Protein sequence requirements for function of the human T-cell leukemia virus type 1 Rex nuclear export signal delineated by a novel in vivo randomization-selection assay. Mol Cell Biol 1996; 16: 4207-14.

132. Gorlich D, Kutay U. Transport between the cell nucleus and the cytoplasm. Annu Rev Cell Dev Biol 1999; 15: 607-60.

133. Chan CK, Jans DA. Using nuclear targeting signals to enhance non-viral gene transfer. Immunol Cell Biol 2002; 80: 119-30.

134. Turner JG, Sullivan DM. CRM1-mediated nuclear export of proteins and drug resistance in cancer. Curr Med Chem 2008; 15: 2648-55.

135. Lobato MN, Rabbitts TH. Intracellular antibodies and challenges facing their use as therapeutic agents. Trends Mol Med 2003; 9: 390-6.

136. Tanaka T, Rabbitts TH. Functional intracellular antibody fragments do not require invariant intra-domain disulfide bonds. J Mol Biol 2008; 376: 749-57.

137. Weisser NE, Hall JC. Applications of single-chain variable fragment antibodies in therapeutics and diagnostics. Biotechnol Adv 2009; 27: 502-20.

138. Mallano A, Zamboni S, Carpinelli G, et al. Generation and characterization of a human single-chain fragment variable (scFv) antibody against cytosine deaminase from Yeast. BMC Biotechnol 2008; 8: 68.

139. Lo AS, Zhu Q, Marasco WA. Intracellular antibodies (intrabodies) and their therapeutic potential. Handb Exp Pharmacol 2008: 343-73.

140. Serruys B, Van Houtte F, Verbrugghe P, Leroux-Roels G, Vanlandschoot P. Llama-derived single-domain intrabodies inhibit secretion of hepatitis B virions in mice. Hepatology 2009; 49: 39-49.

141. Tanaka T, Williams RL, Rabbitts TH. Tumour prevention by a single antibody domain targeting the interaction of signal transduction proteins with RAS. EMBO J 2007; 26: 3250-9.

142. Tanaka TR, TH. Intracellular Antibody Capture Protocol. Nat Methods 2009; *In press*.

143. Visintin M, Quondam M, Cattaneo A. The intracellular antibody capture technology: towards the high-throughput selection of functional intracellular antibodies for target validation. Methods 2004; 34: 200-14.

144. Tse E, Lobato MN, Forster A, Tanaka T, Chung GT, Rabbitts TH. Intracellular antibody capture technology: application to selection of intracellular antibodies recognising the BCR-ABL oncogenic protein. J Mol Biol 2002; 317: 85-94.

145. Visintin M, Settanni G, Maritan A, Graziosi S, Marks JD, Cattaneo A. The intracellular antibody capture technology (IACT): towards a consensus sequence for intracellular antibodies. J Mol Biol 2002; 317: 73-83.

146. Tanaka T, Rabbitts TH. Protocol for the selection of single-domain antibody fragments by third generation intracellular antibody capture. Nat Protoc; 5: 67-92.

147. Tanaka T, Lobato MN, Rabbitts TH. Single domain intracellular antibodies: a minimal fragment for direct in vivo selection of antigen-specific intrabodies. J Mol Biol 2003; 331: 1109-20.

148. Tanaka T, Sewell H, Waters S, Phillips SE, Rabbitts TH. Single domain intracellular antibodies from diverse libraries: emphasizing dual functions of LMO2 protein interactions using a single VH domain. J Biol Chem; 286: 3707-16.

149. McWhirter JR, Galasso DL, Wang JY. A coiled-coil oligomerization domain of Bcr is essential for the transforming function of Bcr-Abl oncoproteins. Mol Cell Biol 1993; 13: 7587-95.

150. Maru Y, Afar DE, Witte ON, Shibuya M. The dimerization property of glutathione S-transferase partially reactivates Bcr-Abl lacking the oligomerization domain. J Biol Chem 1996; 271: 15353-7.

151. Kammerer RA, Jaravine VA, Frank S, et al. An intrahelical salt bridge within the trigger site stabilizes the GCN4 leucine zipper. J Biol Chem 2001; 276: 13685-8.

152. Spek EJ, Bui AH, Lu M, Kallenbach NR. Surface salt bridges stabilize the GCN4 leucine zipper. Protein Sci 1998; 7: 2431-7.

153. Marqusee S, Baldwin RL. Helix stabilization by Glu-...Lys+ salt bridges in short peptides of de novo design. Proc Natl Acad Sci U S A 1987; 84: 8898-902.

154. Ryan SJ, Kennan AJ. Variable stability heterodimeric coiled-coils from manipulation of electrostatic interface residue chain length. J Am Chem Soc 2007; 129: 10255-60.

155. Gurnon DG, Whitaker JA, Oakley MG. Design and characterization of a homodimeric antiparallel coiled coil. J Am Chem Soc 2003; 125: 7518-9.

156. Garg RJ, Kantarjian H, O'Brien S, et al. The use of nilotinib or dasatinib after failure to two prior tyrosine kinase inhibitors (TKI): long-term follow-up. Blood 2009.

157. Fava C, Kantarjian HM, Jabbour E, et al. Failure to achieve a complete hematologic response at the time of a major cytogenetic response with second-generation tyrosine kinase inhibitors is associated with a poor prognosis among patients with chronic myeloid leukemia in accelerated or blast phase. Blood 2009; 113: 5058-63.

158. Martin MG, Dipersio JF, Uy GL. Management of the advanced phases of chronic myelogenous leukemia in the era of tyrosine kinase inhibitors. Leuk Lymphoma 2009; 50: 14-23.

159. Giles FJ, DeAngelo DJ, Baccarani M, et al. Optimizing outcomes for patients with advanced disease in chronic myelogenous leukemia. Semin Oncol 2008; 35: S1-17; quiz S8-20.

160. Shah NP. Advanced CML: therapeutic options for patients in accelerated and blast phases. J Natl Compr Canc Netw 2008; 6 Suppl 2: S31-S6.

161. Radich JP. The Biology of CML blast crisis. Hematology Am Soc Hematol Educ Program 2007: 384-91.

162. Calabretta B, Perrotti D. The biology of CML blast crisis. Blood 2004; 103: 4010-22.

163. Valent P, Deininger M. Clinical perspectives of concepts on neoplastic stem cells and stem cell-resistance in chronic myeloid leukemia. Leuk Lymphoma 2008; 49: 604-9.

164. Jiang X, Zhao Y, Smith C, et al. Chronic myeloid leukemia stem cells possess multiple unique features of resistance to BCR-ABL targeted therapies. Leukemia 2007; 21: 926-35.

165. Jiang X, Smith C, Eaves A, Eaves C. The challenges of targeting chronic myeloid leukemia stem cells. Clin Lymphoma Myeloma 2007; 7 Suppl 2: S71-80.

166. Valent P. Emerging stem cell concepts for imatinib-resistant chronic myeloid leukaemia: implications for the biology, management, and therapy of the disease. Br J Haematol 2008; 142: 361-78.

167. Koldehoff M, Elmaagacli AH. Therapeutic targeting of gene expression by siRNAs directed against BCR-ABL transcripts in a patient with imatinib-resistant chronic myeloid leukemia. Methods Mol Biol 2009; 487: 451-66.

168. Koldehoff M, Steckel NK, Beelen DW, Elmaagacli AH. Therapeutic application of small interfering RNA directed against bcr-abl transcripts to a patient with imatinib-resistant chronic myeloid leukaemia. Clin Exp Med 2007; 7: 47-55.

169. Moll UM, Riou G, Levine AJ. Two distinct mechanisms alter p53 in breast cancer: mutation and nuclear exclusion. Proc Natl Acad Sci U S A 1992; 89: 7262-6.

170. Takenaka Y, Fukumori T, Yoshii T, et al. Nuclear export of phosphorylated galectin-3 regulates its antiapoptotic activity in response to chemotherapeutic drugs. Mol Cell Biol 2004; 24: 4395-406.

171. Kau TR, Way JC, Silver PA. Nuclear transport and cancer: from mechanism to intervention. Nat Rev Cancer 2004; 4: 106-17.

172. Henkel T, Zabel U, van Zee K, Muller JM, Fanning E, Baeuerle PA. Intramolecular masking of the nuclear location signal and dimerization domain in the precursor for the p50 NF-kappa B subunit. Cell 1992; 68: 1121-33.

173. Karpa KD, Lin R, Kabbani N, Levenson R. The dopamine D3 receptor interacts with itself and the truncated D3 splice variant d3nf: D3-D3nf interaction causes mislocalization of D3 receptors. Mol Pharmacol 2000; 58: 677-83.

CHAPTER 2

CONTROLLING SUBCELLULAR LOCALIZATION TO ALTER FUNCTION: SENDING ONCOGENIC BCR-ABL TO THE NUCLEUS CAUSES APOPTOSIS

Abstract

Altering the subcellular localization of signal transducing proteins is a novel approach for therapeutic intervention. Mislocalization of tumor suppressors, oncogenes, or factors involved in apoptosis results in aberrant functioning of these proteins, leading to disease. In the case of chronic myelogenous leukemia (CML), cytoplasmic Bcr–Abl causes oncogenesis/proliferation. On the other hand, nuclear entrapment of endogenous Bcr–Abl (in K562 human leukemia cells) causes apoptosis. The goal of this study was to determine whether ectopically expressed Bcr–Abl could cause apoptosis of K562 cells when specifically directed to the nucleus via strong nuclear localization signals (NLSs). A single NLS from SV40 large T-antigen or four NLSs were subcloned to Bcr–Abl (1NLS–Bcr–Abl or 4NLS–Bcr–Abl). When transfected into K562 cells, only 4NLS–Bcr–Abl translocated to the nucleus. Bcr–Abl alone was found to localize in the cell cytoplasm, colocalizing with actin due to its actin binding domain. 1NLS–Bcr–Abl also

Reprinted by permission from *J Control Release*. 2009 140(3) 245-9

localized with actin. Apoptosis induced by 4NLS–Bcr–Abl was evaluated 24 h post-transfection by morphologic determination, DNA staining, and caspase-3 assay. This is the first demonstration that altering the location of ectopically expressed Bcr–Abl can kill leukemia cells. Multiple NLSs are required to overcome Bcr–Abl binding to actin, thus driving it into the nucleus and causing apoptosis.

Introduction

The causative agent for 95% of all CML cases, Bcr–Abl, is derived from the fusion of the breakpoint cluster region (Bcr) gene on chromosome 22 and the Abelson leukemia oncogene (Abl) on chromosome 9. This reciprocal translocation results in an abnormal, shortened chromosome — 'Philadelphia chromosome" or Ph (+) phenotype (1, 2). The resulting Bcr–Abl fusion protein acts as an oncoprotein, and the constitutive activation of tyrosine kinase activity of Abl leads to cell proliferation. Although Gleevec is currently the "gold standard" drug of choice for Bcr–Abl positive CML (3-5), resistance to treatment with Gleevec occurs. This is mostly due to mutations in the Bcr-Abl kinase domain that render it unable to bind to Gleevec (6-8). Some mutations create a more potent Bcr–Abl oncogene and accelerate disease progression (9). Other mechanisms for resistance include Bcr–Abl amplification or over expression, clonal evolution, a decrease in Gleevec bioavailability or cell exposure, and up regulation of drug efflux pumps (6, 10). Many other tyrosine kinase inhibitors (TKIs) are being studied and developed, with a few already approved. Nonetheless, Bcr–Abl also has the potential to develop resistance to these molecules. In addition, since FDA approval, potentially fatal side effects of Gleevec have been uncovered. These include cardiotoxicity (11), the

possibility of developing other cancers (due to blockade of tumor suppressor p63) (12), and acute renal failure (13). Therefore, finding alternative strategies to Gleevec therapy are necessary.

In the cytoplasm Bcr–Abl acts as an oncogene by interacting with multiple signal transduction pathways that transmit anti-apoptotic and mitogenic signals (14). The key pathways involve ras, MAP kinases, the STAT family, PI3 kinase, and myc, among others (15). In the nucleus, Bcr–Abl may cause apoptosis due to nuclear Abl's ability to stabilize p73 and activate its pro-apoptotic functions. Vigneri and Wang have previously shown that nuclear entrapment of Bcr–Abl in K562 cells results in apoptosis, and requires an active tyrosine kinase domain to do so (2). They used Gleevec to stimulate Bcr–Abl to go to the nucleus (by unknown mechanism), followed by nuclear entrapment by leptomycin B (LMB), a general inhibitor of nuclear export. After washout of Gleevec, Bcr-Abl tyrosine kinase activity is reactivated, and the cells undergo spontaneous apoptosis. Unfortunately LMB causes neuronal toxicity and cannot be used therapeutically. This study attempts to address a fundamental question that remains: Does the apoptosis caused by nuclear entrapment of Bcr–Abl require depletion of Bcr–Abl from the cytoplasm, or is it sufficient to send ectopically expressed Bcr–Abl to the nucleus to cause apoptosis?

Materials and Methods

Subcloning and Construction of Plasmids

Full length Bcr–Abl was removed from pEYK3.1 retroviral vector (a kind gift from Dr. George Daley, Harvard Medical School, Boston) using EcoRI and cloned into

pEGFP-C1 (Clontech, Mountain View, CA) at the EcoRI site to make EGFP–Bcr–Abl. The oligonucleotides 5′-CCGGAAGCCCAAAGAAGAAGAGAAAAGTAGAAT-3′ and 5′-CCGGATTCTACTTTTCTCTTCTTCTTTGGGCTT-3′ were ligated to pEGFP-Bcr-Abl at the BspEI site. The oligonucleotide insert encodes for the nuclear localization signal (NLS) from SV40 large T antigen (amino acids PKKKRKV) and is flanked with the BspEI digested sequence. The ligation resulted in the formation of pEGFP-1NLS–Bcr–Abl and pEGFP–4NLS–Bcr–Abl (a concatemer consisting of four nuclear localization signals). The bases encoding key residues (T65A and Y66A) in the EGFP chromophore (16, 17) of pEGFP–4NLS–Bcr–Abl were mutated using the QuikChange II Site-Directed Mutagenesis Kit from Stratagene (La Jolla, CA) to eliminate EGFP fluorescence (for use in some co-transfection experiments). The primers used for the mutagenesis were 5′-CTCGTGACCACCCTGGCCGCCGGCGTGCAGTGCTTC- 3′ and its reverse complement. This plasmid encodes 4NLS–Bcr–Abl with non-fluorescent EGFP.

Cell Line and Culture Conditions

Bcr-Abl positive K562 cells (human chronic myelogenous leukemia cell line), from our collaborator Dr. K. Elenitoba-Johnson (Univ. of Michigan), were cultured as suspension cells in RPMI 1640 supplemented with 10% FBS (Hyclone Laboratories, Logan, UT), 1% penicillin– streptomycin (100U/ml, GIBCO BRL, Grand Island, NY), 0.1% gentamycin (Hyclone), and 1% L-glutamine (Hyclone). Cells were maintained in a 5% CO2 incubator at 37 °C. Cells were split at a density of 0.5×105/ml 2 days before transfection.

Transfection

Transient transfections were performed using Amaxa Nucleofector II according to the Amaxa protocol for K562 cells. Briefly, 2×10^6 cells were pelleted from a cell density of $1–5\times10^5$ cells/mL, and then resuspended in 100 μL Amaxa Solution V. This solution was then added to 10 μg DNA and transfected in an Amaxa cuvette using program T-013. Following, 500 μL RPMI was added to the cuvette and cells were transferred to 15 mL RPMI and plated in a 75 cm^2 flask for caspase-3 assays. Small aliquots (200 μL) of cells were plated into 4-well live-cell chambers for fluorescent microscopy (Lab-tek chamber slide system, 2 mL, Nalge NUNC International, Naperville, IL) for determination of transfection efficiency. For co-localization experiments where 2 plasmids were transfected simultaneously, 5 μg of each plasmid was used; 5 μg of a single plasmid was used for comparison studies. Cells were incubated for ~20–24 h before any other assays were performed. To calculate the transfection efficiency, four or more fields of cells were counted under the 40× objective. The number of transfected cells (as indicated by the EGFP expression; see methods below for microscope settings) was divided by the total number of cells to obtain transfection efficiency.

Caspase-3 Activity Assay

The induction of apoptosis was monitored through the enzymatic activity of caspase-3 using the EnzChek Caspase-3 Assay Kit #1 (Molecular Probes, Eugene, OR) following the manufacturer's protocol. Briefly, 1.5×10^6 cells were pelleted and resuspended in 50 μL1×cell lysis buffer followed by a freeze-thaw cycle. The lysed cells were centrifuged for 5 min at 2100×g. As a control, 1μL of 1 mM caspase-3 inhibitor was

added to one of the lysates of untransfected K562 cells. 2× substrate (50μL) solution was then added to 50 μL of lysate and incubated at room temperature for 30min. A standard curve was made using known amounts of 7-amino-4-methylcoumarin (AMC). Fluorescence was then measured at an excitation wavelength of 355 nm and an emission wavelength of 460 nm. Caspase assays were performed three or more separate times (n=3). Data was represented as relative fluorescence units per cell, taking transfection efficiencies into account.

Actin Staining and Microscopy

K562 cells transfected with EGFP–Bcr–Abl were fixed with formaldehyde and stained for actin using BODIPY 558/568 Phalloidin from Molecular Probes (Eugene, OR) according to manufacturer's protocol. Briefly, cells were washed with PBS, pelleted, and resuspended in 4% formaldehyde (in PBS). Cells were incubated in formaldehyde solution for 10 min at room temperature and subsequently washed in PBS. Cells were then placed in 1 mL of 0.1% TritonX-100 (in PBS) for 5 min followed again by washing with PBS. The cells were then incubated with staining solution for 20 min at room temperature and then washed with PBS. Following staining the cells were viewed at 40× with an Olympus IX701F inverted fluorescence microscope (Scientific Instrument Company, Aurora, CO) using the HQ:TRITC filter to detect actin, and a high quantity narrow band GFP filter (excitation HQ480/20 nm, emission HQ510/20 nm, with beam splitter Q4951p) to detect EGFP. Cells were photographed using a F-View Monochrome CCD camera.

DNA Staining and EGFP Microscopy

K562 cell nuclei were stained by the addition of 0.8 μL Hoechst 33342 (10 mg/ml) (Invitrogen, Carlsbad, CA) to 1 mL of cells in a Lab-Tek®II 4-well live-cell chamber (Nalge NUNC) and incubated for 30 min at 37°C. Pictures were taken approximately 24h after transfection using a fluorescence microscope with high-quantity narrow band GFP filter (to detect EGFP) and Cyan GFP v2 filter (excitation D436/20 nm, emission D480/40 nm, with beam splitter 455dclp) to detect H33342. To minimize photobleaching of EGFP chromophore, cells were imaged using neutral density filters in combination with short exposure times. An air stream incubator (Nevtek ASI 400, Burnsville, VA) with a variable temperature control was used to maintain the microscope stage and the live-cell chambers at 37 °C. All filters were purchased from Chroma Technology (Brattleboro, VT).

Cell Tracing

Quantitation of Bcr–Abl in the nucleus and cytoplasm was carried out by measuring the fluorescence intensity of EGFP, tagged to the Bcr–Abl, as previously described (18). All the images were analyzed using analySIS® software (Soft Imaging System, Lakewood, CO).

Statistical Analysis

All experiments were done at least in triplicate ($n \geq 3$). The difference between the percent nuclear intensity values was analyzed using an unpaired t-test with Welch's correction. Oneway ANOVA with Tukey's multiple comparisons post-test was used to

assess the differences between relative fluorescence intensity values from the caspase-3 assay. All statistics were calculated using GraphPad Prism (San Diego, CA).

Results

When transfected into K562 cells, Bcr–Abl (pEGFP-Bcr-Abl) localizes in the cytoplasm and forms a distinctive ring around the cell (Figure 2.1). This localization is indicative of binding to actin, and is expected due to previous reports of Bcr–Abl localization with actin (19). Co-localization of EGFP–Bcr–Abl and actin is shown in Figure 2.1.

Additional nuclear localization signal(s) were added to EGFP-Bcr-Abl to attempt to overcome Bcr–Abl binding to actin. Two plasmids were created, one with 1 NLS subcloned to EGFP–Bcr–Abl, and one with 4 NLSs subcloned to EGFP–Bcr–Abl. When transfected into K562 cells, only EGFP–4NLS–Bcr–Abl localized to the nucleus (Figure 2.2G) with the distinct absence of the actin ring surrounding the cell (compared to 2.2A, wt–Bcr–Abl). The 1NLS construct, while somewhat dispersed throughout the cell, still formed a peripheral actin ring (Figure 2.2D), just like wt–Bcr–Abl (Figures. 2.2A and 2.1).

Next, cell studies demonstrating apoptosis were performed on Bcr–Abl, 4NLS–Bcr–Abl, and 1NLS–Bcr–Abl. For comparison, Figure 2.3 shows healthy K562 cells. Phase contrast images show round, healthy cells (Figure 2.3, left panel), while H33342 staining indicates normal (unsegmented) nuclei (Figure 2.3, right panel). Nuclei in

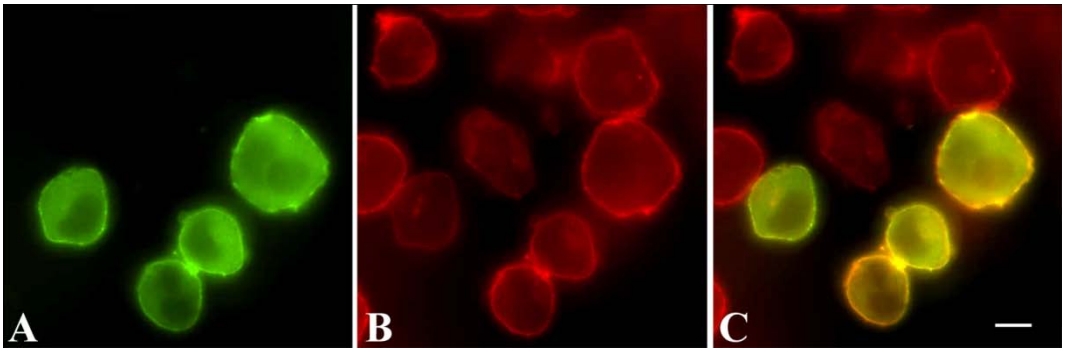

Figure 2.1. EGFP-Bcr-Abl localization in K562 cells. A. localization of Bcr–Abl via EGFP. B. Actin staining of cells. C. Overlay of EGFP–Bcr–Abl localization with actin.White scale bar, 5 μm.

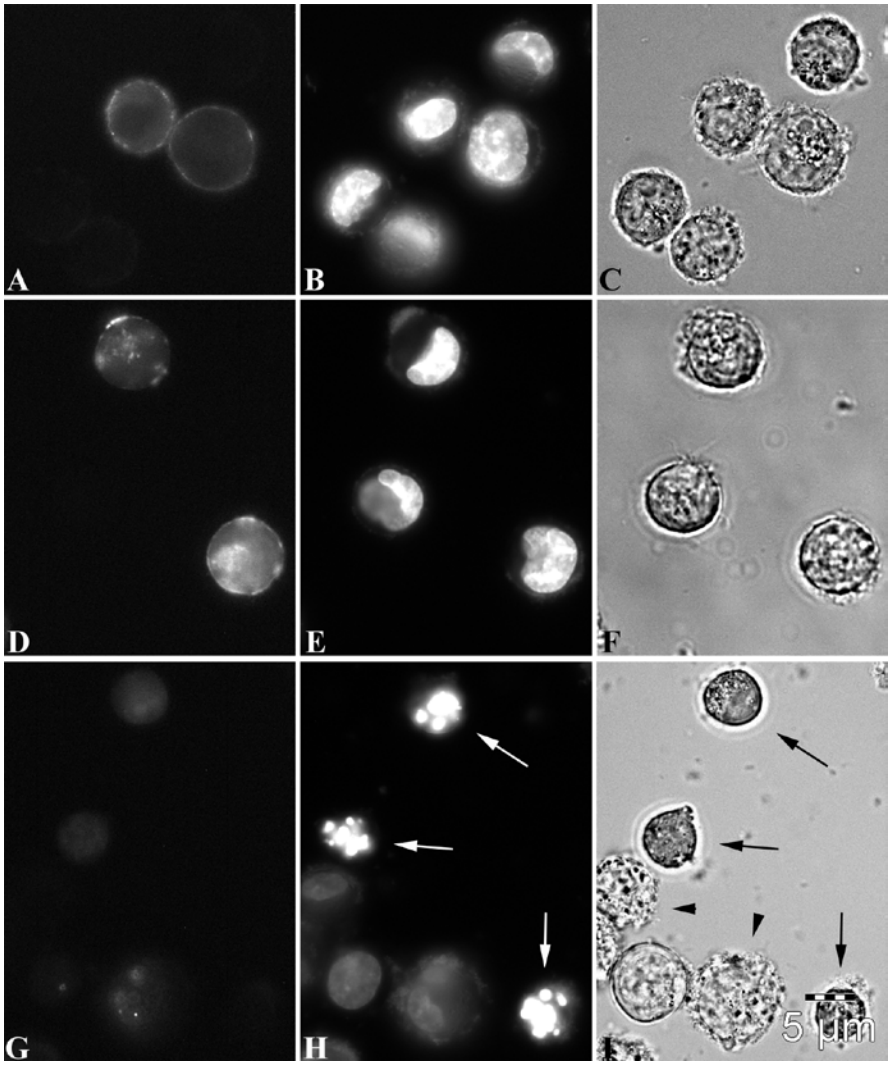

Figure 2.2. K562 cells transfected with 0NLS-, 1NLS-, or 4NLS-Bcr-Abl. A–C. EGFP–Bcr–Abl transfected into K562 cells; fluorescent (EGFP), nuclear staining with H33342, and phase contrast images, respectively. D–F. EGFP–1NLS–Bcr–Abl transfected into K562 cells; fluorescent (EGFP), nuclear staining with H33342, and phase contrast images, respectively. G–H. EGFP–4NLS–Bcr–Abl transfected into K562 cells; fluorescent (EGFP), nuclear stainingwithH33342, and phase contrast images, respectively. White arrows (H) indicate apoptotic cells undergoing massive DNA segmentation. Black arrows (I) indicate that these same cells have undergone cell shrinkage, a morphological hallmark of apoptosis (20-24). Black arrowheads (I) show cells undergoing zeotic/cytoplasmic blebbing. Scale bar (5 μm) representative for all panels (A–I).

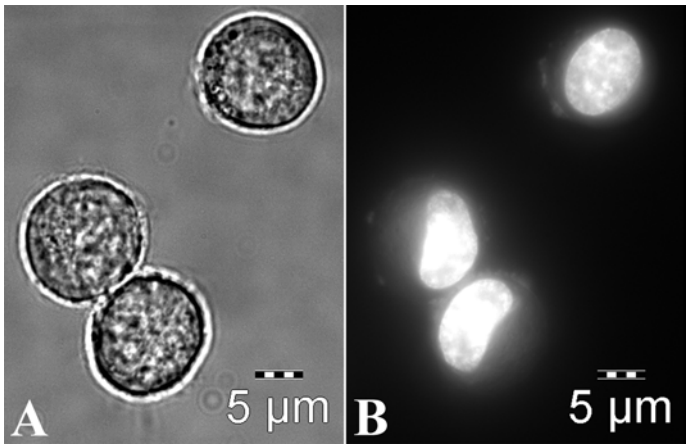

Figure 2.3. Healthy K562 cells. Left panel, phase contrast image. Right panel, nuclear staining with H33342. Nuclei of healthy cells are either round/oval or “kidney” shaped.

healthy K562 cells are round/oval or “kidney” shaped (Figure 2.3, right panel).

Twenty-four hours after transfection, cytochemical analyses of apoptosis, including overall cell morphology (Figure 2.2C,F, and I) and DNA morphology/segmentation (Figure 2.2B,E, and H), were examined.

Morphological changes indicating apoptosis include zeotic and cytoplasmic blebbing, cell shrinkage, and fragmentation of cells into smaller bodies (20-24). These morphological changes are seen obviously in cells transfected with 4NLS–Bcr–Abl, comparing Figure 2.2I (apoptosis) to Figure 2.2C and F (no apoptosis). Black arrows indicate shrunken cells (with cell shrinkage indicating apoptosis). Black arrowheads (2.2I) show cells undergoing zeotic/cytoplasmic blebbing.

The characteristic change in nuclear morphology (DNA segmentation) is “the most accurate indicator of the involvement of apoptosis in the death of a cell” (22), where the nucleus changes shape from the normal round/oval shape into smaller, non-homogeneous segments. As shown in Figure 2.2H, cells transfected with 4NLS–Bcr–Abl show this characteristic DNA segmentation into smaller pieces (white arrows), not seen in other cells (compare to Figure 2.2B and E), including healthy cells (Figure 2.3, right panel).

Transfected cells were also counted for DNA segmentation or nuclear morphology changes, an accurate indicator of apoptosis (22). As shown in Table 2.1, cells transfected with EGFP-4NLS-Bcr-Abl had a higher percentage of cells with apoptotic nuclei than EGFP–1NLS–Bcr–Abl and EGFP–Bcr–Abl. Only cells with obvious DNA segmentation (more than two nuclear fragments formed) were counted as segmented.

Table 2.1. DNA segmentation in K562 cells transfected with EGFP-Bcr-Abl, EGFP-1NLS-Bcr-Abl, or EGFP-4NLS-Bcr-Abl

Construct Transfected	No. of cells transfected	No. transfected cells with segmented DNA	Percentage of cells with segmented DNA
EGFP-Bcr-Abl	178	7	3.9
EGFP-1NLS-Bcr-Abl	154	5	3.2
EGFP-4NLS-Bcr-Abl	375	46	12.3

Bcr–Abl is known to form homodimers (tetramers) (25, 26). To determine if the 4NLS–Bcr–Abl was capable of multimerizing with Bcr–Abl, and altering its localization, a co-transfection (co-localization) experiment was performed. EGFP–4NLS–Bcr–Abl with mutated EGFP chromophore (not fluorescent) was transfected with fluorescent EGFP–Bcr–Abl. If the 4NLS–Bcr–Abl protein is able to drag Bcr–Abl into the nucleus, EGFP fluorescence will be detected in the nucleus. If 4NLS–Bcr–Abl does not drag Bcr–Abl into the nucleus, EGFP–Bcr–Abl will remain in the cytoplasm. For this analysis, a semi-quantitative assay was used that measured the fluorescence intensity in the nucleus in the co-transfected cells vs. the singly transfected (with EGFP–Bcr–Abl) cells, normalized to each cell's cytoplasmic intensity. These nuclear to cytoplasmic intensities were termed “percent nuclear intensity.” 4NLS–Bcr–Abl did not “capture” wt–Bcr–Abl and drag it into the nucleus, since the nuclear intensity of wt–EGFP–Bcr-Abl did not change in the presence of the 4NLS–Bcr–Abl construct (Figure 2.4). This result is not unexpected since the presence of strong NLSs would presumably drive any protein it was attached to immediately into the nucleus. From this result, it was determined that cytoplasmic depletion of Bcr–Abl by 4NLS–Bcr–Abl was not occurring.

Next, the caspase-3 assay was used to determine mid-stage apoptosis. Caspases, from cysteine-aspartate proteases, are a group of proteolytic enzymes that perpetuate the apoptotic signal by cleavage of proteins such as actin, lamins, fodrin, ICAD, and PARP. Prior to receiving the apoptotic signal, caspases are present in cells in an inactive pro-enzyme form. The caspase cascade starts with the activation of the initiator caspases (caspase-2, -8, -9, and -10), which then activate effector caspases (caspase-3, -6, and -7).

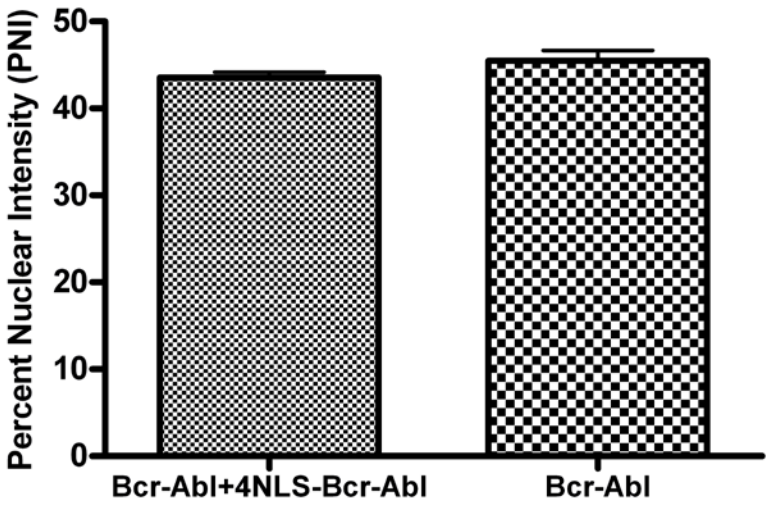

Figure 2.4. Percent nuclear intensity of Bcr-Abl with and without 4NLS-Bcr-Abl. EGFP-Bcr-Abl Percent nuclear intensity for cells transfected with EGFP-Bcr-Abl alone (right column) or EGFP-Bcr-Abl and 4NLS-Bcr-Abl (left column). n=5 cells for each group.

Both caspase-3 and caspase-7 cleave the peptide sequence DEVD, which makes it an ideal substrate for use in measuring apoptosis as a majority of the apoptotic signaling pathways converge on these effector caspases. The caspase-3 assay used measures the cleavage of a substrate with the amino acid sequence DEVD. Caspase-3 activity (Figure 2.5) was determined in several treatment groups, including EGFP–4NLS–Bcr–Abl, EGFP–1NLS–Bcr–Abl, EGFP–Bcr–Abl, or a negative control (transfected with pGL3 basic plasmid which has no promoter or enhancer and hence is not expressed). As shown in Figure 2.5, only cells transfected with EGFP–4NLS–Bcr-Abl showed a statistically significant increase in the caspase activity compared to the negative control.

Discussion/Conclusions

Nuclear localization of Bcr–Abl converts it from an oncogene to an apoptotic factor. The nuclear localization could not be achieved without adding multiple NLSs to Bcr–Abl. Once additional NLSs were added to Bcr–Abl, this caused apoptosis of CML cells (K562 cells) measured by morphologic changes (cytoplasmic blebbing and cell shrinkage), DNA segmentation (nuclear morphology changes), and the caspase-3 assay. This critical finding shows that the change in the location of Bcr–Abl from cytoplasmic to nuclear dramatically alters its function.

Nuclear entrapment and cytoplasmic depletion of wt–Bcr–Abl may have a synergistic effect on cell death. The nuclear entrapment results in apoptosis via the Abl domain which can cause cell death by stabilizing p73 and activating its pro-apoptotic functions (2, 27, 28). Cytoplasmic depletion of wt–Bcr–Abl will remove its ability to

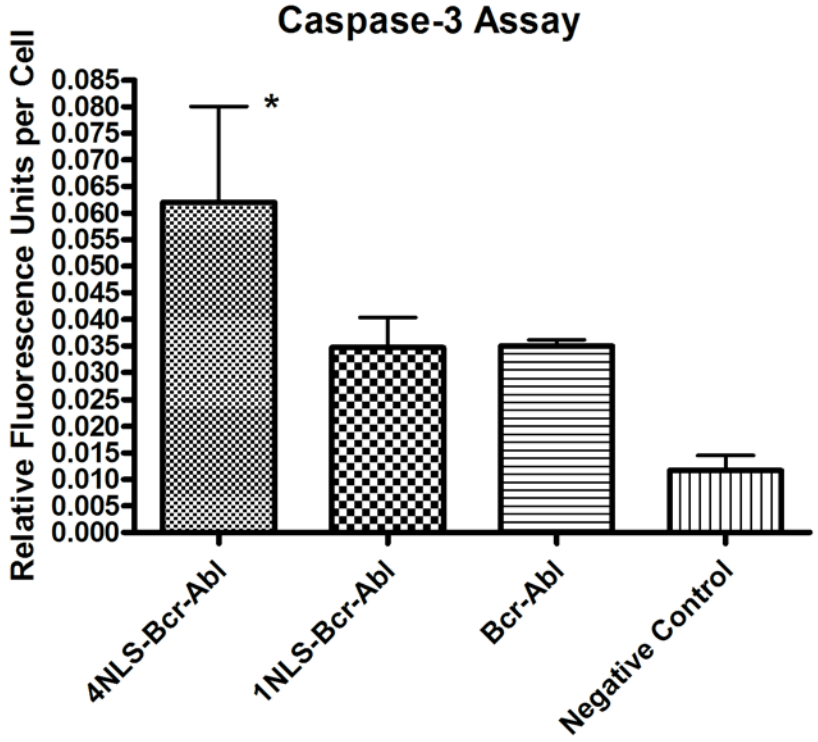

Figure 2.5. Effect of Bcr-Abl localization on caspase activity. Caspase-3 activity in K562 cells transfected with EGFP-4NLS-Bcr-Abl, EGFP-1NLS-Bcr-Abl, EGFP-Bcr-Abl, or pGL3basic plasmid (a negative control; plasmid is promoter- and enhancer-less and therefore nothing is expressed). *p,0.05; n = 3. Statistical significance determined using one-way Anova with Tukey's correction.

interact with the signal transduction proteins involved in gene transcription, mitochondrial processing of apoptotic responses, cytoskeletal organization, and degradation of inhibitory proteins (29). Here we report that ectopically expressed Bcr–Abl directed to the nucleus is sufficient to induce apoptosis without cytoplasmic depletion. However, it may be speculated that coupling cytoplasmic depletion with nuclear entrapment will synergistically enhance the apoptotic signal. To this end, our ultimate goal is to deplete wt–Bcr–Abl from the cytoplasm, and direct it to the nucleus by our previously described "protein switch" technology (18, 30). We exploit known dimerization domains (DD) of proteins to capture them and move them to a different subcellular compartment. An ectopically expressed "protein switch" can be designed to target any protein with a DD. The protein switch also contains inducible signal sequences to localize to a starting compartment in the cell (e.g., cytoplasm). Upon addition of ligand, the protein switch can move to a different subcellular compartment (e.g., nucleus). Our ultimate goal is to use the protein switch (18, 30) to control the subcellular location of Bcr–Abl, and convert Bcr–Abl from an oncogene to an apoptotic factor.

Alternative therapies for CML are needed, despite the "blockbuster" results with Gleevec. Gleevec is not a cure for CML, and patients need to take it for the rest of their lives. Gleevec is also known to have severe side effects including cardiotoxicity (11) and the possibility of developing other cancers (due to blockade of tumor suppressor p63) (12). Importantly, Gleevec resistance mostly occurs due to different point mutations in Bcr–Abl that make traditional small molecule inhibitors (like Gleevec) unable to bind/inhibit Bcr–Abl. In some cases, a decrease in Gleevec bioavailability/cell exposure and upregulation of drug efflux pumps (6, 10) have led to resistance.

The protein switch concept is also being tested in our laboratory with the anti-apoptotic factor survivin, and the tumor suppressor p53 (mislocalized in cancers). Changing localization to alter function may prove to be a new therapeutic strategy for many types of cancer, including CML (31).

Acknowledgements

Funding was provided by NIH R01 CA129528.We acknowledge the use of DNA/Peptide Core supported by the NCI Cancer Center Support Grant P30 CA042014 awarded to Huntsman Cancer Institute. We would like to thank David W. Woessner for technical assistance. We also thank S.W. Kim, K. Elenitoba-Johnson, J. Yockman, T. Cheatham, J. R. Davis, M. Mossalam, and other lab members.

References

1. Rowley JD. Letter: A new consistent chromosomal abnormality in chronic myelogenous leukaemia identified by quinacrine fluorescence and Giemsa staining. Nature 1973; 243: 290-3.

2. Vigneri P, Wang JY. Induction of apoptosis in chronic myelogenous leukemia cells through nuclear entrapment of BCR-ABL tyrosine kinase. Nat Med 2001; 7: 228-34.

3. Druker BJ, Tamura S, Buchdunger E, et al. Effects of a selective inhibitor of the Abl tyrosine kinase on the growth of Bcr-Abl positive cells. Nat Med 1996; 2: 561-6.

4. Oldham R, Dillman R. Gold standard or wrong standard? Cancer Biother Radiopharm 2004; 19: 271-2.

5. Peggs K. Imatinib mesylate--gold standards and silver linings. Clin Exp Med 2004; 4: 1-9.

6. Baccarani M, Saglio G, Goldman J, et al. Evolving concepts in the management of chronic myeloid leukemia. Recommendations from an expert panel on behalf of the European Leukemianet. Blood 2006.

7. Gorre ME, Mohammed M, Ellwood K, et al. Clinical resistance to STI-571 cancer therapy caused by BCR-ABL gene mutation or amplification. Science 2001; 293: 876-80.

8. Shah NP, Sawyers CL. Mechanisms of resistance to STI571 in Philadelphia chromosome-associated leukemias. Oncogene 2003; 22: 7389-95.

9. Roumiantsev S, Shah NP, Gorre ME, et al. Clinical resistance to the kinase inhibitor STI-571 in chronic myeloid leukemia by mutation of Tyr-253 in the Abl kinase domain P-loop. Proc Natl Acad Sci U S A 2002; 99: 10700-5.

10. Melo JV, Hughes TP, Apperley JF. Chronic myeloid leukemia. Hematology (Am Soc Hematol Educ Program) 2003: 132-52.

11. Kerkela R, Grazette L, Yacobi R, et al. Cardiotoxicity of the cancer therapeutic agent imatinib mesylate. Nat Med 2006; 12: 908-16.

12. Ongkeko WM, An Y, Chu TS, Aguilera J, Dang CL, Wang-Rodriguez J. Gleevec suppresses p63 expression in head and neck squamous cell carcinoma despite p63 activation by DNA-damaging agents. Laryngoscope 2006; 116: 1390-6.

13. Francois H, Coppo P, Hayman JP, Fouqueray B, Mougenot B, Ronco P. Partial fanconi syndrome induced by imatinib therapy: a novel cause of urinary phosphate loss. Am J Kidney Dis 2008; 51: 298-301.

14. Calabretta B, Perrotti D. The Biology of CML Blast Crisis. Blood 2004.

15. Goldman JM, Melo JV. Chronic myeloid leukemia--advances in biology and new approaches to treatment. N Engl J Med 2003; 349: 1451-64.

16. Cody CW, Prasher DC, Westler WM, Prendergast FG, Ward WW. Chemical structure of the hexapeptide chromophore of the Aequorea green-fluorescent protein. Biochemistry 1993; 32: 1212-8.

17. Ormo M, Cubitt AB, Kallio K, Gross LA, Tsien RY, Remington SJ. Crystal structure of the Aequorea victoria green fluorescent protein. Science 1996; 273: 1392-5.

18. Kakar M, Davis JR, Kern SE, Lim CS. Optimizing the protein switch: altering nuclear import and export signals, and ligand binding domain. J Control Release 2007; 120: 220-32.

19. Hantschel O, Wiesner S, Guttler T, et al. Structural basis for the cytoskeletal association of Bcr-Abl/c-Abl. Mol Cell 2005; 19: 461-73.

20. Schwartzman RA, Cidlowski JA. Apoptosis: the biochemistry and molecular biology of programmed cell death. Endocr Rev 1993; 14: 133-51.

21. Vermes I, Haanen C. Apoptosis and programmed cell death in health and disease. Adv Clin Chem 1994; 31: 177-246.

22. Willingham MC. Cytochemical methods for the detection of apoptosis. J Histochem Cytochem 1999; 47: 1101-10.

23. Bortner CD, Cidlowski JA. Apoptotic volume decrease and the incredible shrinking cell. Cell Death Differ 2002; 9: 1307-10.

24. Bortner CD, Cidlowski JA. Uncoupling cell shrinkage from apoptosis reveals that Na+ influx is required for volume loss during programmed cell death. J Biol Chem 2003; 278: 39176-84.

25. Zhao X, Ghaffari S, Lodish H, Malashkevich VN, Kim PS. Structure of the Bcr-Abl oncoprotein oligomerization domain. Nat Struct Biol 2002; 9: 117-20.

26. McWhirter JR, Galasso DL, Wang JY. A coiled-coil oligomerization domain of Bcr is essential for the transforming function of Bcr-Abl oncoproteins. Mol Cell Biol 1993; 13: 7587-95.

27. Aloisi A, Di Gregorio S, Stagno F, et al. BCR-ABL nuclear entrapment kills human CML cells: ex vivo study on 35 patients with the combination of imatinib mesylate and leptomycin B. Blood 2006; 107: 1591-8.

28. Wang JY. Regulation of cell death by the Abl tyrosine kinase. Oncogene 2000; 19: 5643-50.

29. Dai Z, Kerzic P, Schroeder WG, McNiece IK. Deletion of the Src homology 3 domain and C-terminal proline-rich sequences in Bcr-Abl prevents Abl interactor 2 degradation and spontaneous cell migration and impairs leukemogenesis. J Biol Chem 2001; 276: 28954-60.

30. Kakar M, Cadwallader AB, Davis JR, Lim CS. Signal sequences for targeting of gene therapy products to subcellular compartments: the role of CRM1 in nucleocytoplasmic shuttling of the protein switch. Pharm Res 2007; 24: 2146-55.

31. Davis JR, Kakar M, Lim CS. Controlling protein compartmentalization to overcome disease. Pharm Res 2007; 24: 17-27.

CHAPTER 3

THE NUCLEUAR TRANSLOCATION ASSAY FOR INTRACELLULAR PROTEIN-PROTEIN INTERACTIONS AND ITS APPLICATION TO THE BCR COILED-COILED DOMAIN

Abstract

Protein interactions are critical for normal biological processes and molecular pathogenesis. While it is important to study these interactions, there are limited assays that are performed inside the cell, in the native cell environment, where the majority of protein-protein interactions take place. Here we present a method of studying protein interactions intracellularly using one protein of interest fused to a localization-controllable enhanced green fluorescent protein (EGFP) construct and the other protein of interest fused to the red fluorescent protein, DsRed. Nuclear translocation of the EGFP construct is induced by addition of a ligand, and the difference in nuclear localization between the induced and uninduced states of the DsRed construct provides an indication of the interaction between the two proteins. This assay, the nuclear translocation assay (NTA), is introduced here as broadly applicable for studying protein interactions in the native environment inside of cells and is demonstrated using forms of the coiled-coil domain from the breakpoint cluster region (Bcr) protein.

Reprinted by permission from *Biotechniques* 49(1) 2010 , 519-524

Introduction

Protein-protein interactions are an essential component of almost every cellular process. These interactions regulate signaling events that result in differentiation, proliferation, regulation of gene transcription, repair mechanisms, and inhibition or induction of apoptosis to name only a few (1). Studying these interactions can provide valuable insights into the molecular mechanisms governing these cellular processes. Furthermore, aberrant protein interactions can lead to diseases such as cancer (2), diabetes (3), cystic fibrosis (4), Alzheimer's (5), and a number of metabolic disorders (6). Thus, the understanding of protein interactions is also critical in the understanding of disease and the development of therapeutic interventions to treat them. The majority of these interactions between proteins occur inside of cells, and intracellular experimental assays for protein-protein interactions are the most relevant. However, currently there are few assays that provide a means to quantify protein-protein interactions in the native cell environment. Resonance energy transfer (RET), including bioluminescence resonance energy transfer (BRET) (7) and Förster (fluorescence) resonance energy transfer (FRET) (8), is one mechanism for detecting intracellular protein interactions but requires a specific combination of the right donor and acceptor, along with the sensitive detection of light emitted at specific wavelengths. Further, the proper orientation of the donor and acceptor dipoles within the Förster distance must be achieved for effective energy transfer. The two-hybrid system (yeast or mammalian) is another assay for intracellular protein interactions (9), but the interaction typically takes place inside the cell nucleus and this assay requires the transcription/translation of a reporter protein which necessitates the expression of three proteins (or even four if normalizing to a second

control protein). CytoTrap® is one variation of the two-hybrid assay that allows the interaction to occur in the cytoplasm. The split ubiquitin assay (10) is similar to the two-hybrid system, but uses truncations of ubiquitin in place of transcription factor domains. Here we present a new method for the qualitative analysis of protein-protein interactions that is performed inside of cells and is based on an optimized ligand-responsive protein and the simultaneous quantification of fluorescence intensity from EGFP and DsRed.

The controlled nuclear translocation in this assay occurs through what we have termed a "protein switch." The protein switches we have developed are chimeric proteins consisting of three components: a nuclear export signal (NES), a nuclear localization signal (NLS), and ligand binding domain (LBD). In the absence of ligand the NES directs the protein switch to the cytoplasm. However, when the ligand binds the LBD it causes a conformational change, exposes the NLS, and the protein is redirected to the nucleus. In our laboratory various combinations of these three components have been studied to identify the optimal combination that results in the greatest amount of nuclear translocation upon ligand induction (11, 12). This nuclear translocation is concentration-dependent and reversible if the ligand is removed (12). One such optimized protein switch, used herein, consists of the NES from HIV rev, the NLS from MycA8, and the LBD from the rat glucocorticoid receptor containing the C656G mutation which renders it 10 times more sensitive to the synthetic glucocorticoid dexamethasone (13). This protein switch provides an easy method for controlling the subcellular shuttling between the cytoplasm and the nucleus.

The ability to control the translocation of a protein into the nucleus has led to a biochemical assay for studying protein-protein interactions we have termed a nuclear

translocation assay (NTA). The general concept of the NTA is depicted in Figure 3.1. A protein of interest is subcloned and expressed as a fusion protein with the protein switch and EGFP. As a result of the protein switch, this fusion protein is responsive to ligand and will translocate into the nucleus upon ligand induction. A second, non-ligand responsive protein tagged with DsRed is co-expressed with the protein switch construct. If the two proteins interact (Figure 3.1, top) the second protein will translocate into the nucleus along with the protein switch. The percentage of DsRed inside the nucleus is quantified before and after the addition of ligand, and the difference (termed percent nuclear increase, PN_L-PN_0)/PN_0*100%) is indicative of the interaction between the two proteins. However, if there is little or no interaction between the two proteins (Figure 3.1, bottom) the protein switch alone moves to the nucleus and there is no change in the subcellular localization of the second protein. Fluorescent protein tags are used as a means of determining the cytoplasmic and nuclear localization of the two proteins through fluorescence microscopy, and thus the fluorescent signals from the two proteins expressed in the same cell need to be distinguishable via excitation/emission filters. Two such fluorescent proteins are EGFP and DsRed that exhibit excitation/emission of 480nm/510nm and 545nm/620nm, respectively.

To demonstrate the NTA in mammalian cells (1471.1: murine adenocarcinoma, and Cos-7: simian kidney), we performed the assay on two forms of the coiled-coil domain from the breakpoint cluster region (Bcr) protein. This domain forms an antiparallel coiled coil responsible for the oligomerization of Bcr (14). Although relatively little is known about the function of the Bcr protein, a reciprocal chromosomal

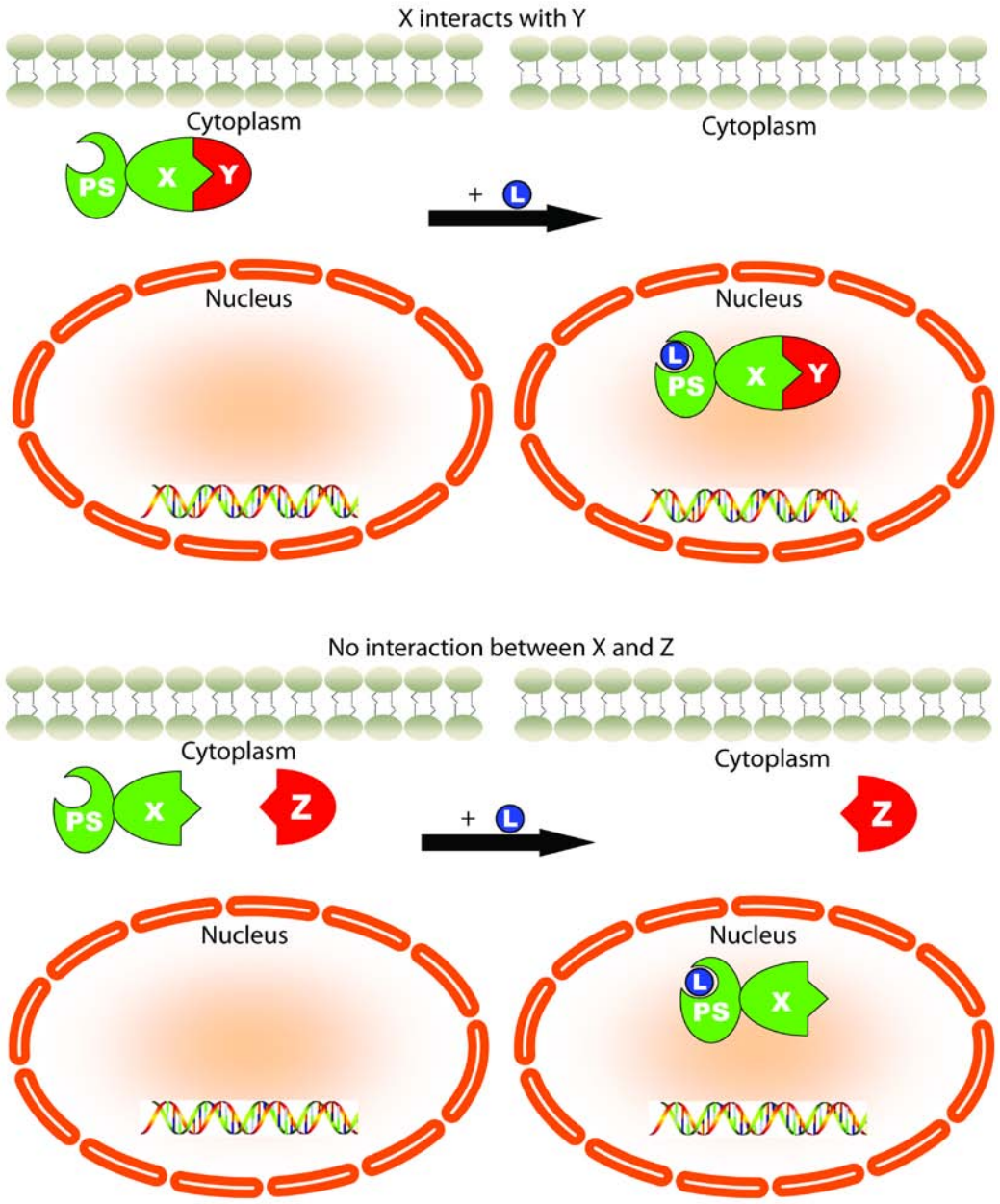

Figure 3.1: The nuclear translocation assay (NTA) concept. If the two proteins interact, as is the case for proteins X and Y in the top half of the diagram, protein X will cause an increase in the nuclear localization of protein Y upon addition of ligand (L) due to the ligand-responsive protein switch (PS) fused to protein X. If two proteins do not interact, as is the case for proteins X and Z in the bottom half of the diagram, the protein switch translocates the fused protein X to the nucleus upon addition of ligand without altering the localization of protein Y. The translocation of the protein switch construct is monitored through the fluorescence of EGFP, and the translocation of the second protein is monitored through the fluorescence of DsRed.

translocation between chromosomes 9 and 22 generates the Philadelphia chromosome which expresses Bcr-Abl consisting of the C-terminus of Bcr fused to the N-terminus of the Abelson kinase protein (Abl) (15). The Philadelphia chromosome and Bcr-Abl are the cause of 95% of chronic myelogenous leukemia (CML) cases (16). Oncogenesis through Bcr-Abl is dependent on the tyrosine kinase activity that is regulated through the oligomerization of Bcr-Abl mediated by the coiled-coil domain (17). Reports have shown an isolated coiled-coil domain (or truncations thereof) can disrupt the oligomerization of Bcr-Abl and reduce the kinase activity and associated oncogenesis (18-21). We have recently altered certain residues (manuscript in progress) of this domain to prevent the homo-oligomerization (i.e., coiled coil:coiled coil) and improve the binding to Bcr-Abl (i.e., coiled coil:Bcr-Abl). As the wild-type coiled-coil domain (herein designated CC, sequence provided in supplementary materials) has no specificity for Bcr-Abl's coiled coil over another exogenously added coiled coil, the homo-oligomerization may be a limiting factor in its efficacy. Our designed coiled coil (herein designated CCmut, sequence provided in supplementary materials) shows reduced homo-oligomerization (mutant:mutant), along with the potential for enhanced hetero-oligomerization (mutant:Bcr-Abl), to increase the binding to the coiled coil of Bcr-Abl.

The NTA is a unique method for studying protein-protein interactions under intracellular conditions. Few assays offer the ability to study these interactions in the cellular environment where they actually take place. The controlled nuclear translocation upon addition of ligand using the protein switch provides the ability to differentiate the nuclear translocation from proteins that localize partially in the nucleus or small proteins that can diffuse into the nucleus, by taking the difference in the nuclear percentage before

and after ligand induction. Thus, proteins smaller than 40kDa that can diffuse through the nuclear pores or nuclear localized proteins will not result in false positives. However, as this assay revolves around nuclear translocation, transmembrane proteins may not be suitable, and nuclear localized proteins may need a modification (mutating the nuclear localization signal, adding a nuclear export signal, or performing the assay with only the binding domain rather than the full protein) for their study. An additional consideration is that the cytoplasmic and nucleoplasmic environments are not the same, and an interaction that normally occurs in the nucleus may be altered in the cytoplasm where this assay originates. Yet in spite of these few limitations, the NTA is relatively simple, does not involve reporter plasmids/proteins, and requires little more than the appropriate fusion proteins, dexamethasone, and a fluorescence microscope to perform.

Materials and Methods

Construction of Plasmids and Mutagenesis

The DNA encoding the coiled-coil domain was amplified through PCR from pEGFP-Bcr-Abl using the primers 5'- tgtaactcgagttatggtggacccggtg-3' and 5'-atgctctcgagaccggtcatagctcttc-3', and subcloned into pEGFP-PS at the XhoI restriction enzyme site. pEGFP-PS is an EGFP mammalian expression plasmid (pEGFP-C1, Clontech, Mountain View, CA, USA) with the optimized protein switch (PS) subcloned at the C-terminus of EGFP (12). Using the resulting pEGFP-PS-CC plasmid as the template, two sequential site-directed mutagenesis reactions were performed using the QuikChange II Site-Directed Mutagenesis Kit (Stratagene, La Jolla, CA, USA). The primers used for the first reaction were 5'-ggagcgctgcaaggcccgcattcggcgcgacgagcagcggg

acaaccaggagcgcttccgcatgatctacctggagacgttgctggccaagg-3' and the reverse complement. For the second reaction the primers were 5'-gcgacgagcagcgggtgaaccaggagcgcttcc-3' (and reverse complement) and 5'-caggagctggagcgcgccaaggcccgcattcg-3' (and reverse complement). These mutations were designed to change bases encoding five amino acids in the coiled-coil domain to increase the number of ionic interactions in the heterodimer (mutant:wild type) and introduce charge-charge repulsions in the mutant homodimer (mutant:mutant) (manuscript in progress). The wild type and mutant forms of the coiled coil were used as the templates for PCR with the primers 5'-tgtaactcgagttatggtggacccggtg-3' and 5'-atgctctcgagccggtcatagctcttc-3', and subsequently inserted into pDsRed2-N1 (Clontech) at the XhoI site.

Cell Line and Transient Transfection

1471.1 and Cos-7 cells grow as monolayers in DMEM and RPMI (GIBCO, Invitrogen, Carlsbad, CA, USA) respectively, both supplemented with 10% FBS (Hyclone Laboratories, Logan, UT, USA), 1% penicillin-streptomycin (GIBCO), 0.1% gentamicin (Hyclone), and 1% L-glutamine (Hyclone). The cells were maintained in a 5% CO_2 incubator at 37 °C. 1471.1 cells were grown to approximately 50% confluency, and 5 x 10^6 cells in 100 μL cold plain DMEM were transiently cotransfected via electroporation as previously described (22, 23). Transfections were performed using the Electrosquare Porator ECM 830 (BTX, Harvard Apparatus, Holliston, MA, USA) with 2 μg of EGFP-protein switch plasmid and 2 μg of DsRed plasmid along with 6 μg pGL3basic (Promega, Madison, WI, USA) carrier DNA for a total of 10 μg DNA. 3 pulses of 140 V were applied for 10 msec. Following the electroporation, the cells were

plated in complete DMEM in a 2-well live cell chamber (Lab-tek II chamber slide system, Nalge NUNC, Rochester, NY, USA), and incubated in a 5% CO_2 incubator at 37 °C overnight. Cos-7 cells were seeded into a 2- or 4-well live cell chamber 24 hrs prior to transfection with Lipofectamine LTX (Invitrogen, Carlsbad, CA, USA) so the confluency was around 90% on the day of the transfection. Transfections were carried out as recommended by the supplier.

Ligand Induction and Fluorescent Microscopy

After 24 hrs, the cells were rinsed with PBS (GIBCO) followed by addition of 2 mL complete phenol red-free DMEM (GIBCO). The protein switch ligand dexamethasone (Sigma, St. Louis, MO, USA) (12) was then added to one well at a final concentration of 200 nM, and the cells were incubated at 37 °C for 1-2 hrs. 0.5 μL H33342 nuclear dye was added to the Cos-7 cells and incubated at 37°C for another 15 min. Following the incubation, the transfected cells were viewed and photographed using an inverted fluorescence microscope, Olympus IX701F (Scientific Instrument Company, Sunnyvale, CA, USA) with high-quality narrow band GFP filter (excitation HQ480/20 nm, emission HQ510/20 nm, beam splitter Q495lp, Chroma Technology Corp., Brattleboro, VT, USA) and high-quality TRITC filter (excitation HQ545/30 nm, emission HQ620/60 nm, beam splitter Q570lp, Chroma Technology Corp.). Cells were photographed with a 40x or 60x objective using an F-view Monochrome CCD camera. Neutral density filters with 500 ms exposure time was used to minimize photobleaching. The microscope stage was maintained at 37 °C with a Nevtek ASI 400 Air Stream Incubator (Nevtek, Williamsville, VA, USA) with temperature control.

Quantification of the Percent Nuclear Increase

Quantification of the fluorescence intensity of EGFP and DsRed correlates to the amount of the respective exogenous protein. The images of cells were analyzed using analySIS® software (Soft Imaging System GmbH, Muenster, Germany), and the amount of protein in the cytoplasm and the nucleus was quantified as previously described (23-26). The following equations were used in the quantification:

$$\textbf{Equation 1:}\ \mathrm{ACI} = \frac{\mathrm{CI}}{\mathrm{CA}}$$

$$\textbf{Equation 2:}\ \mathrm{ANI} = \frac{\mathrm{NI}}{\mathrm{NA}}$$

$$\textbf{Equation 3:}\ \mathrm{PN} = \left(\frac{\mathrm{ANI}}{ANI + ACI}\right) * 100\%$$

$$\textbf{Equation 4:}\ \mathrm{PNI} = \left(\frac{\mathrm{PN_L} - \mathrm{PN_0}}{\mathrm{PN_0}}\right) * 100\%$$

Where ACI= average cytoplasmic intensity, CI=cytoplasmic intensity, CA=area of cytoplasm, ANI=average nuclear intensity, NI=nuclear intensity, NA=area of nucleus, PN=percentage nuclear, PNI=percentage nuclear increase, PN_L=percentage nuclear after ligand induction, PN_0=percentage nuclear without ligand induction.

At least eight cells were analyzed from each group, and each experiment was performed in triplicate. The experimental output, PNI, is a measure of how much the nuclear intensity increases after the addition of ligand, and values reported are the means ± standard deviation. As the percent nuclear increase (PNI) of the DsRed construct is related to the binding and PNI of the protein switch construct, PNI of DsRed was normalized to the PNI of the EGFP (protein switch) construct, $PNI_{DsRed}/PNI_{EGFP}*100\%$.

Results and Discussion

In any assay involving simultaneous expression of two distinct proteins it is essential to ensure both proteins are expressed at consistent levels from experiment to experiment and between groups in each experiment. The NTA exhibits the ability to quantify the amount of protein present in each cell being studied, providing a validation of consistent protein expression. For example, the experiments performed in 1471.1 cells, all resulted in fluorescence intensities in the range of 13,000 RFU/area (no statistical difference at the 95% confidence level using 1-way ANOVA; data not shown). Further, the EGFP PNI (the ligand-responsive protein switch) should be relatively consistent, and can be monitored to ensure the assay is functioning properly. As seen in Figure 3.2a, the nuclear fluorescence intensity from all protein-switch constructs (EGFP) assayed in 1471.1 cells increased in the range of 30% after the addition of ligand (no statistical difference at the 95% confidence level using 1-way ANOVA). After confirmation that the total fluorescence intensities from both DsRed and EGFP, and the percent nuclear increase of EGFP are consistent, the varying levels of DsRed percent nuclear increase will be due to the interaction between the two proteins fused to DsRed and EGFP. Example images demonstrating the localization in the absence and presence of ligand in 1471.1 cells are shown in Figure 3.2b.

The alteration of subcellular localization of a protein is a novel method of studying protein-protein interactions in the complex cellular milieu. This technology harnesses the control over nuclear translocation provided by the protein switch, and uses the fluorescent proteins EGFP and DsRed to monitor their subcellular localization. As a

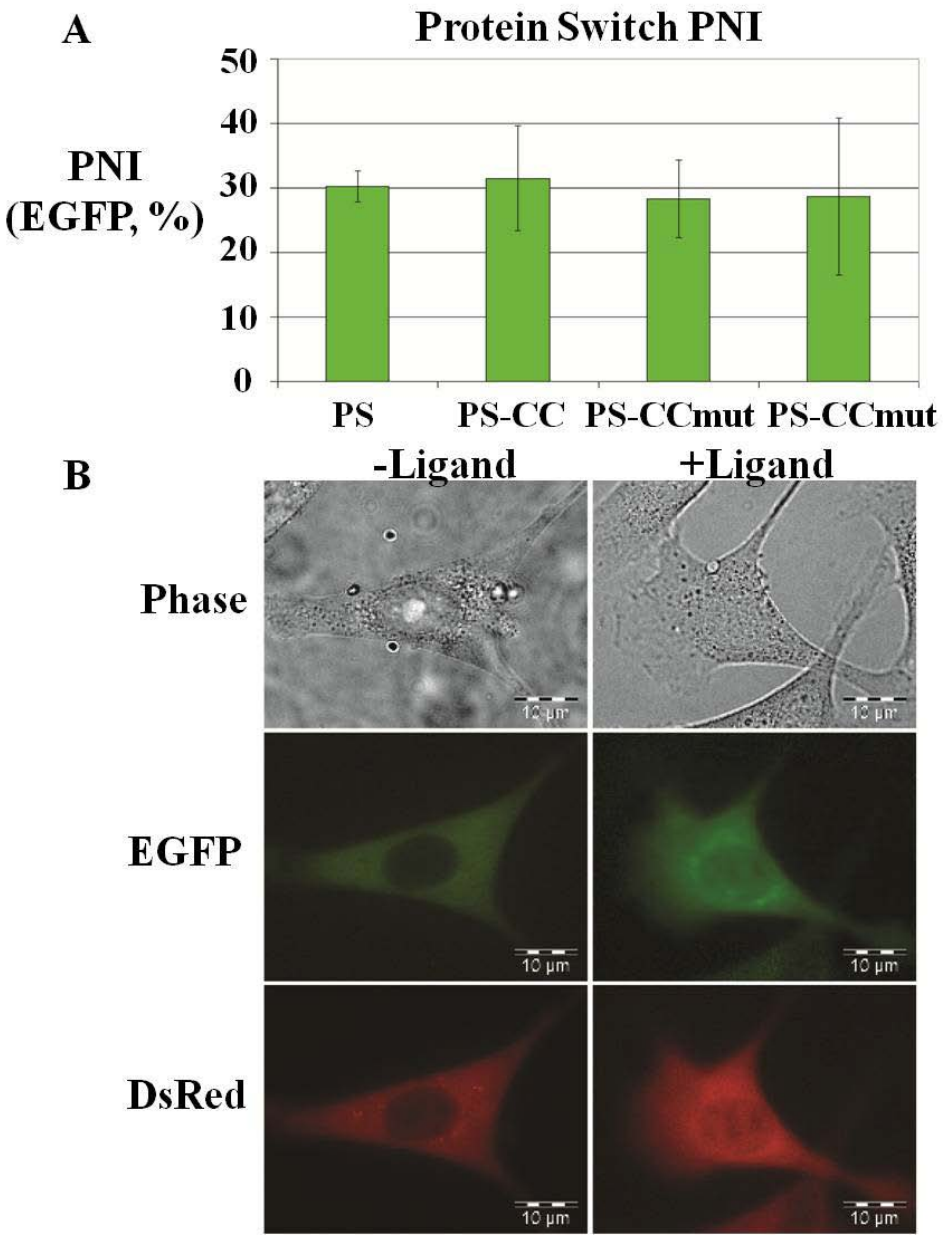

Figure 3.2: Percent Nuclear Increase of Protein-Switch Constructs and Example Cell Images. A. Percent nuclear increase of the protein switch constructs as measured by EGFP fluorescence. The percent nuclear increase of the protein switch being relatively consistent across all groups tested indicates the percent nuclear increase of the DsRed construct is due to the interaction of the fusion proteins. B. Example images of 1471.1 cells cotransfected with EGFP-Protein Switch-CCmut and DsRed-CC. The phase contrast is seen in the top row, the fluorescence from EGFP in the middle row, and fluorescence from DsRed in the bottom row. The left column contains cells without ligand added, and the right column contains cells 2 hrs after ligand was added. For the protein switch construct (EGFP), the initial localization is in the cytoplasm, and after addition of ligand it translocates into the nucleus. The nuclear translocation of the DsRed construct is not as noticeable, but also moves into the nucleus after addition of ligand due to the interaction with the protein switch construct.

negative control, EGFP-PS-CC was cotransfected with DsRed (no coiled-coil domain), as well as EGFP-PS (no coiled coil) cotransfected with DsRed-CC, and both resulted in negligible nuclear translocation after the addition of ligand (Figure 3.3, first column). A particularly challenging interaction to study is the homo-oligomerization of a protein. When utilizing two fusion proteins to study the interaction, difficulty arises due to the formation of homo-oligomerized fusion proteins that compete with the hetero-oligomerization between the two fusion proteins. In the case of the Bcr coiled-coil domain, in spite of the known dimerization of this domain, the homo-oligomerization of the protein switch construct seems to be a limiting factor and minimal nuclear translocation was seen (Figure 3.3, second column). However, when we used a mutant form of the coiled coil that exhibits reduced homo-dimerization, the protein switch construct was more available for interaction with the DsRed construct and a large nuclear increase was observed (Figure 3.3, third column). The prevention of the homo-oligomerization by the mutant coiled coil is also indicated by the absence of nuclear increase when the mutant coiled coil is fused to both the protein switch and DsRed (Figure 3.3, fourth column). The NTA provided a novel way of demonstrating the enhanced binding and specificity of the mutant coiled coil as seen in Figure 3.3. This data has been corroborated with a mammalian two-hybrid assay (data not shown).

One of the cell lines we chose to use for this assay, 1471.1, is an adherent cell line with easily detectable nuclei ideal for imaging fluorescent proteins via fluorescence microscopy. These characteristics make this cell line a suitable candidate for the NTA.

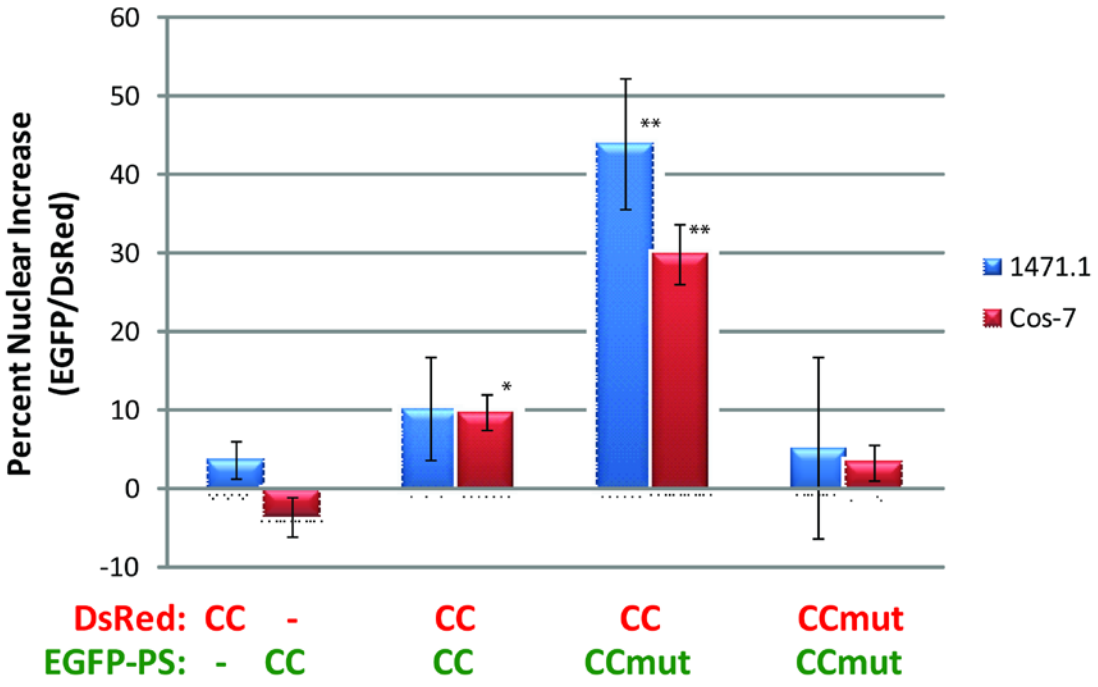

Figure 3.3: NTA results for the Bcr coiled coil and mutant coiled coil. The mutant coiled coil is designed to prevent the homo-oligomerization (CCmut:CCmut) and have improved binding to the wild-type coiled coil. This results in EGFP-PS-CCmut being more available to oligomerize with DsRed-CC, and the greatest nuclear translocation with this combination (CCmut:CC, third column). PS=protein switch, CC=coiled coil, CCmut=mutant coiled coil. * $p<0.01$, **$p<0.001$ compared to control (first column); each experiment performed in triplicate with at least eight cells analyzed per experiment. Statistical significance determined using one-way ANOVA with Tukey's posttest.

Further, the cell nucleus is very large (Figure 3.2b) and the nuclear membrane is easily detectable with a 40x objective, eliminating the need for nuclear stains and reducing the complexity of the assay. We have routinely stained the nuclei of these cells with a Hoechst dye (H33342, similar to DAPI), and confirmed the location of the cell nuclei (data not shown). To further validate the assay, we studied the same interactions in Cos-7 cells, and very similar results were obtained as seen in Figure 3.3.

The protein switch designed in our laboratory originated with an idea for altering the subcellular localization of aberrant functioning proteins as a therapeutic intervention (23). This optimized control over nuclear translocation now serves as an assay to study protein interactions in the intracellular matrix and can be applied to almost any protein of interest. Although in some regards the NTA is similar to the membrane recruitment assay (27), or the translocation biosensor (28), the ability to control the translocation by the presence or absence of a ligand is advantageous. Here we have demonstrated the NTA in murine and simian cells, but as the protein switch is translocated into the nucleus via importin α/β common among most organisms, other cells (including human) could be used to perform this assay. After routine generation of fusion proteins consisting of the proteins of interest fused to EGFP-protein switch and DsRed, the NTA is simple and requires only a fluorescence microscope, software to quantify fluorescence intensities (such as Image J, freeware from the NIH) and the readily available ligand dexamethasone. This assay now adds to the limited repertoire of experimental techniques for studying protein interactions inside of cells.

Acknowledgments

Funding was provided by NIH R01 CA129528. We acknowledge the use of DNA/Peptide Core supported by the NCI Cancer Center Support Grant P30 CA042014 awarded to Huntsman Cancer Institute. We would like to thank T. Cheatham, S. Pendley, Jonathan Constance, Rian Davis, Mohanad Mossalam, and David Woessner for scientific input.

References

1. Stein A, Pache RA, Bernado P, Pons M, Aloy P. Dynamic interactions of proteins in complex networks: a more structured view. Febs J 2009; 276: 5390-405.

2. Davis JR, Kakar M, Lim CS. Controlling protein compartmentalization to overcome disease. Pharm Res 2007; 24: 17-27.

3. Tsukaguchi H, Matsubara H, Taketani S, Mori Y, Seido T, Inada M. Binding-, intracellular transport-, and biosynthesis-defective mutants of vasopressin type 2 receptor in patients with X-linked nephrogenic diabetes insipidus. J Clin Invest 1995; 96: 2043-50.

4. Buchanan PJ, Ernst RK, Elborn JS, Schock B. Role of CFTR, Pseudomonas aeruginosa and Toll-like receptors in cystic fibrosis lung inflammation. Biochem Soc Trans 2009; 37: 863-7.

5. Zhong N, Weisgraber KH. Understanding the Basis for the Association of Apoe4 with Alzheimer's Disease: Opening the Door for Therapeutic Approaches. Curr Alzheimer Res 2009.

6. Gloerich J, Wevers RA, Smeitink JA, van Engelen BG, van den Heuvel LP. Proteomics approaches to study genetic and metabolic disorders. J Proteome Res 2007; 6: 506-12.

7. Pfleger KD, Eidne KA. Illuminating insights into protein-protein interactions using bioluminescence resonance energy transfer (BRET). Nat Methods 2006; 3: 165-74.

8. Miyawaki A, Llopis J, Heim R, et al. Fluorescent indicators for Ca2+ based on green fluorescent proteins and calmodulin. Nature 1997; 388: 882-7.

9. Suter B, Kittanakom S, Stagljar I. Two-hybrid technologies in proteomics research. Curr Opin Biotechnol 2008; 19: 316-23.

10. Johnsson N, Varshavsky A. Split ubiquitin as a sensor of protein interactions in vivo. Proc Natl Acad Sci U S A 1994; 91: 10340-4.

11. Kakar M, Cadwallader AB, Davis JR, Lim CS. Signal sequences for targeting of gene therapy products to subcellular compartments: the role of CRM1 in nucleocytoplasmic shuttling of the protein switch. Pharm Res 2007; 24: 2146-55.

12. Kakar M, Davis JR, Kern SE, Lim CS. Optimizing the protein switch: altering nuclear import and export signals, and ligand binding domain. J Control Release 2007; 120: 220-32.

13. Htun H, Barsony J, Renyi I, Gould DL, Hager GL. Visualization of glucocorticoid receptor translocation and intranuclear organization in living cells with a green fluorescent protein chimera. Proc Natl Acad Sci U S A 1996; 93: 4845-50.

14. Taylor CM, Keating AE. Orientation and oligomerization specificity of the Bcr coiled-coil oligomerization domain. Biochemistry 2005; 44: 16246-56.

15. Rowley JD. Letter: A new consistent chromosomal abnormality in chronic myelogenous leukaemia identified by quinacrine fluorescence and Giemsa staining. Nature 1973; 243: 290-3.

16. Sandberg AA, Gemmill RM, Hecht BK, Hecht F. The Philadelphia chromosome: a model of cancer and molecular cytogenetics. Cancer Genet Cytogenet 1986; 21: 129-46.

17. Zhang X, Subrahmanyam R, Wong R, Gross AW, Ren R. The NH(2)-terminal coiled-coil domain and tyrosine 177 play important roles in induction of a myeloproliferative disease in mice by Bcr-Abl. Mol Cell Biol 2001; 21: 840-53.

18. Guo XY, Cuillerot JM, Wang T, et al. Peptide containing the BCR oligomerization domain (AA 1-160) reverses the transformed phenotype of p210bcr-abl positive 32D myeloid leukemia cells. Oncogene 1998; 17: 825-33.

19. Beissert T, Hundertmark A, Kaburova V, et al. Targeting of the N-terminal coiled coil oligomerization interface by a helix-2 peptide inhibits unmutated and imatinib-resistant BCR/ABL. Int J Cancer 2008; 122: 2744-52.

20. Beissert T, Puccetti E, Bianchini A, et al. Targeting of the N-terminal coiled coil oligomerization interface of BCR interferes with the transformation potential of BCR-ABL and increases sensitivity to STI571. Blood 2003; 102: 2985-93.

21. Huang SF, Liu DB, Zeng JM, et al. Cloning, expression, purification and functional characterization of the oligomerization domain of Bcr-Abl oncoprotein fused to the cytoplasmic transduction peptide. Protein Expr Purif 2009; 64: 167-78.

22. Kanwal C, Li H, Lim CS. Model system to study classical nuclear export signals. AAPS PharmSci 2002; 4: E18.

23. Kanwal C, Mu S, Kern SE, Lim CS. Bidirectional on/off switch for controlled targeting of proteins to subcellular compartments. J Control Release 2004; 98: 379-93.

24. Li H, Fidler ML, Lim CS. Effect of initial subcellular localization of progesterone receptor on import kinetics and transcriptional activity. Mol Pharm 2005; 2: 509-18.

25. Li H, Yan G, Kern SE, Lim CS. Correlation among agonist dose, rate of import, and transcriptional activity of liganded progesterone receptor B isoform in living cells. Pharm Res 2003; 20: 1574-80.

26. Lim CS, Baumann CT, Htun H, et al. Differential localization and activity of the A- and B-forms of the human progesterone receptor using green fluorescent protein chimeras. Mol Endocrinol 1999; 13: 366-75.

27. Grefen C, Stadele K, Ruzicka K, Obrdlik P, Harter K, Horak J. Subcellular localization and in vivo interactions of the Arabidopsis thaliana ethylene receptor family members. Mol Plant 2008; 1: 308-20.

28. Knauer SK, Stauber RH. Development of an autofluorescent translocation biosensor system to investigate protein-protein interactions in living cells. Anal Chem 2005; 77: 4815-20.

CHAPTER 4

DISRUPTION OF BCR-ABL COILED-COIL OLIGOMERIZATION BY DESIGN

Abstract

Oligomerization is an important regulatory mechanism for many proteins, including oncoproteins and other pathogenic proteins. The oncoprotein Bcr-Abl relies on oligomerization via its coiled-coil domain for its kinase activity, suggesting that a designed coiled-coil domain with enhanced binding to Bcr-Abl and reduced self-oligomerization would be therapeutically useful. Key mutations in the coiled-coil domain of Bcr-Abl were identified which reduce homo-oligomerization through intermolecular charge-charge repulsion yet increase interaction with the Bcr-Abl coiled-coil through additional salt bridges, resulting in an enhanced ability to disrupt the oligomeric state of Bcr-Abl. The mutations were modeled computationally to optimize the design. Assays performed *in vitro* confirmed the validity and functionality of the optimal mutations which were found to exhibit reduced homo-oligomerization and increased binding to the Bcr-Abl coiled-coil domain. Introduction of the mutant coiled-coil into K562 cells resulted in decreased phosphorylation of Bcr-Abl, reduced cell

Reprinted by permission from *J. Biol. Chem.* 2011 Aug 5; 286(31):27751-60. The computational work was performed by S. Pendley and appeared in his dissertation.

proliferation, and increased caspase-3/7 activity and DNA segmentation. Importantly, the mutant coiled-coil domain was more efficacious than the wild-type in all experiments performed. The improved inhibition of Bcr-Abl through oligomeric disruption resulting from this modified coiled-coil domain represents a viable alternative to small molecule inhibitors for therapeutic intervention.

Introduction

Coiled-coil domains are ubiquitous protein structural motifs found in approximately 10% of all eukaryotic proteins (1). Characterized by a heptad repeat (sequence of seven amino acids) and association of two or more α-helices, coiled-coils provide oligomerization capabilities (both homo- and hetero-oligomerization) useful for structural scaffolding and protein recognition. Coiled-coil domains are critical for regulating many processes involved in the pathogenesis of various diseases (2). Thus, rationally designed coiled-coils can be used as therapeutics by interfering with the activity of a pathogenic protein through oligomeric disruption. One example is enfuvirtide (Fuzeon®), a fusion inhibitor that disrupts the helix bundle formation necessary for HIV-1[5] viral entry (3), spawning the next-generation of rationally designed fusion inhibitors (4-8). The coiled-coil reported here was designed to bind to the target (Bcr-Abl) better than the target protein binds to itself while exhibiting minimal homo-oligomerization.

Coiled-coils are very well characterized, and the high correlation between their sequence and structure (9) is advantageous for rational design. Coiled-coil oligomerization involves hydrophobic interactions, salt bridge formation, and helicity. In

the heptad repeat, hydrophobic packing at the “a” and “d” positions (see Figure 4.1, green residues) helps drive association with further stability provided by the residues at positions “g” and “e” which are commonly charged and interact to form salt bridges (see Figure 4.1, red and blue residues). Since charged residues are routinely found at the “g” and “e” positions, mutating these residues in a rational manner to add salt bridges to favor formation of hetero-oligomers (10-12) and charge-charge repulsions to reduce the formation of homo-oligomers (13, 14) can change the affinity and specificity of the coiled-coil dimer.

Bcr-Abl exists primarily as a tetramer (more specifically as a dimer of dimers), facilitating the trans-autophosphorylation necessary to activate the tyrosine kinase domain (15, 16). Oligomerization of Bcr-Abl is achieved through a coiled-coil domain at the N-terminus of the protein. Bcr-Abl constructs lacking the N-terminal coiled-coil fail to induce chronic myelogenous leukemia (CML) in a murine model (15, 17) thus setting the stage for oligomeric disruption as a therapy. Proof of concept for using the coiled-coil domain to inhibit Bcr-Abl activity has already been demonstrated through retroviral transfection of the wild-type coiled-coil domain or addition of the purified protein attached to a cytoplasmic transduction peptide (18-22). To further this approach, we designed and tested a mutant coiled-coil (CCmut2) using both computational and *in vitro* experiments. This CCmut2 disfavors self-oligomerization (CCmut2:CCmut2) yet appears to bind more tightly to the target BcrAbl coiled-coil domain (CCmut2:Bcr-Abl) than the target’s native oligomerization partner (Bcr-Abl:Bcr-Abl), and resulted in superior inhibition of Bcr-Abl.

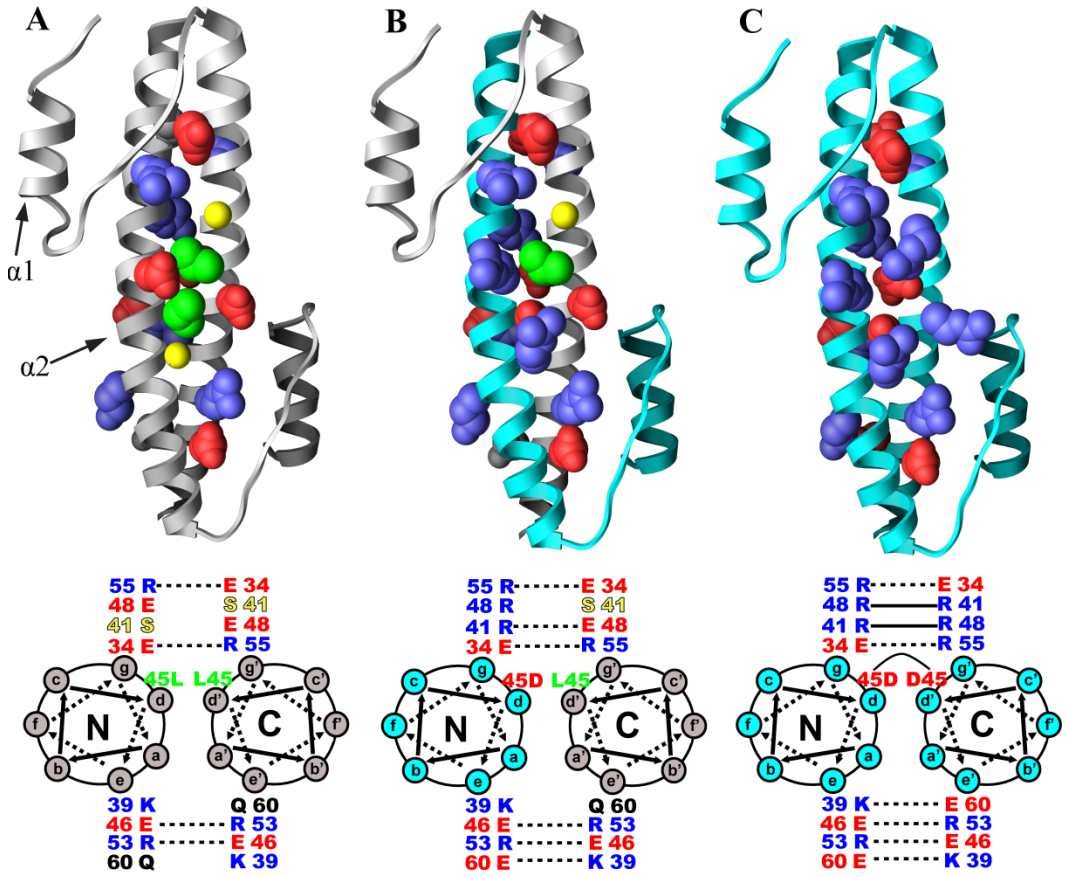

Figure 4.1: Ribbon diagrams, with the corresponding helical wheel diagram below, of the wild-type homodimer (A), wild-type:CCmut2 heterodimer (B), and CCmut2:CCmut2 homodimer (C). Grey ribbon (ribbon diagrams) or dots (helical wheel diagrams) represents the wild-type coiled-coil domain and cyan represents CCmut2. The side chains of key residues (E34, K39, S/R41, L/D45, E46, E/R48, R53, R55, and Q/E60) are shown as red (acidic), blue (basic), green (hydrophobic), yellow (serine), or black (glutamine) spheres (ribbon diagrams) or font (helical wheel diagrams). Dotted lines indicate possible ionic interactions and solid lines indicate charge-charge repulsions. Ribbon diagrams were generated with UCSF Chimera starting with the Bcr coiled-coil domain crystal structure (PDB ID: 1K1F).

The coiled-coil domain from Bcr-Abl consists of 72 amino acids composed of two α-helices (α1: residues 5-15 and α2: residues 28-67) that form an N-shaped configuration with two parallel helices connected by a short linker (see Figure 4.1A) (23). Upon dimerization, the resulting coiled-coil has an anti-parallel orientation with α2 at the core and α1 latching onto the backside of the opposing α2 helix (domain swapping) (1, 23). The majority of the dimer interface is composed of the classic knobs-in-holes type hydrophobic interactions from residues at the "a" and "d" positions (24). Further stabilization comes from 4 inter-chain salt bridges between residues in the α2 helices (Figure 4.1A), as well as packing of aromatic residues from the α1 helix and opposing α2 helix. As seen in Figure 4.1A, there are two uncharged residues (S41 and Q60) that are in the appropriate position for the formation of salt bridges with two charged residues (E32 and E48). Thus, mutation of S41 and Q60 to positively charged amino acids has the potential to provide two additional salt bridges with Bcr-Abl (Figure 4.1B), and thus enhance binding. However, while this provides more salt bridges in the hetero-oligomer, these mutations alone are undesirable as they allow the formation of a greater number of salt bridges in the homo-oligomer. To reduce homo-oligomerization in the mutant coiled-coil, residues proximal to charged residues on the opposing helix were considered as candidates for mutation to introduce charge-charge repulsion (13, 14). L45 and E48 were identified as two such residues (Figure 4.1C). In addition, previous reports have incorporated a C38A mutation primarily for crystallization purposes (1, 23), and this mutation was also studied. Putative mutations were investigated first through molecular modeling and state-of-the-art biomolecular simulation and free energy analysis to ascertain the impact on the coiled-coil structure and stability. Such *in silico* methods

provide a means to efficiently (and inexpensively) assess the influence of mutation. The resulting optimized mutant coiled-coil (CCmut2) contains five mutations (C38A, S41R, L45D, E48R, and Q60E) and was further assessed *in vitro*. Taken together, these results demonstrate the effectiveness of the mutant coiled-coil domain, and importantly, further illustrate the ability to rationally modify an existing coiled-coil domain to improve therapeutic efficacy.

Materials and Methods

Computational Modeling and Simulation

The initial model structure was obtained from the crystal structure (refined to 2.2 Å resolution) of the N-terminal oligomerization domain of Bcr-Abl (PDB ID: 1K1F, chains A and B) (25). Selenomethionine residues were mutated to methionine and position 39 was mutated back to cysteine to maintain consistency with the natural protein. Amino acid side-chain mutations were introduced using Deepview (Swiss PDB Viewer) (26) and by hand with the LEAP module from AMBER 9 (27). Molecular dynamics (MD) and free energy simulations were performed to assess the structure and stability of the model coiled-coil structures. Such methods have proven useful for reproducing and predicting the structure of proteins, including the folding of small proteins and influence of amino acid side chain substitutions (28-34). All simulations were completed using the AMBER modeling suite (27), the AMBER ff03 protein force field (35), with explicit solvent and counter-ions using standard simulation protocols, including minimization and ~40-90 ns of MD sampling with Ewald treatments of the electrostatics (36). For further detail, refer to the supplemental data. Representative plots of the root-mean-squared

deviations (RMSd) to the initial structure of the coiled-coil during the MD simulations can be found in Figure 4.S1 of the supplemental data. The MD trajectory results, effectively the time history of the atomic motions of the model structures at different intervals over the simulation, were analyzed with various tools. Quantification and comparison of the relative helical content was measured by calculating mean residue ellipticities at 222 nm (representative of helix content in CD spectra) of 5 individual 500 ps average structures spanning the final 5 ns of simulation of each coiled-coil dimer using the DichroCalc program (37). Structural helical content, or percent helicity defined as the number of residues in an α-helix divided by the total number of residues, was also calculated based on secondary structure as determined by peptide backbone Ψ and Φ torsions from the final 10 ns of simulation using the DSSP method (38) as implemented in UCSF Chimera (39). Intrahelical hydrogen bonds (i.e. carbonyl oxygen of residue 'i' to the amine nitrogen of residue 'i+4') were calculated over the final 10 ns of MD with distances less than 3.5 Å indicative of a hydrogen bond. To estimate the relative binding free energies of the coils in the dimers, MM-PBSA as implemented in AMBER (40) and described by Gohlke and Case (41) was applied to independent MD trajectories for the dimer and individual monomers. In addition to the post-processing of MD results, calculations of the relative free energy of binding with respect to the wild-type dimer ($\Delta\Delta G_{binding}$) were completed using more detailed thermodynamic integration (TI) methods for the CCmut2 dimers (42). On the basis of a thermodynamic cycle (see supplemental data Figure 4.S2), the relative free energy of binding can be calculated by "mutating" the original protein ($\lambda = 0$) to incorporate designed amino acid side chain point mutations ($\lambda = 1$) in both the dimer and monomeric states over different λ states *in*

silico. Incorporation of the five amino acid mutations considered using this approach was accomplished stepwise (see Figure 4.1B). Two steps were required to incorporate all five mutations to form the heterodimer mutant (CC-CCmut2) and an additional two steps to perturb the transition dimer into the homodimer (CCmut2-CCmut2). Similarly, two steps were used to incorporate the five mutations in the unbound monomer. Relatively long (6 ns equilibration, > 6 ns accumulation) MD simulations were performed at each λ for the TI. Further technical details are provided in the supplemental data.

Construction of Plasmids and Mutagenesis

The gene encoding the coiled-coil domain from Bcr-Abl (43) was amplified via PCR with the primers 5'- tgtaactcgagttatggtggacccggtg-3' and 5'-atgctctcgagaccggtcatag ctcttc-3' and subcloned into the XhoI site of the plasmid pEGFP-PS, an optimized protein switch (PS) (44, 45) for use in the nuclear translocation assay (46), and pEGFP-C1 (Clontech, Mountain View, CA, USA) for other experiments. These plasmids, named pPS-CC and pEGFP-CC respectively, were then used as the template DNA for site-directed mutagenesis using the QuikChange II Site-Directed Mutagenesis Kit (Stratagene, La Jolla, CA, USA) to generate five amino acid mutations (S41R, L45D, E48R, V49D, and Q60E). The primers used for the mutagenesis were 5'-ggagcgctgcaaggcccgcattcggcgcgacgagcagcgggacaaccaggagcgcttccgcatgatctacctggagacgtt gctggccaagg-3' and the reverse complement. Another site-directed mutagenesis was carried out to make C38A and D49V mutations with the primers 5'-caggagctggagcgcgccaaggcccgcattcg-3' (and reverse complement) and 5'-gcgacgagcagcgggtgaaccaggagcgcttcc-3' (and reverse complement). The final constructs

were termed pEGFP-CCmut2 and pPS-CCmut2. The primers 5'-cgcaagggagctcccatcatcatcatcatcttgaagttctttttcaaggtcctatggtggacccggtgggcttc-3' and 5'-agcatggatccctaccggtcatagctcttctttttccttggc-3' were used to PCR amplify wild-type and mutant coiled-coil domains and subcloned into pMAL-c2x (New England Biolabs, Ipswich, MA, USA) at the SacI and BamHI sites to generate pMAL-H6-PP-CC and pMAL-H6-PP-CCmut2 used for protein expression. The primers 5'-tgtaactcgagttatggtggacccggtg-3' and 5'-atgctctcgagccggtcatagctcttc-3' were used to PCR amplify both coiled-coil genes (wild-type and mutant), and each was subsequently subcloned into the XhoI site of pDsRed2-N1 (Clontech) to make pDsRed-CC and pDsRed-CCmut2. Similarly, the primers 5'-tgtaaggcccagccggccatggtggacccggtg-3' and 5'-cggggcgcggccgcccggtcatagctcttctttttc-3' were used to insert the genes into the plasmid pEFVP16 (mammalian two-hybrid prey vector containing the VP16 activation domain, obtained from Dr. T.H. Rabbitts, LIMM, Leeds, UK) at the SfiI and NotI sites to generate pEFVP16-CC and pEFVP16-CCmut2. The primers 5'-tgtaagaattcatggtggacccggtg-3' and 5'-atgctgaattcaccggtcatagctcttc-3' were used to insert the coiled-coils into the vector pM1 (mammalian two-hybrid bait vector containing the Gal4 binding domain, obtained from Dr. T.H. Rabbitts) at the EcoRI site to generate pM1-CC and pM1-CCmut2.

Cell Lines and Transient Transfection

Cells were maintained in a 5% CO_2 incubator at 37°C. K562 (a kind gift from Kojo Elenitoba Johnson, Univ. of Michigan) and Cos-7 cells (ATCC) were grown in RPMI (GIBCO, Invitrogen, Carlsbad, CA, USA) supplemented with 10% FBS (Hyclone Laboratories, Logan, UT, USA), 1% penicillin-streptomycin (GIBCO), 0.1% gentamicin

(Hyclone), and 1% L-glutamine (Hyclone). K562 cells were passaged every two days and maintained between 0.1-1 x 10^6 cells/mL. The Amaxa Nucleofector II (Lonza Group Ltd, Basel, Switzerland), was used to transfect 2 x 10^6 cells with 5-8 μg DNA in solution V following the manufacturer's recommended protocol and nucleofection program (T-013). Cos-7 cells were passaged every 2-3 days and transfected 24 hrs after seeding the cells using Lipofectamine LTX (Invitrogen) as recommended by the supplier.

Protein Purification and Circular Dichroism (CD)

Fusion proteins consisting of maltose binding protein (MBP), a His-tag, a PreScission Protease site, and CC or CCmut2 were expressed in BL21star DE3 E. *coli* cells (Invitrogen) from pMAL-H6-PP-CC or pMAL-H6-PP-CCmut2 plasmids. The proteins were purified over amylose resin (New England Biolabs) with gravity flow, cleaved with PreScission Protease (a kind gift from Dr. Chris Hill, Utah), and MBP-H6 removed by purification over HisPur Cobalt resin, (Thermo Scientific, Waltham, MA, USA). Reverse phase HPLC was performed as a final purification before lyophilizing the protein. CC and CCmut2 purified proteins were confirmed through mass spectrometry (Mass Spectroscopy and Proteomics Core Facilities, U. of Utah). CD experiments were performed on an Aviv 410 CD spectrometer (Biomedical Inc., Lakewood, NJ, USA). Measurements from 190-300 nm (1 nm steps) were taken on 10 μM protein solutions in PBS (50 mM sodium phosphate, 150 mM NaCl, 0.5 mM DTT, pH 7.2) in a 1 mm pathlength cuvette. Three sec equilibration times were allowed prior to each measurement, and the signal was averaged over 3 sec. The average of 3 scans was used for each solution. Thermal denaturation was monitored in a 1 cm cuvette at 222 nm

every 2°C from 10°C to 95°C, and back down to 10°C in 10°C steps. The protein concentrations used were 10 μM CC, 10 μM CCmut2, or 5 μM CC + 5 μM CCmut2. In addition, a mixing cell cuvette was used with 2.5 μM CC in one chamber and 7.5 μM CCmut2 in the other chamber with spectra acquired prior to and post mixing. After mixing and before data acquisition, the sample was incubated at 80 °C for 10 min, and then allowed to re-equilibrate at 10 °C.

Nuclear Translocation Assay

The nuclear translocation assay (NTA) was performed as previously described (46). Briefly, this assay uses a nuclear-localization inducible protein switch fused to a protein of interest and measures its ability to translocate a second protein into the nucleus. Here, the protein fused to the protein switch was either the coiled-coil domain or mutant coiled-coil domain, and its ability to translocate a cotransfected coiled-coil domain or mutant coiled-coil domain into the nucleus was measured. Twenty-four hrs after transient transfection of Cos-7 cells, 200 nM dexamethasone, or an equal volume of ethanol (carrier) was added to the cells and incubated for 1 hr. 0.5 μL H33342 (nuclear dye) was added and incubated for another 15 min. before imaging the cells with a fluorescence microscope as previously described (43). The percentage of protein localized in the nucleus was quantified with and without ligand to determine the nuclear increase after ligand induction.

Mammalian Two-Hybrid Assay

The pM1-CC or pM1-CCmut2 (bait), pEFVP16-CC or pEFVP16-CCmut2 (prey), pG5-Fluc (reporter; obtained from Dr. T.H. Rabbitts), and pRL-CMV (for normalization; obtained from Dr. T.H. Rabbitts) plasmids were co-transfected in RPMI without antibiotics into $7.5x10^4$ Cos-7 cells in a white 96-well plate (Cellstar, Greiner Bio-One, Monroe, NC, USA) in a 10:10:10:1 ratio. Twenty-four hrs after transfection the media was replaced with complete RPMI, and 48 hrs after transfection both the Firefly and Renilla luminescence were measured using the Dual-Glo Luciferase Assay (Promega) reagents per the manufacturer's recommendations. The mean from duplicate samples were taken from 5 separate experiments. pAD-SV40 and pBD-p53 (Stratagene) plasmids were used for the positive control, and pM1 lacking the coiled-coil gene was used as the negative control. A relative response ratio was calculated by first normalizing the individual Firefly luminescence to the Renilla luminescence. The negative control was subtracted from the mean of the duplicate experimental values, and scaled by dividing by the difference between the positive and negative controls ($\frac{Experiment-Ctrl^-}{Ctrl^+-Ctrl^-}$).

Cell Proliferation and Western Blotting

Forty-eight hrs following transfection of K562 cells with pEGFP-C1, pEGFP-CC, or pEGFP-CCmut2, trypan blue exclusion was used to determine cell proliferation (cell viability). Cells were pelleted (3×10^6) and resuspended in 600 μL lysis buffer (62.5 mM Tris-HCl, 2% w/v SDS, 10% glycerol, 50 mM DTT, 0.01% w/v bromophenol blue). Standard western blotting procedures were followed using antibodies to detect the phosphorylated forms of Bcr-Abl, STAT5, CrkL, as well as β-actin as a loading control.

The primary antibodies (anti-pAbl(Y245): 73E5, Cell Signaling Technology; anti-pSTAT5(Y694): E208, Abcam; anti-pCrkl(Y207): #3181, Cell Signaling Technology; anti-actin: mAbcam 8226, Abcam) were detected with anti-mouse (Ab6814, Abcam) or anti-rabbit (#7074, Cell Signaling Technology) HRP-conjugated antibodies before the addition of ChemiGlo (AlphaInnotech, Cell Biosciences, Santa Clara, CA, USA) chemiluminescent substrate and detection with a FluorChem FC2 imager (AlphaInnotech). The resulting bands were quantified through densitometry and normalized to the β-actin bands.

Colony Forming Assay

Twenty-four hrs following transfection of pEGFP-C1, pEGFP-CC, or pEGFP-CCmut2, K562 cells were resuspended in Iscove's modified Dulbecco's media (Stem Cell Technologies, Vancouver, BC, Canada**)** with 2% FBS, and 1000 cells were seeded in Methocult H4230 methylcellulose medium (Stem Cell Technologies) in the absence of cytokines. Imatinib mesylate (IM; a kind gift from Novartis) was added to 1000 untransfected K562 cells seeded in Methocult at the time of seeding. Each group of treated cells was seeded into two separate plates. Colony formation was assessed 7 days after seeding cells by counting colonies in a 200 μm^2 area of the plate and calculating the mean number of colonies per treatment. Experiments were replicated at least 3 times and compared to control (cells transfected with pEGFP-C1).

Caspase-3/7 Assay

Forty-eight hrs following transfection of pEGFP-C1, pEGFP-CC, or pEGFP-

CCmut2, 3 x 10^6 K562 cells were pelleted and resuspended in 50 µL lysis buffer provided in the EnzChek Caspase-3/7 Assay Kit #2 (Invitrogen). Cells were frozen at -80 °C, and then centrifuged at 5,000 x g for 5 min. Lysates were transferred to a black 96-well plate (Cellstar, Greiner Bio-One, Monroe, NC, USA), and 50 µL 2x AMC-DEVD substrate was added and incubated at room temperature for 30 min. Fluorescence was measured with excitation 342 nm and emission 441 nm on a SpectraMax M2 plate reader (Molecular Devices, Sunnyvale, CA, USA).

Fluorescence Microscopy and DNA Segmentation

Forty-eight hrs following transfection of pEGFP-C1, pEGFP-CC, or pEGFP-CCmut2, K562 cells were transferred to 2-well live cell chambers, 1 µL of the nuclear stain H33342 was added, and the cells were incubated at 37°C for 15 min. Cells were then analyzed with an inverted fluorescence microscope (Olympus IX701F, Scientific Instrument Co., Sunnyvale, CA, USA) with high-quality narrow band GFP filter (excitation HQ480/20 nm, emission HQ510/20 nm, beam splitter Q4951p, Chroma Technology Corp., Brattleboro, VT, USA). Cells were photographed with an F-view Monochrome CCD camera using a 60x objective, and were selected based on EGFP fluorescence. The nuclei of at least 50 transfected cells (EGFP fluorescence) per group were classified as either healthy (round or kidney shaped) or segmented (punctate) (47, 48) and the percentage of cells with segmented DNA was calculated.

Results

Computational Modeling

Rational design, molecular modeling, molecular dynamics (MD), and free energy simulations were used to predict favorable attributes, specificity, and energetics in order to facilitate the choice of coiled-coil modifications that stabilize binding of the mutant coiled-coil domain with Bcr-Abl (CCmut2:CC) while destabilizing self-oligomerization (CCmut2:CCmut2). Initial simulations monitored increases in α-helicity as an indirect correlate for improved free energy of binding of mutant pairs (49, 50) and focused on mutations to potentially improve salt bridge interactions, increase stability through formation of a disulfide bond, improve helicity in the backbone though alanine mutations to position "f", and destabilizing mutations to improve specificity.

Alanine mutations in the peptide backbone of the C-terminal coiled-coil region were designed at residues Gln33, Gln47, Phe54, and Thr61 to increase the α-helicity (49-51). Comparisons of the helicity as measured by circular dichroism and secondary structure between the homodimer (CCmut:CCmut) and heterodimer (CCmut:CC) suggested that this design actually decreases the helicity and shows poor specificity for the heterodimer over the homodimer (see Table 4.1, #3, CD and secondary structure) Visualization of the coiled-coil monomer structure suggests that the designed alanine mutations have disrupted local intrahelical hydrogen bonds which may affect secondary structure and protein folding.

Cys38 exists as unbound free thiol in the native protein, and its close proximity to position 52 might allow the formation of a disulfide bond that could further stabilize the

Table 4.1. Overview of comparative helicity calculations for various mutations of the Bcr coiled-coil domain. Helicity of simulated coiled-coil dimers using the calculated circular dichroism of the peptide, the percent of the residue which is defined as α-helical according to Ψ and Φ backbone dihedral torsions (using the DSSP method), and the percent of α-helical specific hydrogen bonds (< 3.5 Å) formed between i and i+4 residues at ps intervals over the final 10 ns of MD relative to the total number of potential interactions (the total number of residues minus 4). Row #6 was the only set of mutations tested that indicated a more favorable homodimer than the heterodimer, and was termed CCmut1 and used in subsequent MM-PBSA experiments as a negative control. Row #8 contains the set of mutations found to exhibit the optimal reduced homo-oligomerization paired with improved hetero-oligomerization and was termed CCmut2 for subsequent MM-PBSA and thermodynamic integration studies, as well as the *in vitro* experiments.

Mutations	Dimer	Circular Dichroism		Secondary Structure		Hydrogen Bonds	
		$[\Theta]_{222}$	S.D.	Helicity (%)	S.D.	i, i+4 hb (%)	S.D.
1. None (wild-type)	Homo	*-20943*	858	*66.6*	1.7	*56.6*	2.7
2. S41R, E48R, Q60E	Hetero	*-21580*	672	*70.0*	2.0	*56.9*	2.8
	Homo	*-20961*	678	*66.5*	2.9	*59.4*	2.7
3. Q33A,Q47A, F54A,T61A	Hetero	*-20884*	477	*66.3*	2.5	*60.6*	2.5
	Homo	*-20787*	760	*65.1*	2.2	*56.4*	3.2
4. E52C	Hetero	*-20521*	796	*67.8*	2.2	*55.9*	2.7
5. S41R, L45D, E48R, Q60E	Hetero	*-20330*	1329	*66.8*	1.9	*52.9*	3.0
	Homo	*-19398*	679	*66.2*	2.0	*56.5*	2.4
6. S41R, L45D, E48R, V49D, Q60E (CCmut1)	Hetero	*-19696*	765	*67.8*	2.0	*56.9*	2.7
	Homo	*-20352*	671	*69.1*	2.5	*59.2*	2.8
7. C38A, S41R, E48R, Q60E	Hetero	*-21493*	90	*70.0*	2.4	*61.5*	2.5
	Homo	*-21463*	265	*70.0*	2.6	*61.4*	2.5
8. C38A, S41R, L45D, E48R, Q60E (CCmut2)	Hetero	*-21186*	695	*67.7*	2.4	*59.1*	2.8
	Homo	*-17964*	507	*59.3*	2.6	*50.7*	2.4
9. C38A, S41R, L45D, E48R, V49D, Q60E	Hetero	*-19651*	456	*64.2*	2.5	*54.0*	2.5
	Homo	*-16770*	312	*64.2*	1.8	*50.4*	3.3

structure. An engineered disulfide was modeled by incorporating a cysteine residue at position 52. Visualization of the heterodimer and analysis of the structure helicity (see Table 4.1, #4, CD) suggests that the geometry of the disulfide is not ideal and introduces structural disturbances.

Three point mutations were designed in the wild-type monomer to improve binding to the oncoprotein: S41R, E48R, and Q60E. When these three designed point mutations were modeled, helicity of the homodimer and heterodimer mutants exceeded the wild-type dimer (see Table 4.1, compare #1 vs. #2) suggesting improved binding due to more favorable electrostatic interactions. The improved helicity of the mutant homodimer over the Bcr-Abl wildtype dimer may, however, result in decreased specificity for the heterodimer form. Destabilizing point mutations to improve the heterodimer specificity included designed aspartate mutations in the hydrophobic core (L45D and L49D), and were evaluated as both single and double mutations. Both mutations together decreased the secondary structure (and stability) of the heterodimer (see Table 4.1, #6 and #9), whereas L45D maintained heterodimer specificity (see Table 4.1, #5). The final mutation converted an exposed thiol group (Cys38) to alanine and, in conjunction with the four prior mutations, stabilized the heterodimer over both the mutant homodimer and the wild-type dimer (see Table 4.1, compare #1 vs. #8). Thus, the optimal mutant coiled-coil domain (termed CCmut2) contains C38A, S41R, L45D, E48R, and Q60E mutations. Specificity as measured by helicity suggests that the mutant homodimer (CCmut2:CCmut2) is significantly less stable than the wild-type (CC:CC) and the heterodimer (CC:CCmut2).

MM-PBSA and thermodynamic integration energy calculation methodologies, the

latter being more quantitative and accurate, were subsequently used to analyze the two sets of mutations. Both approaches validated the previous indications which suggested CCmut2 exhibits improved heterodimer stability compared to the wild-type oligomerization (see Table 4.2). Further, CCmut2 is shown to have reduced homo-oligomerization. Together, MM-PBSA and thermodynamic integration energy calculations suggest improved binding and specificity of CCmut2.

In vitro Experiments Validate the Design

To substantiate the computational circular dichroism calculations, wavelength scans were performed on protein solutions of CCmut2, CC, and a mixture of CCmut2 and CC. As seen in Figure 4.2A, all three protein solutions produced the typical pattern characteristic of α-helices with similar helicity. Given the relatively small number of mutations that distinguish CCmut2 from wild-type CC, and since the mutations are designed to alter oligomerization while retaining helicity, it is reasonable to not expect major differences in their experimentally measured helicity. However, the modifications do clearly destabilize the mutant homodimer as is made apparent in the thermal denaturation of the proteins (Figure 4.2B). While CC demonstrated a melting temperature (T_m) consistent with previous reports of 83 °C (23), a large decrease in T_m is found for the CCmut2, T_m = 63 °C (Figure 4.2B), confirming the decreased stability of the mutant homo-oligomer. When CCmut2 was mixed with CC in a 1:1 ratio two distinct melting transitions are evident (Figure 4.2B, black triangles), however a third T_m was not readily apparent. This suggests the CC-CCmut2 hetero-dimer is either iso-energetic with one of the two homo-dimers or that it simply did not form. To further assess the

Table 4.2. MM-PBSA and thermodynamic relative free energy of binding results (in kcal/mol). MM-PBSA results were found by subtracting the absolute free energies of the unbound monomers from the calculated free energy of coiled-coil dimer using separate MD trajectories. Thermodynamic integration calculations followed the scheme described in supplemental data Figure 4.S2 using intermediate coiled-coil dimers to build a consistent transition from the wild type coiled-coil dimer to the CCmut2 dimers. Results from both calculations were reported relative to the wild-type coiled-coil dimer (CC-CC).

Dimer	MM-PBSA		Thermodynamic Integration	
	$\Delta\Delta G_{binding}$ (kcal/mol)	Stderr (kcal/mol)	$\Delta\Delta G_{binding}$ (kcal/mol)	Stddev (kcal/mol)
CC:CC	0.0	3.2	0.0	0.0
CC:CCmut1	11.7	3.0	-	-
CCmut1:CCmut1	25.5	0.1	-	-
CC:CCmut2	-1.3	3.1	-1.1	0.5
CCmut2:CCmut2	11.4	3.0	3.2	0.8

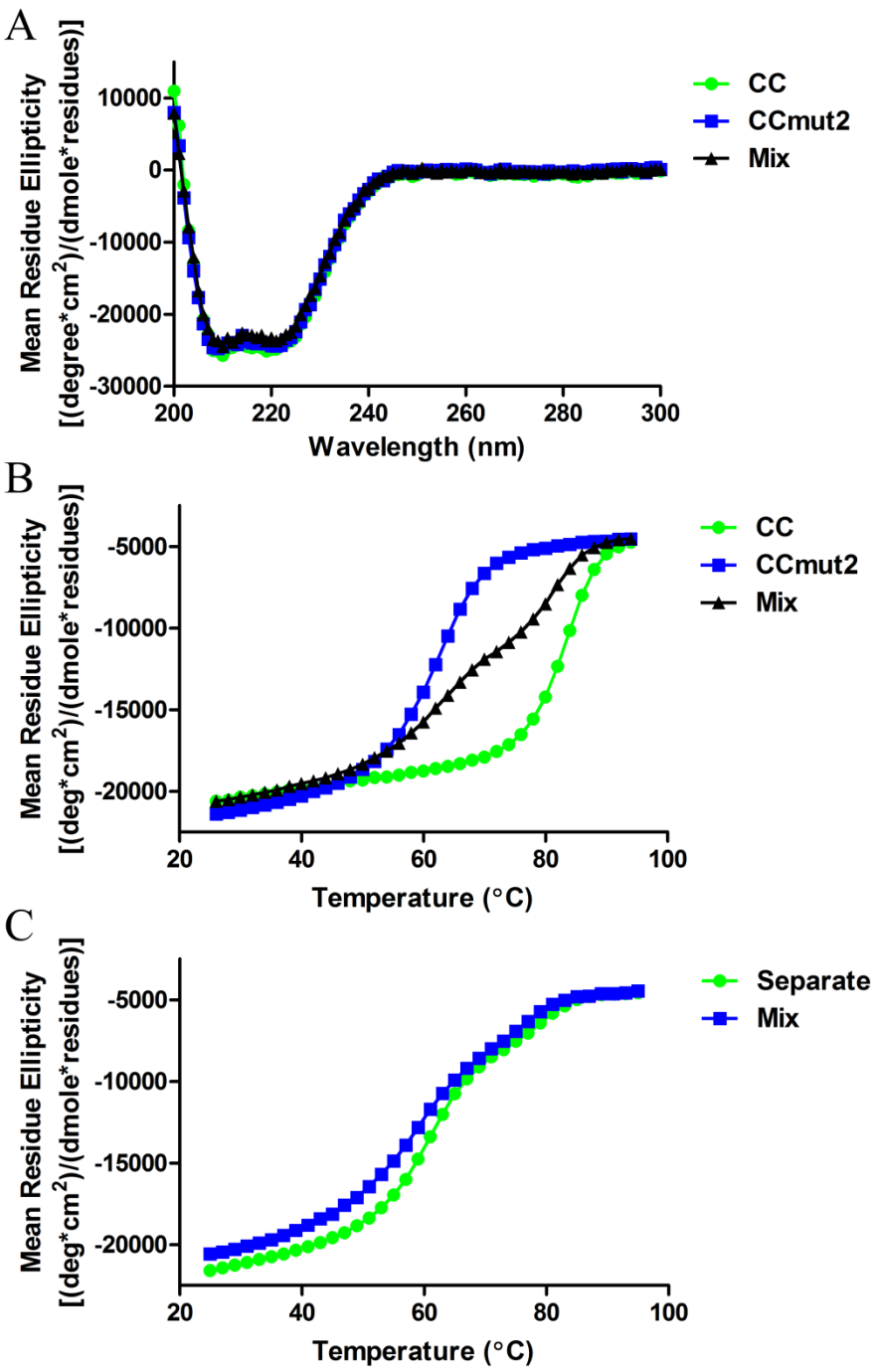

Figure 4.2**:** Circular dichroism wavelength scans and thermal denaturation. A) Alpha-helices exhibit a characteristic double absorption minimum at≈208 nm and 222 nm. CC: green circles, CCmut2: blue squares, Mix: black triangles. The lines represent the average from 3 scans. B) Thermal denaturation curves in 1cm cuvette. Ratio of CC to CCmut2 used in mix was 1:1. CC: green circles, CCmut2: blue squares, Mix: black triangles. C) Thermal denaturation curves in mixing cell cuvette using 2.5 μM CC and 7.5 μM CCmut2. Separate (pre-mixing): green circles, Mix: blue squares.

formation of the hetero-dimer a 3:1 (CCmut2:CC) ratio was studied in a mixing cell cuvette (Figure 4.2C) both before and after mixing. The mixing shifts the curve, most predominantly at lower temperatures and only slightly at higher temperatures, suggesting the formation of a new species (as seen in Figure 4.2C). The shift in the curve at lower temperatures can be accounted for by the decreased CCmut2 concentration due to formation of hetero-dimers. The small difference in the curves at higher temperatures suggests the formation of hetero-oligomers that are nearly iso-energetic or slightly less stable than the CC homo-oligomers. Consistent with the computational modeling, the primary improvement made through these mutations is in the specificity granted by a less stable mutant homo-dimer while retaining the ability to oligomerize with wild-type.

The optimally designed mutant coiled-coil was created through site-directed mutagenesis on a plasmid encoding the Bcr-Abl coiled-coil for cell based *in vitro* experiments and further validation. First, the nuclear translocation assay (NTA) (46) was used to study the interaction (Figure 4.3a). This assay measures the ability of a nuclear-inducible protein switch (PS) fused to one form of the coiled-coil domain to alter the nuclear localization of another form of the coiled-coil domain. Essentially, the interaction between the coiled-coil domains is indicated by an increase in fluorescence in the nucleus. The high level of nuclear translocation resulting from the mutant coiled-coil domain (Figure 4.3a, middle column) is likely to stem from both the reduced homo-oligomerization as well as the improved binding to the wild-type coiled-coil domain. To specifically address whether the designed mutations were limiting the homo-oligomerization, the interaction between two mutant coiled-coil domains (CCmut2:CCmut2) was assayed and found to be indistinguishable from the negative

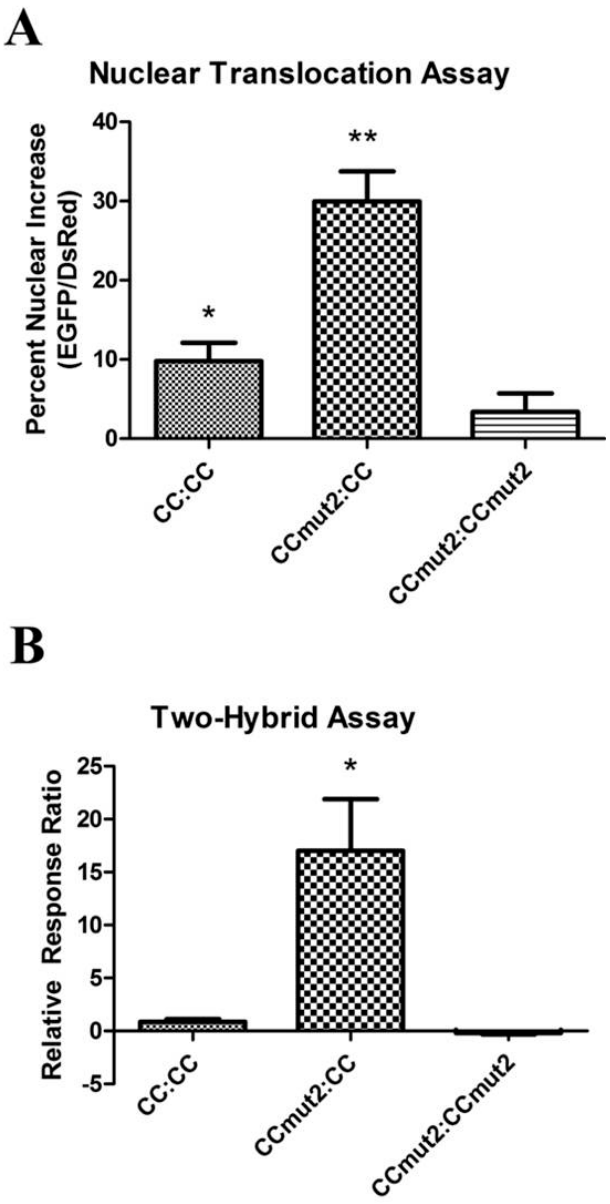

Figure 4.3: Binding of the homo- and hetero-dimers tested through the nuclear translocation assay (NTA) and mammalian two-hybrid assay. A) Figure modified from Dixon and Lim (46). The NTA measures the ability of a nuclear-inducible protein switch (PS) fused to a protein of interest to cause a second interacting protein to translocate into the nucleus, and is monitored through fluorescence microscopy (fused to EGFP and DsRed respectively). The assay was performed in Cos-7 cells that do not contain Bcr-Abl. Each experiment was performed in triplicate with at least eight cells analyzed per experiment. Statistical significance determined using one-way ANOVA with Tukey's posttest. * $p<0.01$, ** $p<0.001$ compared to control (pDsRed2-N1/EGFP-PS-CC, not included in graph); B) Mammalian two-hybrid assay in Cos-7 cells. Statistical significance determined using one-way ANOVA with Tukey's posttest. * $p<0.01$ compared to CC:CC interaction (n=5).

control (not included in graph). These same interactions were also studied in a mammalian two-hybrid assay to further validate the results. Similar to the NTA results, the greatest binding was found between the mutant and wild-type coiled-coil domains (CCmut2:CC, Figure 4.3B, 2nd column), and the homo-oligomerization between two mutants (CCmut2:CCmut2, Figure 4.3B, 3rd column) was not statistically distinguishable from the negative control (not included in graph). Together, the NTA and two-hybrid results indicate the proposed mutations have reduced the homo-oligomerization of the mutant coiled-coil domain and improved the binding to the wild-type coiled-coil domain.

Next, the oligomeric disruption of Bcr-Abl was indirectly measured through assaying the activity of Bcr-Abl. As the oligomeric state of Bcr-Abl is correlated to its activity, if the oligomerization is disrupted it will cause a reduction in Bcr-Abl activity (decrease in phosphorylation). After transfecting either the wild-type or mutant coiled-coil domain into K562 cells, western blotting with an antibody that specifically recognizes the phosphorylated form of Bcr-Abl was used to determine the activity. Under identical experimental conditions, the wild-type coiled-coil domain had minimal effect on the level of phosphorylation of Bcr-Abl (Figure 4.4A, 3rd column), whereas the mutant coiled-coil domain reduced the phosphorylation level to 35% (Figure 4.4A, last column). Further, the phosphorylation of two proteins known to be phosphorylated by Bcr-Abl, STAT5 and CrkL, was also tested. Again, the wild-type coiled-coil domain had minimal effect while the mutant coiled-coil domain reduced the phosphorylation of both proteins (Figure 4.4B, 3rd and 4th columns). The decreased phosphorylation of Bcr-Abl suggests that the mutant coiled-coil domain is capable of interacting with the endogenous Bcr-Abl, and not just the isolated coiled-coil domain as used in the previous NTA and

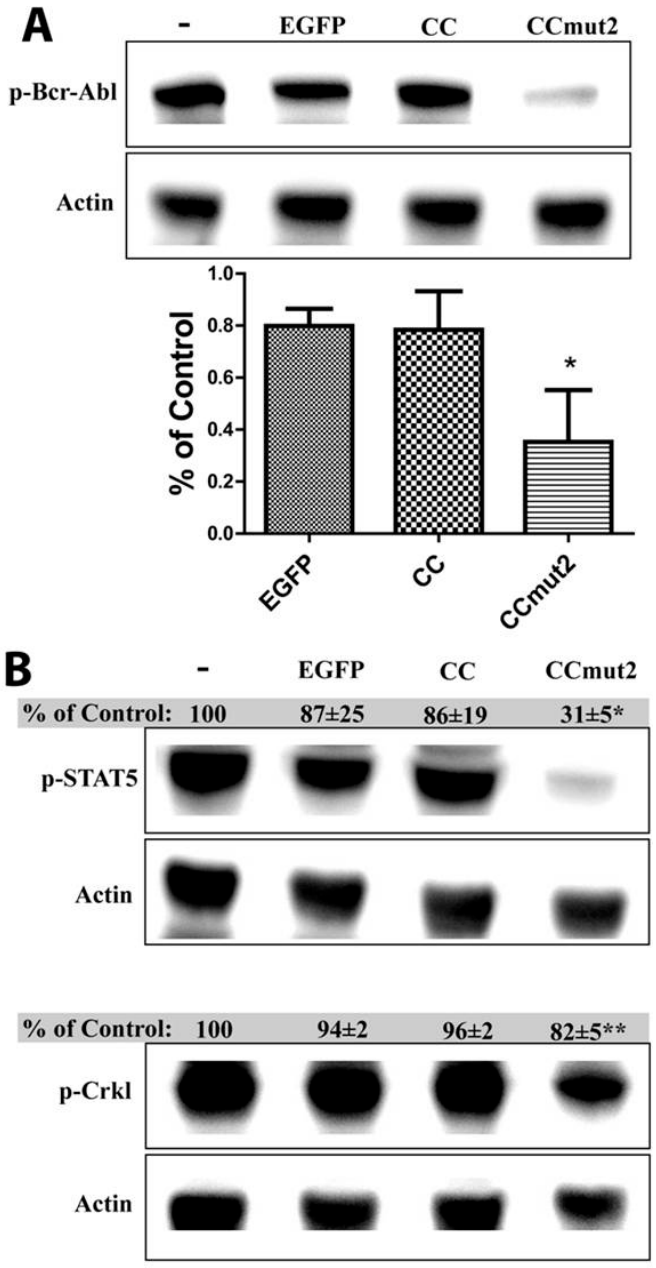

Figure 4.4: Representative images of western blots to detect the phosphorylated form of Bcr-Abl (A) and two substrates of Bcr-Abl, STAT5 and CrkL (B). The phosphorylation of Bcr-Abl is indicative of the tyrosine kinase activity, and is shown to be decreased by the addition of CCmut2 (percent p-Bcr-Abl from untreated K562 cells is indicated graphically). The proteins STAT5 and CrkL are also phosphorylated when Bcr-Abl is active, and are secondary indicators of the Bcr-Abl activity. Western blotting followed by densitometry was replicated three times on lysates from three separate transfections. The level of p-Bcr-Abl, as a percentage of the untreated cells, is shown graphically in A, and the level of p-STAT5 and p-CrkL (±st. dev.) is indicated above the representative images. Statistical significance was determined using one-way ANOVA with Tukey's posttest (n=3). *$p<0.05$, **$p<0.01$ compared to cells transfected with EGFP.

two-hybrid experiments. Moreover, the decreased level of phosphorylation provides insight into the oligomeric disruption and inhibitory potential of the mutant coiled-coil domain.

Inhibition of Bcr-Abl through oligomeric disruption, as with inhibition through tyrosine kinase inhibitors, should relieve the upregulation of signaling pathways resulting in mis-regulated cell proliferation. The effect of the coiled-coil domains on cell proliferation was measured through cell counts with trypan blue exclusion. While the wild-type coiled-coil domain demonstrated a slight effect on the number of proliferating cells, the mutant coiled-coil domain was most effective at decreasing the number of proliferating cells (Figure 4.5A). Furthermore, the effect on proliferation was measured via a colony forming assay, and again the mutant coiled-coil domain was found to cause the greatest reduction in cell proliferation (Figure 4.5B, column 2), similar to that seen with imatinib (Figure 4.5B, column 3).

As CML cells become dependent on the signaling pathways up-regulated by Bcr-Abl, the inhibition of Bcr-Abl and reprieve of that signaling should also induce apoptosis. As one indication of the ability of the coiled-coil constructs to induce apoptosis, the activity of caspase-3/7 was measured in a fluorimetric assay. In a trend similar to that found in all previous experiments, the mutant coiled-coil domain again produced the greatest result, and was the only construct able to induce the activation of caspase activity at a statistically significant level (Figure 4.5C, 3rd column). Similar experiments with CCmut2 in cells that do not express Bcr-Abl (1471.1 and Cos-7), as expected, did not show an increase in caspase activity (data not shown).

Finally, as a measure of late stage apoptosis, DNA segmentation (of K562 nuclei)

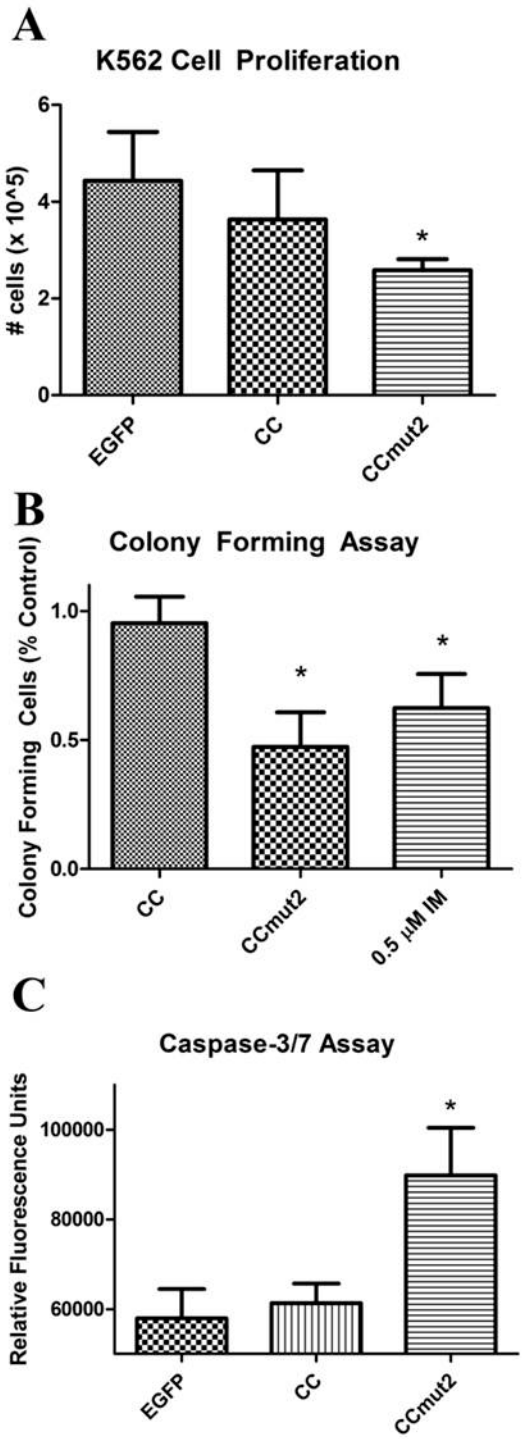

Figure 4.5: Inhibition of the Bcr-Abl through expression of CCmut2 results in decreased proliferation of K562 cells and activation of apoptosis. A) Proliferation of K562 cells as determined by cell counts with trypan blue exclusion. B) Proliferation of K562 cells as determined by colony forming assays; IM, Imatinib mesylate. C) Induction of apoptosis as measured through activation of caspase-3/7. For A-C, statistical significance was determined using one-way ANOVA with Tukey's posttest. * $p<0.01$, ** $p<0.001$ compared to control (cells transfected with pEGFP-C1).

was measured (47, 48). Cells transfected with CCmut2 revealed segmented nuclei, a hallmark of apoptosis as shown in Figure 4.6 (column 3, arrows). CC and control (EGFP) transfected cells had healthy (round) nuclei. The percentage of CCmut2 transfected cells demonstrating apoptosis was 29.4% compared to 4.29% for CC and 0.75% for EGFP control. Additionally, phase contrast images (Figure 4.6, column 1) demonstrated morphological changes indicative of apoptosis including zeotic blebbing, cell shrinkage, and cell fragmentation (43, 48). Finally, in a control cell line (1471.1 cells) minimal DNA segmentation (less than 2%) was observed after EGFP, CC, or CCmut2 was transfected (data not shown). The inhibition of cell proliferation and the induction of apoptosis illustrate the therapeutic potential of oligomeric disruption through this modified coiled-coil.

Discussion

Rational design, molecular modeling, MD simulation, and free energy analysis identified modifications to the Bcr-Abl coiled-coil to improve interaction with Bcr-Abl, while also reducing mutant homodimer (CCmut2:CCmut2) interactions. The optimal set of mutations served as the lead, reducing the need to test an overwhelming number of possible mutations or combination of mutations *in vitro*. The *in vitro* experiments performed with this construct confirmed the computational results and demonstrated that this designed mutant coiled-coil has an enhanced capability to oligomerize with Bcr-Abl. The design incorporated charge-charge repulsions between two mutant coiled-coil domains to reduce the homo-oligomerization, thereby making the mutant more available for interaction with the target, Bcr-Abl. Residues with the potential to form additional

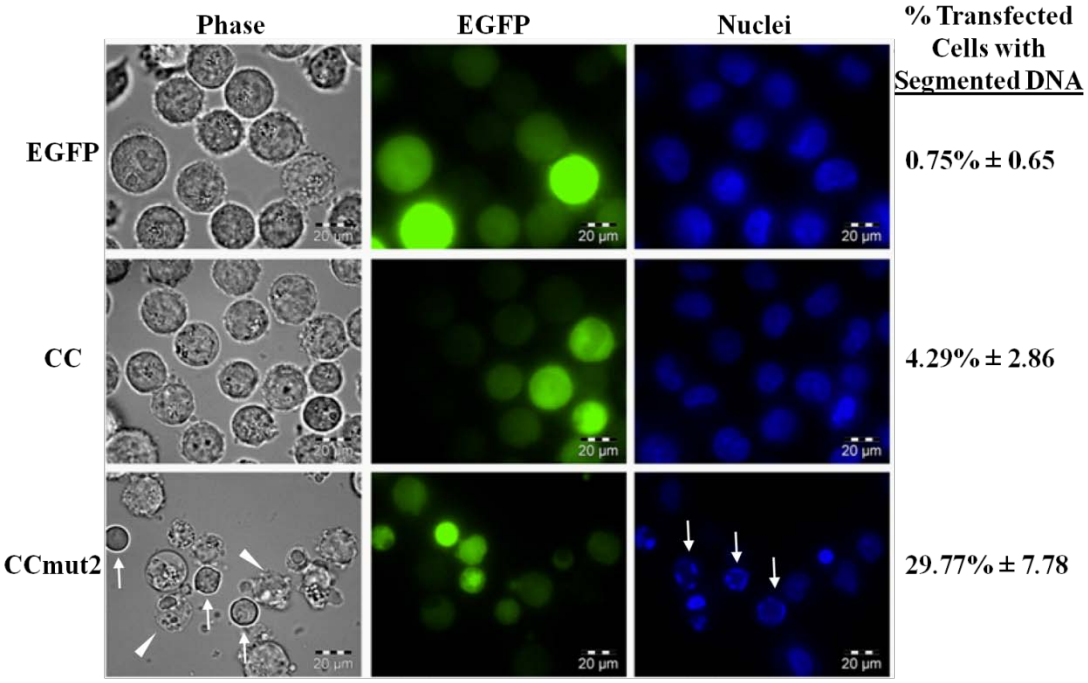

Figure 4.6: Fluorescence microscopy for morphological evaluation of nuclei. Cells transfected with CCmut2 (bottom row) appear shrunken (column 1, arrows) or zeotic (column 1, arrowheads) and exhibit segmented (punctuate) nuclei (column 3, arrows), hallmarks of late apoptotic cells. The far right column summarizes the percentage of transfected cells determined to have segmented DNA. Statistical significance was determined using one-way ANOVA with Tukey's posttest. *$p<0.001$ compared to control (cells transfected with pEGFP-C1).

favorable electrostatic interactions with Bcr-Abl were also introduced to increase the binding affinity between the mutant and Bcr-Abl. Although further structural characterization could confirm that the hypothesized interactions are indeed occurring, both the computational modeling and *in vitro* experiments strongly indicate that the modifications to the coiled-coil domain lead to a more specific, better binding coiled-coil partner for Bcr-Abl.

Although an isolated coiled-coil domain from Bcr-Abl should, in principal, oligomerize with Bcr-Abl, the isolated coiled-coil domain also has the ability to form homo-oligomers. Given that an isolated coiled-coil domain is smaller, there is likely less entropic penalty for formation, and therefore it should be less effective as a therapeutic due to the decreased effective concentration of the monomer and need for dissociation of the dimer for activity. Our approach to a more potent therapeutic involved the design of a coiled-coil domain with reduced ability to self-oligomerize while also exhibiting enhanced oligomerization with the target. This goal was confirmed through both computational modeling and *in vitro* experiments. Alternative treatments for CML are still needed due to the inability to eliminate CML stem cells, resistance to small molecule inhibitors, and ineffective treatment of advanced stages of the disease (52-56). Given the importance the coiled-coil domain has in the regulation of Bcr-Abl activity, it has long been hypothesized that this domain could be used therapeutically. This modified Bcr-Abl coiled-coil domain has a heightened ability to inhibit the oncogenicity of Bcr-Abl and warrants further exploration as an alternative approach to treat CML.

Acknowledgments

We acknowledge the use of DNA/Peptide Core (NCI Cancer Center Support Grant P30 CA042014, Huntsman Cancer Institute), NIH R01-CA129528 (Lim), NIH R01-GM079383 (Cheatham), and computer time from NSF TG-MCA01S027 and the Center for High Performance Computing at U. Utah. We would like to thank Dr. Debbie Eckert for technical assistance in protein purification, and Jonathan Constance, Rian Davis, Mohanad Mossalam, Matthew Weinstock, and Dr. Michael Kay for scientific discussions.

Supplemental Data

Molecular Dynamics Simulation Protocols

The initial models of the coiled-coil proteins were solvated by surrounding the compound with at least a 10 Å water layer in all directions within a truncated octahedron using on the order of 12000 explicit TIP3P (57) waters. Explicit Na^+ and Cl^- salt ions using the AMBER-adapted Aqvist parameters set (58) were added to neutralize the system. Ionization states for the amino acids reflected the expected solvent-exposed pKa states at physiological pH, i.e. charged Arg, Lys, Glu, and Asp residues. Energy minimization was performed for 500 steps first in the system with restrained protein atoms (50 kcal mol^{-1} $Å^{-2}$) and then in an unrestrained system. Initial minimization was followed by heating to 300K at constant volume over a period of 10 ps using harmonic restraints with a force constant of 2 kcal mol^{-1} $Å^{-2}$ on the protein atoms. Subsequent unrestrained equilibration at 300K followed for 500 ps. Bond lengths involving hydrogen atoms were constrained with SHAKE (59, 60) with a geometric tolerance for the constraint of 0.00001 Å during the coordinate resetting. Periodic boundary conditions

were applied using the particle mesh Ewald method (PME) with a less than 1 Å charge grid and cubic B-spline interpolation (36).

All of the production molecular dynamics (MD) simulations were performed with a 2 fs time step and a direct space non-bonded cutoff of 10 Å with the pair list of atomic interactions built out to 11 Å and heuristic update of the pair list triggered when any atom moved more than 0.5 Å since the previous update. During production runs, the center of mass translational motion of the entire system was removed after the initial velocity assignments and subsequently every 5000 MD steps. Constant temperature was maintained with weak coupling to a heat bath with a 2 ps time constant (61). Pressure (1 atm) was maintained using isotropic position scaling with Berendsen weak coupling algorithm with a 1.0 ps pressure relaxation time (61). Production molecular dynamics simulations for each peptide were completed on the 40-90 ns timescale.

Analysis of the MD Trajectories

Quantification and comparison of the relative helical content was measured by calculating mean residue ellipticities at 222 nm (representative of helix content in CD spectra) of 5 individual 500 ps average structures spanning the final 5 ns of simulation of each coiled-coil dimer using the DichroCalc program (37). A Gaussian curve type was assumed with a bandwidth at half maximum of 12.5 nm and two backbone transitions. For these calculations, the Hirst et al. semi-empirical parameter set (62) was used due to its accuracy with helical proteins (37).

MM-PBSA

Standard MM-PBSA methods were employed as described in the main text. Solvent and ion molecules were stripped from the trajectories and the approximate free energy of binding was calculated by subtracting absolute free energies of the monomers from the dimer. For the free energy of binding calculations, 250 snapshots were taken spanning the final 5 ns of stable simulation. Normal mode analysis calculations to determine the translation, rotational, and vibrational entropies of the protein were completed using a subset of 50 snapshots spanning the range of the original 250 snapshot set. Minimization of each snapshot in the gas phase used the conjugate gradient method with a distance dependant dielectric screened by a dielectric constant of 4 until the RMS of the elements of the gradient vector were less than 10^{-6} kcal mol^{-1} $Å^{-1}$. The polar contributions to the solvation free energy of the protein were calculated using the Poisson-Boltzmann (PB) equation as implemented in Delphi II (63). For the calculations, two grid points per Å were used, the solute filled 80% of the grid box, and 5000 finite difference iterations were performed to ensure convergence of the results. Atomic parse radii consistent with prior Amber Delphi parameterization were used (41, 64). For the nonpolar contribution to the free energy of solvation, the molecular surface area was calculated using the molsurf program implemented in AMBER (27) with a 1.4 Å probe radius (41). The surface tension proportionality constant was set to 0.00542 kcal mol^{-1} $Å^{-2}$, and the free energy of nonpolar solvation for a point solute b was set to 0.92 kcal mol^{-1}. This is consistent with the use of Delphi as the PB solver (41). Protein enthalpic components represent the average potential energies of the protein over the snapshots.

Thermodynamic Integration

Calculations of the relative free energy of binding with respect to the wild-type dimer ($\Delta\Delta G_{binding}$) were completed using thermodynamic integration for the CCmut2 dimers. Incorporation of the five amino acid mutations was accomplished stepwise (see Figure 1B from the main text). Two steps were required to incorporate all five mutations to form the heterodimer mutant (CC-CCmut2) and an additional two steps to perturb the transition dimer into the homodimer (CCmut2-CCmut2). Similarly, two steps were used to incorporate the five mutations in the unbound monomer. Transitions from the wild-type dimer to the CCmut2 dimers were accomplished using three stages of thermodynamic integration at each step of the perturbation: the removal of atomic charges for changing atoms, a soft core potential stage for the conversion of atom types, and a stage to add atomic charges to the mutated atoms. All thermodynamic integrations simulations were performed using a particle mesh Ewald (PME) treatment of electrostatics, as previously described, with explicit solvent and neutralizing ions. Equilibrated structures were allowed to relax during 6 ns of molecular dynamics simulation followed by thermodynamic integration sampling for a minimum of 6 ns at each sampling point. Convergence of thermodynamic integration sampling was visualized by a plateau in the $\partial V/\partial\lambda$ time course. The first step transitions which incorporated four of the five mutations required significant sampling time exceeding 12 ns per λ value to affirm that convergence had occurred. For thermodynamic integration calculations involving soft core potentials, nineteen linear sampling points of λ between 0.05 and 0.95 were used. Calculations involving only the removal or addition of atomic charges used ten sampling points of λ between 0.5 and 0.95. Trapezoidal numerical

integration was used to sum the free energy of transitions. Comparing this approach against integrating a polynomial fit of the average weighted energetic value against λ resulted in a difference of less than 0.1 kcal/mol value.

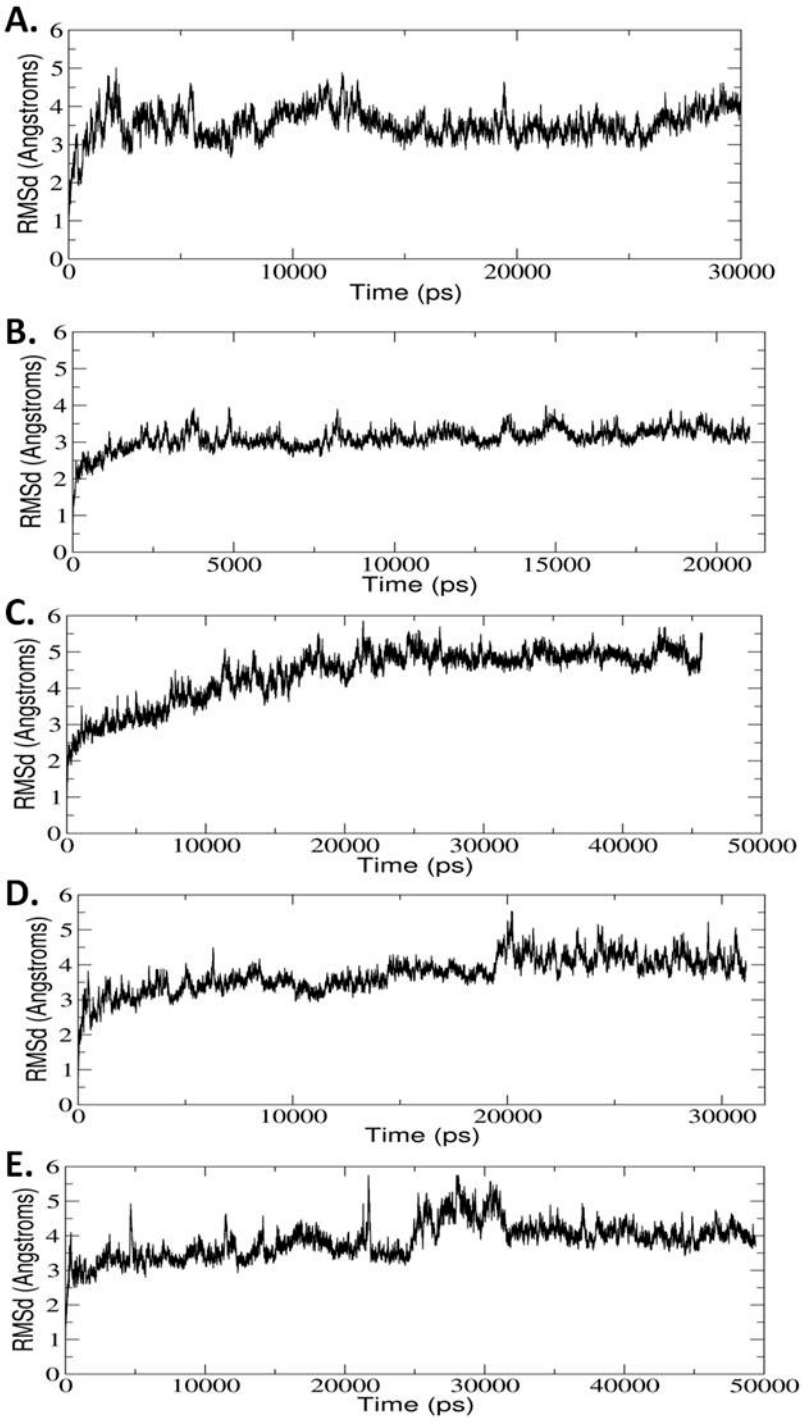

Supplemental Figure 4.S1: One dimensional root mean square deviation (RMSd) of coiled-coil dimers derived from the Bcr protein-protein binding domain. A) CC-CC B) CC-CCmut2 C) CCmut2-CCmut2 D) CC-CCmut1 E) CCmut1-CCmut1

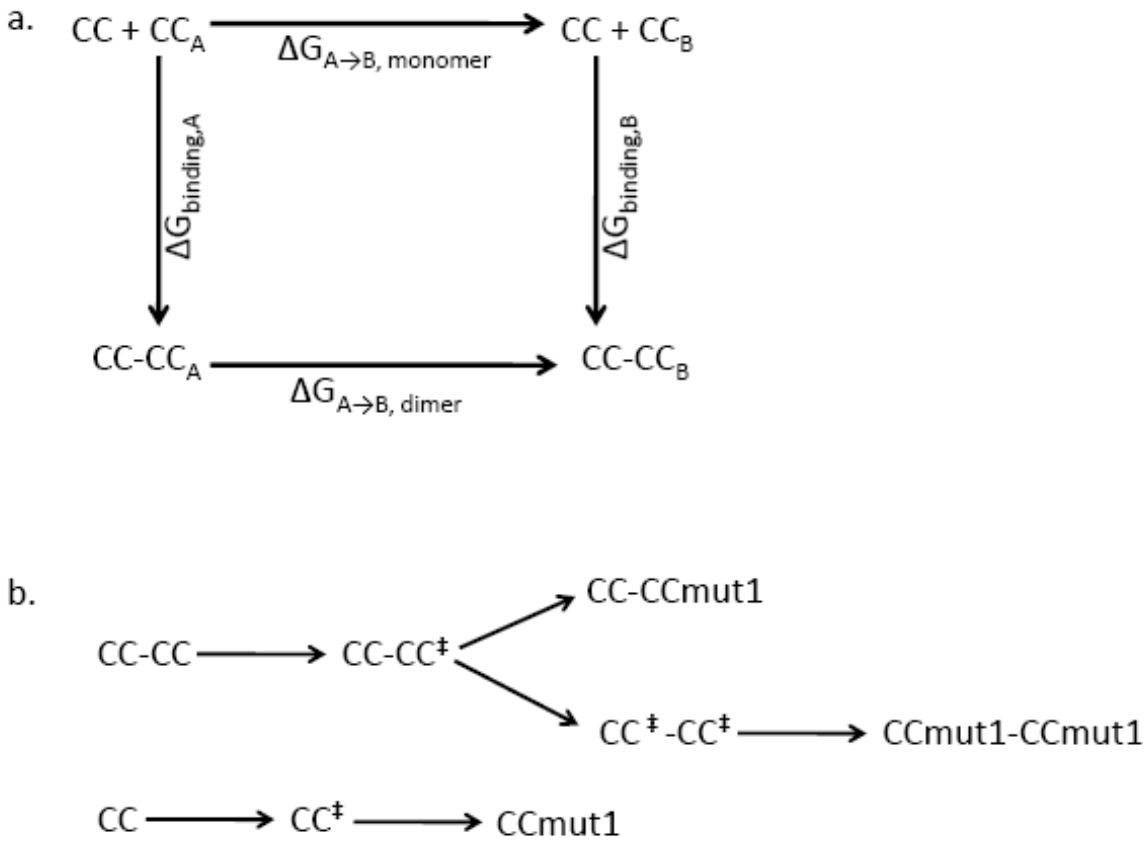

Supplemental Figure 4.S2. Thermodynamic integration approaches to calculate the relative free energy of binding for coiled-coil dimers were based on a thermodynamic cycle (A). Using this cycle the relative free energy of binding ($\Delta\Delta G_{binding}$) can be found using the free energy differences found by incorporating point mutations in the dimer and unbound monomers; $\Delta\Delta G_{binding} = \Delta G_{binding,B} - \Delta G_{binding,A} = \Delta G_{A\rightarrow B,dimer} - \Delta G_{A\rightarrow B,monomer}$. Five point mutations were designed in each monomer using the scheme presented in (B). Note that $CC^{‡}$ represents a transition coiled-coil that incorporates the C38A, S41R, E48R, and Q60E mutations.

References

1. Taylor CM, Keating AE. Orientation and oligomerization specificity of the Bcr coiled-coil oligomerization domain. Biochemistry 2005; 44: 16246-56.

2. Strauss HM, Keller S. Pharmacological interference with protein-protein interactions mediated by coiled-coil motifs. Handb Exp Pharmacol 2008: 461-82.

3. Matthews T, Salgo M, Greenberg M, Chung J, DeMasi R, Bolognesi D. Enfuvirtide: the first therapy to inhibit the entry of HIV-1 into host CD4 lymphocytes. Nat Rev Drug Discov 2004; 3: 215-25.

4. Dwyer JJ, Wilson KL, Davison DK, et al. Design of helical, oligomeric HIV-1 fusion inhibitor peptides with potent activity against enfuvirtide-resistant virus. Proc Natl Acad Sci U S A 2007; 104: 12772-7.

5. Otaka A, Nakamura M, Nameki D, et al. Remodeling of gp41-C34 peptide leads to highly effective inhibitors of the fusion of HIV-1 with target cells. Angew Chem Int Ed Engl 2002; 41: 2937-40.

6. Yan Z, Tripet B, Hodges RS. Biophysical characterization of HRC peptide analogs interaction with heptad repeat regions of the SARS-coronavirus Spike fusion protein core. J Struct Biol 2006; 155: 162-75.

7. Eckert DM, Malashkevich VN, Hong LH, Carr PA, Kim PS. Inhibiting HIV-1 entry: discovery of D-peptide inhibitors that target the gp41 coiled-coil pocket. Cell 1999; 99: 103-15.

8. Sia SK, Carr PA, Cochran AG, Malashkevich VN, Kim PS. Short constrained peptides that inhibit HIV-1 entry. Proc Natl Acad Sci U S A 2002; 99: 14664-9.

9. Parry DA, Fraser RD, Squire JM. Fifty years of coiled-coils and alpha-helical bundles: a close relationship between sequence and structure. J Struct Biol 2008; 163: 258-69.

10. Kammerer RA, Jaravine VA, Frank S, et al. An intrahelical salt bridge within the trigger site stabilizes the GCN4 leucine zipper. J Biol Chem 2001; 276: 13685-8.

11. Spek EJ, Bui AH, Lu M, Kallenbach NR. Surface salt bridges stabilize the GCN4 leucine zipper. Protein Sci 1998; 7: 2431-7.

12. Marqusee S, Baldwin RL. Helix stabilization by Glu-...Lys+ salt bridges in short peptides of de novo design. Proc Natl Acad Sci U S A 1987; 84: 8898-902.

13. Ryan SJ, Kennan AJ. Variable stability heterodimeric coiled-coils from manipulation of electrostatic interface residue chain length. J Am Chem Soc 2007; 129: 10255-60.

14. Gurnon DG, Whitaker JA, Oakley MG. Design and characterization of a homodimeric antiparallel coiled coil. J Am Chem Soc 2003; 125: 7518-9.

15. Zhang X, Subrahmanyam R, Wong R, Gross AW, Ren R. The NH(2)-terminal coiled-coil domain and tyrosine 177 play important roles in induction of a myeloproliferative disease in mice by Bcr-Abl. Mol Cell Biol 2001; 21: 840-53.

16. Arlinghaus RB. Bcr: a negative regulator of the Bcr-Abl oncoprotein in leukemia. Oncogene 2002; 21: 8560-7.

17. He Y, Wertheim JA, Xu L, et al. The coiled-coil domain and Tyr177 of bcr are required to induce a murine chronic myelogenous leukemia-like disease by bcr/abl. Blood 2002; 99: 2957-68.

18. Mian AA, Oancea C, Zhao Z, Ottmann OG, Ruthardt M. Oligomerization inhibition, combined with allosteric inhibition, abrogates the transformation potential of T315I-positive BCR/ABL. Leukemia 2009; 23: 2242-7.

19. Beissert T, Hundertmark A, Kaburova V, et al. Targeting of the N-terminal coiled coil oligomerization interface by a helix-2 peptide inhibits unmutated and imatinib-resistant BCR/ABL. Int J Cancer 2008; 122: 2744-52.

20. Beissert T, Puccetti E, Bianchini A, et al. Targeting of the N-terminal coiled coil oligomerization interface of BCR interferes with the transformation potential of BCR-ABL and increases sensitivity to STI571. Blood 2003; 102: 2985-93.

21. Huang SF, Liu DB, Zeng JM, et al. Cloning, expression, purification and functional characterization of the oligomerization domain of Bcr-Abl oncoprotein fused to the cytoplasmic transduction peptide. Protein Expr Purif 2009; 64: 167-78.

22. Guo XY, Cuillerot JM, Wang T, et al. Peptide containing the BCR oligomerization domain (AA 1-160) reverses the transformed phenotype of p210bcr-abl positive 32D myeloid leukemia cells. Oncogene 1998; 17: 825-33.

23. Zhao X, Ghaffari S, Lodish H, Malashkevich VN, Kim PS. Structure of the Bcr-Abl oncoprotein oligomerization domain. Nat Struct Biol 2002; 9: 117-20.

24. Crick FH. The packing of α-helices: simple coiled-coils. Acta Cryst 1953; 6: 689-97.

25. Zhao X, Ghaffari S, Lodish H, Malashkevich V, Kim P. Structure of the Bcr-Abl oncoprotein oligomerization domain. Nature Structural & Molecular Biology 2002; 9: 117-20.

26. Guex N, Peitsch M. SWISS-MODEL and the Swiss-PdbViewer: an environment for comparative protein modeling. Electrophoresis 1997; 18: 2714-23.

27. Case D, Darden T, Cheatham III T, et al. AMBER 9. University of California, San Francisco 2006.

28. Kollman PA, Massova I, Reyes C, et al. Calculating structures and free energies of complex molecules: Combining molecular mechanics and continuum models. Acc Chem Res 2000; 33: 889-97.

29. Huo S, Massova I, Kollman PA. Computational alanine scanning of the 1:1 human growth hormone-receptor complex. Journal of computational chemistry 2002; 23: 15-27.

30. Grant BJ, Gorfe AA, McCammon JA. Large conformational changes in proteins: signaling and other functions. Curr Opin Struct Biol 2010; 20: 142-7.

31. Lee EH, Hsin J, Sotomayor M, Comellas G, Schulten K. Discovery through the computational microscope. Structure 2009; 17: 1295-306.

32. Meli M, Colombo G. Molecular simulations of peptides: a useful tool for the development of new drugs and for the study of molecular recognition. Methods Mol Biol 2009; 570: 77-153.

33. Klepeis JL, Lindorff-Larsen K, Dror RO, Shaw DE. Long-timescale molecular dynamics simulations of protein structure and function. Curr Opin Struct Biol 2009; 19: 120-7.

34. Steinbrecher T, Labahn A. Towards accurate free energy calculations in ligand protein-binding studies. Curr Med Chem 2010; 17: 767-85.

35. Duan Y, Wu C, Chowdhury S, et al. A point-charge force field for molecular mechanics simulations of proteins based on condensed-phase quantum mechanical calculations. J Comput Chem 2003; 24: 1999-2012.

36. Essmann U, Perera L, Berkowitz ML, Darden T, Lee H, Pedersen LG. A Smooth Particle Mesh Ewald Method. J Chem Phys 1995; 103: 8577-93.

37. Bulheller B, Hirst J. DichroCalc--circular and linear dichroism online. Bioinformatics 2009; 25: 539.

38. Rost B, Sander C. Prediction of protein secondary structure at better than 70% accuracy. Journal of Molecular Biology 1993; 232: 584-.

39. Pettersen E, Goddard T, Huang C, et al. UCSF Chimera—a visualization system for exploratory research and analysis. Journal of computational chemistry 2004; 25: 1605-12.

40. Srinivasan J, Cheatham TE, Cieplak P, Kollman PA, Case DA. Continuum Solvent Studies of the Stability of DNA, RNA, and Phosphoramidateâ˜'DNA Helices. Journal of the American Chemical Society 1998; 120: 9401-9.

41. Gohlke H, Case DA. Converging free energy estimates: MM-PB(GB)SA studies on the protein-protein complex Ras-Raf. J Comput Chem 2004; 25: 238-50.

42. Gouda H, Kuntz ID, Case DA, Kollman PA. Free energy calculations for theophylline binding to an RNA aptamer: Comparison of MM-PBSA and thermodynamic integration methods. Biopolymers 2003; 68: 16-34.

43. Dixon AS, Kakar M, Schneider KM, Constance JE, Paullin BC, Lim CS. Controlling subcellular localization to alter function: Sending oncogenic Bcr-Abl to the nucleus causes apoptosis. J Control Release 2009; 140: 245-9.

44. Kakar M, Davis JR, Kern SE, Lim CS. Optimizing the protein switch: altering nuclear import and export signals, and ligand binding domain. J Control Release 2007; 120: 220-32.

45. Kakar M, Cadwallader AB, Davis JR, Lim CS. Signal sequences for targeting of gene therapy products to subcellular compartments: the role of CRM1 in nucleocytoplasmic shuttling of the protein switch. Pharm Res 2007; 24: 2146-55.

46. Dixon A, Lim C. The nuclear translocation assay for intracellular protein-protein interactions and its application to the Bcr coiled-coil domain. Biotechniques; 49: 519-24.

47. Barrett KL, Willingham JM, Garvin AJ, Willingham MC. Advances in cytochemical methods for detection of apoptosis. J Histochem Cytochem 2001; 49: 821-32.

48. Willingham MC. Cytochemical methods for the detection of apoptosis. J Histochem Cytochem 1999; 47: 1101-10.

49. Jelesarov I, Bosshard HR. Thermodynamic characterization of the coupled folding and association of heterodimeric coiled coils (leucine zippers). J Mol Biol 1996; 263: 344-58.

50. Hodges RS, Saund AK, Chong PC, St-Pierre SA, Reid RE. Synthetic model for two-stranded alpha-helical coiled-coils. Design, synthesis, and characterization of an 86-residue analog of tropomyosin. J Biol Chem 1981; 256: 1214-24.

51. Zitzewitz JA, Ibarra-Molero B, Fishel DR, Terry KL, Matthews CR. Preformed secondary structure drives the association reaction of GCN4-p1, a model coiled-coil system. J Mol Biol 2000; 296: 1105-16.

52. Santos FP, Ravandi F. Advances in treatment of chronic myelogenous leukemia--new treatment options with tyrosine kinase inhibitors. Leuk Lymphoma 2009; 50 Suppl 2: 16-26.

53. Kantarjian HM, Cortes J, La Rosee P, Hochhaus A. Optimizing therapy for patients with chronic myelogenous leukemia in chronic phase. Cancer; 116: 1419-30.

54. Jamieson CH. Chronic myeloid leukemia stem cells. Hematology Am Soc Hematol Educ Program 2008: 436-42.

55. Janssen JJ, Schuurhuis GJ, Terwijn M, Ossenkoppele GJ. Towards cure of CML: why we need to know more about CML stem cells? Curr Stem Cell Res Ther 2009; 4: 224-36.

56. Martin MG, Dipersio JF, Uy GL. Management of the advanced phases of chronic myelogenous leukemia in the era of tyrosine kinase inhibitors. Leuk Lymphoma 2009; 50: 14-23.

57. Jorgensen WL, Chandrasekhar J, Madura JD, Impey RW, Klein ML. Comparisons of simple potential functions for simulating liquid water. J Chem Phys 1983; 79: 926-35.

58. Aqvist J. Ion-water interaction potentials derived from free energy perturbation simulations. Journal of Physical Chemistry 1990; 94: 8021-4.

59. Ryckaert JP, Ciccotti G, Berendsen HJC. Numerical integration of the cartesian equations of motion of a system with constraints: Molecular dynamics of n-alkanes. Journal of Computational Physics 1977; 23: 327-41.

60. Barth E, Kuczera K, Leimkuhler B, Skeel RD. Algorithms for constrained molecular dynamics. Journal of computational chemistry 1995; 16: 1192 - 209.

61. Berendsen HJC, Postma JPM, van Gunsteren WF, DiNola A, Haak JR. Molecular dynamics with coupling to an external bath. Journal of Computational Physics 1984; 81: 3684-90.

62. Cox R, Hirst W. Calculation of the circular dichroism of bihelical ribonucleic acids as a function of nucleotide composition. Biochemical Journal 1976; 155: 292.

63. Rocchia W, Alexov E, Honig B. Extending the Applicability of the Nonlinear Poisson- Boltzmann Equation: Multiple Dielectric Constants and Multivalent Ions†. J Phys Chem B 2001; 105: 6507-14.

64. Massova I, Kollman P. Combined molecular mechanical and continuum solvent approach (MM-PBSA/GBSA) to predict ligand binding. Perspectives in drug discovery and design 2000; 18: 113-35.

CHAPTER 5

SECOND-GENERATION MODIFICATIONS TO THE BCR COILED-COIL DOMAIN: FURTHER MUTANT HOMO-DIMER DESTABILIZATION FOR ENHANCED OLIGOMERIZATION WITH BCR-ABL

Abstract

The oncoprotein Bcr-Abl relies heavily on oligomerization for trans-autophosphorylation responsible for its aberrant activity (1, 2). The formation of Bcr-Abl homo-oligomers is achieved through a coiled-coil domain at the N-terminus of the protein (3, 4). We have previously shown that a modified version of this coiled-coil domain, CCmut2, exhibits improved ability to interfere with the oligomeric state of Bcr-Abl and resulted in decreased proliferation of K562 cells and induction of apoptosis (5). A major contributing factor to these enhanced capabilities is the destabilization of the CCmut2 homo-dimers, increasing the availability to interact with and inhibit Bcr-Abl. Here, we identified an additional residue that could be mutated to further destabilize the mutant homo-dimer. Incorporation of this modification into CCmut2 generated what we termed CCmut3, and resulted in further improvements in the binding properties with the wild-type coiled-coil domain representative of Bcr-Abl. A separate construct containing one revert mutation, CCmut4, did not demonstrate improved oligomeric properties and indicated the importance of the L45D mutation. In spite of the improved oligomerization

capabilities, a distinguishable enhancement in effects on CML cells (versus CCmut2) was not detected and may be attributed to assay sensitivity or the oligomeric disruption already being maximized with CCmut2. In addition to functioning as an alternative to tyrosine kinase inhibitors, the improved binding demonstrated by CCmut3 establishes it as a Bcr-Abl binding domain that may be used to redirect Bcr-Abl to alternative subcellular locations with interesting therapeutic implications.

Introduction

In approximately the past decade, chronic myelogenous leukemia (CML) has been transformed from a deadly cancer into a manageable disease through the development of tyrosine kinase inhibitors (TKIs) (6, 7). Currently, there are three approved TKIs for the treatment of CML; imatinib, nilotinib, and dasatinib. Until only recently, imatinib has been considered the first-line therapy (8), with nilotinib and dasatinib reserved for cases of imatinib resistance, suboptimal outcome, or intolerability. Now, however, all three are FDA-approved for newly diagnosed chronic phase CML (9). While TKI therapy has proven effective for the management of CML, one particular resistant form, harboring an isoleucine mutation in the T315 gate keeper residue, however, is uninhibited by all of the currently approved TKIs (10-13). Ponatinib (14, 15) and DCC-2036 (16) are third-generation TKIs currently in clinical trials that have been shown to be effective against the T315I form. Nevertheless, TKIs are not without problems and are not a cure for CML (8, 9, 17, 18). Patients will need to continually manage the disease by endlessly taking the TKI. Thus, alternative approaches are still of scientific and therapeutic interest.

In healthy cells, the kinase activity of cellular Abelson kinase (c-Abl) is tightly controlled through Src Homology 3 (SH3) and SH2 domains as well as interaction with the myristoylated N-terminus (19-23). Under genotoxic stress and other activating conditions, phosphorylation of the SH2 domain, SH2-Y-kinase linker region, and activation loop of the Y-kinase domain results in activation of c-Abl (24-27). In the majority of CML cases, the Abl protein is fused onto the C-terminus of the breakpoint cluster region protein (Bcr), a fusion protein expressed from the Philadelphia chromosome (28-31). In the fusion protein the myristoylation is lost, and even though both the SH3 and SH2 regulatory domains are retained, the autoinhibition of the Y-kinase domain is relieved (19). The unregulated Y-kinase activity then phosphorylates and activates signaling pathways such as RAS, PI3K/AKT, and Src family kinases such as STAT5, to name only a few (32-34). The net result is inhibition of apoptosis, activation of cell proliferation, and an altered cell adhesion and motility, all engendering growth advantages and cancer.

Key to the constitutive Y-kinase activity found in Bcr-Abl is a trans-autophosphorylation process that phosphorylates critical activating residues (19, 35). This trans-autophosphorylation stems from the oligomeric state achieved through a coiled-coil (or oligomerization) domain at the N-terminus of the Bcr portion of the protein (1, 36, 37). Bcr-Abl constructs lacking the coiled-coil domain have diminished transformation potential (1), validating oligomerization as a pivotal role in oncogenicity through Bcr-Abl. An understanding of the correlation between the Y-kinase activity and oligomerization through the coiled-coil domain has inspired the use of an isolated coiled-coil domain for competition with the Bcr-Abl homo-oligomerization (35, 36, 38).

Formation of hetero-oligomeric structures between Bcr-Abl and the isolated coiled-coil domain prevents the trans-autophosphorylation necessary for constitutive activity leading to cancer, and is an interesting alternative to TKIs that bind at the Y-kinase domain.

The Bcr-Abl coiled-coil domain consists of 72 amino acids that fabricate two parallel α-helices connected through a short linker region (4). The dimerization interface is composed primarily from the second helix (α-2), residues 28-67. The first helix (α-1) functions as a swap domain and folds onto the backside of the opposing α-2 helix after dimerization. This dimer subsequently dimerizes to form a tetrameric dimer-of-dimers. While the tetrameric interface consists primarily of aromatic and hydrophibic interactions and is challenging for rational design, both hydrophobic and ionic interactions contribute to formation of the dimer interface (3, 4). Given that formation of dimers is a preceding step to formation of the tetramer, coupled with the fact that modifications to charged interactions in α-helices are more readily identified, analysis of the dimer interface permits logical modifications for improved oligomerization.

While it is possible to use the wild-type coiled-coil domain to interfere with the Bcr-Abl homo-oligomerization, the drawback is that there is no preference for interacting with Bcr-Abl over another isolated coiled-coil domain. As Bcr-Abl in the cell will already be found in the tetrameric state, the feasibility of using the wild-type domain relies heavily on pushing the equilibrium towards formation of hetero-oligomers through increased concentration of the isolated coiled-coil domain. The ideal coiled-coil domain would exhibit minimal homo-oligomerization and form hetero-oligomers that are more stable than the Bcr-Abl oligomeric structures. In attempt to generate a coiled-coil domain that more closely resembles the properties of the ideal coiled-coil domain, we have

rationally mutated residues in the Bcr-Abl coiled-coil domain. We previously demonstrated that modifications can be made to the Bcr-Abl coiled-coil domain to improve the oligomeric capabilities (5). The design approach was two-fold: decrease homo-dimer stability through incorporation of charge-charge repulsion, and increase hetero-dimer stability through formation of additional salt bridges. The resulting CCmut2 was found to not only have improved oligomeric properties, but further resulted in improved inhibition of Bcr-Abl and enhanced effects on CML cells. In spite of the aforementioned bi-fold design approach, there is much evidence supporting that the improved oligomeric properties stem primarily from decreased stability of the mutant homo-dimer coupled with the retention of the ability to oligomerize with Bcr-Abl, not necessarily the formation of a more stable hetero-dimer. This indicates the importance of reducing the formation of mutant homo-dimers to allow for interaction with Bcr-Abl.

In attempt to increase the hetero-dimer interaction, Q60 was mutated to glutamate in CCmut2 for the formation of an additional salt bridge with K39 of the Bcr-Abl coiled-coil domain. Notwithstanding, in the CCmut2 homo-dimer where both domains contain the Q60E mutation, an unintentional result is the possibility to form two sets of K39:E60 salt bridges (Figure 5.1A). In order to turn these undesired salt bridges that may contribute to stabilization of the mutant homo-dimer into charge-charge repulsions that can decrease the mutant homo-dimer stability, K39 was mutated to glutamate. This mutation, along with the other five mutations previously described for CCmut2, was termed CCmut3 (Figure 5.1B and C).

In analyzing possible mutations that led to CCmut2, it was discovered that

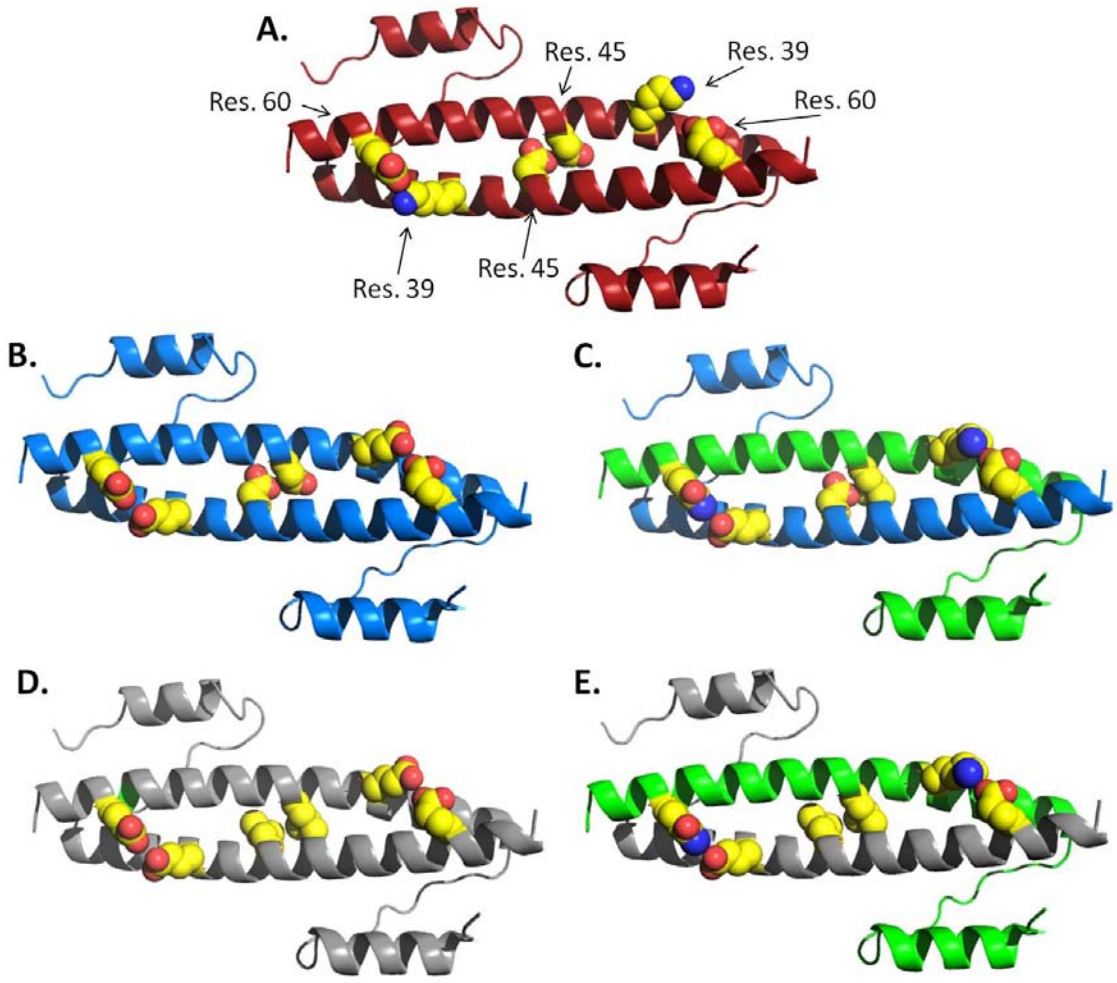

Figure 5.1. Ribbon diagrams of the modified coiled-coil domains. Only side chains from residues 39, 45, and 60 are illustrated as spheres and indicated in A. Red ribbon=CCmut2, Blue ribbon=CCmut3, Green ribbon=wild-type (WT), Gray ribbon=CCmut4. Yellow spheres=carbon, Red spheres=oxygen, Blue spheres=nitrogen. A) CCmut2 homo-dimer. The potential two sets of K39:E60 salt bridges are modeled along with the D45:D45 charge-charge repulsion. B) CCmut3 homo-dimer. The two sets of K39:E60 salt bridges are now replaced with two sets of E39:E60 charge-charge repulsions. The D45:D45 charge-charge repulsion is retained in the middle. C) WT:CCmut3 hetero-dimer. CCmut3 may form a K39:E60 salt bridges with WT as illustrated. As WT does not have negatively charged residue in close proximity to D45 of CCmut3, there is no charge-charge repulsion. D) CCmut4 homo-dimer. Similar to CCmut3 homo-dimer, the two sets of E39:E60 charge-charge repulsion are again illustrated. The D45:D45 charge-charge repulsion is now replaced with L45:L45 hydrophobic interaction in the middle. E) WT:CCmut4 hetero-dimer. The K39:E60 salt bridge is illustrated, and the L45:L45 hydrophobic interaction in the middle.

incorporation of both L45D and V49D mutations, mutations aimed at decreasing homo-dimer stability through charge-charge repuslsions, introduced a kink in the α-2 helix and was unfavorable. However, making either L45D or V49D mutations alone contributed to the specificity of the mutant coiled-coil, and L45D was chosen for incorporation into CCmut2. Residues 45 and 49 are unique among the set of possible mutations analyzed due to the fact that they are not located at "g" or "e" helical positions, but instead are located at the typical hydrophobic "d" and "a" positions. Although the L45D mutation was demonstrated to contribute to the decrease in homo-dimer stability, it may have the drawback of decreased hydrophobic interactions in the hetero-dimer. The additional charge-charge repulsion designed through the K39E mutation may obfuscate the need for charge-charge repulsion through the L45D mutation, and reverting the L45D mutation back to the original leucine may provide the benefit of better hydrophobic interactions with the Bcr-Abl coiled-coil domain (Figure 5.1D and E). Thus, CCmut3 with the revert mutation D45L, was termed CCmut4.

As a second iteration of a rationally designed coiled-coil domain for improved binding to Bcr-Abl, we demonstrate here that CCmut3, but not CCmut4, provides further enhancements of the oligomerization properties. CCmut3 produced similar effects as CCmut2 in inhibiting Bcr-Abl activity, decreasing CML cell proliferation, and inducing apoptosis in CML cells. In addition to an alternative inhibitor of Bcr-Abl, the enhanced binding may further prove beneficial for other interests currently underway in our laboratory involving the escorting of Bcr-Abl to other subcellular compartments.

Materials and Methods

Construction of Plasmids and Mutagenesis

The plasmids pEGFP-CC, pEGFP-CCmut2, pM1-CC, pM1-CCmut2, pEFVP16-CC, and pEFVP16-CCmut2 were constructed as previously described (Chapter 4, Page 78) (5). pM1-CCmut3 and pEFVP16-CCmut3 were created through site-directed mutagenesis using pM1-CCmut2 and pEFVP16-CCmut2 as the templates, respectively. The mutagenic primers were 5'-GCTGGAGCGCGCCGAGGCCCGCATTCGG-3' and 5'-CCGAATGCGGGCCTCGGCGCGCTCCAGC-3'. pM1-CCmut4 and pEFVP16-CCmut4 were created through site-directed mutagenesis using pM1-CCmut3 and pEFVP16-CCmut3 as the templates, respectively. The mutagenic primers were 5'-CCGCATTCGGCGCCTGGAGCAGCGGGTGAAC-3' and 5'-GTTCACCCGCTGCTC CAGGCGCCGAATGCGG-3'. The genes encoding CCmut3 and CCmut4 were then amplified through PCR using pM1-CCmut3 and pM1-CCmut4 as the templates, respectively, and the primers 5'-TGTAACTCGAGTTATGGTGGACCCGGTG-3' and 5'- ATGCTCTCGAGACCGGTCATAGCTCTTC-3'. The PCR products were then inserted into pEGFP-C1 (Clontech, Mountain View, CA, USA) at the XhoI restriction site. To create pmCherry-Bcr-Abl the gene encoding Bcr-Abl was digested out of pEGFP-Bcr-Abl (39) with EcoRI (New England Biolabs, Ipswich, MA, USA), and inserted into pmCherry-C1 (Clontech).

Cell Lines and Transient Transfection

The cells used all experiments were either K562 (model Ph^+ CML cells, a kind gift from Kojo Elenitoba Johnson, Univ. of Michigan) or Cos-7 (simian kidney cells,

ATCC), and were grown in RPMI (GIBCO, Invitrogen, Carlsbad, CA, USA) supplemented with 10% FBS (Hyclone Laboratories, Logan, UT, USA), 1% penicillin-streptomycin (GIBCO), 0.1% gentamicin (Hyclone), and 1% L-glutamine (Hyclone) and maintained in a 5% CO_2 incubator at 37 °C. K562 cells were passaged every two days and maintained between 0.1-1 x 10^6 cells/mL. The Amaxa Nucleofector II (Lonza Group Ltd, Basel, Switzerland), was used to transfect 2 x 10^6 cells with 5-8 μg DNA in solution V using nucleofection program (T-013) following the manufacturer's recommended protocol. Cos-7 cells were passaged every 2-3 days and transfected 24 hrs after seeding the cells using Lipofectamine LTX (Invitrogen) as recommended by the supplier.

Mammalian Two-Hybrid Assay

An in depth description of how the mammalian two-hybrid assay was carried out is described elsewhere (Chapter 4, Page 81) (5). In short, pM1-CC (or mutant), pEFVP16-CC (or mutant), pG5-Fluc (Promega, Madison, WI, USA), and pRL-CMV (Promega) plasmids were co-transfected into Cos-7 cells in a 10:10:10:1 ratio. pAD-SV40 and pBD-p53 (Stratagene, Agilent Technologies Inc., Santa Clara, CA, USA) plasmids were used for the positive control, and pM1 lacking the coiled-coil gene was used as the negative control. Forty-eight hrs after transfection both firefly and renilla luminescence were measured using the Dual-Glo Luciferase Assay (Promega) reagents per the manufacturer's recommendations. The mean from duplicate transfections were taken from five separate experiments. A relative response ratio was calculated using the following equation on the firefly values normalized to the renilla values:

($\frac{Experiment-Ctrl^{-}}{Ctrl^{+}-Ctrl^{-}}$). For ease of comparing to the wild-type coiled-coil interaction, the results were then normalized to the wild-type interaction.

Confocal Microscopy and Co-localization

Twenty-four hrs after seeding K562 cells into 4-well live-cell chambers (Lab-tek chamber slide system, Nalge NUNC International, Naperville, IL, USA) they were transfected with Lipofectamine LTX (Invitrogen). At least 24 hrs after transfection the cells were imaged. All images of cells were acquired on an Olympus IX81 FV1000-XY confocal microscope equipped with 405 diode, 488 argon, and 543 HeNE lasers using a 60X PlanApo oil immersion objective (NA 1.45) using Olympus FluoView software. Excitation and emission filters were as follows: EGFP, 488 nm excitation, emission filter 500-530 nm; mCherry, 543 nm excitation, emission filter 555-655 nm. Images were collected in sequential line mode. The exposure settings and gain of laser were kept constant and below detected pixel saturation for each group of cells. No crosstalk was observed between channels as determined by excitation with either the 488 nm or 543 nm laser lines, independently, while collecting fluorescence in both channels. Pixel resolution was kept at 1024 x 1024 with maximum of 2.5X digital zoom. Prior to statistical co-localization analysis all images were corrected for background noise (i.e., mean background intensity outside of cells). All experiments were completed in triplicate ($n \geq 3$). Region of interests (ROIs) were created around whole cells. Image and statistical analysis was performed with JACoP in ImageJ (http://rsb.info.nih.gov/ij) (40). Costes' automatic threshold was used to generate the quantitative co-localization coefficient (41).

Flow Cytometry

48 hrs following transfection of K562 cells with pEGFP-C1, pEGFP-CC, pEGFP-CCmut2, or pEGFP-CCmut3, 5 mL of cells were pelleted and resuspended in 0.5 mL of 1x annexin binding buffer (Invitrogen). Immediately before flow cytometry analysis, 0.5 μL of 7-aminoactinomycin D (7AAD, Invitrogen, 1 mg/mL) and 5 μL annexin V conjugated with allophycocyanin (annexin-APC, Invitrogen) were added to the cells. Flow cytometric analysis was performed on a FACSCantoII analyzer (Becton Dickinson, Franklin Lakes, NJ, USA) using BD FACSDiva v6.1.3 (BD) software. Both EGFP and 7AAD were excited with a blue laser with 488 nm wavelength, while APC was excited with a red laser with 635 nm wavelength. The fluorescence detector used for EGFP was 530/30 nm, the detector for 7AAD was 660/20 nm, and the detector for APC was 660/20 nm. The untransfected cells were excluded from analysis through gating on the EGFP fluorescence, and the percentage of transfected, apoptotic cells was quantified through combining the number of cells that stained positively for annexin-APC only (Q2) with the number of cells that stained positively for annexin-APC and 7AAD (Q4). All four plasmids were transfected three separate times for separate analysis (n = 3).

Cell Proliferation and Western Blotting

The cell proliferation and western blotting were carried out as previously described for CCmut2 (Chapter 4, Page 82) (5). Briefly, 48 hrs following transfection into 2.5 x 10^6 K562 cells trypan blue exclusion was used to determine the number of viable cells. For western blots, cell pellets were resuspended in 200 μL lysis buffer/10^6 cells and freeze thawed at -80°C. After protein gel electrophoresis and transfer to a

PVDF membrane, the membrane was probed with primary antibodies (anti-pAbl(Y245): 73E5, Cell Signaling Technology; anti-pSTAT5(Y694): E208, Abcam; anti-pCrkl(Y207): #3181, Cell Signaling Technology; anti-actin: mAbcam 8226, Abcam), followed by HRP-conjugated secondary antibodies (Ab6814, Abcam) or anti-rabbit (#7074, Cell Signaling Technology) before the addition of ChemiGlo (Alpha Innotech, Cell Biosciences, Santa Clara, CA, USA) chemiluminescent substrate and detection with a FluorChem FC2 imager (AlphaInnotech). Densitometry was performed on the phospho-bands and normalized to β-actin. Plasmids were transfected three separate times, and a western was performed on each lysate for analysis (n = 3).

Colony Forming Assay

The colony forming assay was carried out as previously described (Chapter 4, Page 83) (5). In short, 24 hrs following transfection into K562 cells, 1000 cells in Iscove's modified Dulbecco's media (Stem Cell Technologies, Vancouver, BC, Canada**)** with 2% FBS were seeded in Methocult H4230 methylcellulose medium (Stem Cell Technologies) in the absence of cytokines. Each group of treated cells was seeded in duplicates, and colony formation was assessed seven days after seeding cells by counting colonies in a 200 μm^2 area of the plate. Experiments were repeated at least three times and compared to control (cells transfected with pEGFP-C1).

Caspase-3/7 Assay

Caspase-3/7 assays were performed as previously described (Chapter 4, Page 83) (5). Briefly, 48 hrs following transfection into K562 cells, cell counts were performed

and 3 x 10^6 cells were resuspended in 50 µL EnzChek Caspase-3/7 lysis buffer (kit #2, Invitrogen). Cells were frozen at -80 °C, thawed, and the cell debris removed by centrifuged at 5,000 x g for 5 min. Lysates were mixed with 50 µL 2x AMC-DEVD substrate in a black 96-well plate (Cellstar, Greiner Bio-One, Monroe, NC, USA), and incubated at room temperature for 30 min. before measuring the fluorescence with excitation 342 nm and emission 441 nm on a SpectraMax M2 plate reader (Molecular Devices, Sunnyvale, CA, USA). Lysates from three separate transfections for each plasmid were assayed for caspase-3/7 activity (n = 3).

Fluorescence Microscopy & DNA Segmentation

A detailed description of the fluorescence microscopy and DNA segmentation can be found elsewhere (Chapter 4, Page 84) (5). In short, 48 hrs following transfection K562 cells were transferred to 2-well live cell chambers, 0.3 µL H33342 (nuclear dye, Invitrogen) was added, and the cells were incubated at 37°C for 15 min. Cells were then analyzed with an inverted fluorescence microscope (Olympus IX701F, Scientific Instrument Co., Sunnyvale, CA, USA) with high-quality narrow band GFP filter (excitation HQ480/20 nm, emission HQ510/20 nm, beam splitter Q4951p, Chroma Technology Corp., Brattleboro, VT, USA) equipped with an F-view Monochrome CCD camera. Fields of view for imaging were selected based on EGFP fluorescence (blinded to nuclei), and were imaged with a 40X oil immersion objective. The nuclei of at least 50 transfected cells (EGFP fluorescence) per group were classified as either healthy (round or kidney shaped) or segmented (punctate) (42, 43) and the percentage of cells with segmented DNA was calculated.

Results

Site-directed mutagenesis was performed on the mammalian two-hybrid plasmids pM1-CCmut2 and pEFVP16-CCmut2 to create CCmut3 constructs. The resulting CCmut3 constructs were then mutated through site-directed mutagenesis to create the corresponding CCmut4 plasmids. Subsequently, mammalian two-hybrid assays were carried out in Cos-7 cells. For the hetero-dimer interactions, both possible fusion constructs were assayed (i.e. pM1-CC/pEFVP16-CCmutX and pM1-CCmutX/pEFVP16-CC). While the same trend was observed regardless of which fusion construct was the wild-type, slightly higher values were obtained when the wild-type were fused to the DNA binding domain (pM1). As illustrated in Figure 5.2A, the greatest interaction resulted from the hetero-dimer between CCmut3 and the wild-type coiled-coil domain (CC) (Figure 5.2A, third column). Equally important, the CCmut3:CCmut3 interaction (homo-dimer) resulted in negligible binding (Figure 5.2A, fourth column). Although it is difficult, if not impossible, in this assay to separate out the binding contributions from increased availability versus increased affinity, the design to decrease the stability of the mutant homo-dimer did correlate to an increased ability to bind wild-type as predicted. The result from the CCmut3 hetero-dimer and homo-dimer together indicate the improved interaction exhibited by CCmut3.

Although the CCmut4 hetero-dimer did result in a slightly greater interaction than wild-type (all results are normalized to the wild-type CC:CC interaction, Figure 5.2A, fifth column), the CCmut4 homo-dimer produced an almost equivalent result (Figure 5.2A, sixth column). This finding indicates the importance of the L45D mutation in

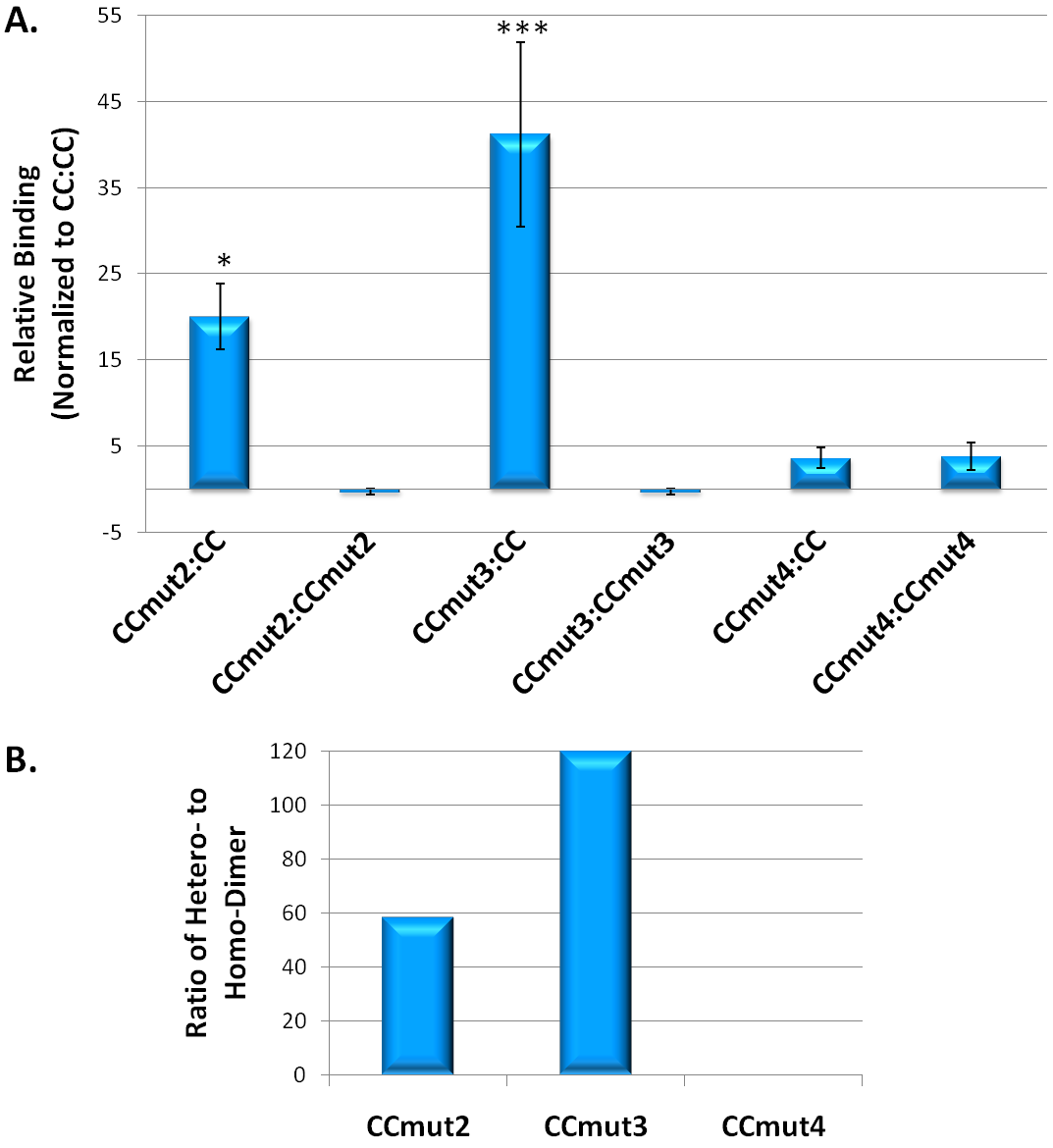

Figure 5.2. Mammalian two-hybrid assay. A) Relative response ratios were first determined for each interaction, and then normalized to the wild-type homo-oligomerization (CC:CC) to indicate the relative binding efficiency. CCmut2, CCmut3, and CCmut4 hetero-dimers resulted in a greater interaction than the wild-type, as did the CCmut4 homo-dimer. CCmut2 and CCmut3 homo-dimer interactions were negligible. Assays were repeated five times, and values indicated are the means ± S.D. Statistics were performed on the values without normalizing to CC so as to include the wild-type interaction in the statistics. Statistical significance was determined by one-way ANOVA with Tukey's posttest. *$p<0.05$, ***$p<0.001$. B) The quotient of the hetero-dimer interaction divided by the homo-dimer interaction (absolute value) is graphed for all three mutants. This ratio provides a means of indicating the preferential binding to CC over the formation of a homo-dimer.

generating a preferential binding towards wild-type. Whereas the other mutations designed for charge-charge repulsion are found on the helix at “g” and “e” postions and may more readily adopt rotamer conformations that position the like charges away from each other, the L45D mutation is in the hydrophobic core where such rotamer flexibility may be more limited. As demonstrated from the dramatic differences between CCmut3 and CCmut4, the L45D mutation is critical.

As both the hetero-dimer and homo-dimer formations are critical in evaluating the improvements made through the mutations, the quotient of the hetero-dimer and homo-dimer can be used to more easily compare the overall effect. Figure 5.2B reports these quotients for CCmut2, CCmut3, and CCmut4. Although the quotient for CCmut2 indicates it is a favorable domain for interacting with Bcr-Abl (at least the wild-type coiled-coil domain of Bcr-Abl), the best set of mutations are those comprising CCmut3. While CCmut4 may interact favorably with wild-type (Figure 5.2A, fifth column), it does not exhibit any preferential binding (Figure 5.2B, third column) and did not result in any improvement as compared to the wild-type domain. Following these results, CCmut4 was dropped from further analysis due to the lack of improvement in oligomerization properties.

While the mammalian two-hybrid assays are a quantitative method of studying the effects of the mutations, these assays were carried out with the isolated coiled-coil domains and not full-length Bcr-Abl. To validate the modifications also correlate to the binding to Bcr-Abl, co-localization experiments were performed in K562 cells. A rigorous analysis for determining co-localization was employed, Costes’ co-localization coefficient (41). Given that CC, CCmut2, and CCmut3 should all bind Bcr-Abl, the co-

localization was aimed at simply confirming the interaction with the full-length protein, and not necessarily at distinguishing their binding affinities. Nevertheless, CCmut3 was found to exhibit a much higher degree of co-localization with Bcr-Abl than the other two (Figure 5.3), and further validated the improved oligomeric properties. Not surprisingly, there was no difference between CC and CCmut2 (Figure 5.3). These co-localization results confirm the CCmut3 set of mutations have improved the ability to interact with Bcr-Abl inside a live cell.

Analysis of the oligomeric disruption of Bcr-Abl was further explored to confirm the interaction of CCmut3. As Bcr-Abl trans-autophosphorylation is dependent on the coiled-coil domain, the formation of hetero-oligomers between a coiled-coil domain and full-length Bcr-Abl should reduce the phosphorylation of Bcr-Abl. As a measure of the phosphorylation state of Bcr-Abl, western blotting was carried out probing K562 lysates with an antibody that recognizes the phosphorylated form of Bcr-Abl. As seen in Figure 5.4A, the phosphorylation of Bcr-Abl was the least after transfection of CCmut3. A secondary measure of the phosphorylation of Bcr-Abl, and its corresponding kinase activity, is the phosphorylation of Bcr-Abl substrates such as STAT5. The phosphorylation of STAT5 was also the least after transfection of CCmut3 (Figure 5.4A). The western blot results correlate with both the mammalian two-hybrid and co-localization data.

Next, the improved Bcr-Abl binding of CCmut3 was analyzed for its effect on CML cells. As CML cells are dependent on Bcr-Abl signaling for growth, inhibition of Bcr-Abl will affect the proliferation rate of the cells. The cell proliferation can be

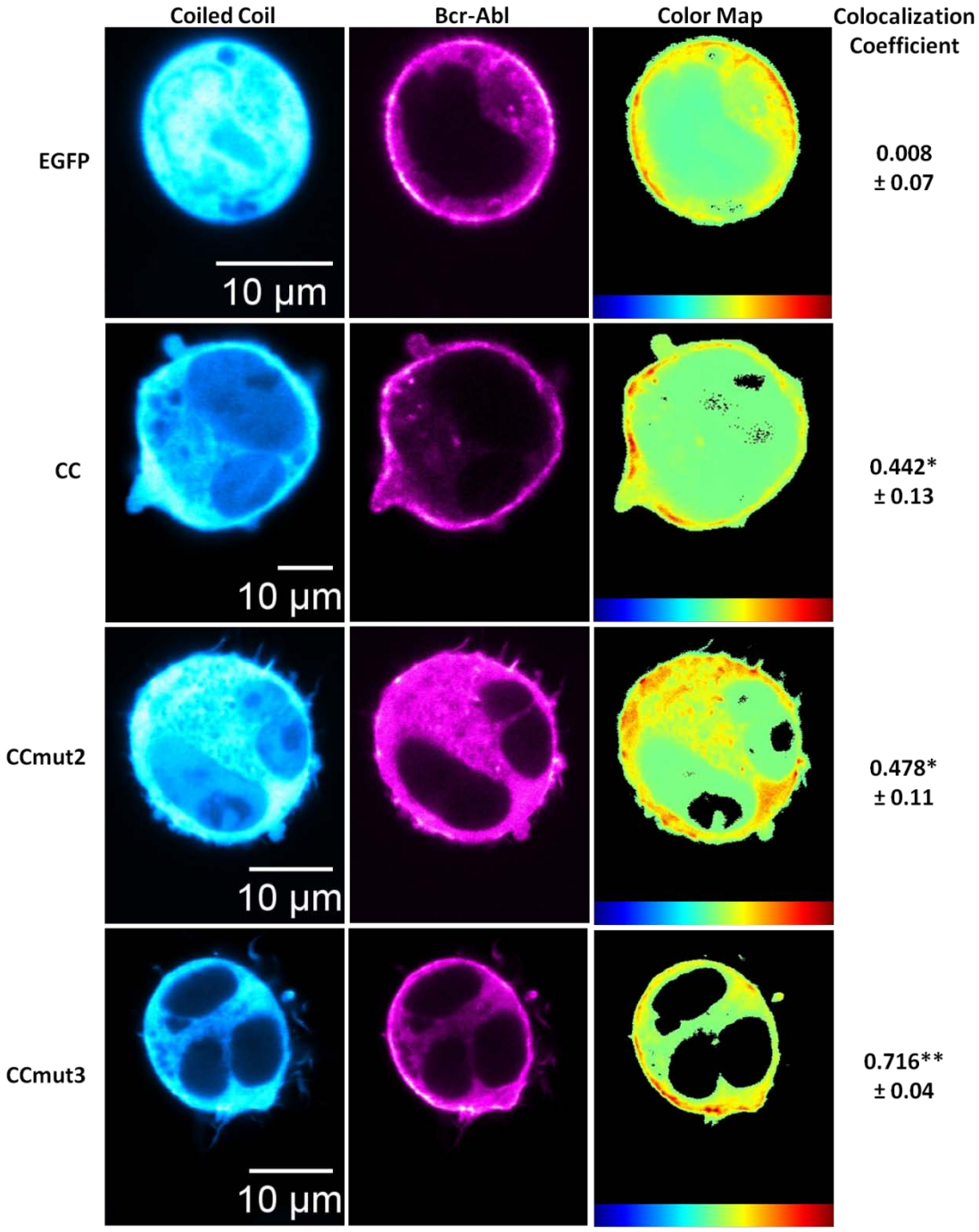

Figure 5.3. Co-localization with Bcr-Abl. Representative images of either EGFP or coiled-coil domain are seen in the left column (cyan). Representative images of Bcr-Abl distribution are seen in the middle column (magenta). Heat maps indicating the co-localization of the two fluorophores are seen in the right column with co-localization scale at the bottom (red highest) followed by the co-localization coefficient. The mean co-localization coefficient was determined from at least three cells per transfection, and repeated four times. The values reported are the means ± S.E.M. Statistical significance was determined by one-way ANOVA with Tukey's posttest. *$p<0.05$, **$p<0.01$.

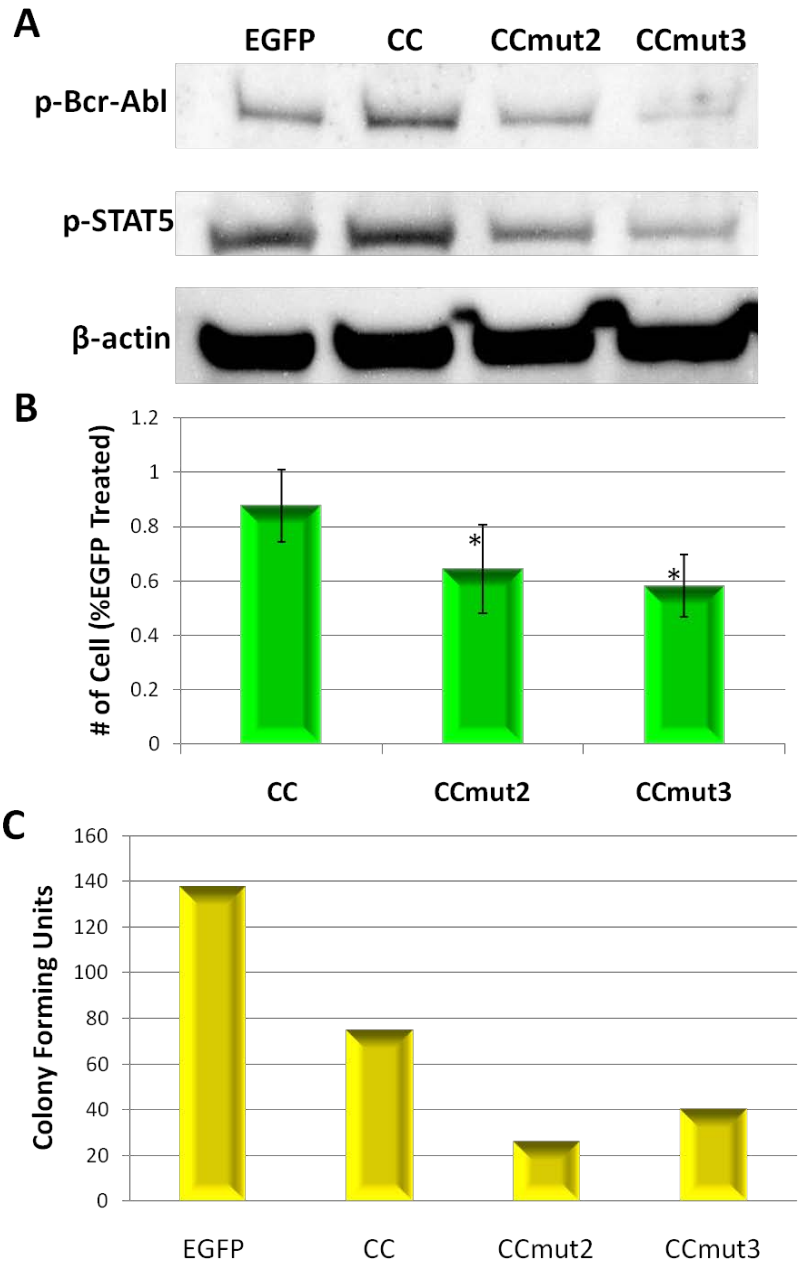

Figure 5.4. Effects of CCs on Bcr-Abl and proliferation of K562 cells. A) A western blot indicating the phosphorylation of Bcr-Abl (top, p-Bcr-Abl) and STAT5 (middle, p-STAT5). B) Viable K562 cells were counted 48 hrs following transfection. The number of proliferating cells was normalized to the number resulting from the EGFP transfection. Each construct was transfected a minimum of three times. Values reported are means ± S.D. Statistical significance was determined by one-way ANOVA with Tukey's posttest. *$p<0.05$. C) Colony forming units were counted 7 days after seeding 10^3 transfected K562 cells into methylcellulose medium. The mean from three separate 200 μm^2 areas was determined.

monitored in a simple fashion through performing cell counts after treatment of the cells. 48 hrs following transfections of either EGFP, CC, CCmut2, or CCmut3 into a CML model cell line (K562), cell counts were performed using trypan blue exclusion. As seen in Figure 5.4A, the proliferation of the cells decreased in the order of EGFP, CC, CCmut2, and CCmut3. Although indirect, this provides evidence of the disruption of Bcr-Abl oligomerization resulting in inhibition of its signaling.

As an alternative method of measuring cell proliferation, a colony forming assay was performed. Twenty-four hrs following transfection of the plasmids into K562 cells, 10^3 cells were seeded into methylcellulose medium and incubated at 37°C for seven days before counting the colony forming units in a 200 μm^2 area. Both CCmut2 and CCmut3 were found to produce the fewest number of colonies, indicative of the decrease in cell proliferation. Notwithstanding, there was no difference in the number of colonies after transfection of CCmut2 or CCmut3. The results achieved by CCmut2 and CCmut3 were comparable to the result after treating K562 cells with 0.5 μM imatinib, demonstrating the therapeutic potential.

Further exploration of the effects on CML cells was carried out though analysis of the induction of apoptosis. First, flow cytometry was used to analyze the number of cells with externalized phosphatidylserine, an established marker of apoptosis. As seen in Figure 5.5A, the level of cell death incrementally increased in the order of CC, CCmut2, and CCmut3. Although the statistical significance compared to the EGFP control was greater for CCmut3 than for CCmut2, there was not a statistical significance between CCmut2 and CCmut3. To further validate the induction of apoptosis, the activity of

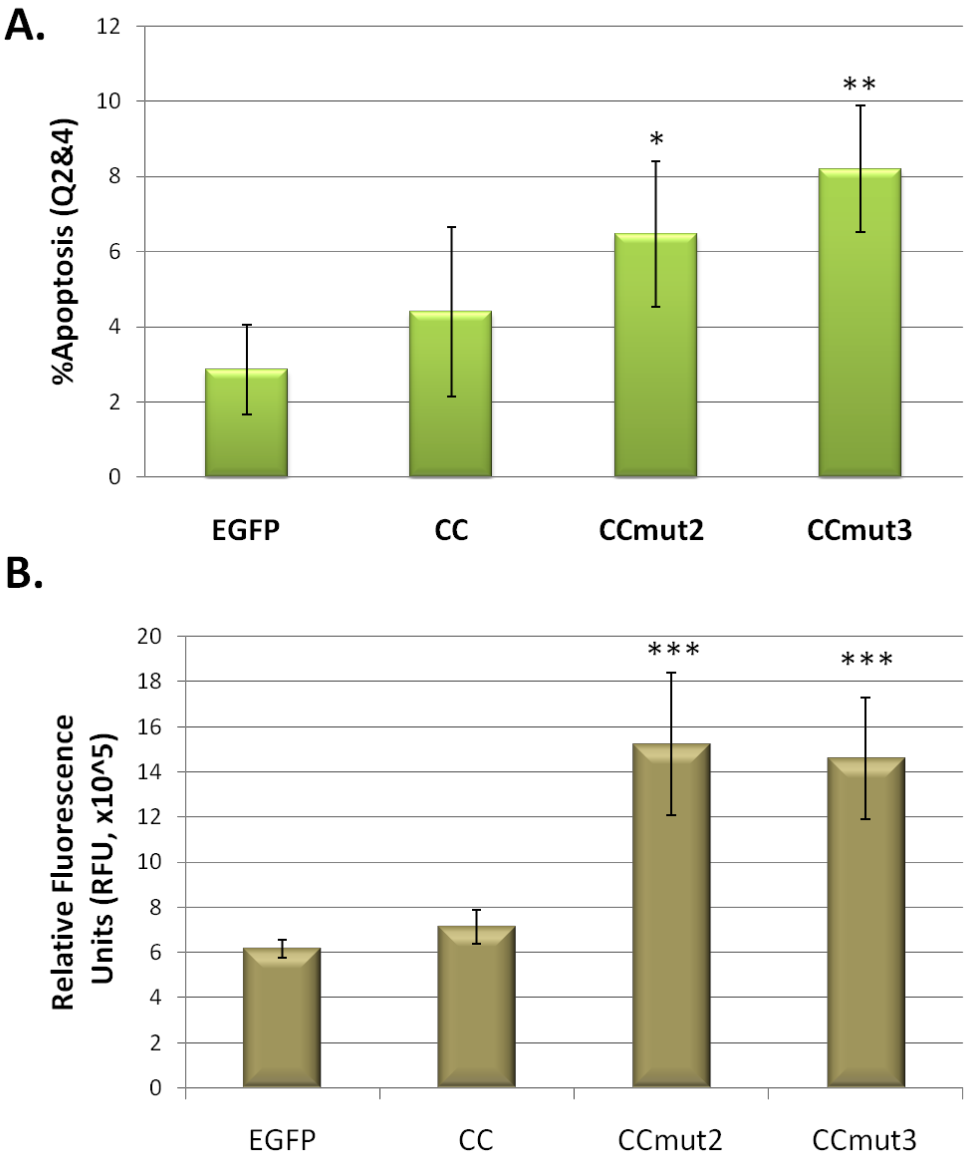

Figure 5.5. Annexin-APC/7AAD staining and caspase-3/7 assays. A) 48 hrs following transfection into K562 cells phosphatidylserine externalization was assessed through flow cytometry. After gating on EGFP fluorescence to select only the transfected cells, the number of $7AAD^-/Annexin^+$ cells (Q2, early apoptosis) was combined with the $7AAD^+/Annexin^+$ cells (Q4, late apoptosis) and used to determine the percentage of apoptotic cells. The values reported are the means ± S.D. from three separate transfections. Statistical significance was determined by one-way ANOVA with Tukey's posttest. *$p<0.05$, **$p<0.01$. B) Forty-eight hrs following transfection into K562 cells the activation of caspase-3/7 was analyzed in the cell lysates through a fluorescence-based assay. Values reported are the means ± S.D. from three separate transfections. Statistical significance was determined by one-way ANOVA with Tukey's posttest. ***$p<0.001$.

caspase-3/7 was also measured. A substantial increase in caspase-3/7 activity was observed after transfection of either CCmut2 or CCmut3 (Figure 5.5B). Again, there was no statistical difference between the caspase-3/7 activities resulting from the CCmut2 or CCmut3 transfected cells.

Analysis of the cell morphology is an alternative method of studying the induction of apoptosis. Healthy K562 cells are relatively large, round cells with kidney shaped (or round) nuclei (Figure 5.6A, top row). Apoptotic cells, however, exhibit very distinct morphological signs readily detectable through microscopy. Some morphological signs of apoptosis include cell shrinkage (as opposed to necrotic cells that may expand), cytoplasmic blebbing, echnoid spikes, and nuclear segmentation (42, 43). Of these signs, nuclear segmentation is one indication that can be quantified (each individual cell determined to have either a normal or segmented nucleus) as a measurement of the induction of apoptosis. Forty-eight hrs after the transfection of the plasmids into K562 cells, the nuclei are stained with H33342, and the cells are photographed on a fluorescence microscope. The fields of view photographed are selected based on the EGFP fluorescence, while being blinded to the nuclear stain, and reduces biased selection of nuclei. Representative images are illustrated in Figure 5.6A. The percentage of transfected cells with segmented nuclei is graphed in Figure 5.6B. Similar to the cell proliferation, and flow cytometry, an incremental effect was observed on nuclear segmentation with CC, CCmut2, and CCmut3. Nevertheless, CCmut2 and CCmut3 produced similar results. Thus, the flow cytometry, caspase assay, and nuclear segmentation together demonstrate the ability of the modified coiled-coils to inhibit Bcr-Abl, decrease cell proliferation, and induce apoptosis in CML cells.

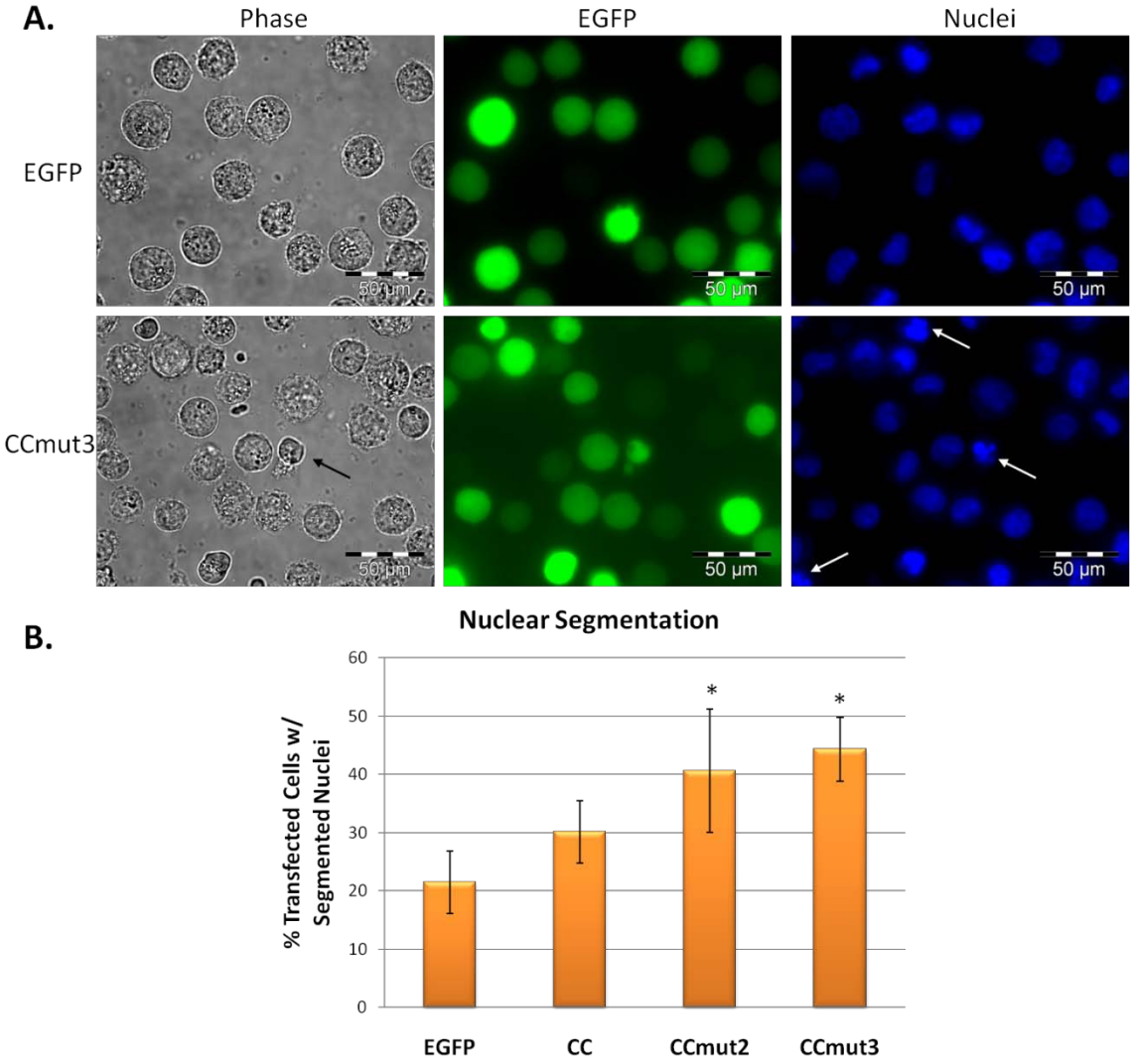

Figure 5.6. Nuclear segmentation of K562 cells. A) Representative images of K562 cells 48 hrs after transfection of EGFP (top row) or CCmut3 (bottom row). The left column depicts the phase contrast images, with an example of cell shrinkage indicated with a black arrow. The middle column depicts the fluorescence from EGFP. The right column depicts the nuclei, with examples of nuclear segmentation indicated by the white arrows. Scale bars are included in the bottom right corners. B) Results from the quantification of nuclear segmentation. The percentage of transfected cells with segmented nuclei was determined from three fields of view and repeated with cells transfected three separate times. Values reported are the means ± S.D. Statistical significance was determined by one-way ANOVA with Tukey's posttest. *$p<0.05$.

Conclusions

Analysis of the structure of the Bcr-Abl coiled-coil domain, and the previously designed CCmut2, guided the identification of residues 39 and 45 as interesting possible mutations. Incorporation of a K39E mutation into CCmut2 produced CCmut3. Subsequently, reverting the CCmut3 L45D mutation back to leucine produced CCmut4. The effects of these modifications on the oligomerization properties were studied through a mammalian two-hybrid assay in Cos-7 cells and compared to CCmut2. While CCmut3 yielded impressive improvements in the binding capabilities, CCmut4 was found to bind almost equivalently to another CCmut4 as it binds CC. The binding results from CCmut4 indicate the importance of the L45D mutation in preventing homo-oligomerization. These binding results, including both CCmut3 and CCmut4, further support the idea that decreased homo-dimer stability is a major driving force in the improved oligomerization with Bcr-Abl. The mammalian two-hybrid assay using isolated coiled-coil domains was then followed by co-localization with full-length Bcr-Abl. CC, CCmut2, and CCmut3 were all found to colocalize with Bcr-Abl, with CCmut3 resulting in the greatest degree of co-localization. The improved binding of CCmut3 to Bcr-Abl also decreased the phosphorylation of Bcr-Abl, a parameter indicative of Bcr-Abl's oligomeric state and activity. These binding studies validated the additional mutation used in CCmut3 led to enhanced oligomeric properties and demonstrated its usefulness as a Bcr-Abl binding domain.

The improved binding by CCmut3 was then tested for its effect on CML cells. Cell proliferation was first measured through cell counts and colony forming assays following transfection of the coiled-coil domains. Both CCmut2 and CCmut3 decreased

the cell proliferation, but there was no statistical difference between CCmut2 and CCmut3.

CCmut3 was also demonstrated to induce apoptosis in K562 cells as measured through 7AAD staining, activation of caspase-3/7, and hallmark morphological signs of apoptosis. Both the decreased cell proliferation and the induction of apoptosis are indirect evidence of the ability of CCmut3 to interfere with the homo-oligomerization of Bcr-Abl. Due to the fact that CCmut3 does not contain the Y-kinase domain necessary for activation through trans-autophosphorylation, the binding between CCmut3 and Bcr-Abl results in inactivation of Bcr-Abl and induction of apoptosis in CML cells.

These results can be divided into two distinct categories of experiments: testing the binding, and testing the effect the construct has on CML cells. The analysis of the binding revealed a marked improvement in CCmut3, even over the proven CCmut2. Nevertheless, this improved binding did not correlate to enhancements over CCmut2 in effects on CML cells. This may be explained by insufficient assay sensitivity to distinguish a modest difference, indicating the improvement is only marginal. An alternative explanation lies in the idea that the disruption of Bcr-Abl oligomerization is already maximized with the binding capabilities of CCmut2. If this is the case, any improvements in binding with an alternative coiled-coil domain would not instigate enhancements in the effect on CML cells. This theory is supported by the inability to increase the effect of CCmut2 on CML cells through combinatorial treatment with CCmut2 and a TKI (unpublished data D.W.W.).

Although use of CCmut3 for interfering with the oligomeric state of Bcr-Abl is an interesting alternative to the standard TKIs, a further application currently in pursuit in

our laboratory is the use as a capture motif for escort of Bcr-Abl to alternative subcellular locations. As opposed to a passive induction of apoptosis when Bcr-Abl is inhibited, we are seeking an active induction of apoptosis that may lead to a more potent therapeutic strategy. With this goal in mind, the improved binding properties are of utmost interest. This work establishes CCmut3 as an efficient binding partner to Bcr-Abl with implications in inhibiting Bcr-Abl as well as other interesting therapeutic strategies that require tight binding to Bcr-Abl.

Acknowledgments

We acknowledge the use of DNA/Peptide Core (NCI Cancer Center Support Grant P30 CA042014, Huntsman Cancer Institute). This work was funded by NIH R01-CA129528. We would like to thank Rian Davis, Mohanad Mossalam, Abdul Okul, and Karina Matissek for scientific discussions.

References

1. McWhirter JR, Galasso DL, Wang JY. A coiled-coil oligomerization domain of Bcr is essential for the transforming function of Bcr-Abl oncoproteins. Mol Cell Biol 1993; 13: 7587-95.

2. Guo XY, Cuillerot JM, Wang T, et al. Peptide containing the BCR oligomerization domain (AA 1-160) reverses the transformed phenotype of p210bcr-abl positive 32D myeloid leukemia cells. Oncogene 1998; 17: 825-33.

3. Taylor CM, Keating AE. Orientation and oligomerization specificity of the Bcr coiled-coil oligomerization domain. Biochemistry 2005; 44: 16246-56.

4. Zhao X, Ghaffari S, Lodish H, Malashkevich VN, Kim PS. Structure of the Bcr-Abl oncoprotein oligomerization domain. Nat Struct Biol 2002; 9: 117-20.

5. Dixon AS, Pendley SS, Bruno BJ, et al. Disruption of BCR-ABL coiled-coil oligomerization by design. J Biol Chem.

6. Okimoto RA, Van Etten RA. Navigating the road toward optimal initial therapy for chronic myeloid leukemia. Curr Opin Hematol; 18: 89-97.

7. Goldman JM. Chronic myeloid leukemia: a historical perspective. Semin Hematol; 47: 302-11.

8. Pavlovsky C, Kantarjian H, Cortes JE. First-line therapy for chronic myeloid leukemia: Past, present, and future. Am J Hematol 2009; 84: 287-93.

9. Wei G, Rafiyath S, Liu D. First-line treatment for chronic myeloid leukemia: dasatinib, nilotinib, or imatinib. J Hematol Oncol; 3: 47.

10. Jabbour E, Cortes JE, Kantarjian H. Second-line therapy and beyond resistance for the treatment of patients with chronic myeloid leukemia post imatinib failure. Clin Lymphoma Myeloma 2009; 9 Suppl 3: S272-9.

11. Quintas-Cardama A, Kantarjian HM, Cortes JE. Mechanisms of primary and secondary resistance to imatinib in chronic myeloid leukemia. Cancer Control 2009; 16: 122-31.

12. Deininger M. Resistance and relapse with imatinib in CML: causes and consequences. J Natl Compr Canc Netw 2008; 6 Suppl 2: S11-S21.

13. Hochhaus A, Erben P, Ernst T, Mueller MC. Resistance to targeted therapy in chronic myelogenous leukemia. Semin Hematol 2007; 44: S15-24.

14. Thomas X. Is AP24534 (Ponatinib) the next treatment of Philadelphia chromosome-positive acute lymphoblastic leukemia? Bull Cancer.

15. Zhou T, Commodore L, Huang WS, et al. Structural mechanism of the Pan-BCR-ABL inhibitor ponatinib (AP24534): lessons for overcoming kinase inhibitor resistance. Chem Biol Drug Des; 77: 1-11.

16. Eide CA, Adrian LT, Tyner JW, et al. The ABL switch control inhibitor DCC-2036 is active against the chronic myeloid leukemia mutant BCR-ABLT315I and exhibits a narrow resistance profile. Cancer Res; 71: 3189-95.

17. Fausel C. Targeted chronic myeloid leukemia therapy: seeking a cure. J Manag Care Pharm 2007; 13: 8-12.

18. Radich JP. Chronic myeloid leukemia 2010: where are we now and where can we go? Hematology Am Soc Hematol Educ Program; 2010: 122-8.

19. Hantschel O, Superti-Furga G. Regulation of the c-Abl and Bcr-Abl tyrosine kinases. Nat Rev Mol Cell Biol 2004; 5: 33-44.

20. Colicelli J. ABL tyrosine kinases: evolution of function, regulation, and specificity. Sci Signal; 3: re6.

21. Barila D, Superti-Furga G. An intramolecular SH3-domain interaction regulates c-Abl activity. Nat Genet 1998; 18: 280-2.

22. Pluk H, Dorey K, Superti-Furga G. Autoinhibition of c-Abl. Cell 2002; 108: 247-59.

23. Nagar B, Hantschel O, Young MA, et al. Structural basis for the autoinhibition of c-Abl tyrosine kinase. Cell 2003; 112: 859-71.

24. Nagar B, Hantschel O, Seeliger M, et al. Organization of the SH3-SH2 unit in active and inactive forms of the c-Abl tyrosine kinase. Mol Cell 2006; 21: 787-98.

25. Hantschel O, Nagar B, Guettler S, et al. A myristoyl/phosphotyrosine switch regulates c-Abl. Cell 2003; 112: 845-57.

26. Sirvent A, Benistant C, Roche S. Cytoplasmic signalling by the c-Abl tyrosine kinase in normal and cancer cells. Biol Cell 2008; 100: 617-31.

27. Brasher BB, Van Etten RA. c-Abl has high intrinsic tyrosine kinase activity that is stimulated by mutation of the Src homology 3 domain and by autophosphorylation at two distinct regulatory tyrosines. J Biol Chem 2000; 275: 35631-7.

28. Rowley JD. Letter: A new consistent chromosomal abnormality in chronic myelogenous leukaemia identified by quinacrine fluorescence and Giemsa staining. Nature 1973; 243: 290-3.

29. Groffen J, Stephenson JR, Heisterkamp N, Bartram C, de Klein A, Grosveld G. The human c-abl oncogene in the Philadelphia translocation. J Cell Physiol Suppl 1984; 3: 179-91.

30. Groffen J, Stephenson JR, Heisterkamp N, de Klein A, Bartram CR, Grosveld G. Philadelphia chromosomal breakpoints are clustered within a limited region, bcr, on chromosome 22. Cell 1984; 36: 93-9.

31. Kurzrock R, Kantarjian HM, Druker BJ, Talpaz M. Philadelphia chromosome-positive leukemias: from basic mechanisms to molecular therapeutics. Ann Intern Med 2003; 138: 819-30.

32. Ren R. The molecular mechanism of chronic myelogenous leukemia and its therapeutic implications: studies in a murine model. Oncogene 2002; 21: 8629-42.

33. Sattler M, Griffin JD. Molecular mechanisms of transformation by the BCR-ABL oncogene. Semin Hematol 2003; 40: 4-10.

34. Hazlehurst LA, Bewry NN, Nair RR, Pinilla-Ibarz J. Signaling networks associated with BCR-ABL-dependent transformation. Cancer Control 2009; 16: 100-7.

35. Beissert T, Puccetti E, Bianchini A, et al. Targeting of the N-terminal coiled coil oligomerization interface of BCR interferes with the transformation potential of BCR-ABL and increases sensitivity to STI571. Blood 2003; 102: 2985-93.

36. Beissert T, Hundertmark A, Kaburova V, et al. Targeting of the N-terminal coiled coil oligomerization interface by a helix-2 peptide inhibits unmutated and imatinib-resistant BCR/ABL. Int J Cancer 2008; 122: 2744-52.

37. McWhirter JR, Wang JY. Effect of Bcr sequences on the cellular function of the Bcr-Abl oncoprotein. Oncogene 1997; 15: 1625-34.

38. Mian AA, Oancea C, Zhao Z, Ottmann OG, Ruthardt M. Oligomerization inhibition, combined with allosteric inhibition, abrogates the transformation potential of T315I-positive BCR/ABL. Leukemia 2009; 23: 2242-7.

39. Dixon AS, Kakar M, Schneider KM, Constance JE, Paullin BC, Lim CS. Controlling subcellular localization to alter function: Sending oncogenic Bcr-Abl to the nucleus causes apoptosis. J Control Release 2009.

40. Bolte S, Cordelieres FP. A guided tour into subcellular colocalization analysis in light microscopy. J Microsc 2006; 224: 213-32.

41. Costes SV, Daelemans D, Cho EH, Dobbin Z, Pavlakis G, Lockett S. Automatic and quantitative measurement of protein-protein colocalization in live cells. Biophys J 2004; 86: 3993-4003.

42. Barrett KL, Willingham JM, Garvin AJ, Willingham MC. Advances in cytochemical methods for detection of apoptosis. J Histochem Cytochem 2001; 49: 821-32.

43. Willingham MC. Cytochemical methods for the detection of apoptosis. J Histochem Cytochem 1999; 47: 1101-10.

CHAPTER 6

RATIONALLY DESIGNED BCR-ABL CAPTURE MOTIFS FOR ESCORT TO THE NUCLEUS

Abstract

The fusion of the breakpoint cluster region (BCR) and Abelson kinase (Abl) proteins generates a highly characterized oncoprotein responsible for the majority of chronic myelogenous leukemia (CML) cases (1-3) attributable to the aberrant signaling through the tyrosine kinase domain (4-7). In addition to the constitutive kinase activity generated by the fusion of these two proteins, a further consequence is the exclusive cytoplasmic localization of Bcr-Abl (8, 9). Bcr-Abl in the cytoplasm allows for oncogenic signaling which leads to proliferation of cells. However, nuclear localization of Bcr-Abl leads to apoptosis (10-12). The purpose of this work was to develop capture motifs capable of binding endogenous Bcr-Abl and escorting it to the nucleus. Binding domains for capture of Bcr-Abl were generated, and subsequently incorporated into a controllable nucleo-cytoplasmic shuttling protein switch (13) or attached to four nuclear localization signals (12). Targeting Bcr-Abl at domains with known interactions that may contribute to the cytoplasmic retention (in particular the actin binding domain at the

C-terminus), we isolated intracellular domain antibodies (iDabs) that bind Bcr-Abl. In addition to the co-localization with Bcr-Abl, the best isolated iDab (ABI7) and a rationally designed coiled-coil domain (CCmut3) provoked a redistribution of the subcellular localization of Bcr-Abl. These binding domains were then tested for their ability to escort Bcr-Abl into the nucleus using the protein switch (13) or attachment of 4 NLSs. Although RIN1, ABI7, and CCmut3 all produced similar co-localization with Bcr-Abl, CCmut3 was the only domain found to produce efficient nuclear translocation of Bcr-Abl, implicating the region of Bcr-Abl being bound, and possibly the resulting Bcr-Abl conformation, are important factors for nuclear translocation and not mere binding affinity alone. This newly found capability to escort Bcr-Abl into the nucleus has the potential of turning the causative agent, Bcr-Abl, against the cancer cell for induction of apoptosis and may provide a potent means of treating CML, even forms resistant to the current and future tyrosine kinase inhibitors (TKIs).

Introduction

As the gene product resulting from the first abnormal chromosome found to be responsible for a specific disease (the Philadelphia chromosome) (14), the oncoprotein Bcr-Abl has been extensively investigated (15, 16). This thorough research has turned a previously fatal cancer, chronic myelogenous leukemia (CML), into what is now a chronically manageable disease (17, 18). The turning point in the treatment of CML was the identification of STI-571 (imatinib, or Gleevec®), a small molecule inhibitor of Bcr-Abl that demonstrated the ability to halt the uncontrolled proliferation of the cancer cells

as well as the progression from the chronic phase of the disease into the deadly blast crisis (19-21).

On the molecular level, Gleevec® binds Bcr-Abl at the tyrosine kinase domain and prevents phosphorylation of its substrates (22, 23), an event critical to the activation of numerous signaling pathways resulting in upregulation of proliferation, inhibition of apoptosis, altered cell adhesion and motility, and inhibition of DNA repair (15), all contributing to the oncogenesis through Bcr-Abl. Due to the essential role of the tyrosine kinase activity in the pathogenesis, the inhibition by Gleevec® has proven to be a remarkable treatment for CML. Nevertheless, numerous mutations in Bcr-Abl have been described which render resistance to Gleevec® (24-27), and second generation tyrosine kinase inhibitors (TKIs) such as AMN107 (nilotinib, Tasigna®) and BMS-354825 (dasatinib, Sprycel®) have already been approved for the treatment of Gleevec®-resistant forms of CML. One resistant form, containing the T315I mutation, remains elusive to all currently approved TKIs (28-31), although AP24534 (Ponatinib) and DCC-2036 have been demonstrated to be effective against the T315I mutation and are currently in clinical trials (32-36). Still, TKIs do not cure CML, and alternative therapeutics are still of interest for the potential to eliminate the necessity of a life-long treatment.

It is well established that the fusion between Bcr and Abl transforms the regulated tyrosine kinase activity from c-Abl into constitutive tyrosine kinase activity in Bcr-Abl. This activity, as described above, has received rightly due attention and has been the focus of much research for CML. In addition to the misregulated kinase activity, it is also well established that this fusion also results in a spatial misregulation at the subcellular level (8, 9). In healthy cells, c-Abl can shuttle between the cytoplasm and

nucleus and plays distinct roles in each subcellular compartment (37-40). This spatial control is important for the role of c-Abl in cell differentiation, division, adhesion, and response to stress signals. In contrast, Bcr-Abl is found to localize exclusively in the cytoplasm where it can be positioned in proximity to the signaling proteins controlled by its activated kinase domain. The combination treatment of Gleevec® and the nuclear export inhibitor Leptomicin B (LMB) have demonstrated the ability to relocate Bcr-Abl to the nucleus, where Bcr-Abl induced apoptosis (11). We have also demonstrated that an exogenous Bcr-Abl construct can be directed to the nucleus through incorporation of nuclear localization signals (NLSs), and established that the induction of apoptosis was dominant over the endogenous Bcr-Abl oncogenic signaling as cytoplasmic depletion of the endogenous Bcr-Abl was not observed (12). Thus, relocalizing Bcr-Abl to the nucleus is a potent method of inducing apoptosis and may be an interesting alternative intervention strategy. However, LMB cannot be used clinically due to neuronal toxicity (41), and treatment with an exogenous Bcr-Abl would also be problematic. In order to harness the apoptotic potential of Bcr-Abl, an alternative method of repositioning the protein is needed.

Numerous proteins are found to shuttle between the cytoplasm and nucleus under normal biological conditions. One of the most notable examples is steroid hormone receptors which are found to localize in the cytoplasm in the absence of hormone (42-44). Upon binding of the hormone and the associated conformational change, the receptor dimerizes and transports into the nucleus where it is a transactivator of various genes. Previous work in our laboratory has exploited the controlled conformational change of the ligand binding domain (LBD) from the glucocorticoid receptor, and through

incorporation of both a nuclear export signal (NES) and a nuclear localization signal (NLS), generated a small (32 kDa) chimeric protein with nucleo-cytoplasmic shuttling control through the addition or removal of the synthetic glucocorticoid dexamethasone (dex) (13). The LBD employed is from the rat glucocorticoid receptor and contains one point mutation, C656G, delivering 10 times more sensitivity to dex (42). This protein, termed the protein switch, localizes to the cytoplasm in the absence of dex due to the NES. When dex is added, the conformational change causes the NLS to become dominant and the protein switch moves to the nucleus. This translocation is reversible, and the protein switch relocalizes to the cytoplasm if dex is washed out (13, 45, 46).

The controlled translocation into the nucleus afforded by the protein switch may be applied to escorting Bcr-Abl into the nucleus through incorporation of a Bcr-Abl binding motif. The ideal binding motif for incorporation into the protein switch will exhibit high affinity and specificity, will be stable inside of cells, and will be small in size. These are all attributes of intracellular domain antibodies (iDabs) (47-56). While it is commonplace for heavy and light chain variable fragments to be connected through a small peptide linker in the scFv format for use in epitope recognition inside of cells, the iDab is a further simplification of an antibody and consists of only one variable domain (from either the heavy or the light chain). As the entire structure is only one domain, the iDab eliminates the necessity for a linker and is half the size of an scFv. The iDab has been demonstrated to function in the absence of any disulfide bonds (54), and is the minimal antibody portion that retains the high affinity and specificity typical of antibodies. A simple method for isolation of an iDab that will bind to an intracellular target has been termed the third generation intracellular antibody capture (IAC^3) (57), and

is based on yeast two-hybrid screening of iDab libraries. In the first round of screening, libraries consisting of randomized CDR3 regions (ranging from 8 to 21 amino acids total in CDR3) are screened. Affinity maturation is achieved through creation of a sublibrary by taking the CDR3 sequences identified in the first round of screening and randomizing CDR2. This process can be repeated a third time for further maturation by randomizing CDR1 and another round of screening. While one limitation of typical yeast two-hybrid screens is the small number of clones that can be screened (as compared to other methods such as phage display), through creation and screening of sublibraries as described in the IAC^3 protocol, it is theoretically possible to screen up to 10^{18} clones (57). This method has been used to generate iDabs that bind LMO2, RAS, RAF, and p53 with high affinity (57, 58).

Using the IAC^3 technology it is possible to not only target a specific protein, but target a specific region of the target protein through screening the libraries against that particular domain or region of interest. In line with the goal of escorting Bcr-Abl to the nucleus, we took the approach that competing with interactions that anchor Bcr-Abl in the cytoplasm may render it more available for transport into the nucleus. In this fashion, the iDab may not solely allow for the capture of Bcr-Abl, but interfere with an interaction contributing to the cytoplasmic localization, and through both mechanisms yield a higher degree of nuclear translocation. Although the list of proteins that interact with Bcr-Abl is lengthy, one of particular interest is actin as it has been demonstrated to play a leading role in the cytoplasmic localization of Bcr-Abl (59-61). As the actin binding domain (ABD) is found at the C-terminus and is contributed by the Abl portion, we also wanted to target a Bcr domain. The Dbl homology and Pleckstrin homology domains (DHPH)

are routinely found together and function to bind inositolphospholipids at the inner surface of the membrane (62-67). Although the Bcr-Abl DHPH domains are less studied and documented in the literature than the ABD, the interaction with phospholipids provides another plausible contribution to cytoplasmic retention. We thus chose the ABD and DHPH domains as the Bcr-Abl subdomains for targeting iDabs, and used these domains as the baits in the screens.

An alternative binding approach is a rationally designed coiled-coil domain based on the coiled-coil domain of Bcr-Abl (68). Through formation of a dimer-of-dimers, Bcr-Abl is found as a tetramer (69, 70). This oligomerization is achieved through the coiled-coil (or oligomerization) domain at the N-terminus, and this domain is another possible way of binding Bcr-Abl. Recently, we have designed mutations in this coiled-coil domain to improve the interaction with Bcr-Abl as an alternative binding motif for controlled nuclear escort (68). Unpublished data in our laboratory indicate a set of mutations, containing one additional mutation than the previously published CCmut2, results in superior interaction with Bcr-Abl, and has been termed CCmut3. In addition to the iDab and CCmut3, we also compared the functionality of the Abl binding domain from RIN1, a known Bcr-Abl interactor, as a binding motif for nuclear escort. This RIN1 domain has been demonstrated to be an efficient binding partner for Bcr-Abl, interacting with the SH3/2 domains and contributing to maintaining Bcr-Abl in a constitutively active state (71-73). The regions of Bcr-Abl targeted by these four binding domains are illustrated in Figure 6.1. Initially we speculated a multivalency approach may be needed

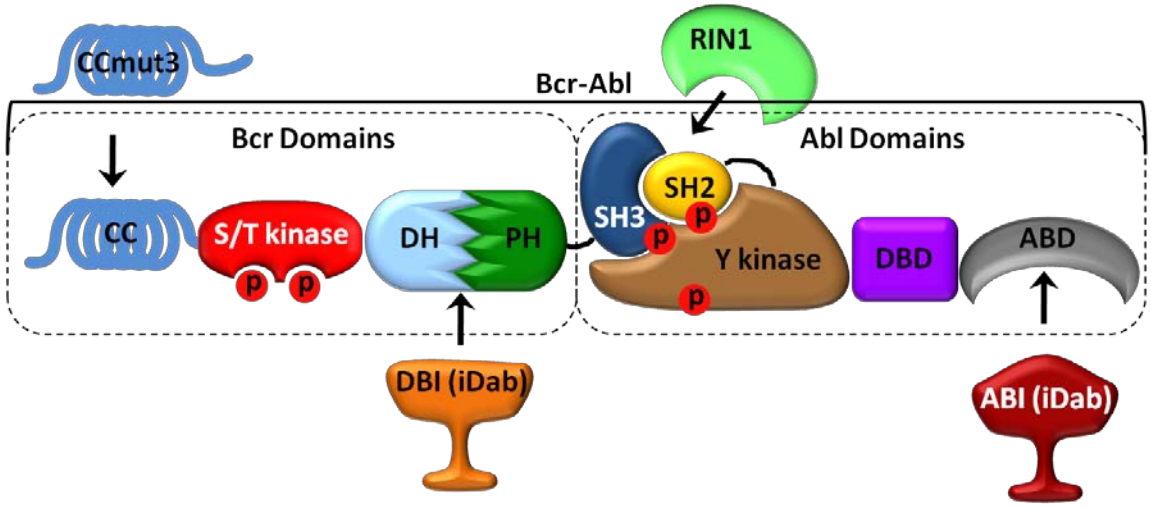

Figure 6.1. Bcr-Abl domains and the targeting regions of the binding domains. CCmut3 binds the coiled-coil domain, DBI binds the DHPH domains, RIN1 binds the SH3/SH2 domains, and ABI binds the ABD. Thus, two Bcr and two Abl domains are targeted with these binding domains. CC = coiled-coil domain, S/T kinase = serine/threonine kinase domain, DH = Dbl homology domain, PH = pleckstrin homology domain, SH3 = Src homology 3 domain, SH2 = Src homology 2 domain, Y kinase = tyrosine kinase domain, DBD = DNA binding domain, ABD = actin binding domain, CCmut3 = coiled-coil mutation set 3, RIN1 = Abl binding domain from RIN1, DBI = DHPH binding iDab, ABI = ABD binding iDab, Red P = phosphorylation site.

to overcome the interactions generating the cytoplasmic retention of Bcr-Abl, and this guided our selection of these distinct regions for targeting Bcr-Abl. Although 4NLS-CCmut3 resulted in efficient nuclear translocation of Bcr-Abl, the effect was enhanced through combining 4NLS-ABI7 and 4NLS-CCmut3.

In this report, the IAC[3] technology was employed for identifying iDabs targeting Bcr-Abl at regions complimentary to where CCmut3 and RIN1 target Bcr-Abl. Next, the effect the expression of these domains had on the subcellular localization of Bcr-Abl was analyzed. In attempt to move Bcr-Abl into the nucleus, the best iDab, as well as CCmut3 and RIN1, were subcloned into the protein switch. The nuclear translocation afforded by these protein switch constructs was then compared to the translocation resulting when the protein switch was replaced with four constitutively active nuclear localization signals.

Materials and Methods

Cell Lines and Transformation/Transfection

First round IAC[3] screening was carried out in L40 yeast cells (T.H. Rabbitts, L.I.M.M., Leeds, UK; MATa, leu2-3, his3Δ200, trp1Δ1, ade2, LYS2::$(LexA\text{-}op)_4$-HIS3, URA3::$(LexA\text{-}op)_8$-lacZ). Second round IAC[3] screening was carried out in AH109 yeast cells (T.H. Rabbitts; MATa, trp1-901, leu2-3, 112, ura3-52, his3-200, gal4Δ, gal80Δ, LYS2::$GAL1_{UAS}$-$GAL1_{TATA}$-HIS3, MEL1, $GAL2_{UAS}$-$GAL2_{TATA}$-ADE2, ura3::$MEL1_{UAS}$-$MEL1_{TATA}$-lacZ). Transformation into yeast cells was performed by a lithium acetate/carrier DNA/PEG precipitation method as described in the IAC[3] protocol (57). Briefly, an overnight culture grown in YC (for transformation of bait) or YC-W (for transformation of library) media was used to inoculate a larger culture that was grown in

YPD to an optical density at 600 nm ($O.D._{600}$) ~0.6. The cells were harvested by centrifugation and washed in sterile water three times. After the final wash, the cells were resuspended in TE-LiAc and maintained on ice. The plasmid DNA being transformed (bait plasmid or library) was mixed with salmon sperm DNA and the DNA mixture was added to the cells and vortexed for 30 sec. A fresh solution of TE/PEG/LiAc was added and the cells were votexed again before incubating at 30 °C for 30 min. Following the incubation DMSO was added and the cells were heat shocked at 42 °C for 15 min with swirling every 2 min. After incubating the cells on ice for 2 min, sterile water was added and the cells harvested by centrifugation. The pellet was washed in water and then resuspended in TE before plating onto 9 cm YC-W (transformation of bait) or 25 x 25 cm YC-WLH (transformation of library) plates. For library screens, serial dilutions were made and plated onto 9 cm YC-WL plates to calculate the transformation efficiency. The plates were grown at 30 °C for 2-3 days.

Mammalian two-hybrid assays were performed in murine adenocarcinoma 1471.1 cells, and fluorescence microscopy was performed in simian kidney Cos-7, or human lymphoblasts K562 (CML model cells expressing Bcr-Abl). 1471.1 cells were grown as monolayers in DMEM (GIBCO, Invitrogen, Carlsbad, CA, USA), and Cos-7 and K562 cells were grown in RPMI (GIBCO, Invitrogen) as monolayers and in suspension, respectively. Both DMEM and RPMI were supplemented with 10% FBS (Invitrogen), 1% pen/strep/L-glu (Invitrogen), and 0.1% gentamicin (Invitrogen). 1471.1 cells were transfected using Lipofectamine 2000 (Invitrogen) following the recommended protocol from the manufacturer. Cos-7 cells were transfected with Fugene HD (Promega, Madison, WI, USA) following the recommended protocol from the manufacturer. K562

cells were nucleofected using Solution V and the Amaxa Nucleofector II (Agilent Technologies Inc., Santa Clara, CA, USA) on program T-013.

Construction of Plasmids and Libraries

The genes encoding the Dbl Homology/Pleckstrin Homology (DHPH) and actin binding (ABD) domains were amplified through PCR using the primers (DHPH) 5'-ACACACACGAATTCGGCTTGGAGATGAGAAAATGGGTCCTG-3' and 5'-CAACCCCAGAATTCCTTCTTCTGCTGCTCCCGGATG-3' and (ABD) 5'-TATGTCTAGAATTCGCAGGGGACCAGCCGTCTTC-3' and 5'-CACTCCACGAATTCCTCAGCCACTGTCATGGGTATG-3' for insertion into the yeast two-hybrid vectors pBTM116 (used in first round screening) and pBD-Gal4-Cam (used in second round screening) at the EcoRI site to create fusions with the LexA and Gal4 DNA binding domains respectively. Oligonucleotides encoding helix 3 from the ABD (5'-AATTCGGCGGTGGGGGATCCGGCGGTGGGGGATCCATGAGGAACAAGTTTGCCTTCCGAGAGGCCATCAACAAACTGGAGAATAATCTCCGGGAGCTTCAGATCG-3' and 5'-AATTCGATCTGAAGCTCCCGGAGATTATTCTCCAGTTTGTTGATGGCCTCTCGGAAGGCAAACTTGTTCCTCATGGATCCCCCACCGCCGGATCCCCCACCGCCG-3') and a linker region between the DH and PH domains (5'- AATTCGGCGGTGGGGGATCCGGCGGTGGGGGATCCTCCAGCATCAATGAGGAGATCACACCCCGACGGCAGTCCG-3' and 5'- AATTCGGACTGCCGTCGGGGTGTGATCTCCTCATTGATGCTGGAGGATCCCCCACCGCCGGATCCCCCACCGCCG-3') were annealed and inserted into the pBD-Gal4-Cam vector at the EcoRI site. The first round iDab libraries screened with randomized CDR3 regions were #4320 and #4325. The construction of

these libraries is described in detail in the IAC^3 protocol (57). For generation of the sublibrary used in the second round of screening, the plasmids encoding the positively interacting iDabs identified in the first round were extracted from the yeast cells and pooled together for use as the template DNA in a PCR to amplify the CDR3 region using the primers VHCDR2Fw (5'- ATATACTATGCAGACTCTG-3') and VP162R (5'-CAACATGTCCAGATCGAA-3'). For the DHPH iDabs, those extracted from screening library #4320 and #4325 were kept separate and used to generate two sublibraries. Another PCR was performed to randomize the bases encoding CDR2 using the primers EFFP2 (5'-GGAGGGGTTTTATGCGATGG-3') and 5RCDR2 (5'-CAGAGTCTGCATAGTATATMNNMNNMNNMNNMNNACTAATGTATGAAACC CAC-3'). A third PCR was performed using the products from the previous two PCRs as the template and the EFFP2 and VP162R primers, fusing the entire iDab sequences together. The product from the final PCR was digested with SfiI and NotI and ligated into the yeast two-hybrid pVP16 vector to generate fusions to the VP16 activation domain. The ligation reaction was transformed into MegaX DH10B^{TM} T1^{R} Electrocomp^{TM} cells (Invitrogen) via electroporation. The transformed cells were plated onto five 25 cm x 25 cm LB plates containing ampicillin, grown overnight, and then harvested by scraping. The plasmids were isolated with a Qiagen EndoFree Plasmid Maxi kit (Qiagen, Hilden, Germany) and used as the sublibrary for second round screening. The ABD and DHPH sequences were digested out from the pBTM116 plasmids, gel purified, and ligated into the mammalian two-hybrid plasmid pM1 for fusion to the Gal4 DNA binding domain. The plasmids encoding the iDabs isolated after second round screening were digested with SfiI and NotI, gel purified, and ligated into

the mammalian two-hybrid plasmid pEFVP16 for fusion to the VP16 activation domain. The ABI7 iDab was amplified through PCR from pEFVP16-ABI7 with the primers 5'-TGCTATCGTCGACATGGCCGAGGTGCAGCTGTTG-3' and 5'- TTTACCTGTCGACCTAGCTCGAGACGGTGACCAGGGTTC-3' and inserted into pEGFP-C1 (Clontech, Mountain View, CA, USA), pPS (protein switch fused to EGFP) (13), p4NLS (containing 4 SV40t antigen nuclear localization signals fused to EGFP, created through removal of Bcr-Abl from p4NLS-Bcr-Abl (12) and re-ligation of the plasmid), and pmCherry-C1 at the SalI site. RIN1 was amplified through PCR from a plasmid containing the human RIN1 gene (NM_004292, OriGene, Rockville, MD, USA) with the primers 5'-TGCTATCGTCGACATGGAAAGCCCTGGAGAGTCAGGC-3' and 5'- TTTACCTGTCGACCTAGTACCCCACTGAGCTCTCCCTCC-3' and inserted into pEGFP-C1, pPS, p4NLS, and pmCherry-C1 at the SalI site. pEGFP-CCmut3 was created through site directed mutagenesis of CCmut2 (68) using the primers 5'- CCGCATTCGGCGCCTGGAGCAGCGGGTGAAC-3' and 5'-GTTCACCCGCTGCTCCAGGCGCCGAATGCG-G-3'. CCmut3 was then amplified through PCR and inserted into pEGFP-C1, pPS, p4NLS, and pmCherry-C1 at the XhoI sites. The gene encoding Bcr-Abl was digested from pEGFP-Bcr-Abl (12) with EcoRI and inserted into the EcoRI site of pmCherry-C1 (Clontech).

X-gal Assay

Colonies growing on the YC-WLH plates from the library screens were picked and streaked onto a 9 cm YC-WLH master plate and incubated at 30 °C for 2-3 days. A nylon membrane (Biodyne, Pall) was placed on top of the master plate and incubated at

30 °C for 15 min. The membrane was then flash frozen in liquid nitrogen, allowed to thaw, and then placed on top of a filter paper soaked in X-gal solution (0.334 mg/mL X-gal, 0.1M sodium phosphate, 0.01M KCl, and 1mM $MgSO_4$, 0.27% (v/v) β-mercaptoethanol, pH 7.0) in a 15 cm petri dish. After incubation at 30 °C for 3 hours, blue colonies were marked.

Mammalian Two-Hybrid Assay

Twenty-four hrs after seeding 5 x 10^4 1471.1 cells into a white 96-well plate (Cellstar, Greiner Bio-One, Monroe, NC, USA), the media was replaced with DMEM with 10% FBS and without antibiotics, and pM1-ABD or pM1-DHPH was cotransfected with pEFVP16-iDab, pG5-Fluc (Promega), and pRL-CMV (Promega) in a 10:10:10:1 ratio using Lipofectamine 2000. Twenty-four hrs after transfection the firefly and renilla luminescence were measured on PlateLumino (Stratec Biomedical Systems) luminometer using the Dual-Glo Luciferase Assay (Promega) reagents following the manufacturer's recommendations. The mean from duplicate samples were taken from three separate experiments. pAD-SV40 and pBD-p53 (Stratagene) plasmids were used for the positive control, and pM1 was used as the negative control. The fold-induction of the luminescence was calculated by subtraction of the luminescence intensity from the negative control and normalizing to the renilla luminescence.

Confocal Microscopy and Co-localization

Twenty-four hrs after transfection into Cos-7 cells seeded in 4-well live cell chambers (Nalge NUNC International, Naperville, IL, USA), fluorescence images were

captured with a FV1000-XY (Olympus) confocal microscope using a 60X PlanApo oil immersion objective (NA 1.45) and Olympus FluoView software. mCherry was excited at 543 nm (HeNe laser), and a 555-655 nm emission filter was used to select the emitted light. EGFP was excited at 488 nm (Argon laser), and a 500-530 nm emission filter was used to select the emitted light. Images were collected in sequential line mode. The exposure settings and gain of laser were kept constant below the detected pixel saturation, and no bleed-through was observed between channels. Pixel resolution was kept at 1024 x 1024 with maximum of 2.5X digital zoom. For each field of view, six images were taken in the z-plane. Image analysis was performed using ImageJ software (freeware, NIH) after converting the images to eight-bit format. The background fluorescence was quantified for each image by selecting a region of interest (ROI) that did not contain cells. This background fluorescence was subtracted from each of the images through use of a plugin set to subtract the mean background fluorescence plus three times the standard deviation in the background. Using ROI manager, the parallel images were duplicated and then analyzed for co-localization with the JACoP plugin (http://rsb.info.nih.gov/ij) (74). The quantitative co-localization coefficient was generated with Costes' automatic threshold (75). All experiments were repeated at least three times.

Fluorescence Microscopy and Nuclear Translocation

The day before transfection between 2 x 10^5 and 3 x 10^5 Cos-7 cells were seeded in each well of a 2-well live cell chamber (Lab-tek II chamber slide system, Nalge NUNC, Rochester, NY, USA). Twenty-four hrs following cotransfection of pmCherry-Bcr-Abl and either pPS, pPS-CCmut3, pPS-ABI7or pPS-RIN1 in duplicate, the media

was replaced with phenol red free RPMI, and 10 µL EtOH (control) was added to one replicate and 10 µL of 20 µM dex was added to the other. After 2-4 hr incubation at 37 °C, 0.5 µL of 10 mg/mL H33342 (nuclear stain) was added, and the cells were incubated at 37°C for 15 min. Cells were then analyzed with an inverted fluorescence microscope (Olympus IX701F, Scientific Instrument Co., Sunnyvale, CA) with high-quality narrow band GFP filter (excitation HQ480/20 nm, emission HQ510/20 nm, beam splitter Q4951p, Chroma Technology Corp., Brattleboro, VT), high-quality TRITC filter (excitation HQ545/30 nm, emission HQ620/60 nm, beam splitter Q570lp, Chroma Technology Corp.). Cells were photographed with an F-view Monochrome CCD camera using a 60x objective. During the microscopy the cells were maintained at 37 °C with an air stream incubator (Nevtek ASI 400, Burnsville, VA) with temperature control. Twenty-four hrs after cotransfection of pmCherry-Bcr-Abl and either p4NLS, p4NLS-ABI7, p4NLS-CCmut3, or p4NLS-RIN1 the cells were imaged using the same microscopy settings and conditions. Following the quantification of the amount of Bcr-Abl in the nucleus as previously described (13, 45, 76, 77), the amount of Bcr-Abl that translocated to the nucleus was calculate using the following equation:

$$\%Nuclear\ BcrAbl = \frac{(BcrAbl\ with\ 4NLS) - (BcrAbl\ alone)}{(4NLS) - (BcrAbl\ alone)} x100$$

Results

The overall results of the IAC[3] screenings are depicted in Figure 6.2. Two libraries, one consisting of nine and the other consisting of 14 amino acids randomized in CDR3, were screened with both the ABD and DHPH baits. For the ABD, 29 colonies were confirmed to be true interactions through the X-gal assay. Of these 29, 9 were

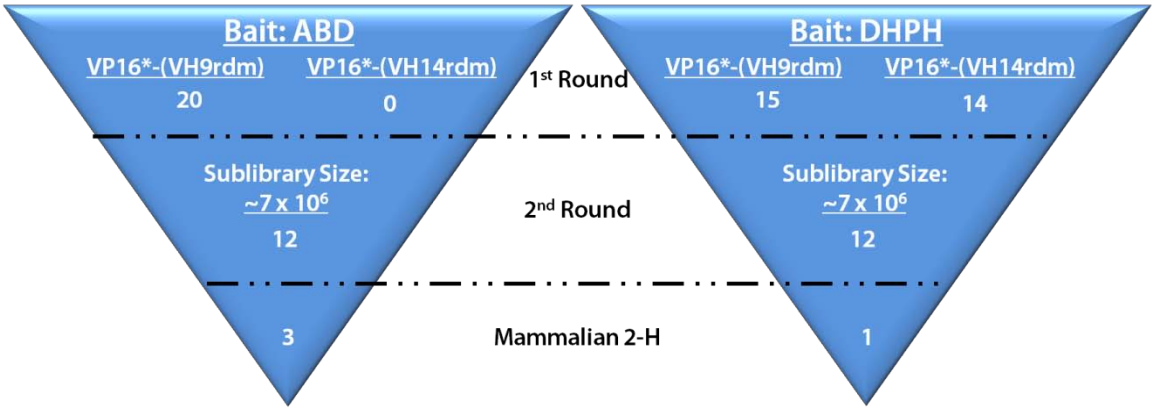

Figure 6.2. Overview of IAC[3] screens against ABD and DHPH baits. Two libraries were screened in the first round. 20 and 15 constructs were isolated using the ABD and DHPH as baits, respectively, from a library that contained nine amino acids randomized in CDR3. Zero and 14 constructs were isolated using the ABD and DHPH as baits, respectively, from a library that contained 14 amino acids randomized in CD3. After generation of sublibraries by randomizing the bases encoding CDR2, the top 12 binders were isolated for each bait. Mammalian two-hybrid assays then identified the top three ABD binders and the top DHPH binder.

determined to be weaker interactions due to their faint blue result and were eliminated to give a total of 20 colonies that were used for creation of the sublibrary. For the DHPH, a much larger number of colonies (159 total) were validated to exhibit true interactions via the X-gal assay. However, the pool was limited to the darkest X-gal results, and 25 were used in creation of the sublibrary. For the DHPH bait, two sublibraries were created, one from the preys extracted from the VP16*-(VH9rdm) screen, and one from the preys extracted from the VP16*-(VH14rdm) screen. The sizes of the sublibraries were estimated to be approximately 7×10^6. The second round of screening produced more than 800 colonies for both the ABD and DHPH targets. 50 of the largest colonies were chosen for validation in the X-gal assay. From the 50 assayed for each bait, the top 12 were selected. The sequences of these 24 are tabulated in Tables 6.1 and 6.2 along with consensus sequences for each. Although no strong consensus is observed, none is truly expected given that each individual iDab may bind at different regions of the target domain.

The sequences of these 24 iDabs were then subcloned into pEFVP16 to generate fusion constructs with the VP16 activation domain in a mammalian expression plasmid for further validation in a mammalian two-hybrid assay. As this assay provides a luminescent readout, the binding affinities can be compared relative to each other for determination of the highest affinity binder. As seen in Figure 6.3, the ABD screens produced better binders overall, with clone A7 exhibiting the greatest binding. Although none of the DHPH binders demonstrated highly efficient binding, the top candidate, D5, was further analyzed through co-localization as any ability to compete with Bcr-Abl

Tables 6.1. Amino acid sequences (one-letter code) of the CDR2 and CDR3 regions of the ABD binding iDabs (ABIs) isolated in the screens. The amino acid (or type of amino acids) in at least 6 of the constructs was termed the consensus amino acid at that position and are in red font and summarized in the bottom row. The sequence of CDR1 was not randomized for screening and is the same for all constructs: GFTFSTFS. The amino acids at positions 1, 2, and 8 of CDR2 were not randomized and are #1-I,#2-S,#8-I. The amino acids at positions 1, 2, 12, 13, and 14 of CDR3 were not randomized and are #1-R, #2-G, #12-F, #13-D, and #14-Y.

ABI	CDR2					CDR3
Position	3	4	5	6	7	3-11
A1	P	S	G	T	L	PLWSFVRMS
A2	Q	S	G	R	L	PLWSFVRMS
A4	K	D	G	K	A	PLWSFVRMS
A5	P	S	G	Y	S	PLWSFVRMS
A7	K	C	G	H	V	PLWSFVRMS
A8	D	T	G	R	A	PLWSFVRMS
A14	R	T	S	K	T	RF
A26	A	T	G	G	A	PLWSFVRMS
A37	A	K	G	N	N	PLWSFVRMS
A45	G	K	G	D	S	PLWSFVRMS
A46	Q	T	G	S	T	PLWSFVRMS
A50	A	N	S	R	T	PLWSFVRMS
Consensus	x	S/T	G	+	φ	PLWSFVRMS

Table 6.2. Tables 6.1. Amino acid sequences (one-letter code) of the CDR2 and CDR3 regions of the DHPH binding iDabs (DBIs) isolated in the screens. The amino acid (or type of amino acids) in at least 6 of the constructs was termed the consensus amino acid at that position and are in red font and summarized in the bottom row. The sequence of CDR1 was not randomized for screening and is the same for all constructs: GFTFSTFS. The amino acids at positions 1, 2, and 8 of CDR2 were not randomized and are #1-I,#2-S,#8-I. The amino acids at positions 1, 2, 12, 13, and 14 of CDR3 were not randomized and are #1-R, #2-G, #12-F, #13-D, and #14-Y.

DBI	CDR2					CDR3
Position	1	2	3	4	5	3-11
D2	E	C	L	D	L	RF
D5	D	T	A	N	E	TFFRPPVRA
D8	P	C	C	R	E	TFFRPPVRA
D9	E	Y	G	S	D	TFFRPPVRA
D12	G	E	S	K	D	TFFRPPVRA
D13	S	M	G	E	D	TFFRPPVRA
D15	K	G	W	C	L	GG
D29	D	T	S	H	E	TFFRPPVRA
D32	S	A	S	E	Q	TFFRPPVRA
D33	D	D	S	G	V	TFFRPPVRA
D34	P	D	S	K	E	TFFRPPVRA
D37	G	C	G	R	D	TFFRPPVRA
Consensus	x	x	S/G	x	-	TFFRPPVRA

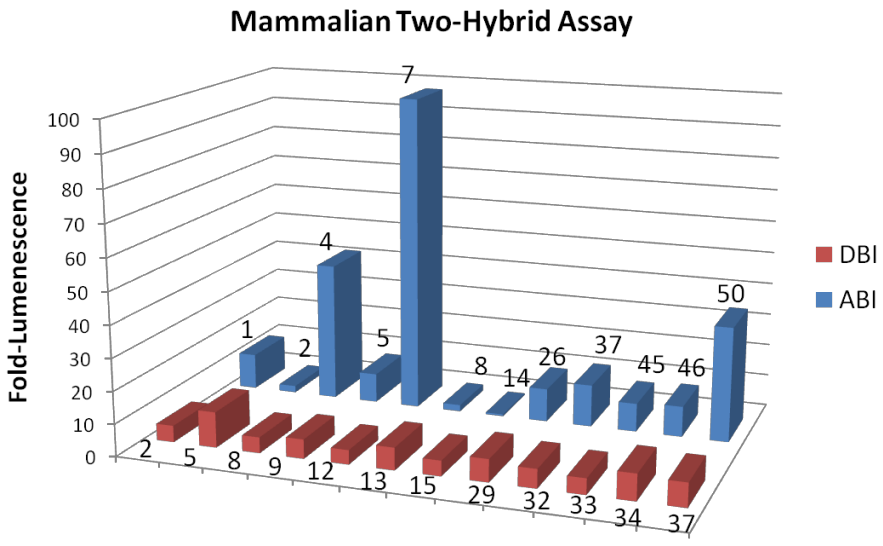

Figure 6.3. Mammalian two-hybrid assays. Blue columns = ABD binding iDabs (ABI), red columns = DHPH binding iDabs (DBI). Based on these mammalian two-hybrid results, the top ABI (ABI7) and the top DBI (DBI5) were selected for further analysis by co-localization with full-length Bcr-Abl.

binding to phospholipids may prove beneficial, and the lack of knowledge regarding the relationship between the mammalian two-hybrid result and the ability to translocate Bcr-Abl justifies further exploration.

The IAC^3 screening and mammalian two-hybrid assays were performed using the isolated ABD or DHPH domains. To confirm these interactions carried over to the full-length Bcr-Abl protein, and to compare their ability to bind Bcr-Abl with CCmut3 and RIN1, co-localization studies were performed with each binding domain and mCherry-Bcr-Abl in Cos-7 cells. A rigorous method for analysis of co-localization, the use of Costes' automatic threshold to determine Costes' coefficient of co-localization (75), was utilized. In this method, fluorescence signals originating from the same location (indicating the interaction between the proteins fused to them) will result in a value greater than 0.5. Noninteracting proteins will generate values close to zero or negative. As seen in Figure 6.4, ABI7, CCmut3, and RIN1 all demonstrated co-localization with Bcr-Abl and confirmed the interactions of these binding motifs with the full protein under biological conditions inside of cells. In agreement with the mammalian two-hybrid result, DBI5 did not result in efficient co-localization (below 0.5 co-localization coefficient with Costes' automatic threshold) with Bcr-Abl. As no iDab was isolated that efficiently interacted with the DHPH region of Bcr-Abl, as determined by the mammalian two-hybrid and co-localization with Bcr-Abl, and due to the other three binding domains functioning superiorly, the DBIs were not analyzed further.

The ABD was selected as a target for the potential advantage of competing with actin binding that may preclude nuclear translocation. Interestingly, upon cotransfection

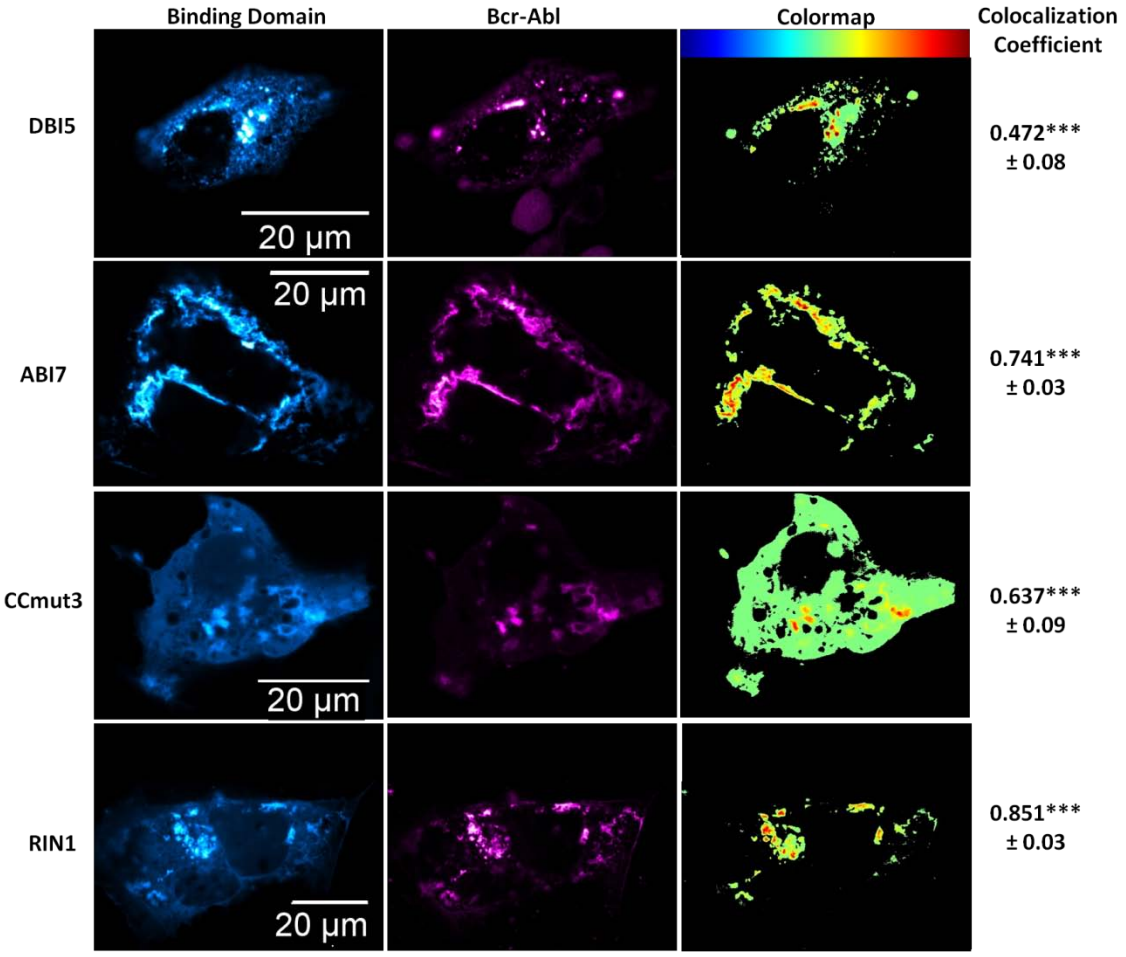

Figure 6.4. Co-localization between Bcr-Abl and the binding domains. Binding domains are in the left columns (cyan), and Bcr-Abl is in the middle column (magenta). Colormaps are illustrated in the right column with the key at the top of the column (highest co-localization = red). The co-localization coefficients are indicated to the right of the colormaps. The mean co-localization coefficient was determined after analyzing at least three cells, and the experiment was repeated three times. The values reported are the means ± S.E.M. Statistical significance was determined by one-way ANOVA with Tukey's posttest. **p<0.01, ***p<0.001.

of ABI7 with Bcr-Abl, a marked redistribution of the subcellular localization pattern was observed. Alone, Bcr-Abl forms a distinct localization pattern similar to the pattern resulting from actin staining, indicating its interaction with actin (Figure 6.5a). However, when ABI7 is coexpressed along with Bcr-Abl this localization pattern shifts to one of punctuate dots throughout the cytoplasm (Figure 6.5b). This observation may be explained by ABI7 preventing Bcr-Abl from binding actin in the same fashion as normally occurs, and may provide evidence for the hypothesized benefit of rendering Bcr-Abl more available for nuclear translocation. Recently it has been demonstrated that the ABD plays a joint role, along with the tyrosine kinase domain, in regulating the NLSs found in Bcr-Abl (59). A further potential implication of targeting the ABD may be a shift to the NLS-active conformation resulting in nuclear accumulation. Although ABI7 did cause an altered localization pattern of Bcr-Abl in the cytoplasm, no substantial increase in nuclear localization was observed. Interestingly, when CCmut3 was co-expressed with Bcr-Abl a dramatic change in the localization pattern occurred, and Bcr-Abl was found to be diffuse throughout the entire cytoplasm and no longer localized to any particular region (Figure 6.5C). This prominent shift may be reflective of the change from tetrameric Bcr-Abl to monomeric Bcr-Abl, and the correlated Bcr-Abl conformations.

In attempt to use the binding motifs for translocation of Bcr-Abl into the nucleus, they were each subcloned into plasmids as fusions with the localization controllable protein switch (13). One potential advantage of using the protein switch for translocating a protein is the initial localization in the same subcellular compartment as the target

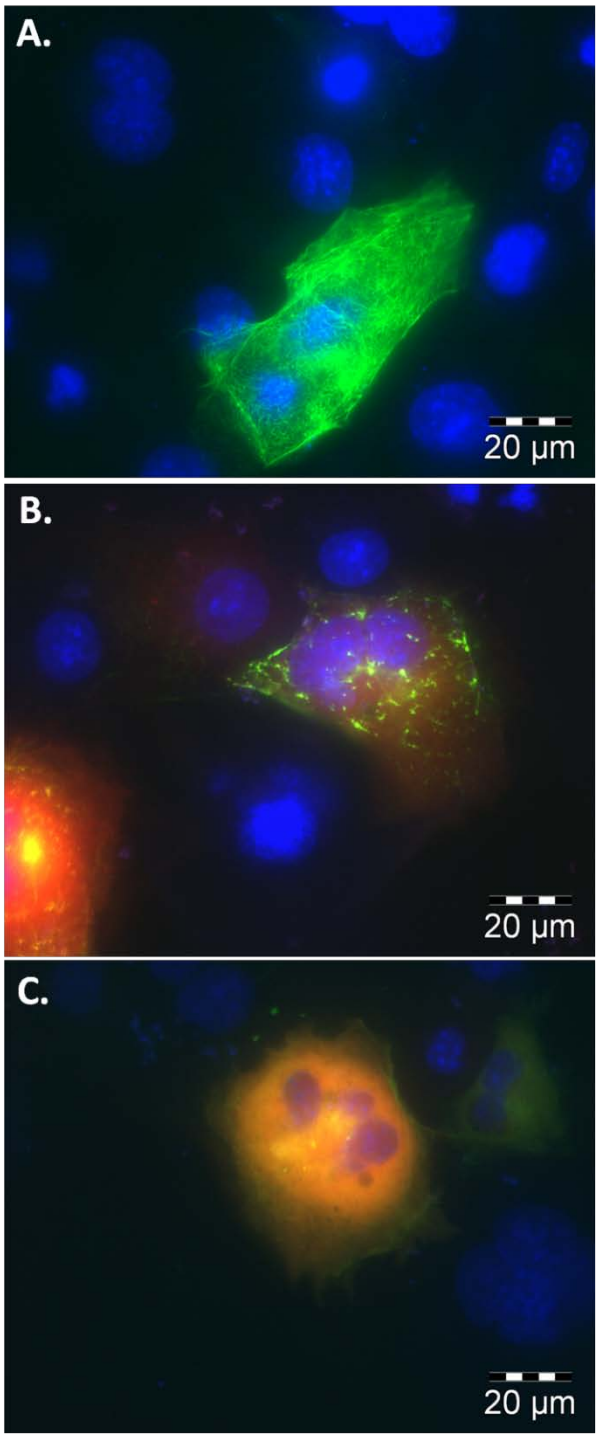

Figure 6.5 Redistribution of Bcr-Abl subcellular localization. A) EGFP-Bcr-Abl expressed alone in Cos-7 cells. Bcr-Abl localizes at actin and forms a pattern characteristic of actin filaments. B) EGFP-Bcr-Abl and mCherry-ABI7. ABI7 affects Bcr-Abls interaction with actin, and results in a distinct localization pattern. C) EGFP-Bcr-Abl and mCherry-CCmut3. CCmut3 causes a Bcr-Abl to become diffuse throughout the cytoplasm.

protein. This allows equilibration time for the interaction between the target protein and the protein switch before any attempt of translocation. After cotransfecting (in duplicate) mCherry-Bcr-Abl with a protein switch construct, ethanol (carrier) or dex was added and fluorescence microscopy used to image the cells 2-4 hrs postligand induction. The percentage of Bcr-Abl inside the nucleus was determined in the presence of ethanol or dex and used to determine a percent nuclear increase (PNI) upon ligand induction. Attempts to move Bcr-Abl with one binding domain (protein switch fused to either CCmut3, ABI7, or RIN1) did not produce any nuclear Bcr-Abl (data not shown). However, when two binding domains were used (two separate protein switch constructs with different binding domains cotransfected) it was possible to find cells with Bcr-Abl inside the nucleus. Some examples are illustrated in Figure 6.6. Nevertheless, the majority of the cells did not have noticeable Bcr-Abl inside the nucleus. While identifying cells with nuclear Bcr-Abl may demonstrate that Bcr-Abl can be moved with this system, the fact that this occurred on a limited basis indicates the inefficiency of the system as applied to Bcr-Abl. As both protein switch constructs are fused to EGFP it is impossible to distinguish cells transfected with only one of the protein switches from those transfected with both protein switch constructs, a fact that may explain why Bcr-Abl could be found in the nucleus of some limited cells. A further note is the level of protein switch that translocated into the nucleus. After incorporation of the binding domain into the protein switch there was a decrease in the nuclear translocation, which may be reflective of the interaction with Bcr-Abl as well as some interference from the binding domain.

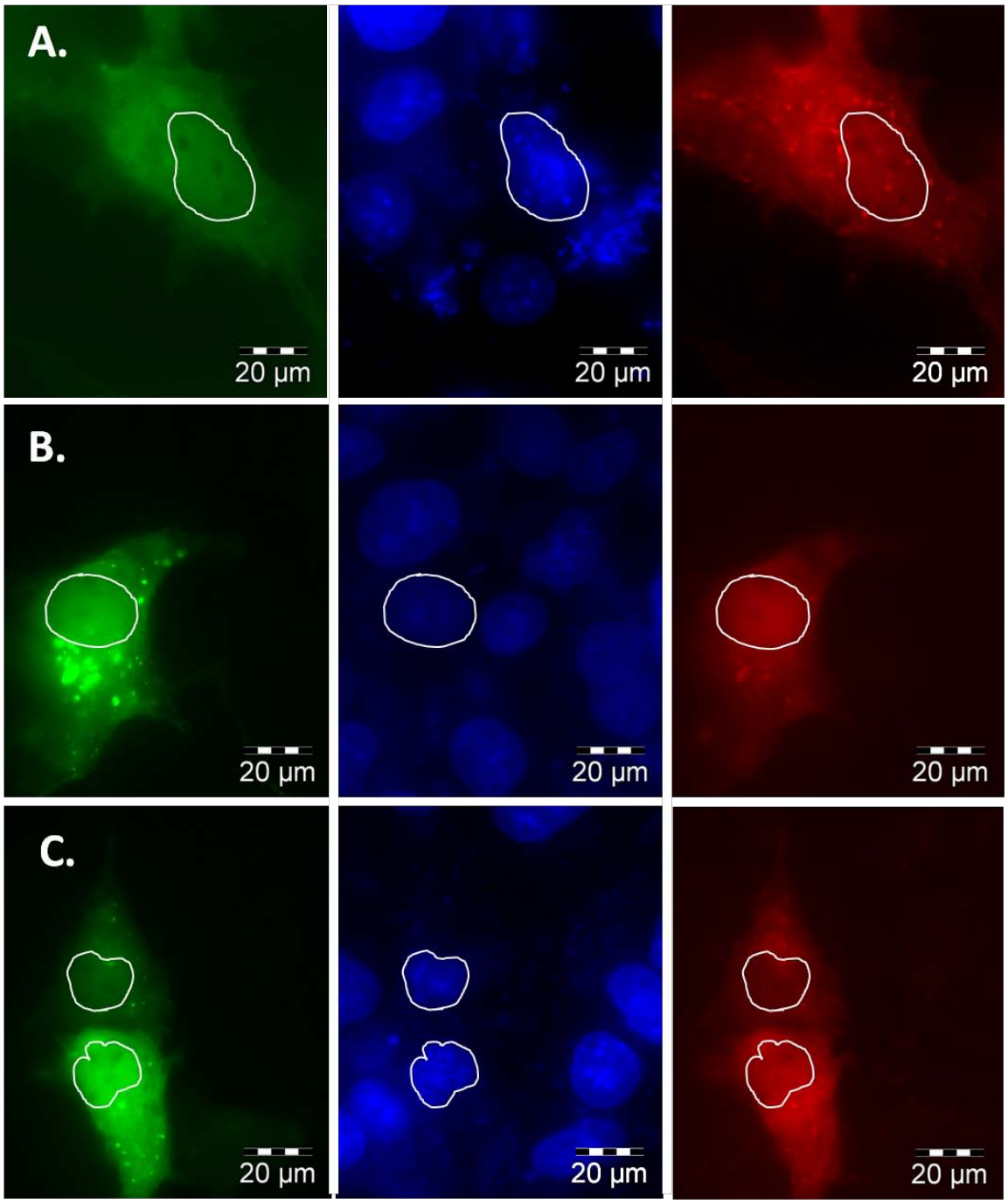

Figure 6.6. Nuclear translocation using the protein switch. Left column = EGFP fluorescence from protein switch; Middle column = Nuclei (H33342); Right column = mCherry from Bcr-Abl. Outlines of the nuclei are included for reference in all images. A) Combination of PS-ABI7 and PS-CCmut3. B) Combination of PS-ABI7 and PS-RIN1. C) Combination of PS-CCmut3 and PS-RIN1.

To increase the force driving nuclear localization and simplify the approach to move Bcr-Abl, the binding motifs were subcloned into a plasmid containing 4 strong NLSs (from SV40t antigen). These constructs, in contrast to protein switch constructs that were only marginally nuclear even in the presence of dex, were exclusively localized to the nucleus (Figure 6.7A-D, green fluorescence). Nevertheless, 4NLS-ABI7 and 4NLS-RIN1 were unable to cause a nuclear accumulation of Bcr-Abl (Figure 6.7B and C). CCmut3, on the other hand, caused the majority of Bcr-Abl to translocate to the nucleus (Figure 6.7D, and Figure 6.8). The percentage of Bcr-Abl inside the nucleus upon cotransfection with the 4NLS constructs was quantified and is indicated in Figure 6.8. While one possible explanation for the inability of 4NLS-ABI7 and 4NLS-RIN1 to translocate Bcr-Abl is that their interaction with Bcr-Abl is not strong enough, all of the binding domains generated statistically indistinguishable co-localization coefficients. That only one of these binding domains exhibited the ability to translocate Bcr-Abl supports the concept that the region of Bcr-Abl where the binding domain interacts is also a critical factor.

In spite of the fact that minimal Bcr-Abl translocated with 4NLS-ABI7, the combination of 4NLS-ABI7 and 4NLS-CCmut3 did result in enhanced nuclear accumulation of Bcr-Abl and only minimal levels were detected outside of the cytoplasm (Figure 6.8C, D, and E). This validates the concept that binding Bcr-Abl through multiple regions is advantageous for nuclear translocation.

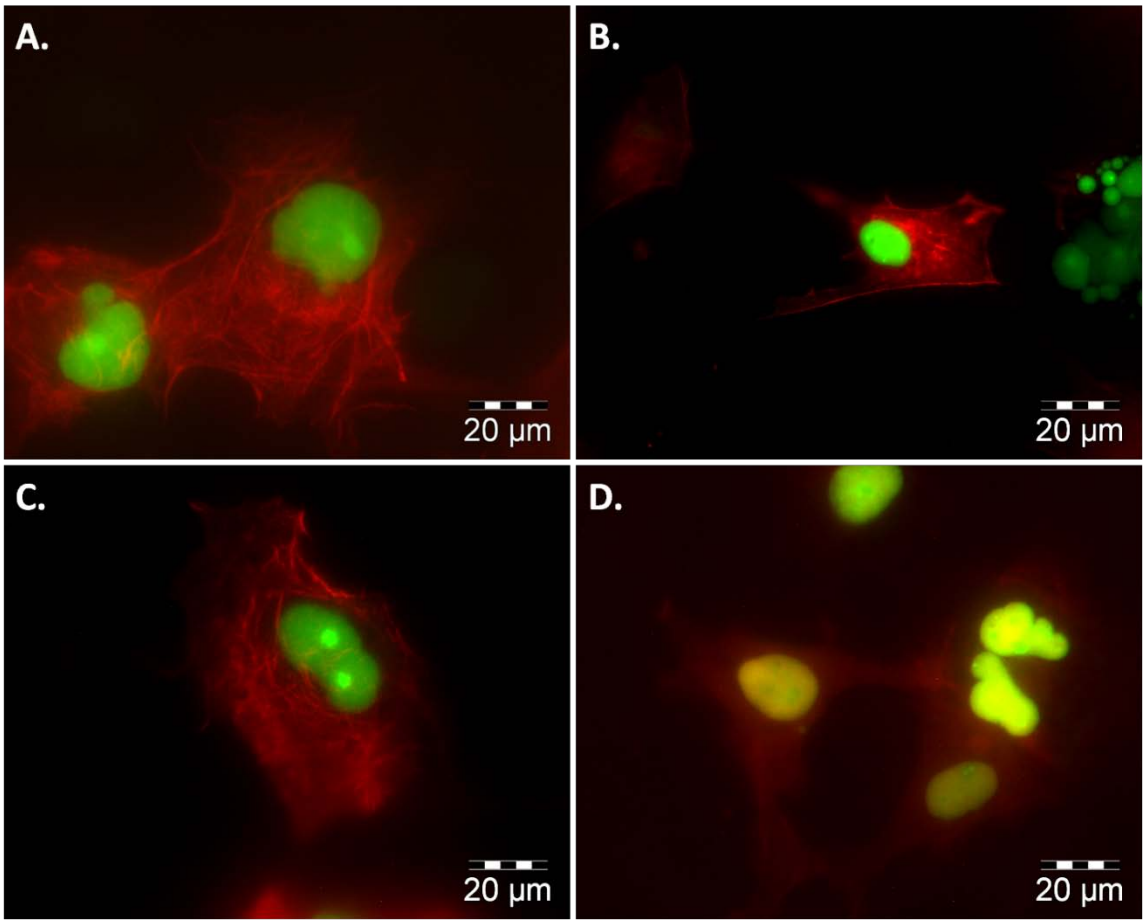

Figure 6.7. Nuclear translocation using 4NLS-binding motif constructs. Bcr-Abl is shown in red (mCherry), and the 4NLS construct is shown in green (EGFP). Images were taken at 60X magnification, and the scale bar is indicated in the lower right corner. A) mCherry-Bcr-Abl and 4NLS (no binding domain). Bcr-Abl localizes in the cytoplasm with actin. 4NLS is exclusively nuclear. B) mCherry Bcr-Abl and 4NLS-RIN1. Bcr-Abl remains cytoplasmic and 4NLS-RIN1 localizes to the nucleus. C) mCherry-Bcr-Abl and 4NLS-ABI7. Bcr-Abl does not accumulate in the nucleus as does 4NLS-ABI7. D) mCherry-Bcr-Abl and 4NLS-CCmut3. As indicated by the overlapping green and red fluorescence (yellow), Bcr-Abl is translocated into the nucleus along with 4NLS-CCmut3.

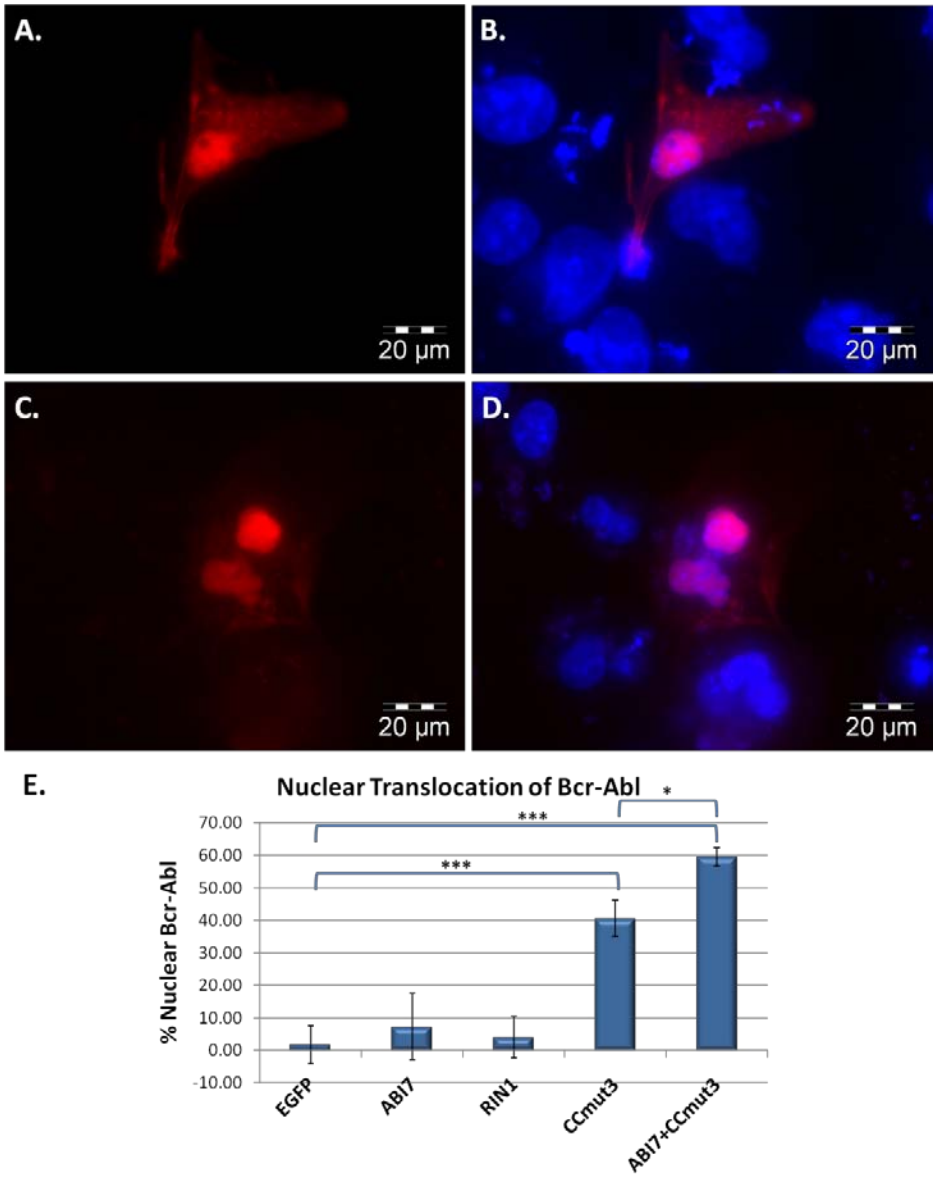

Figure 6.8 Representative images of nuclear Bcr-Abl resulting from 4NLS-CCmut3, and quantification of nuclear Bcr-Abl from all 4NLS constructs. A) To more clearly show the nuclear accumulation of Bcr-Abl upon cotransfection with 4NLS-CCmut3, an image of only the red fluorescence (Bcr-Abl) is shown. B) The image shown in (A) is shown with the nuclear stain (H33342, blue). C) Resulting Bcr-Abl localization after transfecting 4NLS-ABI7 with 4NLS-CCmut3. D) Image from (C) with nuclear stain. E) The percentages of Bcr-Abl found in the nucleus after cotransfection with the indicated constructs was quantified and graphed. At least five cells from each experiment were imaged and analyzed. Each construct was cotransfected with pmCherry-Bcr-Abl three times. Statistical analysis was determined by one-way ANOVA with Tukey's posttest. *$p<0.05$, ***$p<0.001$.

Conclusions

Both the aberrant tyrosine kinase activity and the cytoplasmic localization are important outcomes of the fusion between the Bcr and Abl proteins. Current CML treatments target the tyrosine kinase activity, and an interesting alternative that has not been highly explored is repositioning Bcr-Abl into the nucleus where it is known to be an activator of apoptosis. In this report we have demonstrated the ability to escort Bcr-Abl to the nucleus through Bcr-Abl-binding domains.

In order to compliment the regions of Bcr-Abl already targeted by CCmut3 and RIN1, we screened for iDabs that would bind at the ABD and DHPH. While the protocol outlined for IAC^3 describes the screening of 17 libraries in the first round, followed by screening sublibraries in subsequent second and third rounds of screening, we were able to identify an iDab with efficient binding to Bcr-Abl through screening of only two libraries in the first round and one sublibrary. This demonstrates the versatility and usefulness of the IAC^3 technology. As speculated, this iDab (ABI7) caused a redistribution of Bcr-Abl from its regular localization pattern indicating the ability to interfere with actin interactions. However, ABI7 was unable to efficiently translocate Bcr-Abl to the nucleus without CCmut3. Further affinity maturation of ABI7 could be performed through creation of a randomized CDR1 sublibrary and additional screening. Nevertheless, the combination of 4NLS-ABI7 and 4NLS-CCmut3 produced remarkable accumulation of Bcr-Abl in the nucleus.

Attempts to move Bcr-Abl to the nucleus with the protein switch were unsuccessful with one binding domain, but through two protein switches fused to two distinct binding domains it was possible to identify some cells wherein Bcr-Abl had been

transported into the nucleus. The numerous interactions and large size of Bcr-Abl make it a challenging protein to redirect to alternative subcellular localizations, and other proteins may be more readily translocated. However, the incorporation of the binding domains into the protein switch decreased the nuclear translocation, a factor contributing to the inefficient translocation of Bcr-Abl. This finding highlights the potential need to optimize the protein switch with the binding domain fused to it. The strength of the NES and NLS used in the protein switch could be re-optimized as well as the linker fusing the protein switch to the binding domain and terminus where the binding domain is fused to the protein switch.

In stark contrast to the protein switch constructs, 4NLS-CCmut3 and 4NLS-ABI7 + 4NLS-CCmut3 produced an impressive re-localization of Bcr-Abl to the nucleus. We have long speculated on the advantage and need for some mean-residency time in the location of the target protein to allow the interaction to occur. This mean-residency time is afforded by the controlled translocation in the protein switch. However, that a 4NLS construct (4NLS-CCmut3) was the only construct tested to demonstrate efficient nuclear accumulation of Bcr-Abl strongly supports the claim that mean-residency time is not needed. CML cells where Bcr-Abl is present, and not entirely being co-translated with 4NLS-CCmut3, may exhibit a different dynamic wherein the mean-residency time is more important. Dismissal of the usefulness of the protein switch based on these experiments is not entirely justified, and further exploration into the ability to translocate endogenous Bcr-Abl in CML cells will be needed.

In these experiments four binding domains that bind Bcr-Abl at distinct regions were explored. Interestingly, only one of three binding domains that demonstrated

efficient co-localization with Bcr-Abl resulted in efficient nuclear translocation of Bcr-Abl. This indicates the binding affinity is not the only consideration, and may not be the most important consideration, in determining the ability to translocate Bcr-Abl. Speculatively, the resulting Bcr-Abl conformation upon being bound by the binding domain may contribute to the ability of one domain to translocate Bcr-Abl and not another. RIN1 interacts with the SH3/2 domains of Bcr-Abl, and is known to bind in such a way that Bcr-Abl is maintained in an active conformation (71, 73, 78, 79). This active conformation is correlated with protein interactions thought to cause cytoplasmic retention and inhibition of the Bcr-Abl NLSs (59). However, CCmut3 binds the coiled-coil domain and interferes with the oligomeric state of Bcr-Abl (68-70, 80). The homo-oligomerization of Bcr-Abl is directly correlated with Bcr-Abl activity, and the formation of hetero-oligomers with CCmut3 decreases its activity (unpublished data). This inactive conformation may relieve the cytoplasmic retention as well as activate the Bcr-Abl NLSs. Thus, it is easy to speculate on why CCmut3 was able to translocate Bcr-Abl and RIN1 was not, in spite of the high affinity of RIN1 for Bcr-Abl. As demonstrated with these binding domains, not only binding, but binding Bcr-Abl in an inactive conformation, is critical to the ability to translocate Bcr-Abl.

Capture and escort of Bcr-Abl to the nucleus is an interesting concept for turning the disease causing agent against the diseased cells. Here we demonstrate Bcr-Abl can be redirected to the nucleus by NLSs attached to a Bcr-Abl binding domain. Further, this work validates CCmut3 as an efficient binding partner of Bcr-Abl which can be used for controlling the subcellular localization of Bcr-Abl. Capture and escort of Bcr-Abl would accomplish two goals: nuclear accumulation of endogenous Bcr-Abl, as well as its

cytoplasmic depletion. This ability of CCmut3 to translocate Bcr-Abl has great potential for potent induction of apoptosis in CML cells, and may extend to the ability to induce apoptosis in resistant CML cells and also CML stem cells. This is the subject of future work in our laboratory.

Acknowledgments

We acknowledge the use of DNA/Peptide Core (NCI Cancer Center Support Grant P30 CA042014, Huntsman Cancer Institute). This work was funded by NIH R01-CA129528. We would like to thank Dr. David Stillman, Dr. Jared Rutter, and Danny Li for technical assistance in work involving yeast, and Jonathan Constance, Rian Davis, Mohanad Mossalam, Benjamin Bruno, Geoffrey Miller, David Woessner, Abdul Okul, and Karina Matissek for scientific discussions.

References

1. Rowley JD. Letter: A new consistent chromosomal abnormality in chronic myelogenous leukaemia identified by quinacrine fluorescence and Giemsa staining. Nature 1973; 243: 290-3.

2. Sandberg AA, Gemmill RM, Hecht BK, Hecht F. The Philadelphia chromosome: a model of cancer and molecular cytogenetics. Cancer Genet Cytogenet 1986; 21: 129-46.

3. Kurzrock R, Kantarjian HM, Druker BJ, Talpaz M. Philadelphia chromosome-positive leukemias: from basic mechanisms to molecular therapeutics. Ann Intern Med 2003; 138: 819-30.

4. Lugo TG, Pendergast AM, Muller AJ, Witte ON. Tyrosine kinase activity and transformation potency of bcr-abl oncogene products. Science 1990; 247: 1079-82.

5. Hazlehurst LA, Bewry NN, Nair RR, Pinilla-Ibarz J. Signaling networks associated with BCR-ABL-dependent transformation. Cancer Control 2009; 16: 100-7.

6. Van Etten RA. Mechanisms of transformation by the BCR-ABL oncogene: new perspectives in the post-imatinib era. Leuk Res 2004; 28 Suppl 1: S21-8.

7. Sattler M, Griffin JD. Molecular mechanisms of transformation by the BCR-ABL oncogene. Semin Hematol 2003; 40: 4-10.

8. Wetzler M, Talpaz M, Van Etten RA, Hirsh-Ginsberg C, Beran M, Kurzrock R. Subcellular localization of Bcr, Abl, and Bcr-Abl proteins in normal and leukemic cells and correlation of expression with myeloid differentiation. J Clin Invest 1993; 92: 1925-39.

9. Dhut S, Chaplin T, Young BD. BCR-ABL and BCR proteins: biochemical characterization and localization. Leukemia 1990; 4: 745-50.

10. Aloisi A, Di Gregorio S, Stagno F, et al. BCR-ABL nuclear entrapment kills human CML cells: ex vivo study on 35 patients with the combination of imatinib mesylate and leptomycin B. Blood 2006; 107: 1591-8.

11. Vigneri P, Wang JY. Induction of apoptosis in chronic myelogenous leukemia cells through nuclear entrapment of BCR-ABL tyrosine kinase. Nat Med 2001; 7: 228-34.

12. Dixon AS, Kakar M, Schneider KM, Constance JE, Paullin BC, Lim CS. Controlling subcellular localization to alter function: Sending oncogenic Bcr-Abl to the nucleus causes apoptosis. J Control Release 2009.

13. Kakar M, Davis JR, Kern SE, Lim CS. Optimizing the protein switch: altering nuclear import and export signals, and ligand binding domain. J Control Release 2007; 120: 220-32.

14. Nowell PC, Hungerford DA. Chromosome studies on normal and leukemic human leukocytes. J Natl Cancer Inst 1960; 25: 85-109.

15. Ren R. Mechanisms of BCR-ABL in the pathogenesis of chronic myelogenous leukaemia. Nat Rev Cancer 2005; 5: 172-83.

16. Quintas-Cardama A, Cortes J. Molecular biology of bcr-abl1-positive chronic myeloid leukemia. Blood 2009; 113: 1619-30.

17. Okimoto RA, Van Etten RA. Navigating the road toward optimal initial therapy for chronic myeloid leukemia. Curr Opin Hematol; 18: 89-97.

18. Goldman JM. Chronic myeloid leukemia: a historical perspective. Semin Hematol; 47: 302-11.

19. Druker BJ, Tamura S, Buchdunger E, et al. Effects of a selective inhibitor of the Abl tyrosine kinase on the growth of Bcr-Abl positive cells. Nat Med 1996; 2: 561-6.

20. Deininger MW, Goldman JM, Lydon N, Melo JV. The tyrosine kinase inhibitor CGP57148B selectively inhibits the growth of BCR-ABL-positive cells. Blood 1997; 90: 3691-8.

21. le Coutre P, Mologni L, Cleris L, et al. In vivo eradication of human BCR/ABL-positive leukemia cells with an ABL kinase inhibitor. J Natl Cancer Inst 1999; 91: 163-8.

22. Capdeville R, Buchdunger E, Zimmermann J, Matter A. Glivec (STI571, imatinib), a rationally developed, targeted anticancer drug. Nat Rev Drug Discov 2002; 1: 493-502.

23. Schindler T, Bornmann W, Pellicena P, Miller WT, Clarkson B, Kuriyan J. Structural mechanism for STI-571 inhibition of abelson tyrosine kinase. Science 2000; 289: 1938-42.

24. Baccarani M, Saglio G, Goldman J, et al. Evolving concepts in the management of chronic myeloid leukemia. Recommendations from an expert panel on behalf of the European Leukemianet. Blood 2006.

25. Gorre ME, Mohammed M, Ellwood K, et al. Clinical resistance to STI-571 cancer therapy caused by BCR-ABL gene mutation or amplification. Science 2001; 293: 876-80.

26. Roumiantsev S, Shah NP, Gorre ME, et al. Clinical resistance to the kinase inhibitor STI-571 in chronic myeloid leukemia by mutation of Tyr-253 in the Abl kinase domain P-loop. Proc Natl Acad Sci U S A 2002; 99: 10700-5.

27. Shah NP, Nicoll JM, Nagar B, et al. Multiple BCR-ABL kinase domain mutations confer polyclonal resistance to the tyrosine kinase inhibitor imatinib (STI571) in chronic phase and blast crisis chronic myeloid leukemia. Cancer Cell 2002; 2: 117-25.

28. Weisberg E, Manley P, Mestan J, Cowan-Jacob S, Ray A, Griffin JD. AMN107 (nilotinib): a novel and selective inhibitor of BCR-ABL. Br J Cancer 2006.

29. Weisberg E, Manley PW, Breitenstein W, et al. Characterization of AMN107, a selective inhibitor of native and mutant Bcr-Abl. Cancer Cell 2005; 7: 129-41.

30. O'Hare T, Walters DK, Stoffregen EP, et al. In vitro activity of Bcr-Abl inhibitors AMN107 and BMS-354825 against clinically relevant imatinib-resistant Abl kinase domain mutants. Cancer Res 2005; 65: 4500-5.

31. Lu XY, Cai Q, Ding K. Recent Developments in the Third Generation Inhibitors of Bcr-Abl for Overriding T315I Mutation. Curr Med Chem; 18: 2146-57.

32. Gozgit JM, Wong MJ, Wardwell S, et al. Potent Activity of Ponatinib (AP24534) in Models of FLT3-Driven Acute Myeloid Leukemia and Other Hematologic Malignancies. Mol Cancer Ther; 10: 1028-35.

33. Zhou T, Commodore L, Huang WS, et al. Structural mechanism of the Pan-BCR-ABL inhibitor ponatinib (AP24534): lessons for overcoming kinase inhibitor resistance. Chem Biol Drug Des; 77: 1-11.

34. Huang WS, Metcalf CA, Sundaramoorthi R, et al. Discovery of 3-[2-(imidazo[1,2-b]pyridazin-3-yl)ethynyl]-4-methyl-N-{4-[(4-methylpipera zin-1-yl)methyl]-3-(trifluoromethyl)phenyl}benzamide (AP24534), a potent, orally active pan-inhibitor of breakpoint cluster region-abelson (BCR-ABL) kinase including the T315I gatekeeper mutant. J Med Chem; 53: 4701-19.

35. O'Hare T, Shakespeare WC, Zhu X, et al. AP24534, a pan-BCR-ABL inhibitor for chronic myeloid leukemia, potently inhibits the T315I mutant and overcomes mutation-based resistance. Cancer Cell 2009; 16: 401-12.

36. Eide CA, Adrian LT, Tyner JW, et al. The ABL switch control inhibitor DCC-2036 is active against the chronic myeloid leukemia mutant BCR-ABLT315I and exhibits a narrow resistance profile. Cancer Res; 71: 3189-95.

37. Taagepera S, McDonald D, Loeb JE, et al. Nuclear-cytoplasmic shuttling of C-ABL tyrosine kinase. Proc Natl Acad Sci U S A 1998; 95: 7457-62.

38. Vella V, Zhu J, Frasca F, et al. Exclusion of c-Abl from the nucleus restrains the p73 tumor suppression function. J Biol Chem 2003; 278: 25151-7.

39. Wang JY. Regulation of cell death by the Abl tyrosine kinase. Oncogene 2000; 19: 5643-50.

40. Zhu J, Wang JY. Death by Abl: a matter of location. Curr Top Dev Biol 2004; 59: 165-92.

41. Newlands ES, Rustin GJ, Brampton MH. Phase I trial of elactocin. Br J Cancer 1996; 74: 648-9.

42. Htun H, Barsony J, Renyi I, Gould DL, Hager GL. Visualization of glucocorticoid receptor translocation and intranuclear organization in living cells with a green fluorescent protein chimera. Proc Natl Acad Sci U S A 1996; 93: 4845-50.

43. Baumann CT, Lim CS, Hager GL. Intracellular localization and trafficking of steroid receptors. Cell Biochem Biophys 1999; 31: 119-27.

44. Lim CS, Baumann CT, Htun H, et al. Differential localization and activity of the A- and B-forms of the human progesterone receptor using green fluorescent protein chimeras. Mol Endocrinol 1999; 13: 366-75.

45. Kakar M, Cadwallader AB, Davis JR, Lim CS. Signal sequences for targeting of gene therapy products to subcellular compartments: the role of CRM1 in nucleocytoplasmic shuttling of the protein switch. Pharm Res 2007; 24: 2146-55.

46. Kakar M, Kanwal C, Davis JR, Li H, Lim CS. Geldanamycin, an inhibitor of Hsp90, blocks cytoplasmic retention of progesterone receptors and glucocorticoid receptors via their respective ligand binding domains. Aaps J 2006; 8: E718-28.

47. Ward ES, Gussow D, Griffiths AD, Jones PT, Winter G. Binding activities of a repertoire of single immunoglobulin variable domains secreted from Escherichia coli. Nature 1989; 341: 544-6.

48. Tanaka T, Lobato MN, Rabbitts TH. Single domain intracellular antibodies: a minimal fragment for direct in vivo selection of antigen-specific intrabodies. J Mol Biol 2003; 331: 1109-20.

49. Colby DW, Chu Y, Cassady JP, et al. Potent inhibition of huntingtin aggregation and cytotoxicity by a disulfide bond-free single-domain intracellular antibody. Proc Natl Acad Sci U S A 2004; 101: 17616-21.

50. Paz K, Brennan LA, Iacolina M, Doody J, Hadari YR, Zhu Z. Human single-domain neutralizing intrabodies directed against Etk kinase: a novel approach to impair cellular transformation. Mol Cancer Ther 2005; 4: 1801-9.

51. Verheesen P, de Kluijver A, van Koningsbruggen S, et al. Prevention of oculopharyngeal muscular dystrophy-associated aggregation of nuclear polyA-binding protein with a single-domain intracellular antibody. Hum Mol Genet 2006; 15: 105-11.

52. Gueorguieva D, Li S, Walsh N, Mukerji A, Tanha J, Pandey S. Identification of single-domain, Bax-specific intrabodies that confer resistance to mammalian cells against oxidative-stress-induced apoptosis. Faseb J 2006; 20: 2636-8.

53. Serruys B, Van Houtte F, Verbrugghe P, Leroux-Roels G, Vanlandschoot P. Llama-derived single-domain intrabodies inhibit secretion of hepatitis B virions in mice. Hepatology 2009; 49: 39-49.

54. Tanaka T, Rabbitts TH. Functional intracellular antibody fragments do not require invariant intra-domain disulfide bonds. J Mol Biol 2008; 376: 749-57.

55. Visintin M, Quondam M, Cattaneo A. The intracellular antibody capture technology: towards the high-throughput selection of functional intracellular antibodies for target validation. Methods 2004; 34: 200-14.

56. Visintin M, Settanni G, Maritan A, Graziosi S, Marks JD, Cattaneo A. The intracellular antibody capture technology (IACT): towards a consensus sequence for intracellular antibodies. J Mol Biol 2002; 317: 73-83.

57. Tanaka T, Rabbitts TH. Protocol for the selection of single-domain antibody fragments by third generation intracellular antibody capture. Nat Protoc; 5: 67-92.

58. Tanaka T, Sewell H, Waters S, Phillips SE, Rabbitts TH. Single domain intracellular antibodies from diverse libraries: emphasizing dual functions of LMO2 protein interactions using a single VH domain. J Biol Chem; 286: 3707-16.

59. Preyer M, Vigneri P, Wang JY. Interplay between kinase domain autophosphorylation and F-actin binding domain in regulating imatinib sensitivity and nuclear import of BCR-ABL. PLoS One; 6: e17020.

60. Hantschel O, Wiesner S, Guttler T, et al. Structural basis for the cytoskeletal association of Bcr-Abl/c-Abl. Mol Cell 2005; 19: 461-73.

61. McWhirter JR, Wang JY. An actin-binding function contributes to transformation by the Bcr-Abl oncoprotein of Philadelphia chromosome-positive human leukemias. Embo J 1993; 12: 1533-46.

62. Kin Y, Li G, Shibuya M, Maru Y. The Dbl homology domain of BCR is not a simple spacer in P210BCR-ABL of the Philadelphia chromosome. J Biol Chem 2001; 276: 39462-8.

63. McWhirter JR, Wang JY. Effect of Bcr sequences on the cellular function of the Bcr-Abl oncoprotein. Oncogene 1997; 15: 1625-34.

64. Lemmon MA, Ferguson KM. Signal-dependent membrane targeting by pleckstrin homology (PH) domains. Biochem J 2000; 350 Pt 1: 1-18.

65. Lemmon MA, Ferguson KM, Abrams CS. Pleckstrin homology domains and the cytoskeleton. FEBS Lett 2002; 513: 71-6.

66. Lemmon MA, Ferguson KM, O'Brien R, Sigler PB, Schlessinger J. Specific and high-affinity binding of inositol phosphates to an isolated pleckstrin homology domain. Proc Natl Acad Sci U S A 1995; 92: 10472-6.

67. Lemmon MA. Pleckstrin homology (PH) domains and phosphoinositides. Biochem Soc Symp 2007: 81-93.

68. Dixon AS, Pendley SS, Bruno BJ, et al. Disruption of BCR-ABL coiled-coil oligomerization by design. J Biol Chem.

69. Taylor CM, Keating AE. Orientation and oligomerization specificity of the Bcr coiled-coil oligomerization domain. Biochemistry 2005; 44: 16246-56.

70. Zhao X, Ghaffari S, Lodish H, Malashkevich VN, Kim PS. Structure of the Bcr-Abl oncoprotein oligomerization domain. Nat Struct Biol 2002; 9: 117-20.

71. Afar DE, Han L, McLaughlin J, et al. Regulation of the oncogenic activity of BCR-ABL by a tightly bound substrate protein RIN1. Immunity 1997; 6: 773-82.

72. Lim YM, Wong S, Lau G, Witte ON, Colicelli J. BCR/ABL inhibition by an escort/phosphatase fusion protein. Proc Natl Acad Sci U S A 2000; 97: 12233-8.

73. Han L, Wong D, Dhaka A, et al. Protein binding and signaling properties of RIN1 suggest a unique effector function. Proc Natl Acad Sci U S A 1997; 94: 4954-9.

74. Bolte S, Cordelieres FP. A guided tour into subcellular colocalization analysis in light microscopy. J Microsc 2006; 224: 213-32.

75. Costes SV, Daelemans D, Cho EH, Dobbin Z, Pavlakis G, Lockett S. Automatic and quantitative measurement of protein-protein colocalization in live cells. Biophys J 2004; 86: 3993-4003.

76. Dixon AS, Lim CS. The nuclear translocation assay for intracellular protein-protein interactions and its application to the Bcr coiled-coil domain. Biotechniques; 49: 519-24.

77. Kanwal C, Mu S, Kern SE, Lim CS. Bidirectional on/off switch for controlled targeting of proteins to subcellular compartments. J Control Release 2004; 98: 379-93.

78. Thai M, Ting PY, McLaughlin J, et al. ABL fusion oncogene transformation and inhibitor sensitivity are mediated by the cellular regulator RIN1. Leukemia; 25: 290-300.

79. Cao X, Tanis KQ, Koleske AJ, Colicelli J. Enhancement of ABL kinase catalytic efficiency by a direct binding regulator is independent of other regulatory mechanisms. J Biol Chem 2008; 283: 31401-7.

80. McWhirter JR, Galasso DL, Wang JY. A coiled-coil oligomerization domain of Bcr is essential for the transforming function of Bcr-Abl oncoproteins. Mol Cell Biol 1993; 13: 7587-95.

CHAPTER 7

CONCLUSIONS AND FUTURE WORK

Conclusions

Addition of 4 Nuclear Localization Signals, But Not 1, Sends Bcr-Abl to the Nucleus and Induces Apoptosis

This body of work is hinged on the ability of nuclear Bcr-Abl to induce apoptosis. Bcr-Abl exhibits numerous interactions that have been implicated in its cytoplasmic retention (1-7), and translocating Bcr-Abl to the nucleus is a formidable challenge. To demonstrate that signal sequences can be used to control the subcellular localization of Bcr-Abl, and to demonstrate that nuclear Bcr-Abl causes apoptosis in a model cell line (K562) of chronic myelogenous leukemia (CML), the strong SV40 nuclear localization signal (NLS) was subcloned to Bcr-Abl. When expressed in K562 cells this protein construct did not localize to the nucleus, indicating the interactions anchoring Bcr-Abl in the cytoplasm were stronger than one SV40 NLS. The importin α/β hetero-dimer provides the driving force for nuclear localization upon recognition of the SV40 NLS by importin α (8-11). The strength of this NLS may be increased by having more than one importin α to bind Bcr-Abl, a possibility achieved by conjugating multiple NLSs to Bcr-Abl. When four SV40 NLSs were attached to Bcr-Abl the construct localized to

the nucleus, demonstrating that the factors causing cytoplasmic retention can be overcome through multiple NLSs. This finding provides proof that signal sequences can be used to manipulate the subcellular localization of Bcr-Abl.

Previously it had been reported that nuclear entrapment of Bcr-Abl could be achieved through the combination treatment of leptomycin B (LMB) and imatinib (12, 13). After washout of imatinib, but not LMB, Bcr-Abl induced apoptosis (13). As LMB inhibits all nuclear export through CRM1 and thus affects numerous proteins and cellular processes (14, 15), we sought further validation that nuclear Bcr-Abl induces apoptosis and used the 4NLS-Bcr-Abl construct in K562 cells as a model system. This construct of Bcr-Abl, which localizes to the nucleus, was shown to activate caspase-3/7 after transient transfection into K562 cells. Further demonstration of the induction of apoptosis was shown through morphological evaluation of the K562 cells. Apoptotic cells exhibit morphological phenomena observable through microscopy such as cell shrinkage, cytoplasmic blebbing, echnoid spikes, and DNA segmentation (16, 17). K562 cells expressing 4NLS-Bcr-Abl (determined through fluorescence from EGFP that was fused to the construct) demonstrated an increase in all of these hallmark signs for apoptosis. In particular, DNA segmentation was quantified in the transfected cells, and 4NLS-Bcr-Abl was found to cause higher levels of DNA segmentation than 1NLS-Bcr-Abl or EGFP. One difficulty in these experiments, specifically the caspase assay, was the low transfection efficiency of the large Bcr-Abl plasmids into K562 cells. Unpublished data from our laboratory (J. Constance) involved flow cytometry to analyze the transfected cells for induction of apoptosis based on annexin V binding to phosphatidylserine. This has also demonstrated that nuclear Bcr-Abl induces apoptosis. Together, these

experiments validate that sending Bcr-Abl to the nucleus is a viable method for inducing apoptosis in CML cells.

An important question with these experiments is whether or not the endogenous Bcr-Abl was affected by the localization of the exogenous, nuclear Bcr-Abl. As Bcr-Abl forms tetramers through a coiled-coil domain at the N-terminus of the protein (18-21), it is possible for 4NLS-Bcr-Abl to oligomerize with the endogenous Bcr-Abl and drag it to the nucleus along with it. To assess if the localization of the endogenous Bcr-Abl might be altered by 4NLS-Bcr-Abl, we tested whether the localization of an exogenous EGFP-Bcr-Abl construct would become more nuclear upon cotransfection with 4NLS-Bcr-Abl. Since 4NLS-Bcr-Abl was also fused to EGFP, we mutated EGFP to inactivate the fluorophore. We found the nuclear percentage of EGFP-Bcr-Abl transfected alone to be indistinguishable from the nuclear percentage resulting from cotransfection with 4NLS-Bcr-Abl. The inability to alter the localization of EGFP-Bcr-Abl indicates the endogenous Bcr-Abl is unlikely to be altered. An interesting observation about the inability of 4NLS-Bcr-Abl to alter the localization of endogenous Bcr-Abl, coupled with the ability of 4NLS-Bcr-Abl to induce apoptosis in K562 cells, is that there is competing signals in the cell. While the endogenous cytoplasmic Bcr-Abl signals for cell proliferation and the inhibition of apoptosis (22, 23), 4NLS-Bcr-Abl signals for apoptosis. The fact that 4NLS-Bcr-Abl was found to induce apoptosis in cells containing endogenous Bcr-Abl demonstrates the potent activation of apoptotic signaling by nuclear Bcr-Abl. Jointly, this validates the potential of any method for translocating Bcr-Abl to the nucleus, as all indications are for a high potency when removal of oncogenic signaling from the cytoplasm is coupled with apoptotic signaling in the nucleus.

The Use of the Protein Switch for a Nuclear Translocation Assay for Live-Cell Protein-Protein Interactions

While the protein switch technology has therapeutic potential for altering the subcellular localization of mislocalized proteins responsible for disease (24), a further use is for studying protein interactions inside a live cell. Protein interactions are a critical part of biological functions (25), and misregulation of these interactions is connected to many diseases (26-28). Thus, studying protein interactions is central to a basic understanding of biological processes as well as drug development. Regardless, there are limited assays for studying protein interactions inside a live cell; an essential aspect of studying the interactions in a state that most closely mimics the conditions under which the interactions normally occur.

The ability to control a protein's translocation from the cytoplasm to the nucleus is a valuable tool. Through genetic engineering a protein can be fused to the protein switch to impart the ability to control the nucleo-cytoplasmic shuttling to that protein. This cytoplasmic and nuclear localization can easily be monitored, and quantified, through the fluorescence from EGFP which is tagged to the protein switch. Proteins that interact with that protein can then be studied through subcloning of a second construct consisting of the interacting protein fused to a distinguishable fluorophore such as DsRed or mCherry. This second protein construct is not responsive to dexamethasone, the protein switch ligand. However, if an interaction occurs between the two proteins, the second protein will translocate into the nucleus along with the first protein that is fused to the protein switch. The nuclear accumulation of the second protein is indicative of the

interaction. This concept, termed the nuclear translocation assay (NTA) was demonstrated in chapter two of this dissertation through the interaction between different forms of the coiled-coil domain from Bcr-Abl.

In addition to this assay adding to the limited repertoire of methods to study protein interactions in live cells, an advantage is the confirmation that both of the necessary constructs (EGFP-protein switch-protein 1 and DsRed-protein 2) were transfected into the same cell and are being expressed at similar levels. This is a built-in feature of this assay as it is necessary to quantify the fluorescence intensities of both proteins in order to determine the percentage of the proteins that is in the nucleus. It is typical for cell-based assays to validate the protein expression on a population of cells through a method such as a western blot. The correlated assumption is the expression in the cell population provides evidence regarding the expression level for each protein at an individual cell level. Cotransfection of two fluorescent proteins readily confirms this assumption is not always true, as cells are identified with one or the other fluorescent protein and not both. The NTA does not rely on this assumption, and only cells expressing both constructs are analyzed.

Other advantages of this assay include that it does not require secondary reporter constructs, does not involve an enzymatic reaction, and does not need any kind of added substrate. This design simplifies the experimental set up, and reduces the necessary reagents to include only the plasmids, mammalian cells, a method for transfecting the cells, and a fluorescence microscope.

In summary, the NTA was demonstrated to be a useful way to quantify protein interactions in live cells. The percentage of nuclear proteins was quantified through

fluorescent proteins fused to the proteins of interest, but other methods could also be employed. One such possibility is to fuse the proteins to a transcription factor that would control the expression of a reporter molecule such as luciferase when the transcription factor is in the nucleus. Efforts to create this type of assay are ongoing.

The Rational Design of a Coiled-Coil Domain for Binding Bcr-Abl

With the dual purposes of binding Bcr-Abl for nuclear translocation and inhibiting Bcr-Abl through disruption of its oligomeric state, a modified form of the coiled-coil domain from Bcr-Abl was designed. The design entailed the identification of uncharged residues that are in an appropriate position to form a salt bridge with a charged residue on the opposing helix. These residues, if mutated to the appropriately charged residue, may allow the formation of additional salt bridges between the central helices in the mutant/wild-type dimer and result in a more stable interaction. To reduce the stability of the undesired mutant homodimer, charged residues were also incorporated where they would be positioned in proximity to a residue with the same charge on the opposing mutant helix. Thus, charge-charge repulsion would destabilize the mutant homo-dimer. The initially proposed mutations (S41R, L45D, E48R, V49D, and Q60E) were modeled by Scott Pendley from the Cheatham Laboratory, wherein it was discovered that incorporating both L45D and V49D mutations generates an undesirable kink in the central helix. However, one or the other mutation was demonstrated to provide some specificity along with an additional C38A mutation. The optimal set of mutations was determined to be C38A, S41R, L45D, E48R, and Q60E. This set of mutations was further tested through more extensive computational modeling (thermodynamic

integration and MM-PBSA) and found to form less stable homo-dimers while retaining the ability to oligomerize with the wild-type domain.

To test experimentally the design of these mutations, we carried out site-directed mutagenesis on a plasmid encoding the wild-type coiled-coil domain to generate the mutant coiled-coil domain, CCmut2. Two distinct binding assays, mammalian two-hybrid and nuclear translocation (NTA), were used to validate the modifications made. Both assays indicated the interactions followed the order CCmut2:CCmut2 < CC:CC < CCmut2:CC. This interaction pattern fits the proposed model wherein the modifications reduce the tendency to form mutant homo-dimers and simultaneously provide additional stabilization to the hetero-dimer. Nevertheless, the apparent increase in the hetero-dimer interaction may also be explained by similar wild-type homo-dimer and mutant/wild-type hetero-dimer binding affinities coupled with reduced mutant association rendering it more available to bind the wild-type domain. Regardless of whether the mutant is truly able to bind the wild-type with greater affinity, or simply appears to have a more favorable interaction due to the increased availability, these data indicate the mutations made in the coiled-coil domain do result in an improved oligomerization domain with increased efficacy for interacting with Bcr-Abl.

Oligomerization is important for the trans-autophosphorylation responsible for maintaining Bcr-Abl, specifically its tyrosine kinase domain, in a constitutively active state (18, 19, 29, 30). The oligomerization between CCmut2 and Bcr-Abl would then interfere with the oligomeric state of Bcr-Abl, prevent the trans-autophosphorylation, and shift Bcr-Abl into an inactive state. Indeed, we found that after transiently transfecting CCmut2 into K562 cells the phosphorylation of Bcr-Abl at tyrosine 245 was decreased.

This residue is phosphorylated through trans-autophosphorylation, and its phosphorylation is pivotal for the tyrosine kinase activity of Bcr-Abl (31). Numerous studies have used the phosphorylation of this residue as an indicator of the inhibition of Bcr-Abl, and the ability of CCmut2 to cause a decrease in Y245 phosphorylation demonstrates the ability to disrupt the Bcr-Abl oligomeric state leading to inhibition of Bcr-Abl. The inhibitory effects of CCmut2 were further demonstrated by the reduction in phosphorylation of two substrates phosphorylated by Bcr-Abl, STAT5 and CrkL (32, 33). Importantly, the decreased phosphorylation of all three proteins was a significant improvement from that resulting from the wild-type coiled-coil domain.

The inhibition of Bcr-Abl signaling by CCmut2 was then monitored through the decreased proliferation of the CML cells. CCmut2 was found to decrease the number of proliferating cells as measured through both a colony forming assay and cell counts using trypan blue for exclusion of dead cells. While the wild-type coiled domain did not result in a statistical significant decrease in the proliferation of the K562 cells, CCmut2 was found to decrease the proliferation at a statistically significant level.

Just as tyrosine kinase inhibitors are found to induce apoptosis in CML cells, the inhibition of Bcr-Abl by CCmut2 should also result in apoptosis of CML cells. The induction of apoptosis was measured through activation of caspase-3/7, and CCmut2 produced an increase in active caspase-3/7 in K562 cells. The fact that CCmut2 is functioning through inhibition of Bcr-Abl was further demonstrated by repeating the caspase-3/7 measurements in two cell lines that do not express Bcr-Abl, 1471.1 and Cos-7. No increase in caspase activity was observed in these cells, providing some evidence of the specificity of CCmut2 for cells expressing Bcr-Abl. Apoptosis was also studied

through morphological evaluation of the K562 cells (16, 17). Cells transfected with CCmut2 showed signs of apoptosis such as cell shrinkage, cytoplasmic blebbing, and DNA segmentation. The percentage of transfected cells with segmented DNA was calculated for quantification of the induction of apoptosis, and again CCmut2 demonstrated an improved ability to induce apoptosis in the CML cells. In a cell line lacking Bcr-Abl (1471.1) negligible DNA segmentation was observed after transfection of EGFP, CC or CCmut2. Both the caspase and DNA segmentation assays show the specific induction of apoptosis in CML cells.

As a final bridge between the computational modeling identifying the optimal set of mutations and the *in vitro* experimental work, circular dichroism was used to study the mutations created in the coiled-coil domain. First, both CC and CCmut2 were expressed in *E. coli* as fusion constructs with maltose binding protein (MBP) and six residues of histidine (his-tag, H_6). Wavelength scans produced almost identical spectral patterns for CC, CCmut2, or a mixture of CC and CCmut2, all exhibiting the characteristic pattern of α-helices. Thermal denaturation of CC produced a melting temperature (T_m) of 83 °C in agreement with other published reports. The T_m of CCmut2 was determined to be 63 °C by thermal denaturation, confirming the decreased stability of CCmut2 homo-oligomers. The thermal denaturation of CCmut2 mixed with CC did not produce a T_m higher than 83 °C. If the hetero-dimer has a T_m similar to CC, it may be difficult to distinguish with certainty. The absence of a higher hetero-dimer T_m in combination with a lower homo-dimer T_m for CCmut2, may conform to the list of results from other experiments if the hetero-dimer is isoenergentic with CC homo-dimers. The CD data thus provide insight that the mutations do not increase the stability of the CC:CCmut2 complex, but primarily

improve oligomerization, as substantiated through the *in vitro* experiments, through an increased availability to interact with CC due to decreased CCmut2 stability.

In summary, five mutations were identified in the Bcr-Abl coiled-coil domain. These mutations resulted in improved oligomerization with Bcr-Abl, and efficiently disrupted the oligomeric state of Bcr-Abl. Disruption of Bcr-Abl oligomerization reduced the phosphorylation of Bcr-Abl, decreased the proliferation of K562 cells, and induced apoptosis in cells expressing Bcr-Abl, but not cells that do not express Bcr-Abl. These findings demonstrate the therapeutic capabilities of CCmut2, and also validate CCmut2 as an efficient binding domain for use in binding Bcr-Abl for translocation to the nucleus.

Second Generation Modification to the Coiled-Coil Domain: CCmut3

While the modifications made to the coiled-coil domain improved oligomerization with Bcr-Abl, it seems the improvements stemmed largely from the decreased stability of the mutant coiled-coil rendering it more likely to interact with Bcr-Abl. The design for creating decreased stability was incorporation of charge-charge repulsion between the helices of the dimer interface. In the course of studying CCmut2, an additional residue, K39, was identified as an additional position that could be mutated to create charge-charge repulsion and further destabilize the mutant homo-dimer formation. Based on the structure of the wild-type coiled-coil domain, residue 39 is in a position on the helix to interact with residue 60. For CCmut2 where residue 60 is glutamate, this could mean an additional two salt bridges (two sets of K39:E60) could form in the homo-dimer. The effect of mutating K39 to E39 is to turn the potential to

form undesired salt bridges into possible charge-charge repulsion in the mutant homo-dimer. This additional mutation to CCmut2 was termed CCmut3.

The additional mutation was created in a plasmid encoding CCmut2 to create CCmut3, and mammalian two-hybrid assays were performed to determine the effects of the additional mutation. CCmut3 was found to have an increased interaction with the wild-type coiled-coil domain, and minimal interaction with another CCmut3. This finding confirms the additional mutation improves the oligomerization, at least at the domain level.

Co-localization analysis was then performed to verify the interaction with full-length Bcr-Abl. Although this method is not quantitative in terms of binding affinity, it is a useful way of confirming the interaction with Bcr-Abl inside of a mammalian cell. Interestingly, both wild-type and CCmut2 were found to co-localize at similar levels with Bcr-Abl. However, CCmut3 demonstrated the greatest co-localization with Bcr-Abl, further validating it as the best coiled-coil domain for oligomerizating with Bcr-Abl.

The increased binding by CCmut3 was also assessed for increased effect on CML cells. First, the proliferation was measured through colony forming assays and cell counts with trypan blue exclusion of dead cells. In both assays, CCmut2 and CCmut3 resulted in similar decrease in cellular proliferation. The improved binding through CCmut3 did not correlate with an improved effect on the growth rate of the cells.

Induction of apoptosis by CCmut3 was also studied in CML cells through flow cytometry, DNA segmentation, and caspase-3/7 activation. The number of cells that stained positively with 7-aminoactinomycin D (7AAD) was quantified through flow cytometry after transfection of the coiled-coil domains, and indicated an increase in the

order of EGFP < CC < CCmut2 < CCmut3 as desired. Nevertheless, in spite of CCmut3 exhibiting an improvement over CCmut2 in the statistical probability between EGFP ($p < 0.001$ vs $p < 0.05$, respectively), there was not a statistical difference between CCmut2 and CCmut3. Similarly, when apoptosis was measured through activation of caspase-3/7 and DNA segmentation there was no statistical significance between CCmut2 and CCmut3.

From these studies we can conclude that the additional mutation did improve the ability to oligomerize with Bcr-Abl. However, the improved binding properties did not translate into a further decrease in cell proliferation or enhancement of the induction of apoptosis. Failure to improve the cellular effect may be explained by the disruption of Bcr-Abl oligomerization already being maximized with CCmut2. If this is the case, further advancement in binding properties would not result in an improved effect on the cell proliferation or induction of apoptosis. Alternatively, the assay sensitivity may not be sufficient to distinguish the difference between CCmut2 and CCmut3. The ultimate goal entailing the modified coiled-coil domain is for capturing Bcr-Abl for translocation to the nucleus, and for this purpose the binding is critical. The improvement in binding demonstrated by CCmut3, regardless of the inability to act as a more potent inhibitor of Bcr-Abl activity, will be important to achieve this goal.

Isolation of Intracellular Domain Antibodies for Capture of Bcr-Abl

An alternative approach for binding Bcr-Abl is through isolation of an intracellular domain antibody (iDab) (34, 35) that targets Bcr-Abl. Antibodies exhibit high affinity and specificity, but are generally only useful extracellularly. Antibody

truncations have been made, particularly the scFv format, that are useful for epitope recognition intracellularly (36-39), but the iDab is an even smaller portion that has been shown to retain high binding affinity and specificity without the need for a peptide linker (34, 40). In addition, iDabs are stable inside of cells, do not require any disulfide bridge, and can be expressed at high levels in mammalian cells (35, 41).

The procedure for isolation of an iDab has been termed intracellular antibody capture (IAC) technology (35, 42). The IAC protocol was followed to isolate iDabs that bind Bcr-Abl at either the actin binding domain (ABD) or Dbl homology/pleckstrin homology (DHPH) region. The first round of screening, involving screening libraries with randomized amino acids in the third complementarity determining region (CDR3), was performed in the laboratory of Dr. Rabbitts at the Leeds Institure of Molecular Medicine (LIMM) at Leeds University. Although access to the libraries was limited to the time while I was in the Rabbitts laboratory, 20 and 25 hits were identified for the ABD and DHPH targets respectively. These products from first round screening were then used for generation of sublibraries with amino acids in CDR2 randomized. The sublibraries were then screened in the Lim laboratory where the top 12 ABD and DHPH binders were sequenced and subcloned into plasmids for mammalian two-hybrid screening. Through the mammalian two-hybrid screening four iDabs were identified as the top binders, three that bind to the ABD and one that binds to the DHPH region. Overall, the top binding iDab was found to be ABD binding iDab #7 (ABI7).

Coupled with the goal of using the iDab as a capture motif for translocating Bcr-Abl to the nucleus, the ABD was chosen as the target region of Bcr-Abl in attempt to compete with actin binding anchoring Bcr-Abl in the cytoplasm (1, 43-45). Interestingly,

we found that when ABI7 was co-transfected with mCherry-Bcr-Abl the resulting localization pattern of Bcr-Abl was altered. Under normal conditions mCherry-Bcr-Abl is found to localize at the actin filaments in a distinct pattern of lines. However, this pattern was altered and mCherry-Bcr-Abl was found at distinct punctuate structures when coexpressed with ABI7. As Bcr-Abl interacts with both F-actin and G-actin (44), the resulting localization pattern may be indicative of a shift from interacting with both forms to one or the other. While the exact details of this distinct localization pattern remains to be further elucidated, it does provide evidence ABI7 is able to compete with actin binding to a certain extent and may cause Bcr-Abl to become more available for translocation.

The Use of Capture Motifs for Escorting Bcr-Abl to the Nucleus

The final work of this dissertation was to test the ability of the generated binding domains to capture Bcr-Abl and allow for translocation to the nucleus. As the analysis of the nuclear translocation will be performed through fluorescence microscopy, cells that facilitate imaging and that do not express Bcr-Abl, Cos-7, were chosen for the experiments. Two approaches of translocating Bcr-Abl to the nucleus were tested: incorporation of the binding domain into the inducible protein switch (46, 47), and attachment of nuclear localization signals directly to the binding domain. Along with CCmut3 and ABI7, the top binding domains generated in this dissertation, the previously established Bcr-Abl binding domain from RIN1 (48-50) was also tested and compared with the translocation capabilities of CCmut3 and ABI7. Prior to testing the ability to translocate Bcr-Abl to the nucleus, the binding domains were validated to interact with

Bcr-Abl through colocalization analysis (51). All three constructs (CCmut3, ABI7, RIN1) were found to colocalize with Bcr-Abl indicating their interaction inside a live cell. However, DBI5, the top DHPH binding iDab, was just below the typical threshold used for determining colocalization. This is likely representative of the weak interaction of this binding domain, confirming the modest binding result from the mammalian two-hybrid assays. Due to the evident weak interaction of DBI5 and all other DHPH binding iDabs, these binding domains were not tested further.

The first approach to translocate Bcr-Abl to the nucleus was under the ligand-inducible control of the protein switch. One advantage of this approach is the capability to grant mean residence time for the equilibration of the interaction between the binding domain and Bcr-Abl in the cytoplasm. Nevertheless, the incorporation of the binding domains into the protein switch was found to decrease the nuclear translocation of the fused protein switch construct, and thus reduced the potential to escort Bcr-Abl to the nucleus along with it. Negligible Bcr-Abl was found to accumulate in the nucleus after ligand induction with these protein switch constructs.

As all three of these binding domains interact with a different region of Bcr-Abl, it is possible to use multiple protein switch constructs to bind Bcr-Abl through multiple locations and increase the potential for nuclear translocation. Accordingly, two protein switch constructs were co-transfected with Bcr-Abl and the resulting nuclear translocation was tested. In the majority of the cells negligible Bcr-Abl was found to translocate to the nucleus. However, it was possible to find some cells with minimal nuclear translocation. As both of the protein switch constructs were fused to EGFP, it was impossible to determine if only one, or both, of the protein switch constructs was

transfected into the cells. After identification of cells with apparent nuclear translocation of Bcr-Abl, the percentage of Bcr-Abl in the nucleus was quantified. The combination of protein switch-ABI7 and protein switch-CCmut3 was the only combination to result in a statistical significant accumulation of Bcr-Abl in the nucleus. Although this was a biased screen and represents an inadequate method for translocation of Bcr-Abl, it did demonstrate a slight feasibility of translocating Bcr-Abl to the nucleus.

In a much simpler approach, the binding domains were fused to four strong nuclear localization signals, the signal from SV40. Although these constructs are not ligand-inducible, and thus there will not be any mean residency time for binding in the cytoplasm, these constructs were found to localize almost exclusively in the nucleus. This is in stark contrast to the protein switch constructs, where even the optimized protein switch without incorporation of a binding domain is readily detectable in the cytoplasm even after ligand induction (47). Regardless, both 4NLS-ABI7 and 4NLS-RIN1 were unable to cause a nuclear accumulation of Bcr-Abl. This finding may be due to the minimal time to interact with Bcr-Abl associated with the rapid nuclear accumulation of these constructs, or insufficient binding to overcome the opposing interactions leading to cytoplasmic retention of Bcr-Abl. However, in astounding fashion, 4NLS-CCmut3 resulted in the majority of Bcr-Abl translocating to the nucleus. The fact that CCmut3 was able to translocate Bcr-Abl to the nucleus, but not ABI7 or RIN1, may indicate how Bcr-Abl is bound is important, and not merely how tightly it is bound. Further examination of the binding affinities of these domains will be required to fully make this conclusion. This study demonstrated, for the first time, it is possible to escort Bcr-Abl to the nucleus without use of imatinib or LMB. Moreover, the combination of imatinib and

LMB was previously found to trap approximately 25% of Bcr-Abl in the nucleus, an amount that was sufficient for induction of apoptosis (13). 4NLS-CCmut3 was found to cause approximately 70% of Bcr-Abl to translocate to the nucleus, demonstrating the potential for an even more potent induction of apoptosis.

Future Work

Simplifying CCmut3: Testing Helix 2

The coiled-coil domain from Bcr-Abl is 72 amino acids long and consists of two parallel helices connected by a short loop (20, 21). The first of these helices, termed α-1 and found at the N-terminus, is a short helix of 11 amino acids, residues 5-15. The second helix, α-2, is composed by residues 28-67, and contains the bulk of the residues found at the dimer and tetramer interface. Consistent with α-2 being at the core of the oligomerization, an α-2 peptide composed of residues 23-72 has been shown to be useful for inhibiting Bcr-Abl through interfering with its oligomeric state (52, 53). In this work, we have shown that the coiled-coil domain can be improved by mutating certain residues to achieve enhanced oligomeric properties (54). All of the residues mutated for enhanced oligomerization are found within the α-2 helix. Thus, a CCmut3 peptide can be constructed similar to the previous α-2 peptide, and compared for efficacy against full-length CCmut3 and wild-type α-2 peptide. Both the inhibitory effects on Bcr-Abl and the ability to translocate Bcr-Abl to the nucleus should be studied with this smaller construct. Even if the CCmut3 peptide does not demonstrate enhanced efficacy, and is only equivalent to full-length CCmut3, the peptide will still have the advantage of being

smaller, may be more easily internalized into cells, synthesized synthetically, and may be more readily translated into a useful therapeutic.

In addition to a CCmut3 peptide consisting of residues 23-72 as has been demonstrated for wild-type CC, further truncations such as residues 28-67, or even 30-65, should also be tested. Residues 23-27 and 68-72 are not part of the helix and are not likely to be important in the oligomerization and the corresponding efficacy of the peptide. A peptide consisting of 30-65 has been used to study the structure of the Bcr coiled-coil domain (20, 21), and should also be tested as potentially the minimal peptide to retain binding capabilities. An interesting strategy that has not previously been attempted for this peptide is to add residues at the termini for stabilization of the helix cap. Aspartate residues at the N-terminus provide stabilization to the N-cap through both hydrogen bonding and interactions with the helix dipole (55-58). If only α-2 is used as the peptide (residues 28-67), the N-terminal residue is valine which is slightly destabilizing for the N-cap. This residue could be mutated to aspartate, or an additional aspartate could be added before this valine to help stabilize the N-cap of the helix. At the C-terminus of the helix is a lysine. Although lysines are mildly stabilizing to the C-cap, either this lysine could be mutated to the more stabilizing glycine, or an additional glycine could be added to the C-terminus for added stabilization of the C-cap (58-60). In addition to the incorporation of residues for N- and C-capping of the helix, the termini of the helical peptide could be acetylated and amidated for further stabilization (61, 62).

Continuation of Affinity Maturation Screening of Bcr-Abl-Binding iDabs

Although one iDab, ABI7, has been identified with reasonable affinity for Bcr-Abl, various approaches for further affinity maturation can be explored. This may be of particular interest for the DHPH binders as the isolated iDabs thus far have demonstrated only weak interaction with Bcr-Abl. As further analysis of the ability to induce apoptosis through 4NLS-CCmut3 unfolds it may be discovered that alternative binding strategies that do not interfere with Bcr-Abl oligomerization will be needed. A simultaneous dual binding approach at the ABD and DHPH regions could be a viable alternative with improvements in the affinity of these iDabs.

One of the easiest methods to identify an iDab with higher affinity for Bcr-Abl would be to rescreen the sublibraries with increased concentration of 3-amino-1,2,4-triazole (3-AT). 3-AT is an inhibitor of the HIS3 gene product (35), the gene controlled through the interaction between the iDab and the bait (ABD or DHPH). By increasing the concentration of 3-AT in the screening plates, weaker interactions that activate the pathway to a lesser extent can be inhibited. This allows for the identification of the higher affinity interactions. Before the sublibraries were screened, the auto-activation of the HIS3 gene was assessed, and it was determined that 2 mM 3-AT was sufficient to eliminate the auto-activation. Only this minimal amount, 2 mM, was then used in the screens, leaving ample range for increasing the concentration to screen out the weak interactions and identify the high affinity interactions. As approximately 800 colonies grew on the screening plates with 2 mM 3-AT for both ABD and DHPH baits, increasing the 3-AT concentration would reduce the number of colonies down to a range where all of the colonies could be tested in the X-gal assay.

More extensive approaches could also be undertaken to identify an iDab with higher affinity for Bcr-Abl. The protocol outlined for IAC of iDabs entails the screening of 15 libraries in the first round of screening (35). Time constraints only allowed access to these libraries for a short period of time while in the Rabbitts laboratory, and resulted in the ability to screen only 3 of the 15 libraries. The remaining libraries could be generated in the Lim laboratory, or a possible agreement could be made with the Rabbitts laboratory to continue screening their libraries either in the Lim Laboratory or at the LIMM. A more extensive screening with the all of the potential sequences of CDR3 should allow for the identification of iDabs with higher affinity for Bcr-Abl.

Further affinity maturation of the iDabs could also be achieved through randomization of CDR1 in the creation of a sublibrary for use in another round of screening. Typically IAC^3 consists of all three rounds, screening for the optimal binding sequences of CDR3, CDR2, and CDR1. Continuation of the third round of screening for the optimal CDR1 sequences would increase the affinity of the current iDab constructs.

Translocating Endogenous Bcr-Abl to the Nucleus

While this work has shown that mCherry-Bcr-Abl, when co-transfected, could be translocated to the nucleus with 4NLS-CCmut3, further exploration of the ability to translocate endogenous Bcr-Abl to the nucleus will need to be confirmed. The experimental design wherein the mCherry-Bcr-Abl was shown to translocate to the nucleus along with EGFP-4NLS-CCmut3 may prove easier than translocating the endogenous Bcr-Abl. The major difference being that endogenous Bcr-Abl will already be bound by numerous proteins, and will be in the tetrameric state. Hence, 4NLS-Bcr-

Abl will not only have to compete with the oligomerization of Bcr-Abl, but overcome the other interactions causing the cytoplasmic localization. This is a dramatic difference with the experiment, wherein the Bcr-Abl was being translated simultaneously with 4NLS-CCmut3. This may allow an equal opportunity for 4NLS-CCmut3 to bind Bcr-Abl while homo-oligomerization and other protein binding occur, and result in a more facile nuclear translocation of Bcr-Abl. As the ultimate goal is to translocate endogenous Bcr-Abl to the nucleus, the ability to do so will need to be confirmed without relying on exogenously added Bcr-Abl constructs.

One possible experimental design that may correlate more closely to the ability to translocate endogenous Bcr-Abl, while using mCherry-Bcr-Abl for ease of monitoring the nuclear translocation, is to sequentially transfect mCherry-Bcr-Abl and then 4NLS-CCmut3. In this fashion mCherry-Bcr-Abl would be allowed to form the typical interactions resulting in the cytoplasmic retention. Twenty-four hrs later the same cells could then be transfected with 4NLS-CCmut3, and 24 hrs later the subcellular localization of Bcr-Abl determined through fluorescence microscopy. This would demonstrate the ability of 4NLS-CCmut3 to compete with the cytoplasmic interactions and cause a relocalization of Bcr-Abl into the nucleus.

Nevertheless, this would not replace the testing of endogenous Bcr-Abl in CML cells, and immunocytochemistry will need to be performed to study the subcellular distribution of endogenous Bcr-Abl after transfection of 4NLS-CCmut3. Analysis of the subcellular distribution of Bcr-Abl through an immunocytochemical approach has already been performed in K562 cells (2), and can be followed after transfection of 4NLS-CCmut3. Through this study the percentage of Bcr-Abl that is translocated into

the nucleus can be determined and more appropriately compared with the previous result obtained by the combination treatment of imatinib and LMB (13). If less than 25% of Bcr-Abl is translocated into the nucleus by 4NLS-Bcr-Abl, the result obtained with imatinib and LMB, alternative approaches may need to be explored for increasing the nuclear translocation. Some strategies for achieving this purpose may include combinations of binding domains that bind different regions of Bcr-Abl, pretreatment of cells with CCmut3 or ABI7 (no NLSs) followed by treatment with 4NLS-CCmut3, and combination treatment with imatinib and 4NLS-CCmut3. Additionally, the 14-3-3 inhibitor BV02 (7, 63) could be used in combination with 4NLS-CCmut3 to release Bcr-Abl from 14-3-3 interactions that are also thought to play a role in cytoplasmic retention.

Characterization of the Induction of Apoptosis by Nuclear Bcr-Abl

While translocating Bcr-Abl to the nucleus was a major component of this project, the ultimate goal is to use nuclear Bcr-Abl to induce apoptosis. The induction of apoptosis by Bcr-Abl following translocation to the nucleus by CCmut3 will warrant extensive investigation through multiple experimental approaches. Some apoptosis assays that could be carried out are the analysis of annexin-APC/7AAD staining via flow cytometry, activation of caspases such as caspase-3/7, evaluation of cellular morphology (such as cell shrinkage, cytoplasmic and zeotic blebbing, echnoid spikes, and DNA segmentation), mitochondrial membrane potential (JC-1 assay), cytochrome C release (western blot or ELISA), and PARP cleavage (western blot). An important aspect of analyzing the induction of apoptosis through 4NLS-CCmut3 will be the comparison to the current treatment of CML, imatinib. Inclusion of imatinib into these experiments for

simultaneous evaluation with 4NLS-CCmut3 will provide a reference to the standard of approved CML treatment.

The first step will be to demonstrate the induction of apoptosis in CML model cells such as K562, KU812, BaF3^{p210}, and 32D^{p210}. As 4NLS-CCmut3 functions through altering the localization of Bcr-Abl, cells that do not contain Bcr-Abl should not be affected. The induction of apoptosis should also be measured after transfecting 4NLS-CCmut3 into cells that do not contain Bcr-Abl to demonstrate both the safety of 4NLS-CCmut3 as well as confirm the mechanism of action does in fact depend on Bcr-Abl.

After it has been demonstrated in model cell lines that 4NLS-CCmut3 can escort Bcr-Abl to the nucleus where it induces apoptosis, CML patient samples should be tested. These patient samples provide the closest simulation for therapeutic efficacy in CML patients. A critical aspect of validating the therapeutic potential of 4NLS-CCmut3 will be to demonstrate efficacy in these patient samples. However, a limiting factor is the access to these patient samples, and only after careful vetting of the nuclear translocation of Bcr-Abl and the induction of apoptosis is the use of the limited supply of CML patient samples warranted.

Testing the Ability to Translocate Resistant Forms of Bcr-Abl and the Ensuing Induction of Apoptosis

One of the current problems in CML therapy is the ability to treat TKI resistant forms of Bcr-Abl (64-66). Although ponatinib and DCC-2036 are currently in clinical trials and have been demonstrated to inhibit Bcr-Abl^{T315I} (67-69), there are no currently approved treatments that affect Bcr-Abl^{T315I}. As CCmut3 interacts with Bcr-Abl through

the coiled-coil domain, none of the currently described mutations found in the SH3, SH2, or tyrosine kinase domains should have any effect on the ability of CCmut3 to bind Bcr-Abl (70-72). As a result, 4NLS-CCmut3 should have similar efficacy on Bcr-Abl and all of the resistant forms of Bcr-Abl. The ability to translocate resistant forms of Bcr-Abl to the nucleus, and the resulting induction of apoptosis, should be confirmed experimentally. Moreover, it has been shown that oligomeric disruption of Bcr-Abl^{T315I} does not abrogate the kinase activity as is found for unmutated Bcr-Abl (52, 73). Thus, if the kinase activity is involved in the induction of apoptosis when Bcr-Abl is localized in the nucleus, Bcr-Abl^{T315I} may be a more potent inducer of apoptosis than other forms of Bcr-Abl. In an interesting twist, the only form of Bcr-Abl that is currently untreatable may turn out to be the form which 4NLS-CCmut3 has the highest efficacy against.

Currently our lab has BaF3 cells stably transfected with Bcr-Abl^{T315I}. This is an apt model for studying the ability to translocate Bcr-Abl^{T315I} to the nucleus. After the nuclear translocaion has been confirmed, similar apoptosis assays as were carried out with unmutated Bcr-Abl could be performed. Other cell lines containing Bcr-Abl with other resistant mutations could also be used to demonstrate the ability of 4NLS-CCmut3 to escort Bcr-Abl to the nucleus, and the ability of nuclear Bcr-Abl to induce apoptosis, regardless of the particular mutation. Although extremely difficult to obtain, patient samples from CML patients with Bcr-Abl^{T315I} would be an important demonstration of the efficacy of escorting this particular form of Bcr-Abl to the nucleus and the ensuing induction of apoptosis. Demonstration that 4NLS-CCmut3 can cause induction of apoptosis in cells harboring resistant forms of Bcr-Abl, particularly the T315I mutation,

will validate 4NLS-CCmut3 as a potential strategy for treatment of resistant forms of CML.

Induction of Apoptosis by Nuclear Bcr-Abl in CML Stem Cells

Although TKIs effectively manage CML, they are not curative (74, 75). At the root of the problem resulting in their inability to cure CML is the fact that they do not induce apoptosis in the CML stem cells (76). This inability to induce apoptosis in the stem cells is not due to a lack of Bcr-Abl expression in these cells (77), nor is it due to their inability to inhibit Bcr-Abl in these cells (78). Intriguingly, inhibition of Bcr-Abl in the CML stem cell does not have the same effect as inhibition in the more mature cells. One theory explaining this phenomenon is that these quiescent stem cells are not yet dependent on Bcr-Abl signaling. Regardless of the reasoning for TKIs not affecting the stem cells, it is likely that active induction of apoptosis by nuclear Bcr-Abl will be effective in the stem cells. If indeed nuclear Bcr-Abl induces apoptosis in the CML stem cells, it would demonstrate the potential to turn a disease requiring a life-long management regimen into a curable disease. With enormous ramifications few other approaches, if any, can claim, this therapeutic intervention strategy must be explored.

CML stem cells are typically defined as those cells exhibiting a $CD34^+$ and $CD38^-$ phenotype (79). Addition characteristics have also been used in attempt to accurately identify the homogenous population of CML stem cells. Such attempts include low side scatter, high expression of aldehyde dehydrogenase (79), efflux of Hoescht dye (80), and non-responsiveness to cytokines (80), to name a few. Nevertheless, through FACS it is possible to easily isolate only the $CD34^+/CD38^-$ cells. Although these cells are not a

strict homogenous population of the stem cells, they are enriched with the stem cells and can be used as a model system for the stem cells. Studies in this population of cells will be a critical component of validating the therapeutic potential of nuclear Bcr-Abl. Again, apoptosis assays such as the ones already mentioned could be used to test the induction of apoptosis in these cells. A potential limitation, however, may be the low number of the $CD34^{+}/CD38^{-}$ cells in the sample, requiring the use of assays with high sensitivity that can be performed on minimal numbers of cells. As flow cytometry will be used to sort the cells, some possibilities involve apoptosis analysis via flow cytometry. This affords the ability to treat the entire sample and analyze the effects on different subpopulations of cells simultaneously on the flow cytometer.

While the exact mechanism of inducing apoptosis after Bcr-Abl is transported to the nucleus remains to be further elucidated, the current understanding is that it involves activation of p73 (81-85). As a p53 family member, p73 is a robust tumor suppressor and recently has gained interest as a target for cancer intervention (86). Activation of p73 results in activation of the pro-apoptotic proteins PUMA, Bax, and p21 (87). These signaling pathways are also found in hematopoietic stem cells, and hence the CML stem cells, indicating that activation of p73 by nuclear Bcr-Abl should have the same effect on all Bcr-Abl-containing cells, including the stem cells. This immensely important hypothesis will justify extensive exploration.

Internalization of 4NLS-CCmut3 with a Cell Penetrating Peptide

One of the biggest challenges that will need to be overcome in order to allow the successful use of 4NLS-CCmut3 is the delivery and internalization into the cells. This is

a formidable challenge for macromolecular therapeutics such as 4NLS-CCmut3. One avenue that is currently being explored is the use of a leukemia-specific cell penetrating peptide (CPP) (88). This CPP, the nine amino acid sequence CAYHRLRRC, was identified through screening involving phage display and the specific internalization into leukemia and lymphoma cells. Although CCmut3 is not expected to exhibit toxicity in healthy cells that do not contain Bcr-Abl, specific delivery to only leukemic cells will add an additional level of safety.

As opposed to a typical ligand-receptor based approach to targeting the leukemia/lymphoma cells, this CPP was identified while screening for peptides internalized through macropinocytosis (88). Interestingly, the identified peptide consisted of sequences identified as a lymph-node homing motif (CAY) and an arginine rich sequence (RLRR) typical of cell penetrating peptides. The dual functionality was demonstrated to result in substantially greater internalization into leukemia and lymphoma cells than other non-leukemia/lymphoma cells. Inclusion of this CPP at a terminus of CCmut3 may provide the means for internalization, but will need further validation for larger constructs as it was only demonstrated through conjugation to a peptide of 14 amino acids. As an alternative to CAYHRLRRC, another leukemia-specific CPP has recently been identified that could be explored for internalization of CCmut3 (89).

As mentioned, there is no reason to expect CCmut3 to exhibit toxicity on cells that do not contain Bcr-Abl, and studies thus far confirm this finding. Hence, a leukemia-specific internalization may not be necessary, and if a nonspecific CPP can deliver a greater amount of CCmut3 the loss of specificity may be worth the trade off. As such,

alternative CPPs should be tested and compared for a more comprehensive analysis to guide the selection. Obvious choices include the commonly studied HIV trans-activator of transcription (Tat) (90-95) and the third helix from Antennapedia homeodomain (pAntp) (96-98). These CPPs have been used to deliver a variety of cargos, including proteins, of various sizes into a range of cells and cell types.

Alternatively to the internalization of CCmut3 protein with a CPP, the gene encoding CCmut3 could be delivered with a viral vector. Adenoviral vectors, specifically serotype 5 (Ad5), are one of the most common viral vectors used in clinical trials (99-102), and are a reasonable choice due to improvements reducing immunogenicity along with the epi-chromosomal delivery to both dividing and non-dividing cells. Other options, such as lentiviral vectors, offer the ability to integrate into the host cell genome with continued protein expression in daughter cells but come with an added risk for insertional mutagenesis (103, 104). While no gene therapeutic is currently approved for use in the US, numerous clinical trials are underway. Moreover, two gene therapeutics have been approved for head-and-neck cancer in China (105, 106), Gendicine (SiBiono) (107) and Oncorine (Shanghai Sunway Biotech) (108), and may be a possible indication of technological advancements leading to future US approval of a gene therapeutic. Given the immense potential of viral vectors for gene therapeutics, this mechanism of delivery should also be considered for delivery of CCmut3.

Use of CCmut3 or iDabs for Transport of Bcr-Abl to Other Subcellular Compartments

This body of work has focused on generating binding domains to allow the translocation of Bcr-Abl to the nucleus where it is an active inducer of apoptosis. Directing Bcr-Abl to other subcellular compartments may also prove therapeutically relevant. Two subcellular locations of interest are the proteasome and the mitochondria, and methods to target Bcr-Abl to these areas are being explored by Rian Davis and Jonathan Constance, respectively. Efficient removal of Bcr-Abl by triggering its degradation by sending it to the proteasome may be an alternative to inhibiting its activity. Based on the activity of c-Abl, translocating Bcr-Abl to the mitochondria should result in phosphorylation of protein kinase C delta (PKCdelta) and subsequent induction of apoptosis (109, 110). Both of these projects are underway in the Lim Laboratory and may be facilitated by the increased ability to capture Bcr-Abl with the binding domains generated in this dissertation.

Although signals targeting the proteasome are not as straight forward as other locations such as the nucleus, there are methods to target a protein to the proteasome for degradation. One approach is through the N-end rule, a correlate between the half-life of a protein and the residue at the N-terminus of the protein (111-114). These so-called degradation signals, or degrons, involve either acetylation or arginylation of the residue at the N-terminus. Conjugation of the Bcr-Abl binding domain to a sequence known to be acetylated or arginylated may direct the complex to the proteasome for degradation in a similar fashion as 4NLS-CCmut3 directs Bcr-Abl to the nucleus. An alternative strategy is to use the estrogen receptor ligand binding domain (ER LBD) which has been shown to

be poly-ubiquitinated by ubiquitin ligase and directed to the proteasome after binding to ligand (115-117). Hence, the ER LBD may serve as a proteasomal protein switch. A Bcr-Abl binding domain could be incorporated into this proteasomal protein switch, and after addition of ligand will escort Bcr-Abl to the proteasome for degradation.

Associated with the pivotal role in energy production, the mitochondrion is a highly-characterized cellular compartment. Correspondingly, the signals directing proteins to the mitochondrion are also highly-studied. Various mitochondrial targeting signals (MTS) have been described, including separate signals for targeting the outer membrane (118), the inner membrane (119, 120), the intermembrane space (121), and the matrix (122). To date, in our laboratory the mitochondrial matrix has been efficiently targeted through use of the signal from ornathine transcarbamylase (OTC), MLFNLRILLNNAAFRNGHNFMVRNFRCGQPLQ (122), the outer membrane has been targeted by either the signal from Tom20, MVGRNSAIAAGVCGALFIGYCIYFD RKRRSDPN(123), or from Bcl-XL, RGPGIQKGPGEIQQMVPDRHDRGRRGAAGQP VQQKX , and the innermembrane space has been targeted by the signal from SMAC/Diablo. Similar to the NLSs, these MTS could be incorporated into the binding domain to allow capture of Bcr-Abl followed by redirection to the mitochondrion. In a more elaborate system, Jonathan Constance has designed a cryptic MTS (cMTS) that only results in mitochondrial relocation after phosphorylation by Bcr-Abl. The optimized cMTS exhibits a tight interaction with Bcr-Abl, and no additional binding domain may be necessary. Use of the cMTS would allow translocation of Bcr-Abl to the mitochondria only after activation by phosphorylation.

In addition to the future use of the binding domains generated in this dissertation for translocating Bcr-Abl to other subcellular compartments, the demonstration that Bcr-Abl can be escorted to the nucleus provides proof-of-concept that an exogenously added protein can be used to redirect the subcellular localization of Bcr-Abl. The fact that Bcr-Abl can be moved to the nucleus indeed signifies it can be moved to other compartments as well.

References

1. Preyer M, Vigneri P, Wang JY. Interplay between kinase domain autophosphorylation and F-actin binding domain in regulating imatinib sensitivity and nuclear import of BCR-ABL. PLoS One; 6: e17020.

2. Telegeev GD, Dubrovska AN, Nadgorna VA, et al. Immunocytochemical study of Bcr and Bcr-Abl localization in K562 cells. Exp Oncol; 32: 81-3.

3. Chu S, McDonald T, Bhatia R. Role of BCR-ABL-Y177-mediated p27kip1 phosphorylation and cytoplasmic localization in enhanced proliferation of chronic myeloid leukemia progenitors. Leukemia; 24: 779-87.

4. Hantschel O, Wiesner S, Guttler T, et al. Structural basis for the cytoskeletal association of Bcr-Abl/c-Abl. Mol Cell 2005; 19: 461-73.

5. Wetzler M, Talpaz M, Van Etten RA, Hirsh-Ginsberg C, Beran M, Kurzrock R. Subcellular localization of Bcr, Abl, and Bcr-Abl proteins in normal and leukemic cells and correlation of expression with myeloid differentiation. J Clin Invest 1993; 92: 1925-39.

6. Dhut S, Chaplin T, Young BD. BCR-ABL and BCR proteins: biochemical characterization and localization. Leukemia 1990; 4: 745-50.

7. Mancini M, Corradi V, Petta S, et al. A new nonpeptidic inhibitor of 14-3-3 induces apoptotic cell death in chronic myeloid leukemia sensitive or resistant to imatinib. J Pharmacol Exp Ther; 336: 596-604.

8. Fontes MR, Teh T, Kobe B. Structural basis of recognition of monopartite and bipartite nuclear localization sequences by mammalian importin-alpha. J Mol Biol 2000; 297: 1183-94.

9. Catimel B, Teh T, Fontes MR, et al. Biophysical characterization of interactions involving importin-alpha during nuclear import. J Biol Chem 2001; 276: 34189-98.

10. Jans DA, Xiao CY, Lam MH. Nuclear targeting signal recognition: a key control point in nuclear transport? Bioessays 2000; 22: 532-44.

11. Yoneda Y. Nucleocytoplasmic protein traffic and its significance to cell function. Genes Cells 2000; 5: 777-87.

12. Aloisi A, Di Gregorio S, Stagno F, et al. BCR-ABL nuclear entrapment kills human CML cells: ex vivo study on 35 patients with the combination of imatinib mesylate and leptomycin B. Blood 2006; 107: 1591-8.

13. Vigneri P, Wang JY. Induction of apoptosis in chronic myelogenous leukemia cells through nuclear entrapment of BCR-ABL tyrosine kinase. Nat Med 2001; 7: 228-34.

14. Kudo N, Wolff B, Sekimoto T, et al. Leptomycin B inhibition of signal-mediated nuclear export by direct binding to CRM1. Exp Cell Res 1998; 242: 540-7.

15. Yoshida M, Nishikawa M, Nishi K, Abe K, Horinouchi S, Beppu T. Effects of leptomycin B on the cell cycle of fibroblasts and fission yeast cells. Exp Cell Res 1990; 187: 150-6.

16. Willingham MC. Cytochemical methods for the detection of apoptosis. J Histochem Cytochem 1999; 47: 1101-10.

17. Barrett KL, Willingham JM, Garvin AJ, Willingham MC. Advances in cytochemical methods for detection of apoptosis. J Histochem Cytochem 2001; 49: 821-32.

18. Guo XY, Cuillerot JM, Wang T, et al. Peptide containing the BCR oligomerization domain (AA 1-160) reverses the transformed phenotype of p210bcr-abl positive 32D myeloid leukemia cells. Oncogene 1998; 17: 825-33.

19. McWhirter JR, Galasso DL, Wang JY. A coiled-coil oligomerization domain of Bcr is essential for the transforming function of Bcr-Abl oncoproteins. Mol Cell Biol 1993; 13: 7587-95.

20. Taylor CM, Keating AE. Orientation and oligomerization specificity of the Bcr coiled-coil oligomerization domain. Biochemistry 2005; 44: 16246-56.

21. Zhao X, Ghaffari S, Lodish H, Malashkevich VN, Kim PS. Structure of the Bcr-Abl oncoprotein oligomerization domain. Nat Struct Biol 2002; 9: 117-20.

22. Sattler M, Griffin JD. Molecular mechanisms of transformation by the BCR-ABL oncogene. Semin Hematol 2003; 40: 4-10.

23. Hazlehurst LA, Bewry NN, Nair RR, Pinilla-Ibarz J. Signaling networks associated with BCR-ABL-dependent transformation. Cancer Control 2009; 16: 100-7.

24. Davis JR, Kakar M, Lim CS. Controlling protein compartmentalization to overcome disease. Pharm Res 2007; 24: 17-27.

25. Stein A, Pache RA, Bernado P, Pons M, Aloy P. Dynamic interactions of proteins in complex networks: a more structured view. FEBS J 2009; 276: 5390-405.

26. Tsukaguchi H, Matsubara H, Taketani S, Mori Y, Seido T, Inada M. Binding-, intracellular transport-, and biosynthesis-defective mutants of vasopressin type 2 receptor in patients with X-linked nephrogenic diabetes insipidus. J Clin Invest 1995; 96: 2043-50.

27. Buchanan PJ, Ernst RK, Elborn JS, Schock B. Role of CFTR, Pseudomonas aeruginosa and Toll-like receptors in cystic fibrosis lung inflammation. Biochem Soc Trans 2009; 37: 863-7.

28. Zhong N, Weisgraber KH. Understanding the Basis for the Association of Apoe4 with Alzheimer's Disease: Opening the Door for Therapeutic Approaches. Curr Alzheimer Res 2009.

29. Zhang X, Subrahmanyam R, Wong R, Gross AW, Ren R. The NH(2)-terminal coiled-coil domain and tyrosine 177 play important roles in induction of a myeloproliferative disease in mice by Bcr-Abl. Mol Cell Biol 2001; 21: 840-53.

30. He Y, Wertheim JA, Xu L, et al. The coiled-coil domain and Tyr177 of bcr are required to induce a murine chronic myelogenous leukemia-like disease by bcr/abl. Blood 2002; 99: 2957-68.

31. Brasher BB, Van Etten RA. c-Abl has high intrinsic tyrosine kinase activity that is stimulated by mutation of the Src homology 3 domain and by autophosphorylation at two distinct regulatory tyrosines. J Biol Chem 2000; 275: 35631-7.

32. ten Hoeve J, Arlinghaus RB, Guo JQ, Heisterkamp N, Groffen J. Tyrosine phosphorylation of CRKL in Philadelphia+ leukemia. Blood 1994; 84: 1731-6.

33. Shuai K, Halpern J, ten Hoeve J, Rao X, Sawyers CL. Constitutive activation of STAT5 by the BCR-ABL oncogene in chronic myelogenous leukemia. Oncogene 1996; 13: 247-54.

34. Tanaka T, Lobato MN, Rabbitts TH. Single domain intracellular antibodies: a minimal fragment for direct in vivo selection of antigen-specific intrabodies. J Mol Biol 2003; 331: 1109-20.

35. Tanaka T, Rabbitts TH. Protocol for the selection of single-domain antibody fragments by third generation intracellular antibody capture. Nat Protoc; 5: 67-92.

36. Lo AS, Zhu Q, Marasco WA. Intracellular antibodies (intrabodies) and their therapeutic potential. Handb Exp Pharmacol 2008: 343-73.

37. Lobato MN, Rabbitts TH. Intracellular antibodies as specific reagents for functional ablation: future therapeutic molecules. Curr Mol Med 2004; 4: 519-28.

38. Hagemeyer CE, von Zur Muhlen C, von Elverfeldt D, Peter K. Single-chain antibodies as diagnostic tools and therapeutic agents. Thromb Haemost 2009; 101: 1012-9.

39. Accardi L, Di Bonito P. Antibodies in single-chain format against tumour-associated antigens: present and future applications. Curr Med Chem; 17: 1730-55.

40. Tanaka T, Sewell H, Waters S, Phillips SE, Rabbitts TH. Single domain intracellular antibodies from diverse libraries: emphasizing dual functions of LMO2 protein interactions using a single VH domain. J Biol Chem; 286: 3707-16.

41. Tanaka T, Rabbitts TH. Functional intracellular antibody fragments do not require invariant intra-domain disulfide bonds. J Mol Biol 2008; 376: 749-57.

42. Tanaka TR, TH. Intracellular Antibody Capture Protocol. Nat Methods 2009; *In press*.

43. McWhirter JR, Wang JY. An actin-binding function contributes to transformation by the Bcr-Abl oncoprotein of Philadelphia chromosome-positive human leukemias. Embo J 1993; 12: 1533-46.

44. Van Etten RA, Jackson PK, Baltimore D, Sanders MC, Matsudaira PT, Janmey PA. The COOH terminus of the c-Abl tyrosine kinase contains distinct F- and G-actin binding domains with bundling activity. J Cell Biol 1994; 124: 325-40.

45. Woodring PJ, Hunter T, Wang JY. Regulation of F-actin-dependent processes by the Abl family of tyrosine kinases. J Cell Sci 2003; 116: 2613-26.

46. Kakar M, Cadwallader AB, Davis JR, Lim CS. Signal sequences for targeting of gene therapy products to subcellular compartments: the role of CRM1 in nucleocytoplasmic shuttling of the protein switch. Pharm Res 2007; 24: 2146-55.

47. Kakar M, Davis JR, Kern SE, Lim CS. Optimizing the protein switch: altering nuclear import and export signals, and ligand binding domain. J Control Release 2007; 120: 220-32.

48. Afar DE, Han L, McLaughlin J, et al. Regulation of the oncogenic activity of BCR-ABL by a tightly bound substrate protein RIN1. Immunity 1997; 6: 773-82.

49. Han L, Wong D, Dhaka A, et al. Protein binding and signaling properties of RIN1 suggest a unique effector function. Proc Natl Acad Sci U S A 1997; 94: 4954-9.

50. Lim YM, Wong S, Lau G, Witte ON, Colicelli J. BCR/ABL inhibition by an escort/phosphatase fusion protein. Proc Natl Acad Sci U S A 2000; 97: 12233-8.

51. Costes SV, Daelemans D, Cho EH, Dobbin Z, Pavlakis G, Lockett S. Automatic and quantitative measurement of protein-protein colocalization in live cells. Biophys J 2004; 86: 3993-4003.

52. Beissert T, Hundertmark A, Kaburova V, et al. Targeting of the N-terminal coiled coil oligomerization interface by a helix-2 peptide inhibits unmutated and imatinib-resistant BCR/ABL. Int J Cancer 2008; 122: 2744-52.

53. Beissert T, Puccetti E, Bianchini A, et al. Targeting of the N-terminal coiled coil oligomerization interface of BCR interferes with the transformation potential of BCR-ABL and increases sensitivity to STI571. Blood 2003; 102: 2985-93.

54. Dixon AS, Pendley SS, Bruno BJ, et al. Disruption of BCR-ABL coiled-coil oligomerization by design. J Biol Chem.

55. Anderson TA, Sauer RT. Role of an N(cap) residue in determining the stability and operator-binding affinity of Arc repressor. Biophys Chem 2003; 100: 341-50.

56. Koscielska-Kasprzak K, Cierpicki T, Otlewski J. Importance of alpha-helix N-capping motif in stabilization of betabetaalpha fold. Protein Sci 2003; 12: 1283-9.

57. Dirr HW, Little T, Kuhnert DC, Sayed Y. A conserved N-capping motif contributes significantly to the stabilization and dynamics of the C-terminal region of class Alpha glutathione S-transferases. J Biol Chem 2005; 280: 19480-7.

58. Doig AJ, Baldwin RL. N- and C-capping preferences for all 20 amino acids in alpha-helical peptides. Protein Sci 1995; 4: 1325-36.

59. Ermolenko DN, Thomas ST, Aurora R, Gronenborn AM, Makhatadze GI. Hydrophobic interactions at the Ccap position of the C-capping motif of alpha-helices. J Mol Biol 2002; 322: 123-35.

60. Huttunen-Hennelly HE. An investigation into the N- and C-capping effects of glycine in cavitand-based four-helix bundle proteins. Bioorg Chem; 38: 98-107.

61. Dennison SR, Phoenix DA. Influence of C-terminal amidation on the efficacy of modelin-5. Biochemistry; 50: 1514-23.

62. Greenfield NJ, Stafford WF, Hitchcock-DeGregori SE. The effect of N-terminal acetylation on the structure of an N-terminal tropomyosin peptide and alpha alpha-tropomyosin. Protein Sci 1994; 3: 402-10.

63. Corradi V, Mancini M, Manetti F, Petta S, Santucci MA, Botta M. Identification of the first non-peptidic small molecule inhibitor of the c-Abl/14-3-3 protein-protein interactions able to drive sensitive and Imatinib-resistant leukemia cells to apoptosis. Bioorg Med Chem Lett; 20: 6133-7.

64. Leitner AA, Hochhaus A, Muller MC. Current treatment concepts of CML. Curr Cancer Drug Targets; 11: 31-43.

65. Jabbour E, Cortes J, Kantarjian H. Long-term outcomes in the second-line treatment of chronic myeloid leukemia: a review of tyrosine kinase inhibitors. Cancer; 117: 897-906.

66. Wong SF, Mirshahidi H. Use of tyrosine kinase inhibitors for chronic myeloid leukemia: management of patients and practical applications for pharmacy practitioners. Ann Pharmacother; 45: 787-97.

67. Zhou T, Commodore L, Huang WS, et al. Structural mechanism of the Pan-BCR-ABL inhibitor ponatinib (AP24534): lessons for overcoming kinase inhibitor resistance. Chem Biol Drug Des; 77: 1-11.

68. O'Hare T, Deininger MW, Eide CA, Clackson T, Druker BJ. Targeting the BCR-ABL signaling pathway in therapy-resistant Philadelphia chromosome-positive leukemia. Clin Cancer Res; 17: 212-21.

69. Eide CA, Adrian LT, Tyner JW, et al. The ABL switch control inhibitor DCC-2036 is active against the chronic myeloid leukemia mutant BCR-ABLT315I and exhibits a narrow resistance profile. Cancer Res; 71: 3189-95.

70. Shah NP, Nicoll JM, Nagar B, et al. Multiple BCR-ABL kinase domain mutations confer polyclonal resistance to the tyrosine kinase inhibitor imatinib (STI571) in chronic phase and blast crisis chronic myeloid leukemia. Cancer Cell 2002; 2: 117-25.

71. Hochhaus A, Erben P, Ernst T, Mueller MC. Resistance to targeted therapy in chronic myelogenous leukemia. Semin Hematol 2007; 44: S15-24.

72. Hochhaus A, Schenk T, Erben P, Ernst T, La Rosee P, Muller MC. Cause and management of therapy resistance. Best Pract Res Clin Haematol 2009; 22: 367-79.

73. Mian AA, Oancea C, Zhao Z, Ottmann OG, Ruthardt M. Oligomerization inhibition, combined with allosteric inhibition, abrogates the transformation potential of T315I-positive BCR/ABL. Leukemia 2009; 23: 2242-7.

74. Redner RL. Why doesn't imatinib cure chronic myeloid leukemia? Oncologist; 15: 182-6.

75. Fausel C. Targeted chronic myeloid leukemia therapy: seeking a cure. J Manag Care Pharm 2007; 13: 8-12.

76. Jiang X, Zhao Y, Smith C, et al. Chronic myeloid leukemia stem cells possess multiple unique features of resistance to BCR-ABL targeted therapies. Leukemia 2007; 21: 926-35.

77. Copland M, Hamilton A, Elrick LJ, et al. Dasatinib (BMS-354825) targets an earlier progenitor population than imatinib in primary CML but does not eliminate the quiescent fraction. Blood 2006; 107: 4532-9.

78. Corbin AS, Agarwal A, Loriaux M, Cortes J, Deininger MW, Druker BJ. Human chronic myeloid leukemia stem cells are insensitive to imatinib despite inhibition of BCR-ABL activity. J Clin Invest; 121: 396-409.

79. Gerber JM, Qin L, Kowalski J, et al. Characterization of chronic myeloid leukemia stem cells. Am J Hematol; 86: 31-7.

80. Jorgensen HG, Holyoake TL. Characterization of cancer stem cells in chronic myeloid leukaemia. Biochem Soc Trans 2007; 35: 1347-51.

81. Agami R, Blandino G, Oren M, Shaul Y. Interaction of c-Abl and p73alpha and their collaboration to induce apoptosis. Nature 1999; 399: 809-13.

82. Gong JG, Costanzo A, Yang HQ, et al. The tyrosine kinase c-Abl regulates p73 in apoptotic response to cisplatin-induced DNA damage. Nature 1999; 399: 806-9.

83. Vella V, Zhu J, Frasca F, et al. Exclusion of c-Abl from the nucleus restrains the p73 tumor suppression function. J Biol Chem 2003; 278: 25151-7.

84. Wang JY, Ki SW. Choosing between growth arrest and apoptosis through the retinoblastoma tumour suppressor protein, Abl and p73. Biochem Soc Trans 2001; 29: 666-73.

85. Yuan ZM, Shioya H, Ishiko T, et al. p73 is regulated by tyrosine kinase c-Abl in the apoptotic response to DNA damage. Nature 1999; 399: 814-7.

86. Slade N, Horvat A. Targeting p73--a potential approach in cancer treatment. Curr Pharm Des; 17: 591-602.

87. Zawacka-Pankau J, Kostecka A, Sznarkowska A, Hedstrom E, Kawiak A. p73 tumor suppressor protein: a close relative of p53 not only in structure but also in anti-cancer approach? Cell Cycle; 9: 720-8.

88. Nishimura S, Takahashi S, Kamikatahira H, et al. Combinatorial targeting of the macropinocytotic pathway in leukemia and lymphoma cells. J Biol Chem 2008; 283: 11752-62.

89. Karjalainen K, Jaalouk DE, Bueso-Ramos CE, et al. Targeting neuropilin-1 in human leukemia and lymphoma. Blood; 117: 920-7.

90. Eum WS, Choung IS, Li MZ, et al. HIV-1 Tat-mediated protein transduction of Cu,Zn-superoxide dismutase into pancreatic beta cells in vitro and in vivo. Free Radic Biol Med 2004; 37: 339-49.

91. Jeong MS, Kim DW, Lee MJ, et al. HIV-1 Tat-mediated protein transduction of human brain creatine kinase into PC12 cells. BMB Rep 2008; 41: 537-41.

92. Silhol M, Tyagi M, Giacca M, Lebleu B, Vives E. Different mechanisms for cellular internalization of the HIV-1 Tat-derived cell penetrating peptide and recombinant proteins fused to Tat. Eur J Biochem 2002; 269: 494-501.

93. Tyagi M, Rusnati M, Presta M, Giacca M. Internalization of HIV-1 tat requires cell surface heparan sulfate proteoglycans. J Biol Chem 2001; 276: 3254-61.

94. Vives E, Brodin P, Lebleu B. A truncated HIV-1 Tat protein basic domain rapidly translocates through the plasma membrane and accumulates in the cell nucleus. J Biol Chem 1997; 272: 16010-7.

95. Yang Y, Ma J, Song Z, Wu M. HIV-1 TAT-mediated protein transduction and subcellular localization using novel expression vectors. FEBS Lett 2002; 532: 36-44.

96. Herbig ME, Fromm U, Leuenberger J, Krauss U, Beck-Sickinger AG, Merkle HP. Bilayer interaction and localization of cell penetrating peptides with model membranes: a comparative study of a human calcitonin (hCT)-derived peptide with pVEC and pAntp(43-58). Biochim Biophys Acta 2005; 1712: 197-211.

97. Magzoub M, Eriksson LE, Graslund A. Conformational states of the cell-penetrating peptide penetratin when interacting with phospholipid vesicles: effects of surface charge and peptide concentration. Biochim Biophys Acta 2002; 1563: 53-63.

98. Drin G, Mazel M, Clair P, Mathieu D, Kaczorek M, Temsamani J. Physico-chemical requirements for cellular uptake of pAntp peptide. Role of lipid-binding affinity. Eur J Biochem 2001; 268: 1304-14.

99. Nienhuis A. The growing clinical impact of gene therapy. Mol Ther 2008; 16: 995-6.

100. Merritt JA, Roth JA, Logothetis CJ. Clinical evaluation of adenoviral-mediated p53 gene transfer: review of INGN 201 studies. Semin Oncol 2001; 28: 105-14.

101. Edelstein ML, Abedi MR, Wixon J, Edelstein RM. Gene therapy clinical trials worldwide 1989-2004-an overview. J Gene Med 2004; 6: 597-602.

102. Cotrim AP, Baum BJ. Gene therapy: some history, applications, problems, and prospects. Toxicol Pathol 2008; 36: 97-103.

103. Frecha C, Levy C, Cosset FL, Verhoeyen E. Advances in the field of lentivector-based transduction of T and B lymphocytes for gene therapy. Mol Ther; 18: 1748-57.

104. Escors D, Breckpot K. Lentiviral vectors in gene therapy: their current status and future potential. Arch Immunol Ther Exp (Warsz); 58: 107-19.

105. Shi J, Zheng D. An update on gene therapy in China. Curr Opin Mol Ther 2009; 11: 547-53.

106. Peng Z, Yu Q, Bao L. The application of gene therapy in China. IDrugs 2008; 11: 346-50.

107. Peng Z. Current status of gendicine in China: recombinant human Ad-p53 agent for treatment of cancers. Hum Gene Ther 2005; 16: 1016-27.

108. Raty JK, Pikkarainen JT, Wirth T, Yla-Herttuala S. Gene therapy: the first approved gene-based medicines, molecular mechanisms and clinical indications. Curr Mol Pharmacol 2008; 1: 13-23.

109. Qi X, Mochly-Rosen D. The PKCdelta -Abl complex communicates ER stress to the mitochondria - an essential step in subsequent apoptosis. J Cell Sci 2008; 121: 804-13.

110. Lu W, Finnis S, Xiang C, et al. Tyrosine 311 is phosphorylated by c-Abl and promotes the apoptotic effect of PKCdelta in glioma cells. Biochem Biophys Res Commun 2007; 352: 431-6.

111. Varshavsky A. The N-end rule pathway and regulation by proteolysis. Protein Sci.

112. Hwang CS, Shemorry A, Varshavsky A. N-terminal acetylation of cellular proteins creates specific degradation signals. Science; 327: 973-7.

113. Choi WS, Jeong BC, Joo YJ, et al. Structural basis for the recognition of N-end rule substrates by the UBR box of ubiquitin ligases. Nat Struct Mol Biol; 17: 1175-81.

114. Meinnel T, Serero A, Giglione C. Impact of the N-terminal amino acid on targeted protein degradation. Biol Chem 2006; 387: 839-51.

115. Valley CC, Metivier R, Solodin NM, et al. Differential regulation of estrogen-inducible proteolysis and transcription by the estrogen receptor alpha N terminus. Mol Cell Biol 2005; 25: 5417-28.

116. Lonard DM, Nawaz Z, Smith CL, O'Malley BW. The 26S proteasome is required for estrogen receptor-alpha and coactivator turnover and for efficient estrogen receptor-alpha transactivation. Mol Cell 2000; 5: 939-48.

117. Dennis AP, Haq RU, Nawaz Z. Importance of the regulation of nuclear receptor degradation. Front Biosci 2001; 6: D954-9.

118. Dukanovic J, Rapaport D. Multiple pathways in the integration of proteins into the mitochondrial outer membrane. Biochim Biophys Acta; 1808: 971-80.

119. Peixoto PM, Grana F, Roy TJ, et al. Awaking TIM22, a dynamic ligand-gated channel for protein insertion in the mitochondrial inner membrane. J Biol Chem 2007; 282: 18694-701.

120. Botelho SC, Osterberg M, Reichert AS, et al. TIM23-mediated insertion of transmembrane alpha-helices into the mitochondrial inner membrane. EMBO J; 30: 1003-11.

121. Endo T, Yamano K. Multiple pathways for mitochondrial protein traffic. Biol Chem 2009; 390: 723-30.

122. Morita T, Miura S, Mori M, Tatibana M. Transport of the precursor for rat-liver ornithine carbamoyltransferase into mitochondria in vitro. Eur J Biochem 1982; 122: 501-9.

123. Roise D, Schatz G. Mitochondrial presequences. J Biol Chem 1988; 263: 4509-11.